# INFLUENCE OF CYCLING POSITION AND CROSSWINDS ON PERFORMANCE AND AERODYNAMICS

*"The angle matters"*

By

DANIËLLE MARIA FINTELMAN

A thesis submitted to

The University of Birmingham

For the degree of

DOCTOR OF PHILOSOPHY

School of Sport, Exercise and Rehabilitation Sciences
College of Life and Environmental Sciences
University of Birmingham
April 2015

# ABSTRACT

Wind is fundamentally important to cyclists since it affects their performance, bicycle control, balance and road safety. The overall aim of this research is to improve the understanding of the effect of cycling position and crosswinds on the aerodynamics and performance of a cyclist.

The first part of this thesis focuses on cycling position. To minimise air resistance, cyclists lower their torso to become more aerodynamic. Results show that lowering torso angle is associated with impairment of physiological functioning, which can be explained by a combination of mechanical and muscular factors. Consequently, there is a trade-off between aerodynamic gains and physiological impairment. Therefore a mathematical model has been developed predicting the optimal torso angle at different cycling speeds.

The second part of this thesis aims to understand the flow mechanics around a cyclist subjected to crosswinds. Both wind tunnel experiments and computational fluid dynamics simulations of the flow around a cyclist are used to reveal the effect of crosswinds on cyclists in different cycling positions.

This thesis provides a unique approach to study cycling performance and safety by jointly investigating the human physiology and aerodynamic performance.

# ACKNOWLEDGEMENTS

First and foremost I would like to express my sincere gratitude to my supervisors,
dr. François-Xavier Li, prof. Mark Sterling and dr. Hassan Hemida, for their immense input and continuous support during my PhD. Without their guidance throughout my PhD, this thesis would have never been accomplished. I would like to thank you for your support and understanding over these past three years.

I would also like to thank the undergraduate and postgraduate students who have helped me with the data collection and provided feedback on my research.

Getting through a PhD requires more than academic support, and I have therefore many people to thank for being a listening ear and their support over the past three years. Most important in this were my family and boyfriend. I would like to thank my boyfriend Mark for his support, help and encouragement. Although our time in Birmingham has had its ups and downs, it was an unforgettable experience to study abroad.

# CONTENTS

# LIST OF PUBLICATIONS

This thesis is based on the work contained in the following papers:

**Articles in international journals**

- Fintelman, D. M., Sterling, M., Hemida, H. and Li, F.-X. 2015. The effect of aerodynamic time trial cycling position on physiological and aerodynamic variables. *Journal of Sport Sciences*, doi: 10.1080/02640414.2015.1009936
- Fintelman, D. M., Sterling, M., Hemida, H. and Li, F.-X. 2015. Effect of different aerodynamic time trial cycling positions on crank torque, muscle activation and efficiency. *Scandinavian Journal of Medicine and Science in Sports*, doi: 10.1111/sms.12479
- Fintelman, D. M., Sterling, M., Hemida, H. and Li, F.-X. 2013. Optimal cycling time trial position models: aerodynamics versus power output and metabolic energy. *Journal of Biomechanics*, 47 (8), 1894-1898.
- Fintelman, D. M., Sterling, M., Hemida, H. and Li, F.-X. 2014. The effect of crosswinds on cyclists: an experimental study. *Procedia Engineering*, 72, 720-725.
- Fintelman, D. M., Sterling, M., Hemida, H. and Li, F.-X. 2014. CFD simulations of the flow around a cyclist subjected to crosswinds. *Journal of Wind Engineering and Industrial Aerodynamics*, doi: 10.1016/j.jweia.2015.05.009.

- Fintelman, D. M., Hemida, H., Sterling, M. and Li, F.-X. 2015. Computational fluid dynamics study of the effect of cycling position on the aerodynamic responses in crosswinds, in preparation.
- Fintelman, D. M., Hemida, H., Sterling, M., and Li, F.-X. 2015. Numerical investigation of the flow around a motorbike subjected to crosswinds. *Engineering Applications of Computational Fluid Mechanics*, doi: 10.1080/19942060.2015.1071524.

**Articles published online**

- Fintelman, D. M., Hemida, H., Sterling, M., and Li, F.-X. 2014. Computational fluid dynamics study of the effect of cycling position on the aerodynamic responses in crosswinds. *5th BlueBEAR PG conference*, Birmingham, UK.
- Fintelman, D. M., Hemida, H., Sterling, M., and Li, F.-X. 2013. Numerical investigation of the effect of crosswind on cyclists. *4th BlueBEAR PG conference*, Birmingham, UK.

**Posters**

- Fintelman, D. M., Hemida, H., Sterling, M., and Li, F.-X. 2014. Numerical investigation of the flow around a cyclist subjected to crosswinds. *5th BlueBEAR PG conference*, Birmingham, UK.
- Fintelman, D. M., Sterling, M., Hemida, H. and Li, F.-X. 2013. Cycling time trial position: torso angle affects metabolic and physiological variable. *European College of Sport Science (ECSS) conference*, Barcelona, Spain.

- Fintelman, D. M., Sterling, M., Hemida, H. and Li, F.-X. 2013. Optimal cycling time trial position models. *European College of Sport Science (ECSS) conference*, Barcelona, Spain.
- Fintelman, D. M., Hemida, H., Sterling, M., and Li, F.-X. 2013. Numerical investigation of the flow around a motorbike subjected to crosswinds. *Mid-Plus Engineering Showcase*, Birmingham, UK.

**Oral presentations**

- Fintelman, D. M., Sterling, M., Hemida, H. and Li, F.-X. 2014. The effect of crosswinds on cyclists: an experimental study. *The Engineering of Sport 10, Conference of the International Sports Engineering Association (ISEA)*, Sheffield, UK.
- Fintelman, D. M., Hemida, H., Sterling, M., and Li, F.-X. 2014. The effect of crosswinds on cyclists. *6. International Symposium on Computational Wind Engineering (CWE)*, Hamburg, Germany.

# ABBREVATIONS

| | |
|---|---|
| BDC | Bottom Dead Centre of the pedal stroke |
| Bf | Breathing frequency |
| BF | Biceps femoris muscle |
| BSR | Back-saver sit and reach test |
| CFD | Computational Fluid Dynamics |
| CFL | Courant-Friederichs-Lewy number |
| DDES | Delayed Detached Eddy Simulation |
| DES | Detached Eddy Simulation |
| DNS | Direct Numerical Simulation |
| DP | Dropped cycling position |
| EMG | Electromyography |
| GE | Gross Efficiency |
| GCL | Gastrocnemius lateralis muscle |
| GM | Gastrocnemius medialis muscle |
| GMax | Gluteus maximus muscle |
| HR | Heart rate |
| IE | Metabolic energy and energy of eddies |
| ITU | International Triathlon Union |
| LES | Large Eddy Simulation |
| MAP | Maximal Aerobic Power |
| PO | Power Output |
| PPO | Peak Power Output |
| PSD | Power Spectral Density |
| RF | Rectus femoris muscle |
| RER | Respiratory Exchange Rate |
| RANS | Reynolds Averaged Navier Stokes |
| SENIAM | Surface ElectroMyoGraphy for the Non-Invasive Assessment of Muscles |
| SO | Soleus muscle |

| | |
|---|---|
| TA | Tibialis anterior muscle |
| TDC | Top Dead Centre of the pedal stroke |
| TT | Time Trial |
| UCI | International Cycling Federation |
| UP | Upright cycling position |
| $VCO_{2max}$ | The maximum amount of $CO_2$ that can be consumed by an individual |
| VE | Minute ventilation of breathing |
| VL | Vastus lateralis muscle |
| VM | Vastus medialis muscle |
| $VO_{2max}$ | The maximum amount of oxygen that can be consumed by an individual |
| VT | Tidal Volume |

# NOMENCLATURE

## Greek symbols

| | |
|---|---|
| $\alpha$ | Angle between cyclists' upper arm and lower arm |
| $\beta$ | Angle of the cyclists' torso relative to the ground |
| $\beta_{opt}$ | Optimal cycling torso angle |
| $\gamma$ | Crosswind angle |
| $\delta$ | Dimension of grid cell |
| $\delta_{ij}$ | Kronecker delta |
| $\delta_{99\%}$ | 99% Boundary layer thickness |
| $\varepsilon$ | Turbulent dissipation and relative error between fine and medium mesh |
| $\eta$ | Gross efficiency |
| $\theta$ | Wind direction |
| $\mu$ | Roll friction coefficient |
| $\nu$ | Kinematic viscosity of fluid |
| $\nu_t$ | Turbulent viscosity |
| $\omega$ | Specific turbulent dissipation |
| $\rho$ | Air density |
| $\tau_{ij}$ | Subgrid scale stress tensor |
| $\Delta$ | Largest dimension of the grid cell of the mesh |

## Lower case roman symbols

| | |
|---|---|
| f | Turbulent frequencies in the flow |
| $f_d$ | Van Driest damping function |
| g | Gravitational constant |
| k | Thermal conductivity and turbulent kinetic energy |
| $l_{DES}$ | Modified length scale function |
| $l_{RANS}$ | Turbulent length scale function |
| m | Mass of the bicycle and cyclist |

| | |
|---|---|
| p | Pressure and order of accuracy of simulation results |
| r | Grid refinement factor |
| t | Time |
| $t^*$ | Dimensionless time |
| u | Velocity |
| v | Velocity |
| $v_c$ | Cycling velocity |
| $v_w$ | Wind velocity |
| $x_i$ | Cartesian coordinates |

## Upper case roman symbols

| | |
|---|---|
| A | Projected frontal area |
| Angle $T_{max1}$ | Pedal position at the peak torque of the left down stroke leg |
| Angle $T_{max2}$ | Pedal position at the peak torque of the right down stroke leg |
| $C_D$ | Drag force coefficient |
| $C_i$ | Constant |
| $C_L$ | Lift force coefficient |
| $C_P$ | Pitching moment coefficient, specific heat and pressure coefficient |
| $C_R$ | Rolling moment coefficient |
| $C_S$ | Side force coefficient and Smagorinsky constant |
| $C_Y$ | Yawing moment coefficient |
| $C_DA$ | Drag force coefficient area |
| $C_LA$ | Lift force coefficient area |
| $C_PA$ | Pitching moment coefficient area |
| $C_RA$ | Rolling moment coefficient area |
| $C_SA$ | Side force coefficient area |
| $C_YA$ | Yawing moment coefficient area |
| $CF_X$ | Drag force coefficient |
| $CF_Y$ | Side force coefficient |
| $CF_Z$ | Lift force coefficient |
| $CM_X$ | Rolling moment coefficient |
| $CM_Y$ | Pitching moment coefficient |
| $CM_Z$ | Yawing moment coefficient |
| $F_D$ | Drag force |

| | |
|---|---|
| $F_L$ | Lift force |
| $F_S$ | Side force and safety factor mesh refinement |
| $F_X$ | Drag force |
| $F_Y$ | Side force |
| $F_Z$ | Lift force |
| $GCI_{fine}$ | Grid Convergence Index of the fine mesh |
| H | Height of the cyclist |
| L | Wheelbase of the motorbike |
| $M_P$ | Pitching moment |
| $M_R$ | Rolling moment |
| $M_X$ | Rolling moment |
| $M_Y$ | Pitching moment and yawing moment |
| $M_Z$ | Yawing moment |
| $P_{air}$ | Aerodynamic power losses |
| $P_{gen}$ | Required power generation of cyclist |
| $P_{loss}$ | Power losses due to rolling resistance and aerodynamic drag |
| $P_{PPO}$ | Peak power output |
| $P_{roll}$ | Power losses due to rolling resistance |
| $P_{surplus}$ | Surplus power, the amount of additional power the cyclist has available |
| Q | Second invariant of the velocity gradient tensor |
| St | Strouhal number |
| $S_{ij}$ | Resolved strain rate tensor |
| T | Flow temperature |
| $T_{delta}$ | Difference between minimal and maximal crank torque |
| $T_{maxL}$ | Maximal torque in left leg down stroke |
| $T_{maxR}$ | Maximal torque in right leg down stroke |
| U | Flow velocity |
| $U_\infty$ | Free stream flow velocity |
| $U_{eff}$ | Effective flow velocity |

# LIST OF FIGURES

# LIST OF TABLES

# CHAPTER 1

# Introduction

Due to the competitive nature of sport, cyclists strive to go as fast as possible. In the last few decades, many researchers have tried to improve cycling performance. Methods include amongst others the optimisation of kinematics, training, nutrition, physiology, mechanics and aerodynamics. Since up to 90 % of the total cycling power is used to overcome air resistance when cycling at 50 km/h (Debraux et al., 2011), a beneficial method to improve performance is by reducing air resistance, often called aerodynamic drag. It has been estimated by Bassett et al. (1999) that the improvement in distance of the world hour record between 1967 and 1996 can be attributed for 60 % to aerodynamic gains whilst the other 40 % is due to physiological improvements. Wilson (2004) also stated that '*the greatest potential for improvement in cycling speed is aerodynamics'* (p. 150). Therefore researchers have been focussing on different aspects of reducing aerodynamic drag, including position, equipment optimisation (wheels, frames etc.) and drafting. In addition to performance, cycling safety needs to be maintained. Crosswinds (wind not parallel to the travel direction) could induce additional forces and moments on a bicycle. In particular two-wheeled vehicles are sensitive to crosswinds due to their relatively low weight, but studies addressing this aspect are limited. This introduction chapter is divided in to the following sections. In section 1.1 different aspects of cycling aerodynamics are discussed, whilst section 1.2 focuses on the aerodynamic performance assessment. In section 1.3 an introduction is given about crosswinds on two-wheeled vehicles. Finally in section 1.4 and 1.5, the thesis aims and objectives are given.

## 1.1 Cycling aerodynamics

Aerodynamic drag can be split up in to two components: pressure drag and viscous drag (Faria, 1992, Debraux et al., 2011). The pressure drag, also referred to as form drag, is the drag caused by the pressure difference between the windward and leeward side of an object. The drag caused by the surface friction in the boundary layer of an object is called viscous drag. In cycling, it is estimated that about 90 % is caused by form drag and about 10 % by viscous drag (Defraeye et al., 2010a). The total aerodynamic drag can be calculated by:

$$F_D = \frac{1}{2}\rho A C_D U^2 \tag{1.1}$$

where $\rho$ is the air density, $A$ the frontal area, $C_D$ the aerodynamic drag coefficient and $U$ the free stream flow velocity. The aerodynamic drag coefficient accounts for the combined effect of the pressure and viscous drag. There are several factors that affect the cycling aerodynamics in windless conditions. The dominating factors are the cycling position, cycling equipment, drafting, surface roughness of the clothes, and altitude. As the cyclist accounts for about 70 % of the total aerodynamic drag (Barry et al., 2012, Underwood and Jermy, 2011), optimising position is the most effective method to improve performance. In this research, focus has therefore been given to the optimisation of performance by position alterations. To provide a broader overview of cycling aerodynamics, the most important methods to optimise aerodynamic performance and their drag saving effectiveness are briefly described in section 1.1.1 - 1.1.5.

### 1.1.1 Changing position

There are typically three cycling positions: the upright position (hands on the hoods of the bars), the dropped position (hands on the drops) and the time trial position (hands on the time trial handlebars). The three typical cycling positions are shown in Figure 1.1.

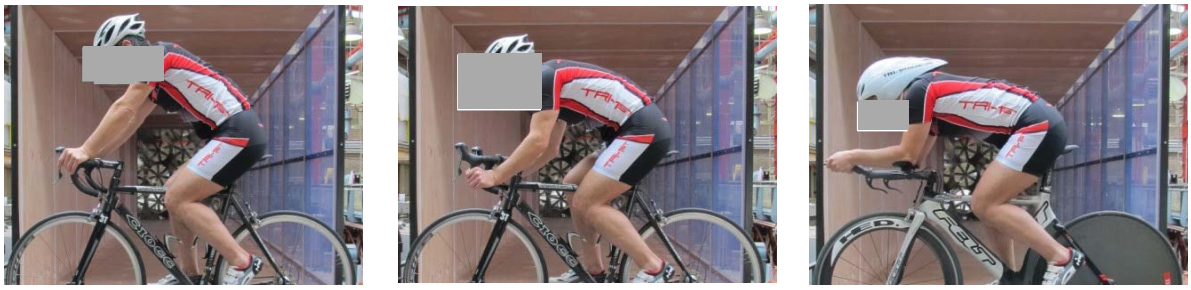

(a) (b) (c)

**Figure 1.1 Typical cycling positions: (a) upright, (b) dropped and (c) time trial.**

The aerodynamic drag can be reduced by changing from an upright to either a dropped position or a time trial position, hence reducing the cyclist's required power output. Average drag reductions of about 10 % in the dropped position and about 22 % in the time trial position are found compared to the upright position, respectively (Zdravkovich et al., 1996, Jeukendrup and Martin, 2001, Chowdhury et al., 2011, Defraeye et al., 2010a). More detailed information about the drag reduction in different cycling positions will be addressed in paragraph 1.2.2. Although the drag significantly reduces when lowering the body position, significant decreases in the power output of the cyclist have been observed (Gnehm et al., 1997, Grappe et al., 1997, Jobson et al., 2008). Previous literature states that for elite cyclists the detriment in power output outweighs the aerodynamic gains (Gnehm et al., 1997, Jeukendrup and Martin, 2001, Lukes et al., 2005). These statements are however based on elite time trial cycling speeds, e.g. > 45 km/h (Gnehm et al., 1997). For trained cyclists, the cycling speeds are usually lower (<45 km/h) and it could therefore be suggested that there is a trade-off between aerodynamics and power output.

In contrast with the reduction of the power output, research on the effect of lowering position on the physiological performance leads to contradicting findings. An overview of several studies investigating the effect of different cycling positions (upright, dropped or time trial

position) on the physiology of trained cyclists is shown in Table 1.1. Although it could be seen in Table 1.1 that there is no consensus about the effect of torso angle on the physiology of cyclists, the most physiological optimal position tends to be the upright position. Several researchers found a significant change of up to 6 % in oxygen consumption and/or heart rate in the upright or dropped position compared to the time trial position (Gnehm et al., 1997, Evangelisti et al., 1995, Faria et al., 1978, Richardson and Johnson, 1994), whilst others show no significant changes between the positions (Berry et al., 1994, Franke et al., 1994, Jobson et al., 2008, Hubenig et al., 2011). Moreover, two studies showed that lowering position significantly increase the minute ventilation by up to 10 % (Faria et al., 1978, Grappe et al., 1998). The inconsistency in the physiological responses on changing position is likely a result of the differences in the exact torso angle positions examined and the methodologies used, such as the tested intensity and duration. There are in particular large variations between the adopted time trial positions examined in the studies.

Finally, it has been shown that changing position could also affect the muscle activation and pedal forces (Savelberg et al., 2003, Chapman et al., 2008, Dorel et al., 2009). Savelberg et al. (2003) have found changes in muscle recruitment in a fully vertical upright cycling position and a 20° forward and backward position. Chapman et al. (2008) have found increased muscle activation during secondary muscle activity (muscle activity between primary bursts) and greater coactivity when cycling in a dropped position compared to an upright trial position as well as the upright compared to the dropped position. In a study by Dorel et al. (2009), a difference in muscle activation and pedal force coordination was found between the three typical cycling positions. It should be noted that the time trial position torso angles examined in Dorel's study position were relatively large (> 21°), thus less optimal in terms of decreasing aerodynamic drag and not commonly used by time trial cyclists, typically around

11 - 12°. Thus although previous studies showed an effect of body position on power output, muscle recruitment and pedal forces / torques, limited information is available about the effect of realistic time trial torso angle changes towards more commonly used joint angles.

**Table 1.1 Overview of research investigating the effect of position on the physiology of trained cyclists. Positions compared are the upright position (UP), dropped position (DP) and time trial position (TT).**

| Researchers | UP | DP | TT | Intensity | HR | VO2 | RER | VE | PO | Nr part. | Torso angle TT |
|---|---|---|---|---|---|---|---|---|---|---|---|
| Faria et al. (1978) | X | X | | Incremental test | No sig. | DP +4% >UP | - | DP+10% >UP | DP +16% > UP | 9 | - |
| Welbergen and Clijsen (1990) | X | X | | 3 min supra-maximal (100W, 200W and max) | - | No sig. | - | - | - | 6 | Near horizontal |
| Johnson and Schultz (1990) | X | | X | 10 min at 80% VO2max | No sig. | No sig. | - | No sig | | 15 | - |
| Ryschon and Stray-Gundersen (1991) [a] | X | X | | 5 min treadmill cycling at 19 km $h^{-1}$ and 4% grade | No sig. | No sig. | No sig. | - | - | 10 | - |
| Origenes et al. (1993) | X | | X | Incremental test with 3 min, 50W stages | No sig | No sig. | - | No sig. | - | 10 | Close to parallel to floor |
| Berry et al. (1994) | X | | X | 1 hour time trial at 80% VO2max, increased thereafter | - | No sig. | - | No sig. | No sig. | 11 | Hip angle 91° |
| Franke et al. (1994) | X | X | X | Incremental test with 3 min, 60W stages | No Sig. | No Sig. | - | - | - | 10 | >24° |
| Richardson and Johnson (1994) | X | | X | 4km at 40 km $h^{-1}$ | - | TT -2% < UP | - | - | - | 11 (elite) | - |
| Evangelisti et al. (1995) | | X | X | 1 hour time trial at 70% VO2max (lab) | TT +6% > DP | TT +5% > DP | - | - | - | 8 | - |

| Researchers | UP | DP | TT | Intensity | HR | VO2 | RER | VE | PO | Nr part. | Torso angle TT |
|---|---|---|---|---|---|---|---|---|---|---|---|
| Gnehm et al. (1997) | X | X | X | 5 min at 70% VO2max | TT +3% > UP | TT +3% > UP | TT+1.3% > UP | - | UP 3% > TT | 14 (elite) | 20° |
| Grappe et al. (1998) | X | X | X | 10 min at 70% VO2max | No sig. | No sig. | TT+1% > UP | DP +4% > UP | - | 9 | - |
| Jobson et al. (2008) [b] | X | X | X | 40.23 km time trial (≈1 hour, lab) | No sig. | No sig. | No sig. | No sig. | UP 6% > TT | 9 | 15±3° |
| Dorel et al. (2009) | X | X | X | VT +Δ20% (6 min) | No sig. | No sig. | No sig. | No sig. | - | 12 | 21±4° |
| Hubenig et al. (2011) | X | | X | VT1 and VT2 | No sig. | No sig. | - | - | At VT1 UP 5% > TT | 18 (female) | 20° |

*HR, heart rate; VO2, oxygen consumption; RER, respiratory exchange ratio; VE, minute ventilation; PO, power output; VT1, first ventilatory threshold;VT2, second ventilatory threshold.*

[a] more positions were analysed
[b] compared to road cycling time trial

### 1.1.2 Cycling equipment

Aerodynamic optimised bicycles are developed to improve performance. For example, it has been shown that changing the wheels from spoke wheels to disc wheels can decrease the aerodynamic drag of the wheels up to 50 % (Tew and Sayers, 1999). The overall drag reduction of the wheels can be in the order of about 2 to 3 % in windless conditions (Greenwell et al., 1995, Barry et al., 2012). However, in crosswinds the wheel type has a significant effect on aerodynamic side forces and the bicycle stability (Barry et al., 2012, Tew and Sayers, 1999, Greenwell et al., 1995). For example, side forces acting on a cyclist can increase by up to 38% when using a disc wheel compared to a spoke wheel at a 30° crosswind yaw angle (i.e., the angle the wind makes with the cyclists' direction of travel) (Barry et al., 2012). The aforementioned research accentuates the importance of taking into consideration

the side forces, rolling moments and yawing moments imparted on a cyclist. For safety reasons, the international cycling federation, UCI, decided to ban disc wheels in mass start competitions, in both the road and cyclo-cross disciplines (Article 1.3.018). In addition, a front disc wheel is only permitted in track or time trials on the road (Article 1.3.018). Similarly, the international triathlon union, ITU, only allows wheel covers or disc wheels on the rear wheel in non-drafting events (Article 5.2c). Disc wheels are also prohibited at the Ironman World Championships in Hawaii, as large crosswinds are common and could affect the safety of the cyclists (Article 5.02a).

### 1.1.3 Surface roughness clothes

Research has shown that the aerodynamic drag around a cyclist is dominated by form drag (Defraeye et al., 2010a). Consequently, changing the surface roughness has a small effect on the total aerodynamic drag; drag reductions up to about 5 % at cycling speeds above 50 km/h have been reported (Brownlie et al., 2009). The legs and arms have the greatest potential for changes in surface roughness to reduce the aerodynamic drag. The limb segments are the only parts of the body that are perpendicular to the flow and can transform the boundary layer from laminar to turbulent, hence reducing the aerodynamic drag. The speed at which this flow transition occurs depends on the surface roughness; rougher fabrics can lower the critical speed, but will have a higher drag at higher flow speeds. At the critical speed, the flow separation is delayed and hence reduces the pressure drag (Chowdhury et al., 2010, Brownlie et al., 2009, Oggiano et al., 2009, Underwood and Jermy, 2011). For a static leg, the critical speed has been shown to be at around 50 km/h (Oggiano et al., 2009). As the torso is generally close to parallel to the flow, viscous drag dominates and hence a smooth fabric is usually beneficial (Brownlie et al., 2009). A study by Brownlie et al (2009), showed that

optimisation of their track suit reduced the drag by up to 2.7 % at speeds of 53 km/h compared to 2003 time trial suits that were used by competitive cyclists. This is predominantly accomplished by: (1) reducing the skin friction attached flow regions, (2) placement of the seams in areas of separated flow, (3) minimising the wrinkles and loose fabrics, and (4) inducing boundary layer transition from laminar to turbulent around the arms and legs, hence altering the position of flow separation.

### 1.1.4 Drafting

Drafting is a situation when two or more cyclists are aligned in a close group where the riders are within the wake of each other, hence reducing the overall drag exerted on the cyclists. A reduction of up to 49 % of the aerodynamic drag has been measured for the trailing cyclist (See Table 1.2). This reduction is exploited by cycling in the decreased flow velocity of the turbulent wake of the leading cyclist. Of the three typical cycling positions, the largest drag reduction has been found for two cyclists in an upright position (Blocken et al., 2013).

When increasing the number of cyclists to four, Computational Fluid Dynamics (CFD) simulations have shown that the reduction increase can be up to 40 % (Defraeye et al., 2014). A novel finding is the fact that the drag of the leading cyclist also reduces whilst drafting (Blocken et al., 2013, Barry et al., 2014, Iniguez-de-la Torre and Iniguez, 2009). It has been demonstrated in theoretical, physical and numerical work that the drag reductions can be between 3 – 5 % for the leading cyclist in the time trial position. When two cyclists are riding side-by-side, a drag increase of over 6 % has been reported (Barry et al., 2014).

**Table 1.2 Overview of several studies investigating the effect of drafting. Savings expressed for the trailing cyclist.**

| Researchers | Savings | Method |
|---|---|---|
| Kyle (1979) | Power output savings: 35 % | Coastal down test |
| Kyle and Burke (1984) | Drag savings: 40 % | Wind tunnel and coastal down tests |
| Zdravkovich et al. (1996) | Drag savings: 37 % - 49 % (UP) | Wind tunnel |
| Broker et al. (1999) | Power output savings: 30 % | Track power measurements |
| Edwards and Byrnes (2007) | Power output savings: 33 % (DP)<br>Drag coefficient reduction: 42 % (DP) | Field power measurement |
| Blocken et al. (2013) [a] | Drag savings CFD simulations: 27 % (UP), 23 % (DP) and 14 % (TT) | Wind tunnel and CFD |
| Barry et al. (2014) | Drag savings: 49 % (TT) | Wind tunnel |

*UP, upright position; DP, dropped position; TT, time trial position; CFD, computational fluid dynamics.*

[a] results shown of a cyclist without bicycle

### 1.1.5 Altitude

The density of the air decreases with higher altitude, hence decreasing the aerodynamic drag. The maximal oxygen consumption is however also reduced with higher altitude. It is estimated that the cycling time can be improved by 4 % to 4.5 % when cycling at 3200m-3500m compared to sea level (Olds, 1992). Capelli and Diprampero (1995) estimated that the optimal altitude for the one hour world record is 4000m. However, they suggest that the reduction of oxygen resulting from altitude used in their model might be higher for athletes than for trained cyclists. The advantage of the reduced aerodynamic drag at altitude is particularly useful when cycling at high speeds on a flat course, whilst at a high altitude hilly course the performance will decrease (Hahn and Gore, 2001).

## 1.2 Assessment of aerodynamic performance

Since the 1970's, researchers have begun to investigate and more importantly have started to understand the importance of cycling aerodynamics. To be able to optimise the aerodynamic performance, the cycling aerodynamics has to be determined. Methods range from deterministic approaches where the drag is estimated by a linear relationship of the drag with the frontal area towards more advanced methods such as wind tunnel experiments and Computational Fluid Dynamics (CFD) simulations. This section is focused on the most commonly used scientific methods to assess the aerodynamic drag in cycling and their application in cycling position optimisation.

### 1.2.1 Linear relationship

The easiest method to estimate the aerodynamic drag is to use the correlation of the drag forces with the projected frontal area as presented in equation 1.1. This method is rooted on the correlation of drag with the frontal area (Underwood et al., 2011). The frontal area is often determined by means of analysing a frontal photograph in an image processing software (Debraux et al., 2009, Barelle et al., 2010, Heil, 2001) or computer-aided design software (Debraux et al., 2011, Debraux et al., 2009). More detailed information about the image processing software technique is given in section 2.2.2. Albeit this linear relationship method is low-cost and relatively fast, it provides a rather rough estimate of the drag.

### 1.2.2 Wind tunnel experiments

Wind tunnel experiments are a reliable and controllable method to access aerodynamic drag and are most commonly used in aerodynamic cycling research, despite the high costs and limited flow field data. Some guidelines for cycling wind tunnel experiments are outlined by

Chowdhury and Alam (2012). An overview of several cycling wind tunnel experiments is shown in Table 1.3, from which a large spread in drag area results are witnessed for the different cycling positions. These variations can be related to several factors:

1. The static or dynamic movement of the legs.
2. Anthropometric differences between the cyclists.
3. The blockage ratio of the wind tunnel, which could cause an increased flow velocity in a closed wind tunnel. In particular in the studies with a blockage area > 10 %, this has to be corrected for.
4. Differences in used equipment, such as helmet, frame and wheels.
5. Accuracy of the measurement equipment.

Wind tunnel experiments are used to determine the effect of different typical cycling positions on the aerodynamic drag (Zdravkovich et al., 1996, Jeukendrup and Martin, 2001, Gibertini et al., 2008, Chowdhury et al., 2011, Defraeye et al., 2010a). In addition, the most aerodynamic efficient position for individuals is commonly determined by wind tunnel experiments (Underwood et al., 2011, Underwood and Jermy, 2013, Chabroux et al., 2012, García-López et al., 2008). When systematically changing the position, the 'optimal' position can be determined by means of trial and error. For example, Underwood et al. (2011) investigated the effect of torso angle and shoulder angle on the aerodynamic drag. In another study by Underwood and Jeremy (2013), for each cyclist the aerodynamically optimal handlebar height and handlebar separation distance taken from the cyclists' current cycling position was examined. Both studies demonstrated that there is a correlation between torso angle and drag area ($R^2$=0.44), however individual differences between the optimal handlebar positions were observed between riders. Due to the cyclist's individual approach, the cycling position was

not systematically controlled. Thus, extrapolating to large sample sizes is fraught with difficulties. Chabroux et al. (2012) examined the aerodynamic influence of the cyclists' posture and helmet. With the hand positions closer together the drag is reduced, whilst raising the saddle height by 10 mm increased the aerodynamic drag by about 3 % (Chabroux et al., 2012). In addition, the helmet inclination was shown to affect the total aerodynamic drag. Although wind tunnels can be used to optimise the aerodynamic drag of an individual cyclist, information about the flow mechanics that influence the aerodynamic forces and moments are lacking.

### 1.2.3 Computational Fluid Dynamics

Computational Fluid Dynamics (CFD) can be used to determine the aerodynamic forces acting on a cyclist and to visualise the flow structures within the fluid. CFD application in cycling is however still in its infancy (Defraeye et al., 2010a, Griffith et al., 2014, Lukes et al., 2004, Hanna, 2002). A study by Defraeye et al. (2010b) showed that CFD could provide reliable and accurate results compared to wind tunnel experiments (relative difference of about 9 %) and is therefore a valuable tool to investigate the flow field in cycling. Griffith et al. (2014) has explored the flow mechanics around a cyclist and found a visually fair agreement of the wake flow structures between experiments and computational results. The numerical simulation also revealed the transient nature of the entire flow field in greater detail. It has been found that in particular the flow separation from the cyclist can be directly related to drag changes. Defraeye et al. (2010a) are the first researchers to compare different cycling positions (upright, dropped and time trial) by means of CFD. It should be noted that the bicycle was excluded in the simulations thus neglecting the bicycle-cyclist interaction.

**Table 1.3 Overview of several drag area results and other wind tunnel experiment details in one of the three typical cycling: upright position (UP), dropped position (DP) and time trial position (TT).**

| Researchers | Drag area, CdA ($m^2$) | | | Static/dynamic | Body mass (kg) | Body height (m) | Blockage ratio[d] | Nr cyclists |
|---|---|---|---|---|---|---|---|---|
| | UP | DP | TT | | | | | |
| Kyle and Burke (1984) | | 0.32 | | Static | | | 8 % | 1 |
| Dalmonte et al. (1987) | | | 0.246-0.254 | | | | 1 % | |
| Kyle (1991) | | | 0.221±0.010 | Static | | | 8 % | 3 |
| Zdravkovich et al. (1996) | 0.26 – 0.38 | 0.230-0.34 | 0.17-0.23 | Static | 69 | 1.72 | 14 % | 2 |
| Martin et al. (1998) | | | 0.269±0.006 | Dynamic Pedalling (90rpm) | 71.9±6.3 | 1.77±0.05 | 8 % | 6 |
| Padilla et al. (2000) | | | 0.244 | | 81.0 | 1.88 | - | 1 |
| Jeukendrup and Martin (2001) | 0.358 | 0.307 | 0.269 | Static | - | - | - | 1 |
| García-López et al. (2008) | | | 0.260±0.011<br>0.341±0.013 | Static<br>Dynamic (pedalling) | 71.6±2.7 | 1.79±0.03 | 8 % | 5 |
| Gibertini et al. (2008) | | 0.275 | 0.223 | Dynamic (Rotating wheels) | - | 1.8 | 3 % | 1 |
| Defraeye et al. (2010a) | 0.270 | 0.243 | 0.211 | Static | 72 | 1.83 | 7 % | 1 |
| Chowdhury et al. (2011) [a] | 0.419 | 0.413 | 0.334 | Static | - | - | 8 % | 1 |
| Underwood et al. (2011) [b] | | | 0.277±0.018 | Dynamic (Pedalling) | 71.7±5.9 | 1.76±0.03 | 22 % | 3 |
| Barry et al. (2012) [c] | | | 0.195-0.200 | Dynamic (Rotating disc wheels) | - | - | 5 % | 1 |
| Chabroux et al. (2012) | | | 37.67N±1.56 | Dynamic Pedalling (90rpm) | 69.3±5.5 | 1.79±0.06 | 8 % | 9 |
| Griffith et al. (2012) | | | 0.15-0.23 | Quasi-dynamic (different leg positions) | - | - | 5 % | 1 |

[a] different wheels tested
[b] lowest drag after adjusting shoulder and torso angle
[c] only drag forces recorded; drag area estimated

The results were in good agreement with their experiments and showed the value of CFD simulations in determining the aerodynamic responses. However, no attempt has been made to understand the flow mechanisms. Other areas where CFD has been used in cycling are: to investigate the effect of drafting (Blocken et al., 2013, Defraeye et al., 2014), to determine the convective heat transfer of individual body segments (Defraeye et al., 2011) and to study mountain bike aerodynamics (Lukes et al., 2004). The only numerical crosswind cycling study is reported by Hanna (2002). In this study a comparison has been made between isolated disc and spoke rear wheels at different crosswind flow velocities (0-48 km/h). The crosswind was imposed at an angle of 90 degrees to the cycling direction. The study showed that a disc wheel lowers the overall drag by about 2 % compared to spoke wheels; in a crosswind of about 32 km/h the side forces are doubled. As the research has been conducted for the British Cycling team, details of the simulations are limited and without validation, precaution has to be taken about the validity of the results. It should be noted that cycling manufactures (e.g. Cervelo, Felt and Trek) and cycling teams (e.g. British Cycling and United Kingdom Sport Institute, Hanna (2002) ) take advantage of CFD, but due to the competition in the commercial and sporting cycling world, data is rarely published or peer reviewed.

In conclusion, CFD has been shown to be a reasonably accurate tool to investigate the fluid flow around cyclists. Although recent research has addressed the effect of position, the positions are limited and an in depth fluid analysis is lacking. Moreover, the effect of crosswinds on the flow field is unknown, despite the fact that crosswinds can significantly affect the stability and safety of a cyclist.

## 1.3 Crosswinds on two-wheeled vehicles

Cyclists are commonly subjected to crosswinds (Guzik et al., 2013). Even though only about 5 % of all reported cycling accidents are caused by crosswinds, it is reported that the majority lead to severe or fatal accidents (Schepers and Wolt, 2012). In addition, there is evidence to suggest that about two-thirds of the total number of road accidents are unreported (Transport, 2012). Several crosswind accidents have been reported (7 News The Denver Channel, 2011, ABC News, 2012, Ryan, 2012, The Argus, 2014). In England in 2014, a cyclist was severely injured when he was blown off his bicycle by a strong gust of wind. The cyclist fell into the road where he was hit by a car which was travelling behind (The Argus, 2014). Another severe accident was reported in the USA in 2011, where a man suffered from traumatic injuries including head and pelvis injuries when blown over by heavy wind in a National Park (7 News The Denver Channel, 2011). In Australia in 2005, a cyclist died after a strong gust of wind blew her into the path of a car (Barnes, 2005). High rise buildings have also been shown to lead to increased wind speeds and concurrently cycling accidents on windy days. High flow velocities around high rise buildings are caused by the downstream bending of the wind to the cycling-level, coupled with the corner streams at the sides of the building (Blocken and Carmeliet, 2004). In particular single high rise buildings surrounded by low rise buildings could significantly increase the flow velocity of the crosswind; the wind speeds can be amplified by up to two times the upcoming wind flow velocity (Blocken and Carmeliet, 2004, Murakami et al., 1979). Examples of single high rise buildings are the 90 m tall EWI building in Delft, The Netherlands (Delta, 2007) as shown in Figure 1.2 and the 112 m tall Bridgewater Place in Leeds, UK (Best, 2013). The Leeds City council has recently decided to ban traffic and pedestrians during strong winds (>72 km/h), after the death of a pedestrian at a predicted wind speed of about 120 km/h (BBC, 2014). Lorries could also induce increased

flow velocities. The combination of the suddenly increased wind velocity and change in direction of the wind together with the vortex structures inside this flow affects the overtaken cyclist (Walton et al., 2005). In particular the sudden change in side force components of the flow induced by the vehicle can influence the stability of the cyclist.

In conclusion, despite the occurrence of severe and fatal accidents due to crosswind, there are limited studies investigating the aerodynamic responses of cyclists under such conditions. These accidents are caused by the lack of ability to control the bicycle when subjected to crosswinds and are often severe / fatal primarily due to deviation of the cyclist into the path of other vehicles. Similar problems arise in other two-wheeled vehicles in crosswinds, such as motorbikes. Albeit the crosswind yaw angle is usually smaller for motorbikes compared to bicycles, several accidents are reported due to crosswinds (Gauger, 2013, Carr, 2011, Donell, 2010). There are however a limited number of investigations of the aerodynamic performance of motorbikes in crosswinds (Ubertini and Desideri, 2002).

**Figure 1.2 Example of an isolated high rise building and the effect on cyclists on windy days. The stability of cyclists is affected due to high velocity crosswinds induced by the corning streams at the side of the high rise EWI building, Delft The Netherlands. Images courtesy of http://siebeswart.photoshelter.com.**

## 1.4 Goal and aims of this thesis

The main aim of this thesis is:

> *To get an improved understanding of the effect of cycling position and crosswinds on the aerodynamics and performance of a cyclist*

To accomplish this aim, the following two objectives and hypothesizes are developed:

1. Investigate the effect of position on the cyclists' physiology and aerodynamics. It is hypothesized that although lowering the time trial position improves the aerodynamics, it impairs the physiological and mechanical performance; and therefore a trade-off between the physiological detriment and the aerodynamic gain is postulated.
2. Investigate the effect of crosswinds on two-wheeled vehicles. Firstly, it is hypothesized that crosswinds significantly increase the side forces and rolling moments acting on a cyclist and motorbike rider. Secondly, it is hypothesized that lowering torso angle in cycling only reduces the drag force coefficients, whilst the side force and rolling moment coefficients remains unchanged.

Aerodynamic optimisation of cycling performance and safety includes different methodologies and requires therefore a multidisciplinary approach. As it has been previously demonstrated that the power output of the cyclist changes by altering position, the performance cannot be solely assessed by means of aerodynamic measures, but physiology has to be taken into account. Additionally, aerodynamic forces can be estimated by the frontal area or measured with wind tunnel experiments. It is however difficult to capture with wind tunnel experiments the highly turbulent flow around the cyclist which changes in both place

and time, as the data collection is limited to certain measurement points. To get an improved understanding of the flow field, a computational fluid dynamics approach is required, which needs to be validated with experimental work, e.g. wind tunnel research. All the aforementioned methodologies are used in this thesis to get a comprehensive insight in to the effect of cycling position and crosswinds on the aerodynamics and performance of a cyclist.

The work in this thesis is divided into seven studies with different objectives and is summarised in the following points:

1. *The effect of torso angle on metabolic and physiological variables.* The objective of this study is to perform physiological and metabolic measurements on trained cyclists in different time trial positions. Graded cycling exercise in four commonly used time trial cycling positions is performed by trained cyclists. In conjunction, the frontal area method is used to estimate the aerodynamic benefit when lowering position.
2. *The effect of torso angle on the muscle recruitment, crank torques and efficiency.* The focus of this study is to investigate the influence of time trial torso angle position on the muscle activation patterns, crank torques and cycling efficiency. Submaximal intensity exercise in three different time trial positions is performed by trained cyclists.
3. *Optimisation of position based on power output and metabolic energy.* Whilst decreasing the torso angle reduces aerodynamic drag, it is hypothesized that it limits the physiological functioning of a cyclist. Therefore the objective of this study is to predict the optimal time trial cycling position as a function of the cycling speed and to determine at which speed the aerodynamic power losses start to dominate. Two mathematical models are developed to determine the optimal torso angle.

4. *Experimental investigation of the effect of crosswind on cyclists.* The objective is to investigate the effect of crosswinds on the aerodynamic responses of cyclists for crosswind yaw angles ranging from 0 to $90^{o}$ with $15^{o}$ increments. With wind tunnel experiments the aerodynamic responses of a cyclist subjected to different crosswinds are obtained.
5. *Numerical investigation of the effect of crosswinds on a cyclist.* The first aim of this study is to determine the accuracy of different turbulence models in crosswinds. Secondly it is aimed to investigate the effect of crosswinds on the fluid mechanics in both the instantaneous and time-averaged flow. In this study, CFD simulations, based on the Reynolds Averaged Navier Stokes (RANS), Detached Eddy Simulations (DES) and Large Eddy Simulations (LES) are carried out on a bicycle and cyclist to obtain the flow structures and fluid mechanics.
6. *Numerical investigation of the effect of crosswind on cyclists in different cycling positions.* The objective of this study is to investigate the effect of cycling position on the flow field around a cyclist and bicycle subjected to different crosswinds. The Reynolds Averaged Navier Stokes method is used to determine the flow structures around the cyclist and bicycle. Positions analysed are three different time trial positions and two different dropped positions.
7. *Numerical investigation of the effect of crosswind on a motorbike.* Similar to cycling, several fatal accidents are reported for motorbikes due to crosswinds. The objective of this study is to numerically investigate the flow around a motorbike subjected to different crosswind yaw angles ranging from 15 - 90°.

## 1.5 Thesis outline

In chapter 2 the main general methods used in this thesis are described. The first part of the experimental chapters is focused on the human performance when cycling in different torso angle positions.[1] Chapter 3 describes the effect of position on the physiology and aerodynamics of a cyclist. To help to explain the findings, in chapter 4 a description of the mechanical and muscular consequences when lowering position is given. This is followed by chapter 5, in which a model is developed to determine the optimal cycling position based on physiology and aerodynamic data recorded in chapter 3. The second part of the thesis is concentrated on the effect of crosswinds on the aerodynamics. In chapter 6, the effect of crosswinds on the aerodynamic forces and moments of a cyclist is discussed. To get an improved understanding of the flow field around the cyclist in crosswinds, CFD simulations are carried out in chapter 7. In chapter 8, the flow characteristics in different cycling positions are considered, including the positions studied in chapter 3-5. This is followed by an investigation of crosswinds on another two-wheeled vehicle, the motorbike, in chapter 9. Finally, an overall discussion and conclusion of the findings are presented in chapter 10.

[1] It should be noted that the content of all submitted / published experimental chapters is identical to that of the submitted / published papers.

# CHAPTER 2

# General methods

The research area covers two branches of science: sport sciences and wind engineering. This chapter provides a brief introduction to definitions and measurements relating to these branches which are pertinent to the current research.

## 2.1 Kinesiology

Human performance analysis methods used in this thesis includes measurements of the torso angle, oxygen consumption, muscle activation and crank torques. The aforementioned measurement methods are described in this section.

### 2.1.1 Torso angle

The torso angle is used to systematically change the position of the cyclists. The torso angle is defined as the angle between torso and the ground, measured from the centre of rotation of the glenohumeral axis and the greater trochanter as shown by β in Figure 2.1. A digital inclinometer (Fisco EN17, Ficso Tools Limited, Essex, UK) is used to check the torso angle. The upper arm angle, α, is defined as the angle between the upper arm and the torso.


**Figure 2.1 Definition of the torso angle, β, and upper arm angle, α**

### 2.1.2 Oxygen consumption

Maximal oxygen consumption ($VO_{2max}$) can be used to assess the aerobic capacity and cardio respiratory fitness of an athlete. The oxygen consumption can be quantified by collecting the volume and composition of the expired gasses in a fixed time span or by analysing each single breath directly. Analysing each single breath provides detailed information about ventilatory changes and has therefore been used in all studies presented in this thesis. Before each test, the concentration settings of the gas analysers (Jaeger Oxycon Pro, Erich Jaeger GmbH, Hoechberg, Germany) are calibrated with known gas concentrations of 14.95 % $O_2$ and 4.99 % $CO_2$ respectively. The respiratory volumes are calibrated with a 3L syringe. To determine the maximal oxygen consumption and thus the physiological limits to performance, an incremental test is used in the current research. During an incremental test, the cycle ergometer load increases over time with fixed increments. Before starting the incremental test, a warming-up is performed. During the tests, the athletes are asked to breathe through a small mouthpiece. Recordings of the $O_2$ consumption, $CO_2$ exhale, breathing frequency (numbers of

breaths per minute), minute ventilation (respiratory volume per minute), heart rate (beats per minute) and the cadence (pedal revolutions per minute) are taken. The incremental test is terminated when the athlete has reached their maximal performance, the heart rate exceeds the age limit restriction (220 - age) or the respiratory exchange ratio (RER) exceeds 1.12. The RER is the ratio between the amount of $CO_2$ produced and the amount of $O_2$ consumed in one breath. An example of the expired gas data of a cyclist during an incremental test with stages of 25W is shown in Figure 2.2. At rest, the number of $O_2$ molecules inhaled is higher than the number of $CO_2$ molecules exhaled; the RER is around 0.7. The primary source of energy in rest is fat. When the $O_2$ inhaled is equal to the $CO_2$ exhaled, the RER has a value of 1.0. This indicates that carbohydrate is the predominant source of energy.

Based on the oxygen consumption and RER, the gross efficiency can be calculated. The gross efficiency is a measure for how much metabolic energy is transferred into effective power output. The metabolic energy, IE, can be determined using the formula of Garby and Astrup (1987):

$$\mathrm{IE}(\mathrm{J}\cdot\mathrm{s}^{-1}) = \mathrm{VO}_2\left[\frac{(4.940\cdot\mathrm{RER}+16.040)}{60}\right] \tag{2.1}$$

The gross efficiency, GE, is defined as:

$$\mathrm{GE}(\%) = \frac{\text{Work load (W)}}{\text{IE (J}\cdot\text{s}^{-1})}\cdot 100\ \% \tag{2.2}$$

where the Work load is the power exerted by the cyclist on the ergometer. The gross efficiency is calculated for every work load stage until the RER exceeds 1.0. To provide the steady state average metabolic intensity of each stage, all metabolic variables are averaged over 8 breaths and finally averaged over the last 2 minutes of each stage of the incremental test.

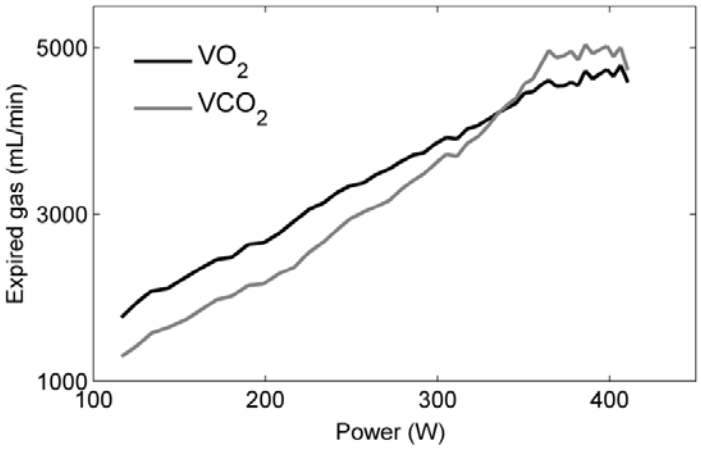


**Figure 2.2 Example of the expired gas of an individual competitive time trial cyclist during an incremental test.VO2, oxygen consumption; VCO2, carbon dioxide exhale.**

### 2.1.3 Crank torque

The muscles generate forces on the pedals producing torque that moves the bicycle forward. Assessing this crank torque is important in the analysis of the pedal technique. In this research, the crank torque is recorded with a SRM ergometer (SRM, Jülich, Germany) at a sampling frequency of 200 Hz. The torque is measured by strain gauges placed on the front chain ring. The measured torque is the combined crank torque of the left and right leg and shown over the 360 degrees of the pedal revolution. A one minute ensemble averaged torque during the pedal stroke of a competitive cyclist is calculated and displayed in Figure 2.3 as a chart 2.3(a) and as a polar view 2.3(b). The polar view can be used to provide feedback to a cyclist about their pedalling technique. There are three distinctive pedal positions in the crank cycle: 1) the pedal is in the top dead centre, TDC, i.e. 12 o'clock position, 2) the pedal is in the bottom dead centre, BDC, i.e. 6 o'clock position, 3) pedal is in the most forward position, i.e. 3 o'clock position. In Figure 2.3, the crank positions from 0-180 degrees corresponds to the left leg down stroke starting at the top dead centre of the pedal revolution and finishing at

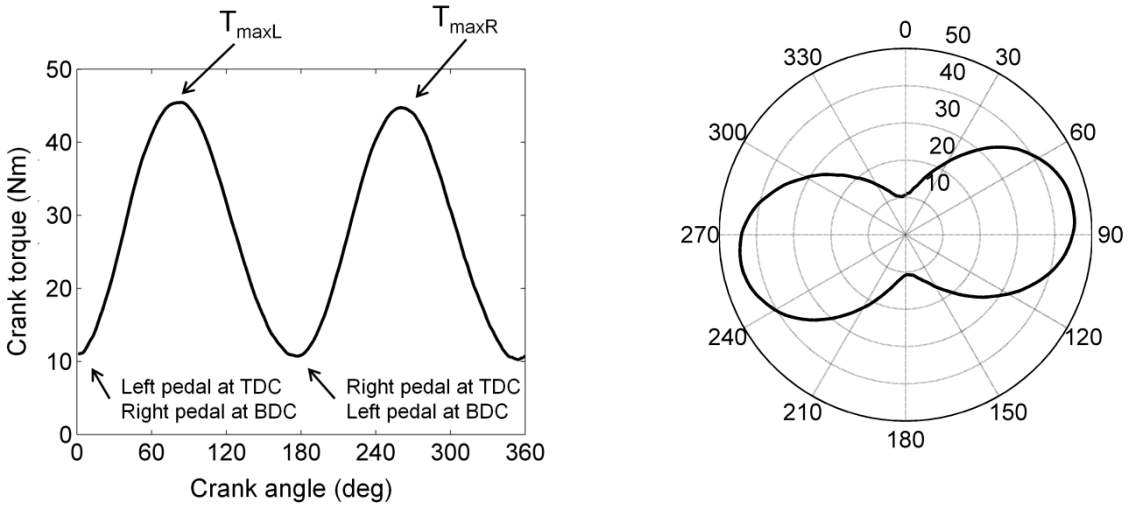


(a) (b)

**Figure 2.3 An example of the crank torque over the crank revolution of 21 competitive cyclists, presented as a chart (a) and polar plot (b).**

the bottom dead centre. From 180-360 degrees corresponds to the right leg down stroke. The maximal torque, $T_{max}$, occurs when one of the pedals is in the most forward position. The lowest torque is observed when one of the pedals is in the top dead centre.

### 2.1.4 Muscle activation

Recording of muscle activation allows the quantification of the muscular performance and the assessment of muscle activation changes due to external alterations. These alterations include among others changes in body position, cadence, power output, training and fatigue (Hug and Dorel, 2009). In addition, recordings of the muscle activation give insight into the physiological processes that cause the muscle to generate force and hence forward motion of the bicycle. Electromyography (EMG) is a procedure to access the electrical activity produced by the skeletal muscle. The EMG can be measured invasively by needles/fine wires or non-invasively on the surface by electrodes. Needle EMG allows for examination of deeper

muscles and reduces the crosstalk among muscles. In cycling research however, EMG is commonly recorded non-invasively with surface EMG (Hug and Dorel, 2009, Dorel et al., 2009, Duc et al., 2005, Savelberg et al., 2003). Surface EMG provides information regarding the combined action potential from a large mass of the muscle, which is therefore correlated with the generated forces. To standardise the procedure of the preparation and application of surface EMG, guidelines are set by the Surface ElectroMyoGraphy for the Non-Invasive Assessment of Muscles project, SENIAM (Hermens et al., 1999) and are applied in the EMG study presented in chapter 4. These guidelines include recommendations for the skin preparation and the sensor placement on individual muscles. For example, the SENIAM recommendation for skin preparation recommend that the skin needs to be shaved at the location at which the sensor will be placed, after which the skin will be cleaned with an alcohol swipe. The sensor location is described as a point on a line between two anatomical landmarks.

An illustration of the applied surface EMG sensors is shown in Figure 2.4 (Delsys Myomonitor III, Delsys Inc, Natick, United States). EMG electrodes with an inter-distance of 10 mm are utilised. To reduce the electrode-skin impedance, electrolyte gel is put on the conductive areas of the electrodes.

The muscles typically recorded in cycling research are the gluteus maximus, biceps femoris, vastus lateralis, vastus medialis, rectus femoris, gastrocnemius lateralis, gastrocnemius medialis, soleus and tibialis anterior. A schematic overview of these muscles and their primary function (e.g. extension or flexion) are shown in Figure 2.5.

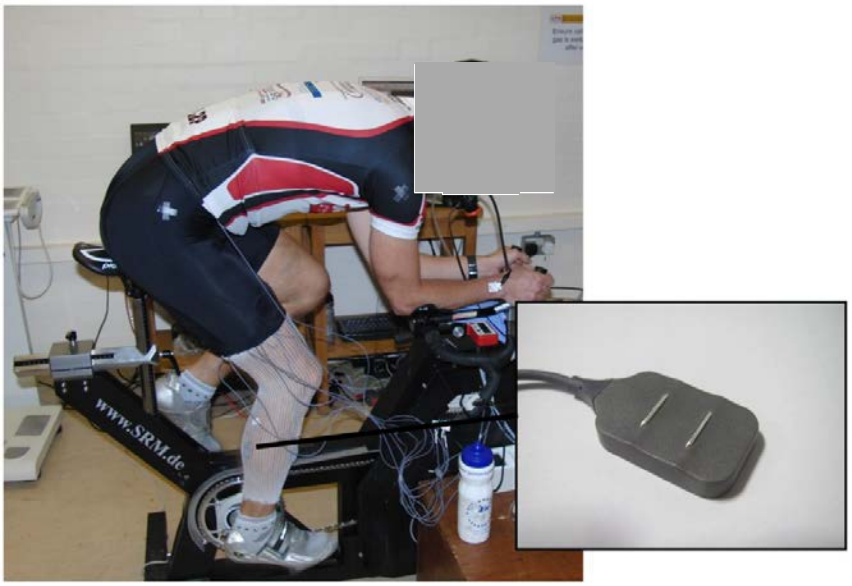


**Figure 2.4 Illustration of the experimental setup to study the effect of position on the muscle activation during cycling. The cables are tied together and the lower leg electrodes covered with a net bandage to minimise motion artefacts. Inset shows a close-up of the EMG electrode with an inter-space distance of 10 mm, which is placed on the skin.**

In the current research, all aforementioned muscle are recorded except the gastrocnemius medialis and vastus medialis due to the limited number of channels of the EMG hardware used in the course of this research. The gastrocnemius medialis and vastus medialis are excluded as their actions are similar to that of the gastrocnemius lateralis and vastus lateralis muscles.

The muscle activation is commonly presented as a function of crank angle. The pedal revolutions are measured with a magnetometer, which detects when the left leg is in the top dead centre. The magnetometer is synchronised by an external 5V trigger from the EMG hardware. The raw EMG data is analysed before meaningful interpretations can be made. Firstly, the raw signal is full wave rectified; all negative values are converted to positive values. Secondly, the signal needs to be filtered. In this research, a $4^{th}$ order Butterworth filter with a cut-off frequency of 10 Hz is applied (Connick and Li, 2013, Prilutsky et al., 1998).

The application of a high order filter minimises the phase shift. Thirdly, the EMG during each

pedal revolution is determined and ensemble averaged; for each crank angle the EMG values of all pedal revolutions are averaged. Finally, the muscle activation is normalised to be able to compare between different muscles and different subjects. The dynamic peak method is used to normalise the EMG (Hug and Dorel, 2009). In this method, the maximal recorded muscle activation of the ensemble averaged EMG data of each individual muscle and participant is used for normalisation. An example of the ensemble averaged EMG of 7 different muscles as a function of the crank angle of a competitive cyclist is shown in Figure 2.6. In addition, the muscle activation timing of 19 participants is shown in Figure 2.7. The muscle activation timing provides important information about the onset and offset that determine the activation duration. The EMG threshold is set to 20 % of the peak EMG of each individual muscle of the participant (Dorel et al., 2009, Savelberg et al., 2003).

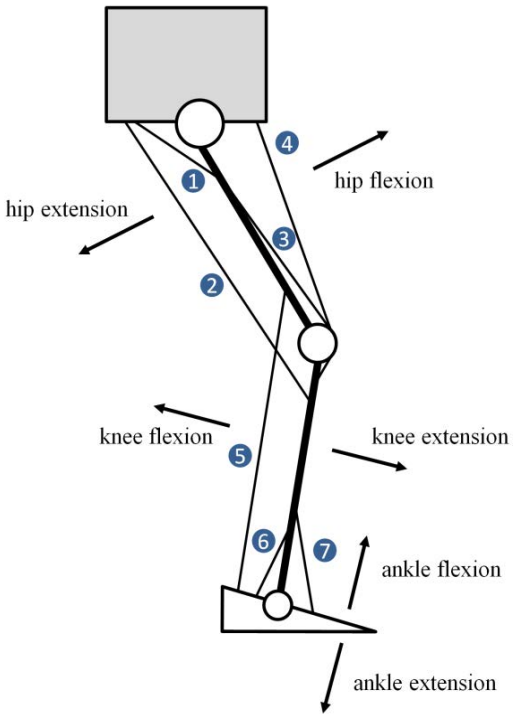


**Figure 2.5 Schematics of the main cycling muscles (1) gluteus maximus – hip extensor, (2) biceps femoris – hip extensor / knee flexor, (3) vastus lateralis and vastus medialis – knee extensor, (4) rectus femoris – knee extensor / hip flexor, (5) gastrocnemius lateralis and gastrocnemius medialis – knee flexor / ankle extensor, (6) soleus – ankle extensor, (7) tibialis anterior – ankle flexor. Adapted from Hug and Dorel (2009)**

This allows for determination of changes in the crank angle (0-360°) at which the onset or offset of the muscle activation occurs. In Figure 2.6 and Figure 2.7, it can be seen that the pedal is in the BDC at a crank angle of 0°. The tibialis anterior muscle is active from a crank angle of 90° to slightly after the TDC. The region of activity of the rectus femoris is in the second half of the upstroke pedal stroke (about 120°) and is terminated at about 270°. Just before the TDC the vastus lateralis becomes active, whereas just after the TDC the gluteus maximus is activated. Large activation is observed for the knee extensors, rectus femoris and vastus lateralis, at the TDC. The highest muscle activation of the ankle extensor soleus and the hip extensor gluteus maximus are observed when the pedal is at a crank angle of 270°, where the pedal is in the most forward position. At this position, large forces are applied on the pedals that accelerate the bicycle. The region of activity of the gastrocnemius lateralis starts just after the termination of the tibialis anterior and finishes just before the activation of the tibialis anterior.

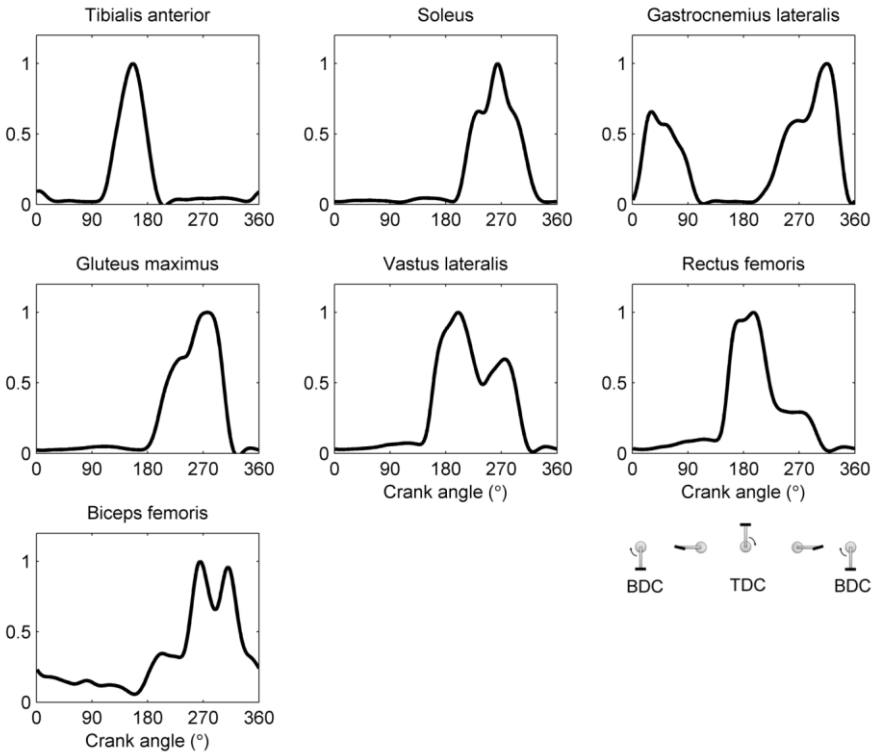


**Figure 2.6 Example of ensemble averaged EMG of 7 different muscles as function of the crank angle of an individual competitive cyclist. The EMG data is averaged over 1 minute and the cyclist was asked to cycle at a constant intensity of 70 % of their peak power output. The EMG recordings are normalised to the maximal ensemble averaged muscle activation of the individual muscle. The 0° crank angle represents the bottom dead centre (BDC), whereas the 180° represents the top dead centre (TDC).**

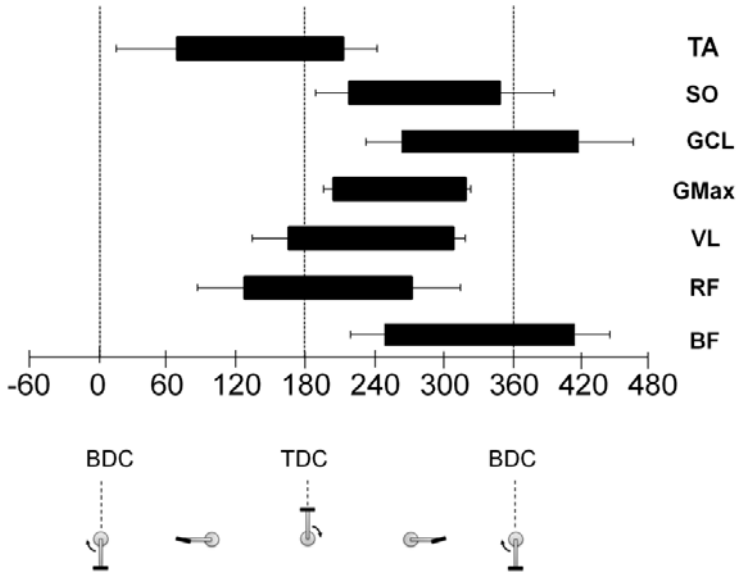


**Figure 2.7 Example of the mean onset, offset and duration of 19 competitive cyclists of the EMG muscle activation timing of 7 muscles: tibialis anterior (TA), soleus (SO), gastrocnemius lateralis (GCL), gluteus maximus (GMax), vastus lateralis (VL), rectus femoris (RF), and biceps femoris (BF). BDC, bottom dead centre; TDC, top dead centre.**

## 2.2 Aerodynamics

Several methods are used in the current research to investigate the aerodynamic forces and moments acting on a cyclist. The aerodynamic coefficients are predicted by frontal area measurements, determined experimentally by wind tunnel experiments and simulated with CFD simulations to provide detailed insight into the flow mechanics.

### 2.2.1 Aerodynamic forces and moments

Analysing the aerodynamic forces and moments assists in the understanding of the loads acting on a cyclist and helps to improve cycling performance and safety. The aerodynamic forces on a cyclist subjected to crosswinds are the drag force, $F_X$, the side force, $F_Y$, and the lift force, $F_Z$. The aerodynamic moments are the rolling moment, $M_X$, the pitching moment, $M_Y$, and the yawing moment, $M_Z$. Figure 2.8 shows the aerodynamic forces and moments acting on a bicycle and cyclist subjected to crosswinds. The coordinate system is placed in the bicycle reference frame and hence independent of the flow direction.

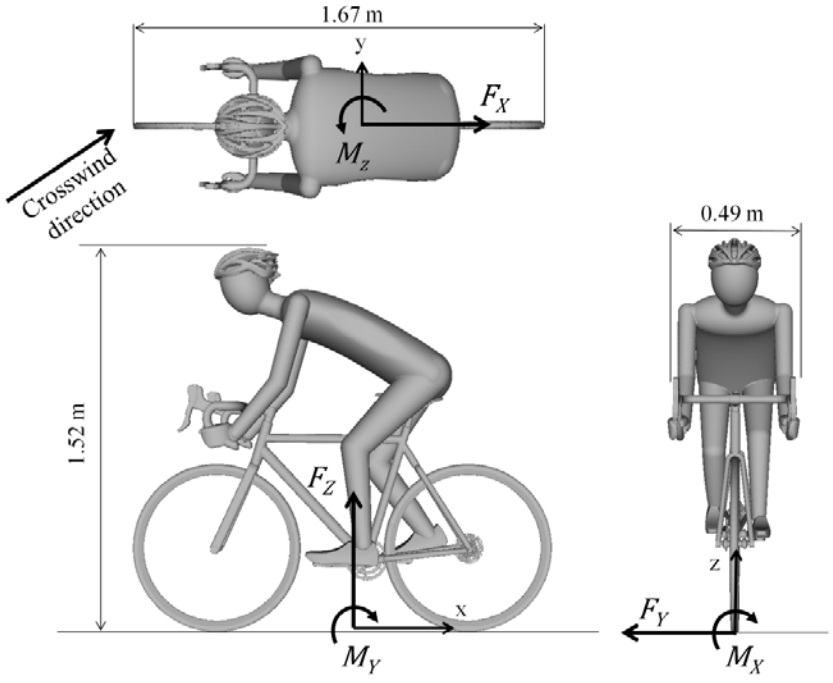


**Figure 2.8 Directions of the forces and moments acting on a cyclist in crosswinds. $F_X$, drag force; $F_Y$, side force; $F_Z$, lift force; $M_X$, rolling moment; $M_Y$, pitching moment; $M_Z$, yawing moment.**

### 2.2.2 Frontal area

The frontal area is used to provide a prediction of the aerodynamic performance of cyclists. With an image processing software technique, the frontal area is determined. In this technique, a calibration frame is positioned at the side of the cyclist as shown in Figure 2.9. In the ImageJ 1.45s image processing software (ImageJ, National Institutes of Health, USA), the pixels of the cyclist and bike in the photograph are selected and counted. This is also performed for the reference frame with a known area. By calculating the ratio between the pixels in the reference frame and the cyclist, the total frontal area is estimated.

**Figure 2.9 Frontal area determination by means of image processing software technique. A frontal photograph is taken from the cyclist and the calibration frame shown on the left side. With the image processing software, the projected frontal area is quantified as shown on the right side. This Figure is repeated in chapter 3.**

### 2.2.3 Wind tunnel

To determine the aerodynamic forces on a cyclist, the wind tunnel facility at the University of Birmingham was used. The wind tunnel is a subsonic open return wind tunnel with a cross-sectional area of 2 x 2 m. The wind tunnel is equipped with 49 individual fans of 60 kW that can produce a maximal flow velocity, $U_\infty$, of 10 m/s in the centre of the tunnel. The wind

speed was measured with a 3-axis ultrasonic anemometer at a sampling frequency of 10 Hz (Gill Windmaster, Gill Instruments Ltd, Lymington, UK). The turbulence intensity at the end of the wind tunnel was 0.67 %. The turbulence intensity is associated with eddies in the turbulent flow. The boundary layer thickness, $\delta_{99\%,}$ has been estimated by CFD simulations and found to be around 145 mm. More detailed information about the wind tunnel calibration and the boundary layer thickness simulations is given in Appendix A.

The aerodynamic forces and moments are recorded with a multi-component piezoelectric force plate (Kistler type 9281B, Kistler Instruments, Winterthur, Switzerland) which is integrated in a custom built turntable as shown in Figure 2.10. The turntable and measurement frame are designed with Autodesk Inventor software (Autodesk Inc., San Rafael, USA). The turntable is level with the wind tunnel floor and allows experiments in the full 360 degrees range of yaw angles (i.e., the angle the wind makes with the cyclists direction of travel). The wheels of the bicycle are connected to the force platform by means of a frame with uprights (insert of Figure 2.10). The force plate is capable of measuring the aerodynamic forces and moments around the three axes at a sampling frequency of 1000 Hz. The aerodynamic force data is recorded with Kistler BioWare software and analysed with a bespoke Matlab script.

**Figure 2.10 Wind tunnel experimental setup to measure the forces on a bicycle and cyclist under the influence of crosswinds. To investigate a variety of crosswind yaw angles, the bicycle is placed on a turntable. The aerodynamic forces are measured with a force platform, which is placed underneath the turntable floor. Inset shows a close-up of the measurement frame and force platform.**

The force platform is calibrated in all three force application directions (e.g. side force, drag force and lift force) by means of calibration weights with a known weight. To calibrate the lift forces, the weights are placed directly on the frame with uprights. The side and drag forces are calibrated with a force calibration setup as shown in Figure 2.11, in which a rope is connected to the bicycle, Figure 2.11(a), and the uprights, Figure 2.11(b), respectively. The rope is connected via a pulley to a hanger, on which the calibration weights are placed. For all force directions, the force calibration is performed in the full range of the expected aerodynamic forces for crosswind yaw angle varying between 0 - 90 degrees. All calibration measurements are repeated 10 times. Correction factors for the sensitivity of the force platform are calculated and applied on all recorded data. The aerodynamic forces are repeatable within ± 0.05 N and have a standard deviation of 0.0424N.

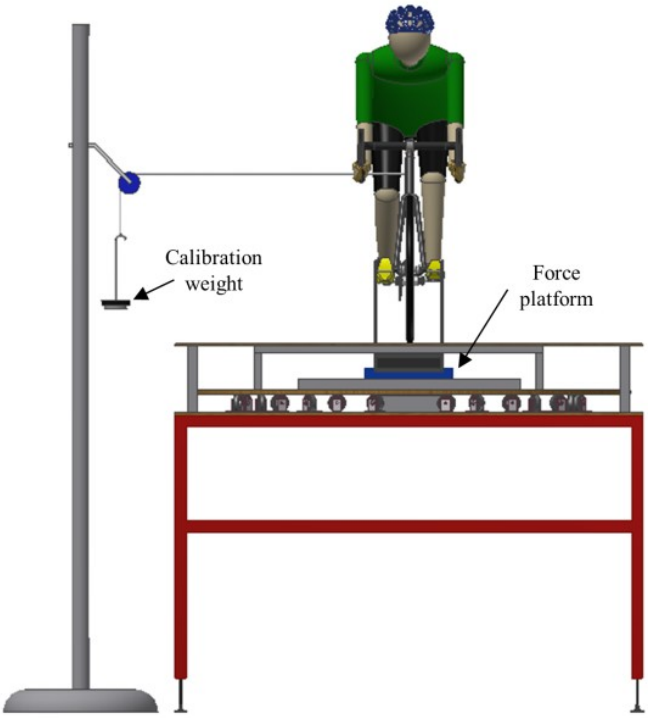


(a)

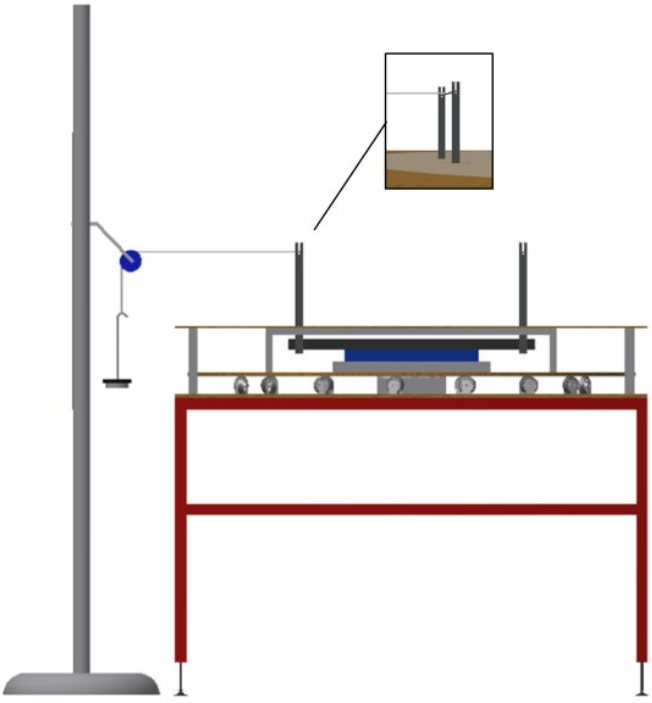

(b)

**Figure 2.11 Schematics of the force calibration setup. Calibration weights, hook and a rope are used to calibrate the system in the side direction (a) and drag direction (b), respectively. The lift forces were calibrated by placing calibration weights on top of the force platform.**

In the experiments a standard road bicycle (CIOCC Dragster, CIOCC ISB SRL, Bergamo, Italy) with spoked wheels (Bianchi SGHEZ, F.I.V. E. Bianchi S.p.A., Treviglio, Italy) is used. A mannequin is placed on the bicycle to closely resemble a cyclist, whilst maintaining accurate results, i.e. minimal movements of the cyclist during the experiments. The height of the mannequin is 1.80 m (PolyStar Man, Creatif Leven Displays Ltd, Gloucester, UK). Yaw angles between 0 - 90 degrees with increments of 15 degrees are analysed. Every yaw angle trial is repeated at least 3 times. A confidence interval analysis is applied to determine the minimal number of samples per yaw angle. The analysis is based on a data set of 10 trials at each yaw angle and the significance level is set to 95 %. Results revealed that the minimum number of samples at every yaw angle needs to be 3. The measured period is 80 seconds. The environmental temperature and humidity are measured and recorded before each trial to compensate for temperature fluctuations during the experiments (Davis Perception II, Davis Instruments Corp., Hayward, California, USA). The weather station has a temperature resolution of 0.1 °C and humidity resolution of 1 %. Detailed information about the aerodynamic coefficient corrections can be found in Appendix B.

### 2.2.4 CFD fundamentals

CFD is a powerful tool to investigate fluid flow dynamics. The availability of fast computers, together with reduced costs of CFD software packages has advanced CFD as a useful technique to optimise sports equipment and human performance. In this section, the fundamentals and methods involved in CFD analysis are discussed.

***Governing equations***

CFD is based on the fundamental governing equations of fluid dynamics. They represent mathematical statements of the laws of conservation.

The three conservation laws are:

1. Conservation of momentum: change of momentum equals the forces acting on a fluid particle
2. Conservation of mass: equation of continuity
3. Conservation of energy: rate of energy change equals the sum of the work done on a particle and the rate of heat addition

For an infinite small element fixed in space these equations can be written in a differential and conservation form. When assuming a homogeneous, isotropic, Newtonian and incompressible flow, these equations can be written as:

Momentum equation:

$$\rho\left(\frac{\partial u}{\partial t} + u\nabla u\right) = -\nabla p + \rho\nu\nabla^2 u \tag{2.3}$$

Mass equation:

$$\frac{\partial p}{\partial t} + \nabla\rho u = 0 \tag{2.4}$$

Energy equation:

$$\frac{\partial T}{\partial t} + u\nabla T = \frac{k}{\rho C_p}\nabla^2 T \tag{2.5}$$

where u is the flow velocity, ρ the fluid density, p the pressure, T the temperature, ν the fluid kinematic viscosity, k the thermal conductivity and $C_p$ the specific heat. Equations 2.3-2.5 are also known as the Navier Stokes equations. The body forces such as gravity are not considered.

***CFD process***

There are different steps in the CFD simulation process. Firstly, in the pre-process of a CFD analysis, the geometry has to be created. The classical method is to define every single point, line and surface of the geometry in a CFD package directly (e.g. OpenFOAM) or specialised meshing software (e.g. Ansys ICEM). The geometry can also be directly imported from other sources. For example one could import data from a 3D scanner, which can capture the specific properties of objects and / or humans. Another option is to import the geometry from that created with CAD software, which has been used in this thesis. This method is cheap and allows for parameterisation. By parameterisation of the position variables, such as torso and arm angles, influences of position alterations on the fluid flow can easily be analysed.

Secondly, after geometry creation the control volume has to be discretised. The mesh density should be high enough to capture all relevant flow features, whilst keeping the computational time minimal. In turbulent regions, like the boundary layers, the mesh density has to be high. The mesh size has impact on the computer power, accuracy of the results and the convergence rate of the model. For simple geometries, a structured mesh is preferred. In large and complex models such as the bicycle model in this thesis, an unstructured mesh with hexa-triangular mesh elements is commonly used. In this research, the snappyHexMesh utility of OpenFOAM has been used to create the unstructured mesh.

Thirdly, the boundary conditions have to be defined, like the inlet flow velocity, inlet and outlet pressure and the definition of boundary layers along walls. Finally, the physics and flow properties of the model have to be selected. In aerodynamic cycling studies, it is generally assumed that the air is incompressible.

After pre-processing, a CFD solver is used to calculate the flow. The finite volume method is the standard numerical solution technique for almost all commercial CFD codes. After

solving the flow the output can be post-processed. The output from the CFD software can be visualised by plots, such as streamline path plots, pressure plots, velocity vector plots or by numerical output. Visualisation of the flow enhances correct data interpretation. Flow field animations can be used to visualise the time varying fluid flow phenomena's and have become increasingly popular.

### 2.2.5 Turbulence and CFD

A cyclist can be characterised as a bluff body. The fluid flow around a bluff body becomes turbulent. Turbulent flow is caused by the interaction between the viscous and inertia terms of the momentum. Visually, turbulent flows are usually chaotic and random.

A deterministic approach of turbulence is very difficult, due to the closure problem: there are more unknowns as equations. Therefore the problem can only be solved by introducing additional hypotheses. Scientists are still searching for accurate methods to predict turbulent flows. Although the velocity of a fluid is highly disorganised and unpredictable, its statistical properties are reproducible. This implies that all turbulence theories are statistical theories. The time averaged flow pattern is a statistic property of the flow and therefore the flow variables (i.e. velocity, pressure, temperature) are decomposed in a mean flow and fluctuating part. For example, at each location in a steady flow the velocity will be

$$u = u' + \bar{u} \tag{2.6}$$

where $u'$ is the fluctuating part of the motion and $\bar{u}$ is the time averaged motion.

A turbulent flow can be characterised by "eddies"; fluid flows which are moving contrary to the direction of the main flow and usually in a circular motion. A turbulent flow has different eddy scales. The eddy scales are characterised by the length scales. The large scale eddies contain most of the turbulent kinetic energy. These large scale eddies cascade into smaller

eddies with lower kinetic energy as shown in the Kolmogrov energy cascade in Figure 2.12. Finally, the small eddies dissipate the energy into heat. The size of the eddy scales that are resolved depends on the CFD approach used.

In the Reynolds Navier Stokes equations (RANS) all eddies are modelled. In RANS models, equations are developed that predict the time averaged velocity, pressure and temperature fields instead of calculating the complete flow pattern as a function of time. The interaction of the mean flow and the turbulence is modelled by the Reynolds stresses. The Reynolds stresses represent the flux of momentum caused by turbulent fluctuations. Kolmogorov stated that for high Reynolds numbers, the turbulent motions of the small eddies are statistically isotropic and the statistics of small scale motions have a universal form which is determined by the

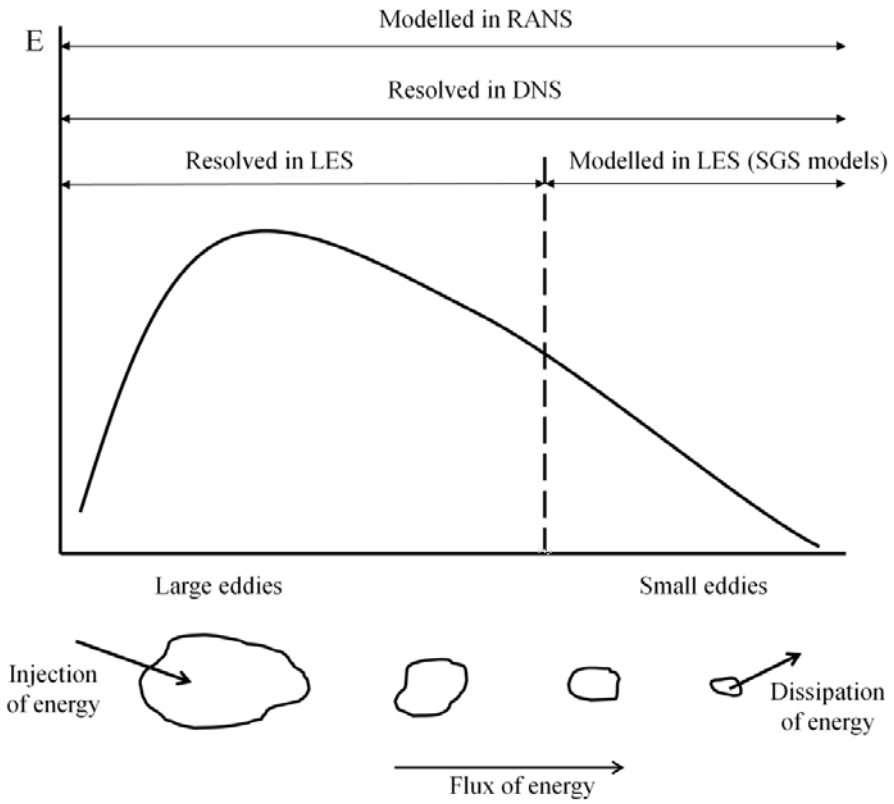


**Figure 2.12 Kolmogorov energy cascade**. **The large scales eddies contain most of the turbulent kinetic energy. The large eddies cascade into smaller eddies with lower kinetic energy. Finally, the small eddies dissipate the energy into heat. The size of the resolved eddies is dependent on the applied CFD approach. RANS, Reynolds Averaged Navier Stokes; DNS, direct numerical simulations; LES, Large Eddy Simulations; SGS, sub-grid scale.**

turbulent energy ε and the turbulent kinematic viscosity $\nu_t$ (Kolmogorov, 1941). A variety of methods are used to predict the turbulence viscosity. The most commonly used RANS models are the k-ε and the k-ω model. In the two equation k-ε model it is assumed that fluctuations in pressure induced by the turbulent eddies are used to spread the turbulent kinetic energy from regions of strong turbulence to those of low intensity turbulence and that this redistribution of energy is a diffusive process. The turbulent viscosity is predicted by a relationship between the dissipation energy and kinetic energy of the turbulence. The two equation k-ω model predicts the turbulent viscosity by a relationship of the kinetic energy k and the specific dissipation, ω. A transport equation is used for the vorticity of the turbulence.

Other CFD approaches are the Large Eddy Simulation (LES) and the Direct Numerical Simulation (DNS). This class of turbulence methods solves the time dependent equations. The LES method calculates only the large eddies in the flow and models the smallest eddies. The small eddies are modelled by a sub-grid scale model. In a DNS model all eddies are explicitly resolved. DNS and LES are more accurate than RANS based turbulence models, but require higher computer power and data storage. To reduce the computational costs whilst maintaining time varying flow data, the hybrid Detached Eddy Simulation (DES) method was developed. In the DES method, the RANS formulations are combined with the LES methods. In detached regions the model is based on the LES model, whilst in the boundary layer the RANS formulations are used. For highly turbulent flows, such as the flow around a cyclist, the DES is more cost efficient in comparison to the LES and DNS methods. It should be noted that the LES and DNS methods provide in general more accurate results.

In this research, a variety of CFD methods are used to determine the accuracy of different turbulence models of two-wheeled vehicles subjected to crosswinds. Methods included are the commonly used steady RANS k- ε and k-ω models and the unsteady DES and LES method.

# CHAPTER 3

# Position and physiology

**Abstract** [1]

To reduce aerodynamic resistance cyclists lower their torso angle, concurrently reducing Peak Power Output (PPO). However, realistic torso angle changes in the range used by time trial cyclists have not yet been examined. Therefore the aim of this study was to investigate the effect of torso angle on physiological parameters and frontal area in different commonly used time trial positions. Nineteen well-trained male cyclists performed incremental tests on a cycle ergometer at five different torso angles: their preferred torso angle and at 0, 8, 16 and 24°. Oxygen uptake, carbon dioxide expiration, minute ventilation, gross efficiency, PPO, heart rate, cadence, and frontal area were recorded. The frontal area provides an estimate of the aerodynamic drag. Overall, results showed that lower torso angles attenuated performance. Maximal values of all variables, attained in the incremental test, decreased with lower torso angles ($p<0.001$). The 0° torso angle position significantly affected the metabolic and physiological variables compared to all other investigated positions. At constant submaximal intensities of 60, 70 and 80 % PPO, all variables significantly increased with increasing intensity ($p<0.0001$) and decreasing torso angle ($p<0.005$). This study shows that for trained cyclists there should be a trade-off between the aerodynamic drag and physiological functioning.

[1] This chapter has been published as: The effect of aerodynamic time trial cycling position on physiological and aerodynamic variables. *Journal of Sport Sciences* (2015), doi: 10.1080/02640414.2015.1009936

## 3.1 Introduction

During cycling, up to 90 % of the power output is used to overcome air resistance (Debraux et al., 2011). To reduce air resistance, or aerodynamic drag, cyclists adopt a characteristic time trial position using time trial handlebar extensions (Kyle, 1988, Kyle, 2003). This position results in a significant decrease in frontal area that has been found to be predominately a result of changes in torso angle (Chabroux et al., 2012, Oggiano et al., 2008), where the torso angle is defined as the angle between the torso relative to the ground. García-López et al. (2008) showed that decreasing the torso angle position can decrease the aerodynamic drag up to 16 %. Although reducing torso angle effectively decreases the aerodynamic drag, it negatively affects the peak power output (PPO) (Gnehm et al., 1997, Grappe et al., 1997, Jobson et al., 2008). Moreover, results of the effect on the metabolic and physiological functioning of the cyclist are inconclusive.

Since the introduction of the time trial handlebars in the 80's, the time trial position has been subject of several investigations. In the literature three typical cycling positions are usually compared: upright position, dropped position and time trial position. These correspond respectively to a large, medium and small torso angle. When comparing these positions, in terms of oxygen consumption ($VO_2$) and heart rate, results are equivocal. For example three studies failed to show an effect of torso angle on $VO_2$ and heart rate (Origenes et al., 1993, Franke et al., 1994, Dorel et al., 2009). Both Dorel et al. (2009) and Origenes et al. (1993) examined submaximal intensity exercise; however different time trial positions were adopted. Whereas Dorel et al. (2009) examined a 21° torso angle time trial position, Origenes et al. (1993) failed to standardise the adopted time trial torso angle position. Franke et al (1994) examined maximal intensity exercise and standardised the position of the handlebars to be 5 cm lower than the saddle, corresponding with large torso angles, e.g. > 24°. In contrast with

the aforementioned studies, Richardson et al. (1994) reported in the cyclists' preferred time trial position an increase in $VO_2$ compared with upright position at a submaximal intensity. Ghnem et al. (1997) also found an increase in $VO_2$ and heart rate in the time trial position (20° torso angle) compared to the upright position under submaximal conditions. An increased $VO_2$ and heart rate in the time trial position compared to the dropped position was also found by Evangelisti et al. (1995), but the adopted positions were not reported. These conflicting results in metabolic and physiological functioning are likely to be a consequence of the heterogeneity in the cycling positions adopted and methodological dissimilarities.

By examining the three typical road cycling positions, rather large position changes were examined, which does not complement the body of knowledge of time trial cycling position optimisation. To allow for comparison and optimisation, the torso angle needs to be systematically changed and the complete range of commonly used torso angle examined. Although Heil et al. (1997) have systematically changed the time trial position (10°, 20°, 30°), according to the knowledge of the authors, all previous studies examined rather large time trial torso angle positions (>10°). In competitive time trial cycling nowadays often smaller time trial positions are used. For example, in our study about 40 % of the participants ride with torso angles smaller than 10°. Although these low torso angle positions (up to 0°) are optimal in terms of aerodynamics (Kyle, 2003) and are often cited as optimal in non peer-reviewed cycling periodicals, knowledge on its effect on physiological performance is lacking. These small torso angle positions also require more extreme hip joint angles and hip flexibility of the cyclist. Therefore it is generally accepted by professional bike fitters that hip flexibility is a limiting factor in adopting a smaller torso angle positions. However, there is no scientific evidence supporting this assumption.

In addition to the physiological variables at small torso angle positions, air resistance needs to

be investigated. The frontal area of the cyclist is one of the most important parameters to characterise air resistance and therefore is often used to predict the total aerodynamic drag (Debraux et al., 2011). However, according to the authors' knowledge, determining the physiological performance in conjunction with frontal area is rarely achieved in literature. Based on this information a model evaluating the trade-off between physiological responses and aerodynamic gains can be developed (e.g. Fintelman et al., (2014c)).

Therefore the main aim of this study was to determine the effect of torso angle on physiological functioning and frontal area in five different commonly used time trial positions. A secondary aim was to determine whether the hip flexibility affects the preferred cycling position. It was hypothesized that decreasing the torso angle towards smaller joint angles would negatively affect the physiological parameters but decrease frontal area and consequently the aerodynamic drag, and that a lower level of flexibility would be associated with a higher preferred torso angle.

## 3.2 Methods

Nineteen healthy, trained male competitive triathletes and cyclists aged between 20 - 55 years, volunteered to take part in the experiment. Participants reported to ride on average 7.2 ± 2.4 hours a week and had used time trial handlebars for at least the last 2 years. They had no physical impairment preventing them from a competitive cycling activity. Participants' preferred time trial torso angle ranged from 2 - 21°. The group characteristic means and standard deviation of the participants in their preferred time trial cycling position are presented in Table 3.1. The study was approved by the Universities Science, Technology, Engineering and Mathematics ethics committee (ERN_12-1223) and all participants gave written informed consent at the beginning of the study.

**Table 3.1 Group characteristics (n=19), assessed in the participants' preferred time trial position. Values are reported as mean ± SD.**

| Variable | Value |
|---|---|
| Age (yr) | 34.8 ± 10.7 |
| Body weight (kg) | 74.3 ± 8.0 |
| Height (cm) | 181.3 ± 6.0 |
| Preferred torso angle (°) | 11.9 ± 5.6 |
| $VO_{2max}$ (mL/min) | 4151.5 ± 406.0 |
| $VO_{2max}$ (mL/min/kg) | 56.1 ± 5.2 |
| PPO (W) | 354.1 ± 36.5 |
| Flexibility BSR Left (cm) | 13.8 ± 9.2 |
| Flexibility BSR Right (cm) | 14.6 ± 9.5 |

*$VO_{2max}$, maximal oxygen consumption; PPO, peak power output; BSR, back saver sit and reach test*

The participants were also asked to fill out a questionnaire about their cycling characteristics, and potentially cycling related back pain. The participants performed five incremental test sessions in a time trial position on a bicycle ergometer (Lode Excalibur Sport, Lode BV, Groningen, The Netherlands); in their preferred torso angle and at 0, 8, 16 and 24° torso angles, β (see Figure 3.1). Time trial clip-on handlebars (Profile Design Carbon Stryke, Long Beach, United States) were mounted on the ergometer. The sessions were separated by at least 48 hours, whilst all trials were performed within a maximum of 17 days. Measurements of the heart rate, torso angle, power output, cadence, oxygen consumption ($VO_2$), carbon dioxide expiration ($VCO_2$), respiratory exchange ratio (RER), gross efficiency and minute ventilation were performed throughout each session. At the end of each session a frontal photograph was taken to calculate frontal area, which has been shown to give a reasonable estimate of the aerodynamic drag (Debraux et al., 2011).

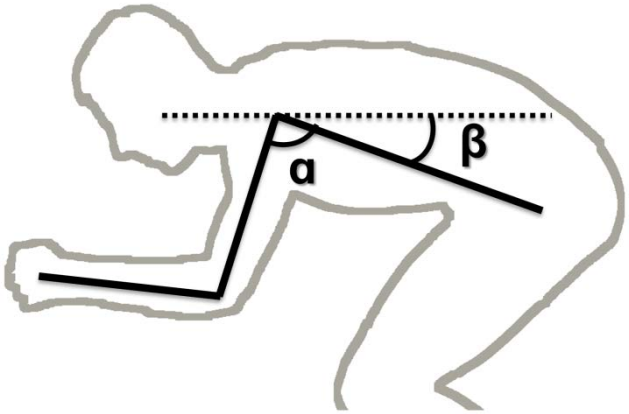


**Figure 3.1 Torso angle β relative to the ground and shoulder angle α. The torso angles analysed were 0, 8, 16 and 24°, whilst the shoulder angle remained constant. The shoulder angle was measured in the participant initial preferred position.**

Each participant reported to the laboratory at the same time each session and had fasted for at least 8 hours, and they were asked to standardise their exercise the day before the sessions.

In the first session the saddle and time trial handlebar positions of the participants' time trial bike were reproduced on the ergometer and referred to as their 'preferred' position. The mean distance between the handlebars of the participants was 10 ± 1 cm. In the remaining sessions, the handlebar height was adjusted to fit one of the predefined torso angles (0, 8, 16 or 24°), which was checked with a digital inclinometer (Fisco EN17, Ficso Tools Limited, Essex, UK) and measured from the centre of rotation of the glenohumeral axis and the greater trochanter. The order of torso angle was randomised across participants. The angle between the upper arms and the torso, α, was maintained constant across all trials and was based on the participants' preferred cycling position. The participants used their own clip-in pedals and shoes. It should be noted that out of the nineteen participants, it was not possible for four of them to reach 0° torso angle due to ergometer position limitations. In this situation the smallest reachable torso angle was used, ranging between 1.1 - 4.9°.

The incremental test started with a 5 minutes warm up at 95 W, after which the intensity was increased by 35 W every 3 minutes. The participants were asked to maintain their normal road cycling cadence during the test. The tests were stopped when the participant was exhausted, the heart rate exceeded the age limit restriction (220 - age) or the RER exceeded 1.12. Cycling in a standing position was not permitted. The participants were allowed to have an electric fan in front of them to provide cooling. No visual feedback or encouragement was given to the participant during the tests.

During the session the $VO_2$, $VCO_2$, minute ventilation and RER were measured constantly with a breath-by-breath gas analyser (Jaeger Oxycon Pro, Erich Jaeger GmbH, Hoechberg, Germany), except for the first minute of the 200 W stage where the participants were allowed to have a drink. A small mouthpiece was used. The system was calibrated prior to each test with gas concentrations of 14.95 % $O_2$ and 4.99 % $CO_2$ and a 3 L calibration syringe. All measurements took place under similar environmental conditions (18 - 20°C), using the same measurement equipment. Heart rate was recorded every minute (Polar FT1, Polar Electro, Kempele, Finland). The cadence was continuously measured on the ergometer with a sampling frequency of 4 Hz.

The hip range of movement of the cyclists was assessed with the back savers sit-and-reach test (Chillón et al., 2010). A standard sit-and-reach box with a measurement scale was used (Cranlea Medical electronics, Birmingham, UK), with the level of the feet at 15 cm. The flexibility of the left and right leg were measured directly after warming up and performed according to the protocol used by Chillón et al. (2010). The tests were carried out by one instructor to ensure repeatability and that the same method was applied. The flexibility tests were repeated two times for each leg and the scores averaged.

All metabolic variables were averaged over 8 breaths and finally averaged over the final 2

minutes of each stage. The gross efficiency was derived according to the formulae of Garby and Astrup (1987). The gross efficiency was calculated until the RER exceeded 1.00. The PPO was defined as the sum of the final power stage reached and the fraction of the partly completed workload performed before exhaustion (Moseley and Jeukendrup, 2001). Furthermore, the recorded variables were evaluated in all torso angle positions at a submaximal intensity of 60 %, 70 % and 80 % of the PPO obtained in the participants' preferred position. The frontal area of the cyclists in each torso angle position was estimated by analysing frontal photographs of the cyclist (Barelle et al., 2010, Debraux et al., 2011). In this method a reference frame with a known area was placed between the participant's shoulders and hip (See Figure 3.2). The frontal photographs were analysed with the ImageJ 1.45s image processing software (ImageJ, National Institutes of Health, USA). By determining the ratio of pixels of the projected frontal area of the isolated cyclist and the known reference frame area, the actual frontal area of the cyclist was calculated.

The mean and standard deviation of all variables were calculated. A one-way repeated measures ANOVA was used to compare the maximal and submaximal variable values in all torso angles. Prior to these tests, a Maulchy test of sphericity was conducted. If sphericity was violated, a Greenhouse-Geisser correction was applied. Post hoc tests with Bonferroni correction were used to locate the differences. Effect sizes were reported as partial eta-squared ($\eta^2$). A linear regression analysis was performed to determine whether the participants' flexibility could predict their preferred torso angle. This will help to determine if flexibility is a limitation to cycle with small torso angles. Another linear regression was performed to determine whether the torso angle could predict the frontal area, to confirm that lowering torso angle reduces frontal area and hence aerodynamic drag. Finally, the effect of the preferred torso angle on the peak power output has been investigated with a second order


**Figure 3.2 Example of photographs of a cyclist used to measure the frontal area. (a) before image processing (b) after image processing.**

polynomial regression analysis. In the regression the relative torso angle, which was defined as the measured position (0, 8, 16 or 24°) minus the participants' preferred position, was laid out against the PPO of each individual cyclist. In all statistical tests significance was set at $p<0.05$.

## 3.3 Results

There was a significant main effect of torso angle on all recorded variables ($p<0.001$). All maximal values of the variables recorded decreased with lower torso angles (Table 3.2). The mean PPO was reduced by 14 % (51 W) when changing from a 24° to a 0° torso angle position. Post hoc tests revealed that the 0 ° torso angle position significantly decreased the $VO_2$ ($p<0.015$), heart rate ($p<0.007$), cadence ($p<0.041$) and minute ventilation ($p<0.017$) compared with all other torso angles. A reduction of 2.6 % (78 mL/breath) in gas volume per breath was recorded between the 0° and 24° torso angles.

The responses of the heart rate, minute ventilation, gross efficiency and $VO_2$ at different submaximal cycling intensities of 60, 70 and 80 % of PPO in the different positions are

shown in Figure 3.3. All variables showed a statistically significant increase with increasing intensity ($p<0.0001$). Furthermore, the heart rate, minute ventilation and $VO_2$ significantly increased when cyclists were in a lower torso angle position ($p<0.005$), whilst the gross efficiency significantly decreased ($p<0.001$) at the analysed submaximal intensities (i.e. 60, 70 and 80 % of PPO). The heart rate, minute ventilation and $VO_2$ were increased by 4.2 % (6.0 bpm), 14.4 % (12.0 L/min) and 4.1 % (1.8 mL/min/kg) respectively in the 0° position compared to the 24° position at submaximal intensities. The gross efficiency dropped by approximately 4.6 % (1.0 %) with a lower torso position. For the minute ventilation and heart rate the 0° position elicited a significant increase compared with all other positions, whilst for the gross efficiency and $VO_2$ the largest differences were found for the 24° torso angle position.

The relative torso angle versus the peak power output of all participants together with the least square fit second order polynomial ($R^2=0.341$, $p<0.0001$) are shown in Figure 3.4. No optimum has been observed at the cyclists' preferred cycling position.

Furthermore, a reduction of 14 % frontal area was observed between the 24° and 0° torso angle positions. Statistically significant differences were found between the frontal areas for all torso angles ($p<0.001$). The linear regression results showed that the torso angle significantly predicted the frontal area ($R^2=0.359$, $p=0.001$).

The participants' mean left and right leg back savers sit-and-reach test scores were 13.8 ± 9.2 cm and 14.6 ± 9.5 cm respectively. The linear regression analysis showed that the flexibility of the left and right leg did not significantly predict the chosen preferred torso angle of the participants respectively ($R^2=0.014$, $p=0.632$ and $R^2=0.011$, $p=0.655$). Questionnaires revealed that none of them experienced regular lower back pain during cycling, or adjusted their bicycle settings as a result of back pain.

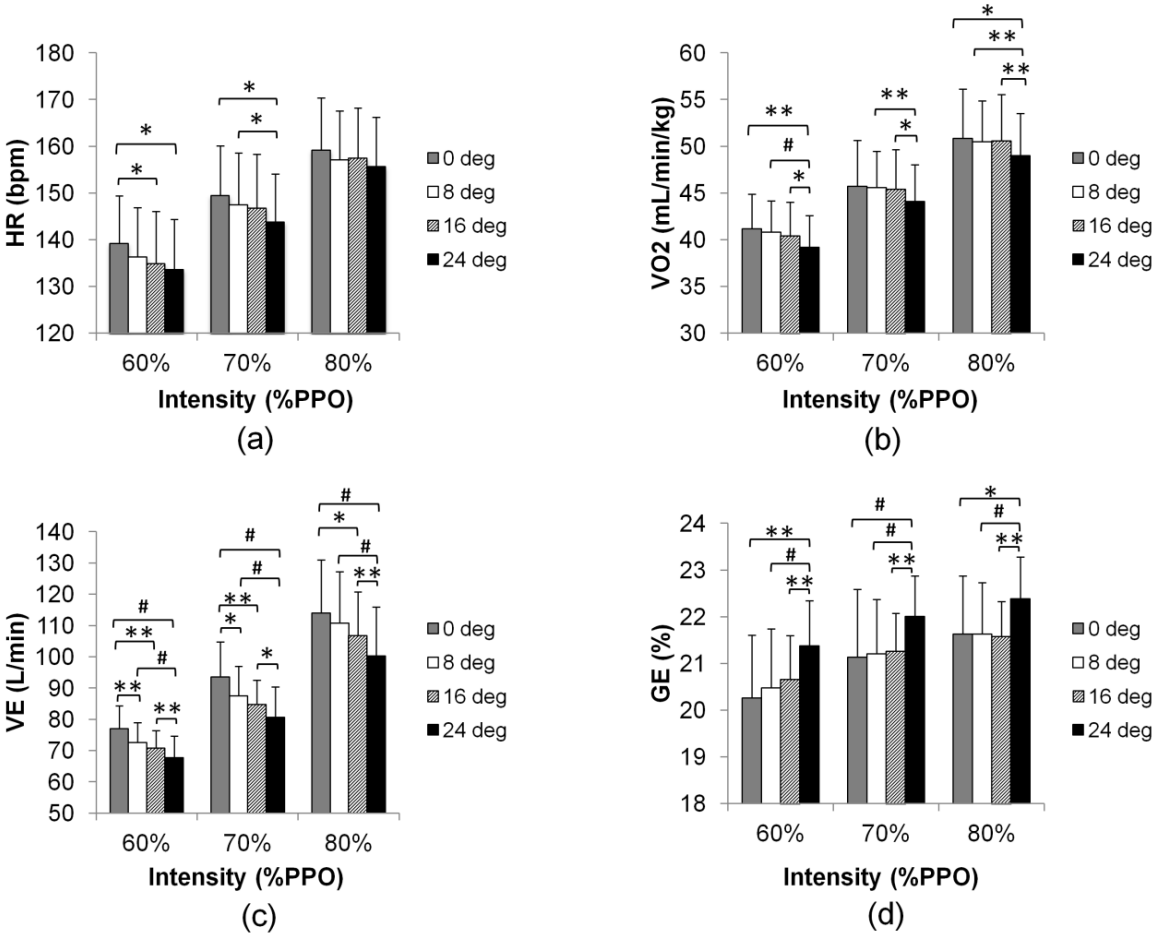


**Figure 3.3 Response of selected variables at different submaximal cycling intensities (60 %, 70 % and 80 % PPO) at different torso angle positions (0, 8, 16 and 24°). The submaximal intensity was related to the peak power output (PPO) in the participants preferred position. (a) HR, heart rate response, (b) $VO_2$, oxygen consumption response, (c) $V_E$, minute ventilation response, (d) GE, gross efficiency response. * Significant different at p<0.05, ** Significant different at p<0.01, # Significant different at p<0.001.**

**Table 3.2 The maximal values of the main physiological variables and frontal area at all torso angles obtained during the incremental tests (mean ± SD). Time trial torso angle positions evaluated were 0, 8, 16 and 24° and their preferred position. The mean preferred torso angle position of all participants was 11.9° ± 5.6°. The repeated measures ANOVA results show a statistically significant main effect for all variables analysed.**

| Variable | 0° | 8° | 16° | 24° | Preferred (11.9° ± 5.6°) | F statistic |
|---|---|---|---|---|---|---|
| PPO (W) | 318.5± 34.1[a,b] | 343.4± 37.7[a] | 357.2± 36.7[a] | 369.4± 38.4[a] | 354.1± 36.5 | F(1.66,29.82)= 48.70, p<0.0001, $\eta^2$=0.730 |
| $VO_{2max}$ (mL/min/kg) | 51.76 ± 6.78[b] | 54.95± 5.79 | 56.81± 6.57 | 56.89± 5.86 | 56.14± 5.24 | F(3,54)=13.98, p<0.0001, $\eta^2$=0.437 |
| Max HR (bpm) | 165.8 ± 12.3[b] | 169.9± 10.6 | 173.1± 10.0 | 175.2± 10.2 | 175.1± 10.0 | F(2.12,38.08)= 12.24, p<0.0001, $\eta^2$=0.405 |
| Max $V_E$ (L/min) | 130.4 ± 24.2[b] | 145.0± 23.5 | 153.8± 22.6 | 154.8± 22.8 | 150.9± 17.7 | F(1.93,34.89)= 19.12, p<0.0001, $\eta^2$=0.515 |
| Mean GE (%) | 18.38± 1.62 | 18.75± 1.53 | 19.04± 1.10 | 19.85± 1.26[c] | 18.88± 1.17 | F(3,54)=18.71, p<0.0001, $\eta^2$=0.510 |
| Mean Cadence (rpm) | 81.53± 8.11[b] | 85.64± 7.83 | 87.43± 7.98 | 86.46± 7.82 | 90.73± 6.55 | F(3,54)=8.00, p<0.0001, $\eta^2$=0.308 |
| Frontal area ($m^2$) | 0.288± 0.023[a] | 0.302± 0.021[a] | 0.318± 0.024[a] | 0.335± 0.027[a] | 0.307± 0.021 | F(3,54)=130.70, p<0.0001, $\eta^2$=0.879 |

*PPO, peak power output; $VO_{2max}$, maximal oxygen consumption; HR, heart rate; $V_E$, minute ventilation; GE, gross efficiency.*

[a] Significant difference between all torso angles (p<0.001)
[b] Significant difference between 0° and 8 - 24° torso angle (p<0.05)
[c] Significant difference between 24° and 0 - 16° torso angle (p<0.001)

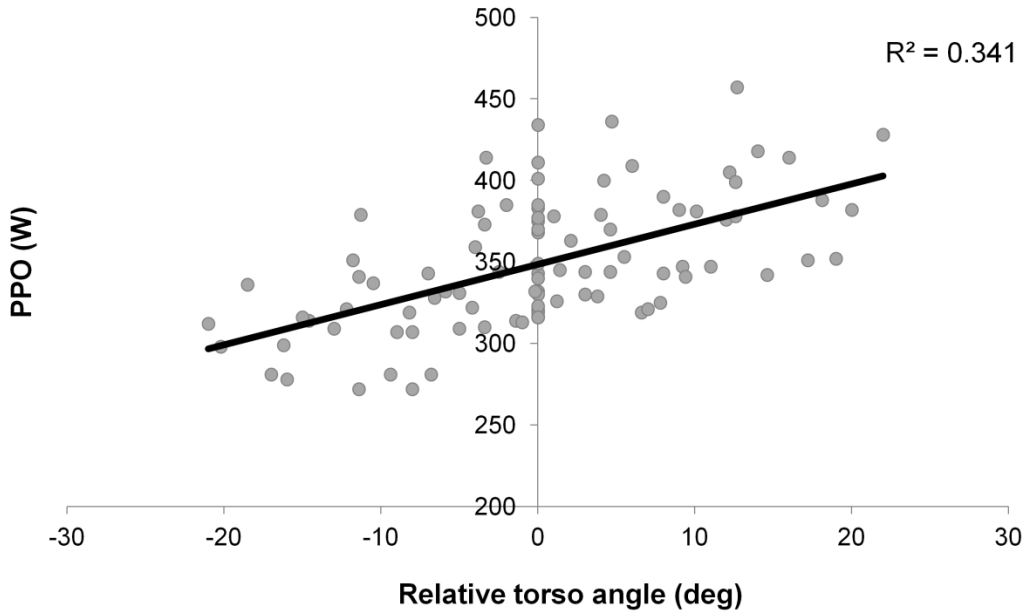


**Figure 3.4 Relative torso angle of each participant versus the peak power output (PPO). The relative torso angle was defined as the measured torso angle position (0, 8, 16 or 24°) minus the preferred torso angle. The second order polynomial regression revealed no optimum at the participants preferred cycling position, e.g. at a relative cycling position of 0°.**

## 3.4 Discussion

The main aim of this study was to investigate the effect of torso angle on physiological parameters and frontal area in different commonly adopted cycling time trial positions. The results showed that torso angle affected all recorded variables. In particular, small torso angles limited physiological functioning. Although the power output was reduced with a lowering of the torso angle, the frontal area significantly decreased. This would suggest that a trade-off exists between the physiological losses and the aerodynamic gains of a cyclist.

Here we report significant physiological losses and reduced PPO associated with lowering time trial torso angle in the range often used by cyclists. This supports and complements previous findings (Gnehm et al., 1997, Grappe et al., 1997, Jobson et al., 2008) and shows that this reduction can also be observed for small time trial torso angle changes. We also demonstrated that at maximal intensity the heart rate and $VO_2$ decrease, contrasting with other experiments that fail to show impairments of the physiological performances when lowering

torso angle (Origenes et al., 1993, Franke et al., 1994, Dorel et al., 2009, Heil et al., 1997). This discrepancy could be a result of heterogeneity in the torso angle adopted in the various experiments (torso angles > 10°), together with the large range of torso angles that were applied (often comparison upright, time trial and dropped position). However, the submaximal intensity results of the present study are in line with those reported by Gnehm et al.(1997) and Evangelisti et al. (1995), albeit for different torso angle positions. The heart rate and $VO_2$ differences between the 0° and 24° torso angle were comparable to the results of Gnehm et al. (1997), in which an upright position (large torso angle position) was compared with a 20° torso angle position. We also demonstrated that at a 0° torso angle, the $VO_{2max}$, heart rate, cadence and minute ventilation were significantly reduced compared to all other positions. This trend of reduced physiological performance when lowering position has also been observed at different cycling intensities during the incremental test. This demonstrates that at both maximal and submaximal cycling intensities, the physiological performance is impaired at 0° torso angle. In general, the 0° torso angle position should be therefore avoided in trained male competitive cyclists.

Several factors could influence physiological responses at small torso angles. The hip and leg muscles operate at a different, less optimal length to produce optimal force of contraction (Dorel et al., 2009). The abdominal compression occurring at this low angle could hinder the work of the diaphragm and therefore limit lung volume resulting in reduced $VO_{2max}$ (Ashe et al., 2003). The more extreme hip angles could also cause increased activation of the adductor to keep the leg movement in the sagittal plane (Gnehm et al., 1997). Finally, as the torso is lowered, the force that the neck and upper limbs have to exert, to maintain the position, marginally increases (Gnehm et al., 1997). The present experiments cannot clarify the origin of the changes observed when lowering torso angle and future research should attempt to

reveal the exact underlying mechanisms.

Although small torso angles impair the physiological functioning, the frontal area linearly decreased when torso angle is lowered; hence the aerodynamic drag is likely to have been reduced. Several studies have also investigated the effect of torso angle on aerodynamic drag with wind tunnel experiments by recording the drag area, which is the combination of frontal area and drag coefficient (Underwood et al., 2011, García-López et al., 2008). They reported a significant positive correlation between drag area and torso angle, which is similar to our findings. Therefore there is a clear aerodynamic advantage to lowering the torso, and from the findings on this single variable, one could conclude that reducing torso angle is a good strategy when setting a time trial position. However, physiological findings do not support this simple argument and this emphasises the existence of trade-off for non-elite cyclists. In a recent study by Fintelman et al. (2014c) it has been shown that for cycling speeds commonly used by time trial cyclist (24-50 km/h), a trade-off exists between the power output/efficiency and aerodynamics. The model used in the aforementioned study shows that the optimal time trial torso angle position is a function of the frontal area, human physiology, cycling speed, course profile and cycling duration. Therefore all these factors, including the physiological impairment and power losses, need to be taken into account when optimising position.

In addition, when optimising position other factors like training and flexibility could have an effect on the optimal position. Previous literature has demonstrated that training could also improve cycling performance and hence affect the optimal cycling position (Jeukendrup and Martin, 2001, Peveler et al., 2005). Heil et al. (1997) found that the optimal time trial position of cyclists was close to their preferred cycling position. In contrast to these results, our study demonstrated that the preferred position did not show an increase in peak power output or decreased oxygen consumption compared to the positions analysed. This suggests that when

changing position towards low torso angle positions (0°), a performance reduction can be observed independently of the preferred position. From this it could be implied that in the torso angle range we analysed, the training effect is likely to be limited, but further work is needed. With regard to hip range of movement potentially affecting the optimal cycling position, this study has demonstrated that flexibility, as measured by the back-savers sit and reach test, did not affect the preferred cycling position of cyclists. In the population tested, the flexibility required for time trial position is already within the range of motion of our participants. As in previous literature no correlation was found between low back pain in cyclists and low back inflexibility (Brier and Nyfield, 1995), it can be suggested that hip flexibility of the participants is not a limitation to cycling with small torso angles. However, decreasing torso angle will affect the comfort of the cyclist.

Finally, it should be mentioned that all reported results are based on laboratory performances. In previous literature it has been shown that there are discrepancies between road based and laboratory based performances. Body size has been shown to highly contribute to these discrepancies (Jobson et al., 2007), but other factors including thermoregulation, motivation and course profile could also affect the performance. However, a study by Jobson et al. (2008) have shown that the physiological demand for cycling in a time-trial position in the laboratory is similar to that of cycling in the field. In addition, previous literature has shown that the PPO output, as assessed by an incremental test, is a valid and reliable measure of endurance performance and can be used to predict average power in upright cycling (Hawley and Noakes, 1992) and time trial cycling (Balmer et al., 2000). This reinforces the ecological validity of laboratory based performance assessment. Moreover, in conjunction with the model of Fintelman et al. (2014c), which relies predominantly on the power output, efficiency and frontal area, the data of the current study is of value in optimising time trial cycling

position. It should however be noted that this study is limited to male competitive cyclists and therefore precaution has to be taken on the extrapolation of the results to less trained male cyclists and potentially for female cyclists.

## 3.5 Conclusion

Whilst systematically controlling the time trial position, the effect of the torso angle on physiological functioning and frontal area was investigated. The results demonstrated that decreasing torso angle results in a reduction in metabolic and physiological responses at maximal and submaximal intensity, whilst the frontal area linearly decreases. In particular the lowest torso angle position (0°) showed a significant reduction in the physiological performance and should be avoided in trained male competitive cyclists. For trained cyclists, there exists a trade-off between aerodynamic gains and physiological losses. The flexibility of the cyclists does not limit the participant to cycle with small torso angles. Moreover, results suggest that training in lower torso angle positions will improve to some extent the power output. When optimising position, one should bear in mind that decreasing torso angle will affect the performance.

## Acknowledgements

This study was not supported by any external funding. The authors would like to thank P. Highton and T. Adams for their assistance with the data collection.

# CHAPTER 4

# Position, muscle activation and torque

**Abstract** [1]

To reduce air resistance, time trial cyclists and triathletes lower their torso angle. The aim of this study was to investigate the effect of lowering time trial torso angle positions on muscle activation patterns and crank torque coordination. It was hypothesized that small torso angles yield a forward shift of the muscle activation timing and crank torque. Twenty-one trained cyclists performed 3 exercise bouts at 70 % maximal aerobic power in a time trial position at three different torso angles (0°, 8° and 16°) at a fixed cadence of 85 rpm. Measurements included surface electromyography, crank torques and gas exchange. A significant increase in crank torque range and forward shift in peak torque timing was found at smaller torso angles. This relates closely with the later onset and duration of the muscle activation found in the gluteus maximus muscle. Torso angle effects were only observed in proximal monoarticular muscles. Moreover, all measured physiological variables (oxygen consumption, breathing frequency, minute ventilation) were significantly increased with lowering torso angle and hence decreased the gross efficiency. The findings provide support for the notion that at a cycling intensity of 70 % maximal aerobic power, the aerodynamic gains outweigh the physiological/biomechanical disadvantages in trained cyclists.

[1] This chapter has been published as: Effect of different aerodynamic time trial cycling positions on crank torque, muscle activation and efficiency. *Scandinavian Journal of Medicine and Science in Sports* (2015). doi: 10.1111/sms.12479.

## 4.1 Introduction

Aerodynamic drag is the dominant resistance force during cycling on a flat road (Debraux et al., 2011, Kyle and Burke, 1984). To minimize drag, cyclists and triathletes adopt a time trial position and lower their torso angle to reduce frontal area (Lukes et al., 2005). However, conflicting results on the effect of torso angle on the physiological measures at submaximal intensity were presented in the literature. For example, whilst comparing different typical cycling positions (i.e. upright, dropped and time trial position) no position effects were found (Berry et al., 1994, Dorel et al., 2009, Jobson et al., 2008). In contrast, other studies demonstrated that riding in a time trial position negatively affects physiological measures (Evangelisti et al., 1995, Gnehm et al., 1997, Grappe et al., 1998). Remarkably, only a few studies have investigated the effect of position changes on the muscle recruitment and crank torques.

Examples of studies examining the effect of position alterations on the muscular and mechanical factors are the investigations of Savelberg et al. (2003), Chapman et al. (2008) and Dorel et al. (2009). Savelberg et al. (2003) have observed changes in muscle recruitment in a fully vertical upright cycling position and a 20° forward and backward position. Likewise, Chapman et al. (2008) have found increased muscle activation during secondary muscle activity (muscle activity between primary bursts) and greater coactivity when cycling in a dropped position compared to an upright position. No changes were found in the leg or foot kinematics between the two aforementioned positions. The only study that simultaneously recorded crank forces and muscle activations in the three typical cycling positions (upright, dropped and time trial) is the study of Dorel et al. (2009). They observed increased muscle activation in the gluteus maximus (Gmax) in the time trial position compared to the upright and dropped positions. This was closely related to higher observed

down stroke peak forces and later force application during the pedal stroke in the time trial position. The higher down stroke peak forces compensate for the lower negative upstroke peak forces observed in the time trial position. Dorel's study has been focused on comparing different typical cycling positions and therefore the torso angles examined were relatively large (>21°). The analysed positions in the latter study are consequently less optimal in terms of decreasing aerodynamic drag. To reduce air resistance whilst riding in a time trial position, a horizontal torso has been recommended by Martin and Cobb (2002). Thus although previous studies showed an effect of body position on muscle recruitment and pedal forces/ crank torques in classic road cycling positions, no information is known about the effect of realistic time trial position torso angle changes towards more aerodynamic torso angles. In particular, the effect of lowering torso angle on muscle activation, force application and physiological variables remains unknown.

The aim of this research was to determine the effect of changes in realistic time trial torso angle position on the muscle activation patterns and crank torques. It was hypothesized that small torso angles will result in a forward shift of the muscle activation timing and crank torque.

## 4.2 Materials and methods

Twenty-one male competitive time trial cyclists and triathletes volunteered to participate in the study. The participants' physical characteristics were: age 40.0 ± 9.9 years, height 1.79 ± 0.06 m, body mass 75.3 ± 6.1 kg, Maximal Aerobic Power (MAP) 368 ± 41 W, $VO_{2max}$ 4200 ± 448 mL/min or $VO_{2max/kg}$ 56.0 ± 5.8 mL/min/kg (mean ± SD). The average preferred torso angle was 11.0 ± 3.7° (range of 5° - 17°) relative to the ground. All participants performed regular cycling exercise with time trial handlebars. The study was approved by the local ethics

committee (ERN_13-0941) and at the beginning of the study the participants gave their informed written consent. The participants were asked to refrain from high intensity training at least 24 hours prior to the sessions. They were also not allowed to eat or drink 4 hours before the sessions.

Using a within subject design, each participant visited the laboratory on two occasions, separated by at least 48 hours. Visit one consisted of completing a 1-min incremental cycling test on an ergometer to determine the MAP. The MAP was defined as the sum of the final fully completed stage and the fraction of the last stage (Moseley and Jeukendrup, 2001). Testing was performed upon a fully adjustable cycling SRM ergometer (SRM, Jülich, Germany) with time trial handlebars mounted on top of the ergometer handlebar (Profile Design Carbon Stryke, Long Beach, United States) and equipped with the subjects' own pedals. The ergometer was set in hyperbolic mode to hold the cyclists' power to a fixed level. The time trial handlebars were set 100 mm apart. The participants' preferred time trial cycling position was replicated on the ergometer by measuring the dimensions of the participants' own time trial bike. To standardize the position, the handlebar height was adjusted so that the torso angle was set at 16° during the incremental test. The torso angle was measured with a digital inclinometer (Fisco EN17, Ficso Tools Limited, Essex, UK) from the centre of rotation of the glenohumeral axis to the greater trochanter. The test started with a 10 minute warm up at 100 W. Then the load was increased every minute by 25 W until either exhaustion or when the cadence dropped below 60 rpm. During the session the power output, oxygen consumption ($VO_2$), heart rate (HR), minute ventilation (VE), cadence, breathing frequency (Bf) and tidal volume (VT) were constantly recorded. The physiological variables were measured with a breath-by-breath gas analyser (Jaeger Oxycon Pro, Erich Jaeger GmbH, Hoechberg, Germany) with a small mouth piece. The SRM ergometer and gas analyser were

calibrated before each test according to the manufacturers' recommendations.

The second visit consisted of submaximal cycling exercise in 3 different torso angle positions. Torso angles positions were 0, 8 and 16° relative to the ground. The participants were asked to cycle at a constant cadence of 85 rpm throughout the tests to avoid interaction between cadence and muscle activation (Marsh and Martin, 1995, Neptune et al., 1997, Sarre et al., 2003). The protocol started with a 10 min warm-up at 100 W, followed by the three exercise bouts. The order of the exercise bouts was counter balanced. All bouts were at 70 % MAP intensity with duration of 4 min and at least 6 min recovery to prevent fatigue. The participants finished with a 10 min recovery at 100 W. During the session the crank torques, cadence, physiological responses (VE, Bf, VT, $VO_2$), and EMG of 7 muscles were recorded (tibialis anterior (TA), soleus (SO), gastrocnemius lateralis (GCL), GMax, vastus lateralis (VL), rectus femoris (RF) and biceps femoris (BF)). The skin of the right leg was shaved, abraded and cleaned with alcohol before electrode application. Single differential surface EMG electrodes with an inter-space distance of 10 mm (Delsys Myomonitor III, Delsys Inc, Natick, United States) were placed according to the SENIAM guidelines (Hermens et al., 1999). The EMG system recorded data at a sampling frequency of 1000 Hz and was synchronised with the cadence by means of an external 5 V trigger. The cadence sensor was placed at the top dead centre of the left pedal revolution. The torque and crank angle was measured with a SRM Torque Analysis system (SRM, Jülich, Germany) and sampled at a frequency of 200 Hz. The angular position of the crank/pedal was estimated based on the assumption of constant crank angular velocity. The torque measured is the combined torque of the left and right pedal.

The gas measurements were averaged over the last minute of the submaximal exercise bout, in which steady state was reached. Gross efficiency (GE), the ratio of work generated to

metabolic energy, was calculated according to the method of Garby and Astrup (1987). The efficiency was calculated until the respiratory exchange ratio exceeded 1.00. The torque data was analysed and ensemble averaged over the pedal strokes of the last minute of the exercise bout. The difference between the minimal and maximal mean torque during the pedal revolutions, $T_{delta}$ was determined. The $T_{delta}$ provides information about the effectiveness of the pedal stroke. Furthermore the pedal position at the mean peak torque of the left pedal down stroke, Angle $T_{maxL}$ and right pedal down stroke, Angle $T_{maxR,}$ was determined. The mean crank torque during the left pedal down stroke was split into angular quarters: quarter 1 represented 0-45°; quarter 2, 45-90°; quarter 3, 90-135° and quarter 4, 135-180° (Figure 4.3(a)). The variability of the torque profile over the pedal stroke was expressed as the mean standard deviation of all pedal cycles in each exercise condition.

The EMG data was corrected for baseline offsets and full wave rectified. A fourth order Butterworth filter with a cut-off frequency of 10 Hz was applied to create a linear envelope (Connick and Li, 2013, Prilutsky et al., 1998). The ensemble averaged EMG data over the pedal stroke was normalised by the maximum filtered peak EMG data of the participant in the 0° torso angle position (peak dynamic method) (Hug and Dorel, 2009). The EMG is presented as function of the phase of the pedal cycle to eliminate duration differences in muscle activation due to cadence. The on-set and off-set of the muscle threshold value was set to 20 % of the mean peak EMG recorded during the pedal cycle (Dorel et al., 2009, Savelberg et al., 2003). To allow the muscles to adapt to the new position and to reach steady state, the final minute of the EMG data was analysed (Saunders et al., 2000, Shinohara and Moritani, 1992).

***Statistics***

A one-way repeated measures ANOVA (IBM SPSS Statistics 21) was performed to determine

the effect of all considered variables among the three different torso angle positions. The data was checked for normality and sphericity. When sphericity could not be assumed, a Greenhouse-Geisser correction was applied. Post-hoc testing was performed with Bonferroni adjustments to identify the locations of the differences. The significance level of all statistical tests was set at p=0.05 and all data is presented as mean values ± standard deviation.

## 4.3 Results

*Data overview*

All participants successfully completed both sessions. EMG data of two participants was excluded due to technical malfunctioning and therefore all EMG data was analysed for 19 participants. For the VL muscle recordings, one additional participant was excluded due to technical problems. Three participants were excluded from the gross efficiency data, because they did not fulfil the RER criteria.

***Electromyography***

The results showed that there was no significant main effect of torso angle on the mean normalized muscle activation. However, the onset of the main burst of the GMax appeared significantly later during the pedal cycle when lowering torso angle ($F(2,36)=16.70$, $p<0.001$), see Figure 4.1. The onset in the 0° ($p<0.001$) and 8° ($p<0.05$) torso angle positions occurred significantly later compared with the 16° position (4° and 3° later, respectively). In addition, the duration of the GMax muscle activity was observed over a significantly shorter period ($p<0.05$) in the 0° position compared to the 16° position (3° shorter). For the VL offset timing, a significantly later offset of muscle activation during the pedal stroke was found in the 0° ($p<0.005$) and 8° ($p<0.01$) position compared with the 16° position (3° later).

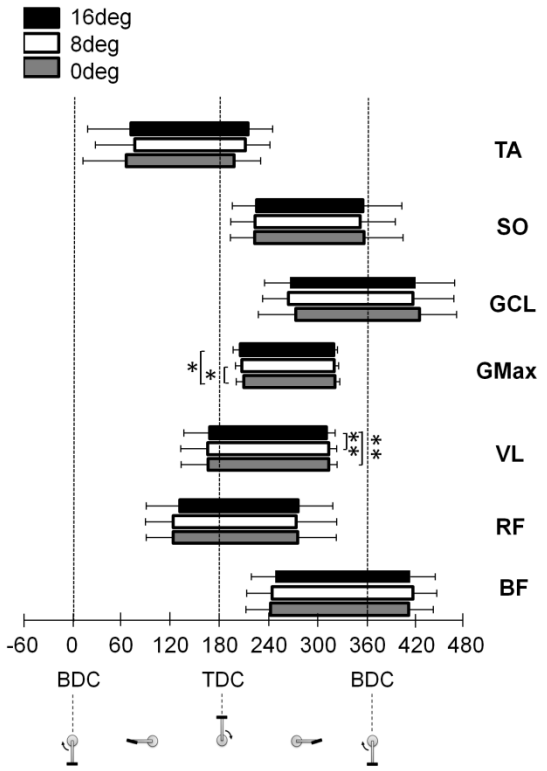


**Figure 4.1 Muscle onset and offset of main burst as function of crank angle among the different cycling positions. * p<0.05 and ** p<0.01 significant difference between the two conditions. Bottom Dead Centre (BDC); Top Dead Centre (TDC).**

### *Torque measures*

The mean torque profile of all participants and the crank torque variables among the different torso angle positions are shown in Figure 4.2 and Table 4.1 respectively. $T_{delta}$ significantly increased with lowering torso angle ($F(2,40)=5.85$, $p<0.01$). A significantly higher torque of approximately 7 % was observed in quarter 3 of the crank stroke ($F(2,40)=12.25$, $p<0.001$), see Figure 4.3. Furthermore, the position of the peak torque in the pedal revolution was significantly changed when lowering position (Angle $T_{maxL}$: $F(2,40)= 2.72$, $p<0.05$; Angle $T_{maxR}$: $F(2,40)=8.25$, $p<0.001$). Post-hoc tests revealed that the peak torque appeared about 5° later during the pedal cycle in the 0° compared to the 16° torso angle position ($p<0.005$). Moreover, the variability of the crank torque profile significantly increased when lowering the torso angle ($F(2,40)=6.57$, $p<0.005$). A significantly larger variability (7 %) was found in the 0° position than in the 16° position ($p<0.005$).

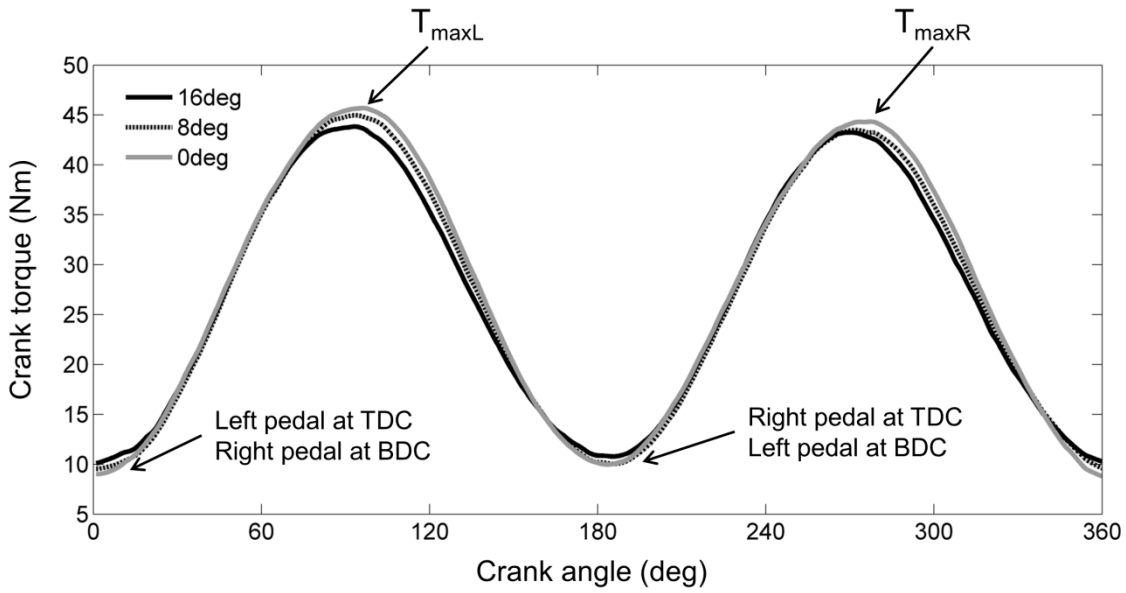


**Figure 4.2 Mean crank torque over the pedal cycle among different cycling positions: 0°,8° and 16° torso angle relative to the ground (n=21). BDC, Bottom Dead Centre; TDC, Top Dead Centre; TmaxL, maximal torque in left leg down stroke; TmaxR, maximal torque in right leg down stroke.**

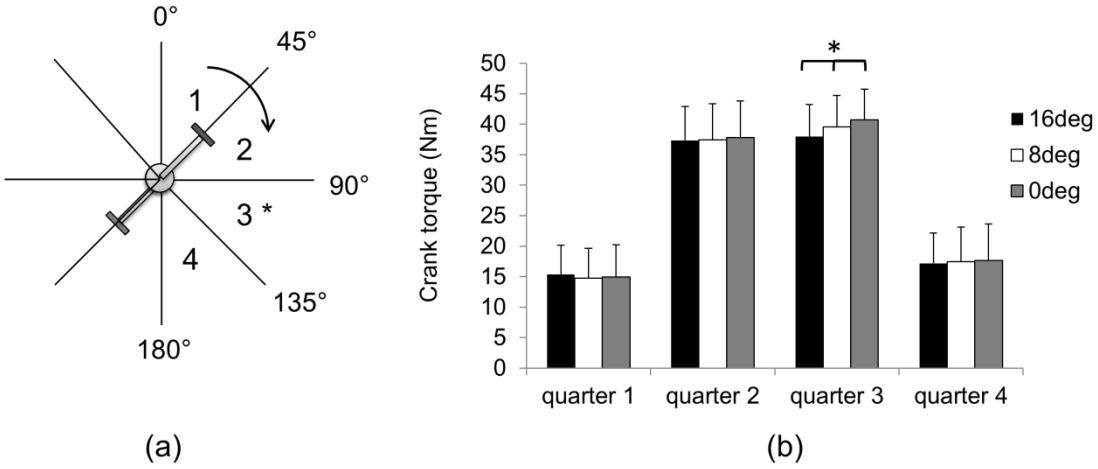


**Figure 4.3 Mean crank torque at different stages during the pedal revolution between different cycling torso angle positions. Stage 1 range between 0-45°, stage 2 between 45-90°, stage 3 between 90-135° and stage 4 between 135-180°. (a) Schematic representation of the quarters; (b) Mean crank torque at the different stages. * p<0.005 significant difference between the two conditions.**

***Physiological measures***

The results of the physiological measures at different torso angle positions are shown in Table 4.1. Results showed that the torso angle had a significant main effect on all physiological variables measured ($p<0.001$), except the VT. The mean VE, Bf and $VO_2$ significantly increased by lowering the torso angle, whilst the GE significantly decreased. Post hoc test revealed that the GE in the 16° torso angle position was significantly higher compared to the 8° and 0° position. The results of the VE in all torso angle positions were significantly different from each other ($p<0.05$). The $VO_2$ was significantly increased in the 0° compared to the 16° position ($p<0.005$), whilst for the Bf the 0° was significantly different from both the 8° and 16° position ($p<0.005$).

## 4.4 Discussion

This study investigated the effect of changing the aerodynamic time trial cycling position on muscle activation patterns, crank torques and physiological measures under submaximal intensity. The results showed that peak crank torque increased and occurred later during the pedal revolution. This is closely related with the significantly later onset and shorter duration found for the GMax when lowering the torso and the later offset of the main burst in the VL. Furthermore, a significant increase in all measured physiological variables were observed when lowering the torso angle and hence a decrease in gross efficiency.

This research showed that for the muscles crossing the hip (e.g. RF, BF and GMax), altering torso angle position only changes the muscle activation of the monoarticular GMax muscle, whilst no difference were observed in the biarticular muscles RF and BF. It has been shown by Li and Caldwell (1998) that the monoarticular muscles show a greater effect in muscle activity when changing position (seating to standing) than the biarticular muscles.

**Table 4.1 Torque and physiological variables measured at a fixed cadence of 85 rpm. All torque measurements and physiological data were averaged over the final minute of the exercise bout (n=21).**

| Torso angle | β=16° | β=8° | β=0° |
|---|---|---|---|
| $T_{delta}$ (Nm) | 40.0±5.9 | 41.3±5.8 | 42.5±5.3 [a] |
| Angle $T_{maxL}$ (°) | 98.0±9.5 | 100.1±7.3 | 102.0±10.1 [a] |
| Angle $T_{maxR}$ (°) | 277.9±8.3 | 282.7±9.2 | 283.5±10.0 [a] |
| Variability (Nm) | 12.0±1.9 | 12.5±2.2 | 12.8±2.1 [b] |
| Cadence (rpm) | 85.8±1.0 | 85.9±0.8 | 85.7±1.2 |
| VE (L/min) | 90.7±12.4 | 94.6±13.9 [b] | 99.8±14.8 [b,c] |
| Bf (breaths/min) | 32.2±6.7 | 33.2±6.8 | 34.7±7 [b,c] |
| VT (L) | 2.88±0.45 | 2.90±0.40 | 2.93±0.38 |
| $VO_2$ (mL/min) | 3565±301 | 3603±309 | 3635±286 [b] |
| $VO_2$(mL/min/kg) | 47.5±4.4 | 48.0±4.6 | 48.4±4.0 [b] |
| GE (%) | 21.1±1.2 | 20.9±1.1 [a] | 20.6±1.2 [b] |

*$T_{delta}$, difference between the maximal and minimum torque during the pedal revolution; Angle $T_{maxL,}$ crank angle that corresponds with the maximal torque in left leg down stroke; Angle $T_{maxR,}$ crank angle that corresponds with the maximal torque in right leg down stroke; Variability, standard deviation of the torque profile over all pedal strokes; VE, minute ventilation; Bf, breathing frequency; VT, tidal volume; $VO_2$, oxygen consumption; GE, gross efficiency*

[a] different from 16° degrees torso angle position, $p<0.05$
[b] different from 16° torso angle position, $p<0.01$
[c] different from 8° torso angle position, $p<0.05$

Moreover, the EMG activity level as percentage of their isometric maximal voluntary contraction tend to be lower in biarticular muscles compared to monoarticular muscles (Ericson, 1986). Our results are in line with the latter statements which could provide an explanation for the non-significant findings in the biarticular muscles crossing the hip. The results from the knee muscles showed that only the monoarticular VL muscle timing was

affected by torso angle changes whilst the biarticular muscles acting on the knee remained unchanged. The ankle flexor and extensor activation were also not altered due to position changes. These results are in agreement with previous literature (Chapman et al., 2008, Dorel et al., 2009) and support the notion that muscle coordination patterns of the distal leg segments are very stable.

The peak crank torque and timing changed whilst altering position. There are a limited number of studies investigating the effect of cycling position on pedal forces and crank torques (Brown et al., 1996, Dorel et al., 2009). To the best knowledge of the authors, only Dorel et al. (2009) investigated pedal forces in different ecological cycling positions. Whilst the analysed positions are not comparable, our findings are similar with their results showing an increased down stroke peak torque and a later occurrence of this peak torque in the pedal stroke when lowering torso position.

The EMG data demonstrates that the increased crank torque $T_{delta}$ could be explained by the timing changes in the knee extensor VL and hip extensor GMax. Whilst the EMG activation of the VL is directly related to the crank torques, there is no such direct relationship for the GMax as torso angle affects its length. However, the later onset in both the crank torque and GMax suggests that the cyclists changed their pedalling technique during the down stroke pedal phase in different time trial positions.

This study showed that small torso angles elicit an increase in metabolic cost in submaximal conditions. There are several factors that can explain the underlying mechanism of the detriment in physiological responses. Firstly, the observed crank torque changes could have contributed to the increased energetic costs. Secondly, it is hypothesized by several researchers that changing torso angle positions elicit changes in muscles length, predominantly in the muscles crossing the hip (Ashe et al., 2003, Dorel et al., 2009, Savelberg

et al., 2003, Too, 1990). Savelberg et al. (2003) have demonstrated that the length of these muscles changes by about 3 – 4 % when lowering the torso angle by 20° from a fully vertical upright cycling position. When lowering the torso, the RF shortens whilst the BF and GMax lengthen, hence likely affecting the length-force relationship of the muscles and cycling efficiency (Too, 1990). Although the actual angles tested by Savelberg et al. (2003) are larger than in the present study, nevertheless the principle should still apply and potentially explain the results found here. Increased activation of other muscles not examined in this study, could have also contributed to the increased oxygen consumption. Another explanation for the detriment in physiological responses could be the restricted movement of the diaphragm in low positions (Ashe et al., 2003). Although in this study increases were observed in the Bf and VE, the tidal volume was unaffected by position changes. Likewise, Berry et al. (1994) showed that the lung volume and lung capacity between an upright and time trial position are not significantly different. Franke et al. (1994) also revealed no differences in the central haemodynamic responses between these positions. However, rather large time trial torso angles positions were examined in the two aforementioned studies. Craig (1960) on the other hand, demonstrated that the respiratory reserve volume significantly increased when changing from a sitting position to a leaned forward sitting position. This suggests that increased expiratory changes are likely to be more noticeable at higher cycling intensities, and further research targeting specifically this level of intensity should be conducted. Besides the aforementioned factors, the increased pressure on the shoulders and neck could affect the increase in physiology responses (Gnehm et al., 1997), but will more likely play a major role in the cycling comfort than in the neuromuscular and cardiovascular functions. Finally, greater adductor activation (Gnehm et al., 1997) and altered cardiovascular responses (Gnehm et al., 1997) could also likely have a small effect on the physiological performance.

The study was limited to alterations in torso angle positions, whilst keeping the saddle position constant. By setting the saddle position in the participants' preferred position, all relationships between the different parts of the bike were inherently taken into account. However, to reduce aerodynamic drag, time trial cyclists and triathletes commonly move their saddle up and forward (Burke and Pruitt, 2003, de Vey Mestdagh, 1998). It has been shown that a forward seat position and steep seat tube angle could also reduce the oxygen consumption (Heil et al., 1995, Price and Donne, 1997) and improve gross efficiency (Price and Donne, 1997). As all participants were time trial cyclists and triathletes, they were already using relatively large seat tube angle (77.1°±2.0°). Increasing the seat tube angle for these cyclists will likely have a small effect on the metabolic costs.

## 4.5 Perspectives

This study demonstrated that lowering torso angle results in a small but significant increase in crank torque and a significant decrease in cycling efficiency. The 2 % increase in metabolic costs when lowering position will likely result in a reduction of power output of about 2 – 3 %. On the other hand, lowering torso angle effectively reduces the frontal area. The projected frontal area of 8 participants has been assessed by analysing photographs in the 3 different cycling positions according to the method of Barelle et al. (2010). From this data, the frontal area is estimated to be reduced by about 10 % when lowering the time trial torso angle position from 16° to 0°. As the frontal area has been shown to provide a reasonable estimate of the aerodynamic drag (Debraux et al., 2011), it could be suggested that the aerodynamic advantage outweigh the metabolic costs at the investigated cycling intensity. The mean cycling intensity of 276 W used in this study corresponds to a cycling velocity of about 38 km/h in the 16° time trial position. Based on mathematical performance models it could be

estimated that at this cycling intensity, the 40km time would be reduced by approximately 91s when lowering position (Fintelman et al., 2014c, Martin et al., 2006). It should be noted that lowering torso angle position significantly reduces maximal power output and efficiency (Gnehm et al., 1997, Jobson et al., 2008, Fintelman et al., 2015) and therefore a small torso angle position might not be the optimal position.

As in many studies, the cyclists here were exposed to an acute change in position. It is possible that some of the detrimental effects of a lower position can be attenuated via training. Therefore, how cyclists adapt through training to lower torso angle should be investigated. Similarly, it is not clear how changes in time trial position interact with fatigue.

## Acknowledgements

The authors would like to thank C. Milton and D. Onions for their help in the data collection. The authors gratefully acknowledge also the use of the facilities and equipment of the HI Performance Centre at the University of Birmingham SPORT, UK.

# CHAPTER 5

# Optimisation of position

**Abstract** [1]

The aerodynamic drag of a cyclist in time trial position is strongly influenced by the torso angle. Whilst decreasing the torso angle reduces the drag, it limits the physiological functioning of the cyclist. Therefore the aims of this study were to predict the optimal time trial cycling position as function of the cycling speed and to determine at which speed the aerodynamic power losses start to dominate. Two models were developed to determine the optimal torso angle: a 'Metabolic Energy Model' and a 'Power Output Model'. The Metabolic Energy Model minimised the required cycling energy expenditure, whilst the Power Output Model maximised the cyclists' power output. The input parameters were experimentally collected from 19 time trial cyclists at different torso angle positions (0 - 24°). The results showed that for both models, the optimal torso angle depends strongly on the cycling speed, with decreasing torso angles at increasing speeds. The aerodynamic losses outweigh the power losses at cycling speeds above 46 km/h. However, a fully horizontal torso is not optimal. For speeds below 30 km/h, it is beneficial to ride in a more upright time trial position. The two model outputs were not completely similar, due to the different model approaches. The Metabolic Energy Model could be applied for endurance events, whilst the

[1] This chapter has been published as: Optimal cycling time trial position models: aerodynamics versus power output and metabolic energy. *Journal of Biomechanics* (2013), 47 (8), 1894-1898.

Power Output Model is more suitable in sprinting or in variable conditions (wind, undulating course, etc.). It is suggested that despite some limitations, the models give valuable information about improving the cycling performance by optimising the time trial cycling position.

## 5.1 Introduction

In order to minimise the aerodynamic drag, cyclists adopt a time trial position (often called the 'aerodynamic position'). The time trial handlebars allow the rider to adopt this aerodynamic position, resulting in a decreased frontal area and hence aerodynamic drag experienced by the rider. A reduction in aerodynamic drag of approximately 35 % is found between an upright position and a time trial position (Hennekam, 1990). In addition, Underwood et al. (2011) showed with wind tunnel experiments that in a time trial position the total aerodynamic drag is strongly influenced by the torso angle. A difference in drag area of approximately 16 % was found for torso angles between 2° - 20°. Moreover, Garcia-Lopez et al. (2009) showed a significant decrease in aerodynamic drag of about 14 % when the height of the time trial handlebars was lowered. Kyle and Burke (2003) also stated that in general the aerodynamic drag is minimal with an almost flat back. From these findings it can be concluded that cyclists should adopt an almost flat (0°) torso angle position to minimise the aerodynamic drag.

However, along with the drag the cyclists' peak power output decreases with lower torso angle (Gnehm et al., 1997, Grappe et al., 1997, Jobson et al., 2008, Fintelman et al., 2013). For instance a reduction of 14 % peak power output was recorded between an upright (24°) and flat (0°) torso angle time trial position (Fintelman et al., 2013). It is suggested by Dorel et al. (2009) that this peak power output reduction could be related to: (1) muscles not working

in their optimal range, (2) a difference in muscle recruitment, (3) greater muscular fatigue, (4) increased pressure on shoulder griddle, neck and arms, (5) increased adductor activation to keep the leg movement in the sagittal plane due to the extreme hip angles, or a combination of these factors. These experiments imply that cyclists should not adopt an almost flat position.

Clearly there are two conflicting constraints, with aerodynamics requiring a flat position and biomechanics favouring a more upright position. Therefore it can be inferred that combining the results obtained for aerodynamic drag and peak power in different time trial positions, a trade-off can be found between the loss in power output and drag as function of cycling speed. This is supported by the energy expenditure (*IE*) which is a function of the workload divided by the gross efficiency ($\eta$). The workload to overcome drag decreases with smaller torso angles, whilst also the $\eta$ decreases.

In previous literature (Gnehm et al., 1997, Jeukendrup and Martin, 2001, Lukes et al., 2005), suggestions have been made that the aerodynamic gains outweigh the loss in peak power output for time trial cyclists. However, these statements are based on elite time trial cycling speeds, e.g. > 45 km/h (Gnehm et al., 1997). Contrary, Underwood et al. (2011) have estimated the optimal cycling position for a relative wind speed of 40 km/h in terms of power output performance and aerodynamic losses. They introduced a new method to analyse the optimal cycling position, the so-called 'surplus power'. The surplus power was defined as the maximal power output of the cyclist minus the aerodynamic power losses and rolling resistance of the tires with the road. In their study, no consistent results about the optimal position were found, which could be due to the limited number of participants (n=3). Nevertheless, they have demonstrated the existence of an optimal torso angle at cycling speeds of 40 km/h. To the best knowledge of the authors, the speed of the cyclist at which the aerodynamic power loss starts to dominate has not been defined. Therefore the aims of this

investigation were to predict the optimal time trial cycling position as function of the cycling speed and to determine at which cycling speed the aerodynamic power losses starts to dominate. It has been hypothesized that an optimal torso angle exists for each cycling speed and type of event. In the presented work, the torso angle of non-elite cyclists are optimised by using two mathematical models.

## 5.2 Method

Two models were developed to determine the optimal torso angle cycling position for a certain cycling speed: the 'Metabolic Energy Model' and the 'Power Output Model'. The Metabolic Energy Model minimised the required cycling energy, whilst the Power Output Model maximised the surplus power. The inputs for the models came from experimental data of 19 participants in different torso angle positions, $\beta$, from 0 – 24° relative to the ground (Figure 5.1). Main input parameters were the cycling speeds ranging between 28 – 40 km/h with increments of 1 km/h and torso angle positions with increments of 0.1°. Output of the models was the optimal torso angle position as function of cycling speed.


**Figure 5.1 Definition of torso angle β and shoulder angle α. The torso angles analysed were 0,8,16 and 24° relative to the ground, whilst the shoulder angle remained constant. The head position can affect the aerodynamic drag (Lukes et al., 2005). However, for obvious safety reasons cyclists have to maintain their head upright and therefore the current model assumes this position is adopted.**

### 5.2.1 Mathematical models

#### *5.2.1.1Fundamental principles*

During cycling on a flat road, the two main factors of resistance are aerodynamic drag and friction of the wheels with the road. The amount of power loss, $P_{loss}$, can be estimated by the summation of the aerodynamic drag power losses of the cyclist, $P_{air}$, and the roll resistance power losses of the wheels, $P_{roll}$:

$$P_{loss} = P_{air} + P_{roll} \ . \tag{5.1}$$

The aerodynamic power losses are defined by:

$$P_{air} = \frac{1}{2}\rho A C_d v^3 \ , \tag{5.2}$$

where $\rho$ the air density, $A$ the total frontal area of the cyclist and bicycle, $C_d$ the drag coefficient, and $v$ the speed of the cyclist relative to the wind. The roll resistance power losses are defined by:

$$P_{roll} = \mu m g v \ , \tag{5.3}$$

where $\mu$ the roll friction coefficient, $m$ the mass of the bicycle and cyclist and $g$ the acceleration due to gravity (9.81 m/s$^2$).

#### *5.2.1.2 Models*

*Metabolic Energy Model* The Metabolic Energy Model minimised the energy expenditure of the cyclist for a given speed. A schematic block scheme of the model is shown in Figure 5.2. In the first step, the cyclists' power loss was calculated by using equations 1-3, for every degree torso angle between 0 – 24° at a given initial speed and under the given assumptions. Input parameters were the torso angle, cycling speed, mass and frontal area of the individual cyclist. In the second step it was assumed that the cyclist power losses due to drag and rolling

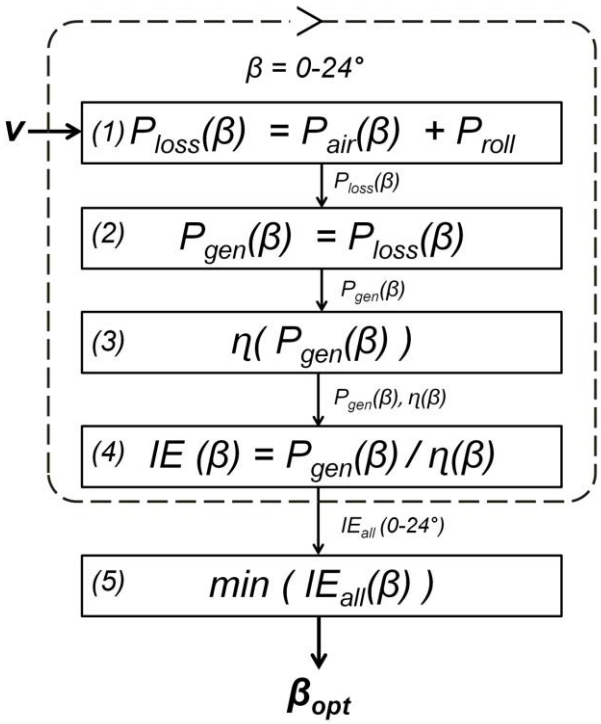


**Figure 5.2 Metabolic Energy Model step diagram to calculate optimal cycling torso angle as function of the cycling speed.**

resistance were equal to the required power generation of the cyclist, hence constant speed assumed. This was followed by model step 3, in which for the calculated power generation, the gross efficiency, $\eta$, was determined. From the gross efficiency, the corresponding energy expenditure (*IE*) of the cyclist was obtained in step 4. Model steps 1-4 were repeated for all different torso angle positions of the cyclist in the range between 0 – 24°. Finally, the optimal torso angle, $\beta_{opt,}$ which has the lowest energy expenditure for each given cycling speed, was determined in step 5.

*Power Output Model* This model maximised the amount of additional power the participant has available, which could be used for example to accelerate. This so called surplus power is the remainder of the peak power output (*PPO)* in a position with a particular torso angle

minus the losses due to the roll resistance and drag in that position, as previous defined by Underwood (2011):

$$P_{surplus} = P_{PPO} - P_{loss} \, . \tag{5.4}$$

In Figure 5.3, the Power Output Model block scheme is shown. Firstly, the power loss for a given speed in one of the different torso angle positions (0 - 24°) was calculated by using equations 1-3. This was followed by calculating the surplus power in step 2, in which the calculated power losses were subtracted from the recorded *PPO* of the individual cyclist in the corresponding torso angle position (Eq. 6). Model steps 1 and 2 were repeated for all different torso angles ranging between 0 – 24°. Finally the optimal torso angle position, $\beta_{opt,}$ of the individual cyclist corresponding to the maximal surplus power was determined for each given speed in step 3. It should be noted that only cycling speeds with a positive surplus power for all different torso angle positions were analysed.

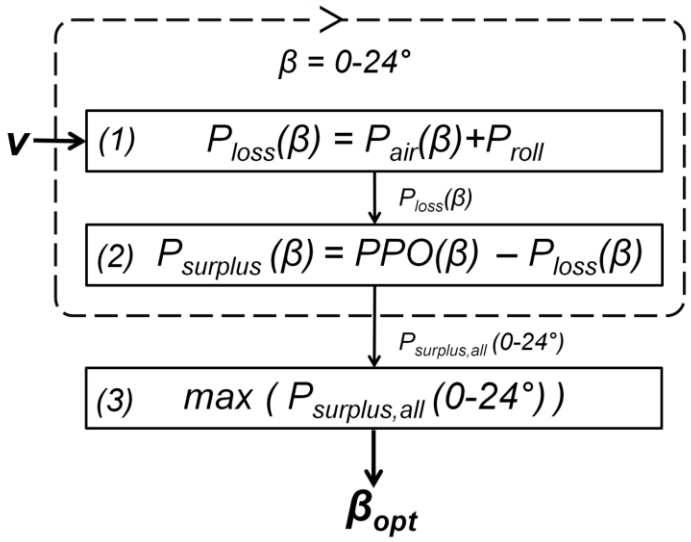


**Figure 5.3 Power Output Model step diagram to calculate optimal cycling torso angle as function of the cycling speed.**

#### *5.2.1.3 Implementation*

Both models have been implemented in the commercial software package MATLAB 7.5.0 (MATLAB, The MathWorks Inc., Natick, MA). For each participant the optimal torso angle was determined for every km/h in the range of 28 - 40 km/h. The optimal torso angles of all participants for each speed were averaged. The cycling speed range was restricted by the maximal power output of the participants. Therefore, outside the 28 - 40 km/h range the data was extrapolated based on the experimental data, to obtain a speed range of 18 - 50 km/h. No centripetal forces, acceleration forces or gravitational forces due to uphill or downhill cycling were implemented. This implies the assumption that the cyclist is riding on a flat course, in a straight line and does not accelerate. Also bearing and drive train friction were not implemented, as it accounts only for 1 - 2 % of the total power output (Martin et al., 1998), which was within the workload accuracy of the ergometer. In addition, no wind was acting on the cyclist in the models. Consequently, the speed of the cyclist relative to the wind equals the cycling speed. As a result, all mentioned speeds in this paper could be considered as cycling speeds. Nevertheless, the models are still applicable for head and tail wind, where the relative speed of the cyclist respectively decreases or increases. Contrary, crosswind effects cannot be predicted, as both the relative wind speed and the drag area are altered.

#### *5.2.1.4 Model input*

The *PPO* was calculated for every cyclist. The gross efficiency values, $\eta$, of each individual cyclist were interpolated to power and torso angle increments of respectively 1 W and 0.1° torso angle. The $P_{loss}$ was interpolated to obtain a value for every 0.1°. Finally a moving average filter with a window of 10 samples was applied, to avoid model optimisation to the

measured torso angle positions. The total frontal area was the sum of the frontal area of the cyclist, time trial bicycle and helmet. The frontal area of the isolated cyclist was estimated by using frontal view photographs in all different torso angle positions. The photos were analysed following the method of Barelle et al. (2010). To account for the time trial bicycle and helmet frontal area, 0.086 $m^2$ was added to the frontal area of the cyclist. The additional frontal area was calculated by taking photographs of an isolated bike and cyclists with and without a time trial helmet in all torso angle positions. There was a significant correlation between torso angle and the frontal area ($r = 0.600$, $p < .0001$). The total mass included contributions of the cyclist, shoes and time trial bicycle. The weight of each individual cyclist was taken and 8 kg was added to account for the shoes and time trial bicycle. A rolling resistance coefficient, $\mu$, of 0.002 (Kyle, 2003) was applied, representing riding on smooth asphalt. It was assumed that the friction coefficient remains constant, irrespectively of the cycling speed. The air density, $\rho$, was set to 1.205 $kg/m^3$, representing air at 20°C at sea level. A constant $C_d$ value of 0.86 (Chowdhury and Alam, 2012) was used, independently of the shape and roughness of the cyclist or the cycling speed.

### 5.2.2 Experimental data collection

Nineteen healthy male trained competitive triathletes and cyclists, aged between 21 - 52 years participated in the study. The main participants' characteristics are shown in Table 5.1. All participants completed 4 identical incremental tests on a bicycle ergometer (Lode Excalibur Sport, Lode BV, Groningen, The Netherlands) with time trial handlebars (Profile Design Carbon Stryke, Long Beach, United States). The test started with an intensity of 95W and increased with 35 W every 3 minutes till exhaustion. The distance between the handlebars (10 ± 1 cm) was replicated from the cyclists' bicycle. The tests were performed in 4 different torso angle positions, $\beta$: 0, 8, 16 and 24° relative to the ground (Figure 5.1). The torso angle

was measured with a digital inclinometer (Fisco EN17, Ficso Tools Limited, Essex, Uk) with an accuracy of 0.1 degree and attached to a 1m stick. The inclinometer was placed on the centre of rotation of the glenohumeral axis and the greater throchanter. The shoulder angle, *a*, was measured from the cyclists' preferred position and remained constant in all sessions. All participants performed regularly cycling exercise with time trial handlebars. The study was approved by the University of Birmingham's Science, Technology, Engineering and Mathematics ethics committee (ERN_12-1223) and participants gave written informed consent at the beginning of the study. The torso angle, power output, oxygen consumption, carbon dioxide exhaled and respiratory exchange ratio (*RER*) were measured throughout the session. At the end of each session a frontal photograph was taken. From the data the gross efficiency, $\eta$ ,was calculated by the formula of Garby and Astrup (1987) and only determined until the *RER* exceeded 1.00.

**Table 5.1 Participant characteristics (mean ± std). Torso length was measured from the centre of rotation of the glenohumeral axis to the centre of rotation of the greater throchanter. The saddle height is the vertical distance between the bottom bracket and the top of the saddle. The torso angle, shoulder angle and Peak Power Output were measured in the participants' preferred cycling position (n=19).**

| | Value |
|---|---|
| Age (yr) | 34.8 ± 10.7 |
| Height (cm) | 181.3 ± 6.0 |
| Weight (kg) | 74.3 ± 8.0 |
| Torso length (cm) | 47.5 ± 3.3 |
| Frontal area cyclist at β=0° ($m^2$) | 0.287 ± 0.024 |
| Saddle height (cm) | 79.0 ± 3.7 |
| Preferred torso angle, β (°) | 11.9 ± 5.6 |
| Shoulder angle, α (°) | 90.7 ± 5.3 |
| Peak Power Output (W) | 354.1 ± 36.5 |

## 5.3 Results

### 5.3.1 Models outcome

Two different models were used to predict the optimal torso angle, $\beta_{opt}$. The optimal torso angle was determined for torso angles between 0-24°. In Figure 5.4 the results of both models and the corresponding confidence intervals (significance level p=.05) for non-elite time trial cyclists are shown for speed between 28-40 km/h. Outside this range, the torso angle was predicted based on extrapolation of the experimental data. It could be seen that the optimal torso angle is dependent on the cycling speed, with torso angle decreasing with increasing speed. Nevertheless, a fully horizontal torso is not optimal. For speeds above 45 km/h, the drag outweighs the power losses. The Power Output Model curve was shifted to a higher speed compared to the Metabolic Energy Model. The Metabolic Energy Model showed a decreased optimal torso angle if the speed of the cyclist increased from approximately 22° at 28 km/h, up to 4° at 40 km/h. The optimal torso angle in the Power Output Model was almost constant in the 28-40 km/h speed range. For speeds between 32-39 km/h a torso angle of approximately 17° was found to be optimal, whilst above 46 km/h the aerodynamic losses outweigh the power losses resulting in an optimal torso angle of 3°. A two-way repeated measures ANOVA examining the effect of cycling speed and model type on the optimal torso angle was conducted. In all statistical tests the significance level was set to p = .05.There was a statistically significant interaction between the speed and the model type on the optimal torso angle within the subjects $F(4,72)= 23.22$, $p<.0001$. A multiple regression was performed to predict optimal torso angle from a group of anthropometric variables of each participant for cycling speeds between 28-40 km/h, with increments of 3 km/h. Variables included were torso length, weight, height and frontal area. For the Metabolic Energy Model, only the frontal area significantly predicted the torso angle for speeds of 28 and 31 km/h ($F(1,17)=9.41$

p= .007 $R^2$=.318 and F(1,17)=3.27 p= .088 $R^2$=.112). In the Power Output Model analysis, the power output difference between the 24° and 0° torso angle position was added and resulted in the best predictor ($R^2$ between .321-.492, p<.01).

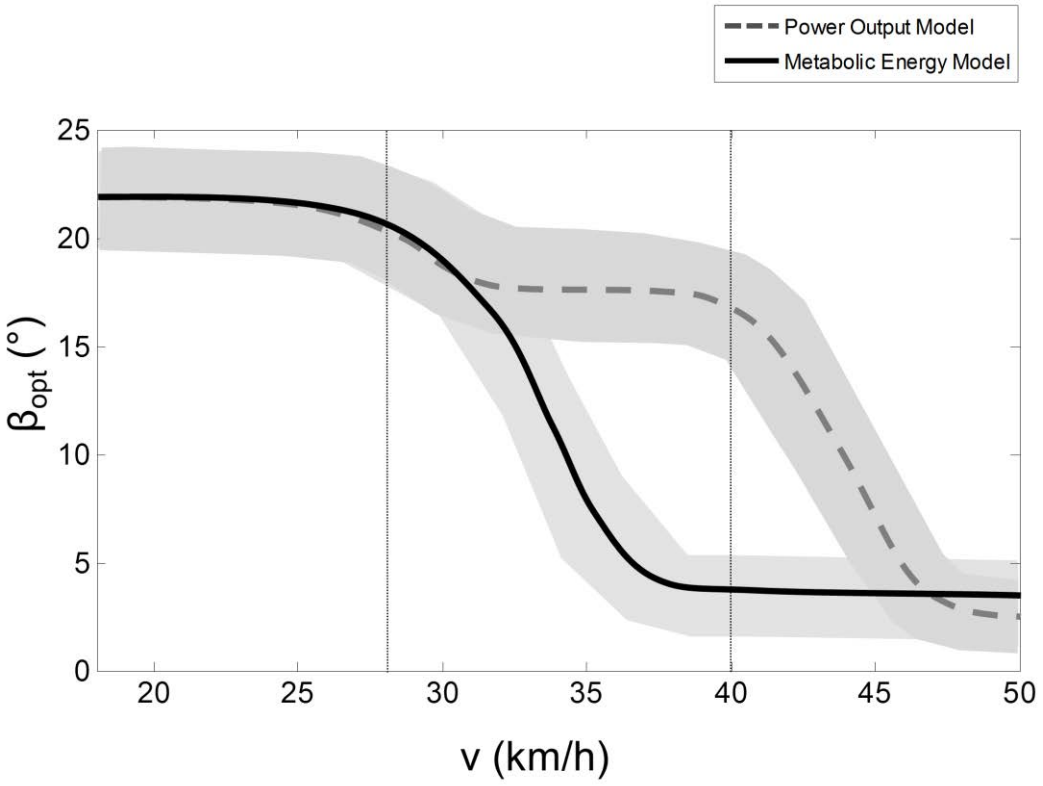


**Figure 5.4 Optimal torso angle as function of cycling speed with confidence levels with a significance level set on p=.05. For speeds between 28 and 40 km/h the optimal torso angle curves as function of cycling speed is based on the Power Output Model and Metabolic Energy Model. Outside this range, the optimal torso angle positions are predicted based on extrapolation of the experimental data.**

### 5.3.2 Experimental data

The mean of the recorded maximal power output of the participants in the 0° and 24° torso angles were 318 W and 369 W respectively. The reduction in *PPO* was found to be approximately 14 % (51 W). The calculated power losses due to aerodynamic drag and rolling friction of the wheels on the road for speeds between 28 - 40 km/h are shown in Table 5.2. For the extreme torso angles, 0° and 24°, the power loss differences were calculated for each speed. The absolute differences between the losses in these two extreme positions are shown in Table 5.3.

**Table 5.2. Mean and standard deviation of the power losses at different speeds ranging between 28 - 40 km/h and in different torso angle positions (0-24°) of all participants (n=19). The power losses included contributions of the aerodynamic drag and road friction power losses of each individual participant.**

| Power losses (W) | Cycling speed (km/h) | | | | | | |
|---|---|---|---|---|---|---|---|
| | 28 | 30 | 32 | 34 | 36 | 38 | 40 |
| $P_{loss(0°)}$ | 103.7±6.8 | 125.5±8.2 | 150.3±9.8 | 178.4±11.5 | 209.8±13.5 | 244.8±15.8 | 283.5±18.2 |
| $P_{loss(8°)}$ | 107.2±6.0 | 129.9±7.2 | 155.6±8.6 | 184.7±10.2 | 217.3±11.9 | 253.6±13.9 | 293.9±16.0 |
| $P_{loss(16°)}$ | 110.7±7.2 | 134.2±8.7 | 160.9±10.4 | 191.0±12.3 | 224.8±14.5 | 262.4±16.9 | 304.1±19.5 |
| $P_{loss(24°)}$ | 115.2±7.3 | 139.7±8.8 | 167.6±10.5 | 199.1±12.4 | 234.4±14.6 | 273.7±17.0 | 317.3±19.7 |

**Table 5.3 Mean and standard deviation of the absolute difference of the calculated mean of the power losses in two time trial torso angle positions at different speeds of all participants, i.e. 0 and 24°(n=19). The total power losses are the total of the aerodynamic drag and road friction power losses.**

| Cycling speed (km/h) | 28 | 30 | 32 | 34 | 36 | 38 | 40 |
|---|---|---|---|---|---|---|---|
| $\Delta P_{loss(0°, 24°)}$ (W) | 11.6±2.9 | 14.2± 3.6 | 17.3±4.3 | 20.7±5.2 | 24.6±6.1 | 28.9±7.2 | 33.7±8.4 |

## 5.4 Discussion

Two models were developed to predict the optimal torso angle position at different cycling speeds: the Metabolic Energy Model and the Power Output Model. The results showed that the optimal torso angle depends strongly on the cycling speed, with decreasing torso angles at increasing speeds. However, a fully horizontal back is not optimal. At speeds above 46 km/h, the aerodynamic losses outweigh the power output losses, which is in line with previous literature (Gnehm et al., 1997, Jeukendrup and Martin, 2001, Lukes et al., 2005) .The Power Output Model and Metabolic Energy Models outputs were not similar. This is not surprising as the fundamental principles underpinning these two models are different. The model type application depends on the type of event. The Power Output Model is more relevant if a

cyclist is cycling in a short distance event or need to have additional power available to accelerate, cycle up-hill or is subjected to head or side wind. In these situations, the energy consumption is less dominant. However, the optimal cycling position based on Metabolic Energy Model is more relevant for long distance races. If a cyclist is more efficient, they will save energy which can be used later during the race for like sprinting, change in wind conditions or overall higher performance. If for instance the energy saved riding at 36 km/h in a 3° crouched position compared to a 16° upright position will be used to increase the cycling speed in the crouched position, a time saving of about 3 minutes will be experienced in case of a 40 km time trial under windless conditions. In conclusion, for speeds between 32-40 km/h in an endurance event it is advisable to lower the torso despite the fact that the power output in a more aerodynamic position is decreased. In contrast, in sprinting or in variable conditions (wind, undulating course, etc) at these speeds it is more beneficial to ride in a more upright time trial position.

Although the models provide a practical general prediction of the optimal torso angle, the authors acknowledge that there are individual differences between the optimal torso angle predictions. Individual differences in position optimisation were also found in the study of Underwood et al. (2011). The multiple regressions analysis has shown that all analysed anthropometric parameters inadequately predict the optimal torso angle. This might be a result of the homogeneity of the participant group. On the other hand, there is no evidence that our sample was not representative of the time trial population. Besides participant differences, training in a lower torso angle position can have a positive effect on the power output and Oxygen consumption (Peveler et al., 2005, Heil et al., 1997). However, it has been shown that when cyclists adopt more extreme torso angle positions (in particular close to 0°), the physiological performance significantly drops independently of the cyclists' training position

(Fintelman et al., 2013). To investigate the effect of training on the cycling performance, all participants performed one additional incremental test in their preferred position. These experiments demonstrated that in general the participants' maximal power output did not correspond to the cyclists preferred position. Although no training effect was observed in this study, it is possible that training at lower torso angle positions could slightly improve the power output (Jeukendrup and Martin, 2001, Peveler et al., 2005). In particular for cyclists with a relatively large preferred torso angle, the optimal torso angle might decrease at lower speeds. Nonetheless, it can be concluded that anthropometrical differences and training will only have a small effect on the optimal torso angle model predictions.

In the models a constant $C_d$ value was estimated for all participants. It should be noted that the selection of $C_d$ affects the location of the large torso angle decrease in the model output. In previous literature, the drag coefficient in the time trial position has been reported in the range of 0.63 - 0.99 (García-López et al., 2008, Underwood et al., 2011, Chowdhury et al., 2011). It has been shown that the $C_d$value is not constant and the variations complex, which could explain the variation in $C_d$ values between different studies and therefore difficult to estimate. In this study only the handlebar height was alternated, whilst the shoulder angle and position of the hands were kept constant. Therefore it could be considered that only a small variation in the flow structures and therefore $C_d$values exists between the different torso angles. Still, these deductions have to be tested either experimentally or numerically by using Fluid Dynamic Simulations.

In conclusion, two models were developed to determine the optimal cycling position as function of cycling speed. A trade-off between the aerodynamic performance and power output is shown. For speeds above 46 km/h the aerodynamic power losses dominates. For lower speeds, the optimal torso angle is dependent on the cycling event. The presented models

can be used to advise non-elite cyclists about the optimal torso angle time trial position, taking into account aerodynamics and physiology. Future research should attempt to implement the effect of side wind.

# CHAPTER 6

# Crosswinds: Experimental Study

**Abstract** [1]

The aims of this research were to firstly investigate the effect of crosswinds on the aerodynamic behaviour of cyclists and secondly, to determine which parameters (cyclist position and bike type) influenced the aerodynamic forces on cyclists the most. The aerodynamic response of two different full-scale bikes with and without a mannequin has been recorded for a variety of crosswind angles ranging from $0^o$ – $90^o$ (in $15^o$ increments). The results showed that the wind induced force is a function of the crosswind angle. The actual aerodynamic loads arising from such winds can be up to about 2.5 times the aerodynamic drag. It has also been observed that the torso angle has little effect on the lateral force coefficient. In contrast, the bike type significantly affects the aerodynamic forces: at large yaw angles, a road bike is responsible for approximately 60 % of the total lateral force coefficient. This study is the first step in the process of determining the effect of crosswind from a full range of angles of attack on cyclists, and will help to improve the safety of cyclists and equipment, and to define guidelines for cycling lanes.

[1] This chapter has been published as: The effect of crosswinds on cyclists: an experimental study. *Procedia Engineering* (2014), 72, 720-725.

## 6.1 Introduction

During cycling, crosswinds can have a significant impact on the performance, stability and safety of a cyclist. Even though only about 5 % of all cycling accidents are caused by crosswind, it is reported that the majority leads to severe or fatal accidents (Ryan, 2012, Schepers and Wolt, 2012). Nevertheless, there is evidence to suggest that about two-thirds of the total number casualties (slight injuries, serious injuries and fatalities) in road accidents are unreported (Transport, 2012). Despite the occurrence of fatal accidents due to crosswinds, there are limited studies investigating the aerodynamic responses of cyclists under such conditions. Current literature mainly focuses on windless environmental conditions (Chabroux et al., 2012, Gibertini et al., 2008, Lukes et al., 2005). Whilst these experiments provide important information about the aerodynamic performance of cyclists, it is a poor approximation for conditions which regularly occur. Recent studies showed that equipment has a significant effect on the aerodynamic load of a cyclist (Barry et al., 2012). However, only a limited range of yaw angles (i.e., the angle the wind makes with the cyclists direction of travel, i.e., $\beta$ in Figure 6.1) have been analysed, i.e. up to $30^{o}$. In contrast, in the rail and automotive industry a wide range of yaw angles (0 - $90^{o}$) are often considered, since it is appreciated that the worst case conditions can occur for yaw angles greater than $30^{o}$. In conclusion, although it has been suggested that crosswinds have a significant effect on the aerodynamic forces of cyclists, influencing their performance and stability, this is the first comprehensive study to provide vital information relating to cyclist stability.

## 6.2 Method

### 6.2.1. Wind tunnel

A subsonic open return wind tunnel with a cross-sectional area of 2x2 $m^2$ was used for the work outlined below. The wind speed was measured with a 3-axis ultrasonic anemometer at a sampling frequency of 10 Hz (Gill Windmaster, Gill Instruments Ltd, Lymington, UK). The turbulence intensity (i.e., the standard deviation / mean wind speed) at the edge of the wind tunnel was 0.67 %. The aerodynamic forces and moments were recorded with a multi-component piezoelectric force plate (Kistler type 9281B, Kistler Instruments, Winterthur, Switzerland) which was integrated in a custom built turntable. The wheels of the bike were connected to the force platform by means of a frame with uprights (Figure 6.1). The force plate was capable of measuring the aerodynamic forces and moments around the three axes at a sampling frequency of 1 kHz. The aerodynamic forces were repeatable to within ± 0.05 N. The coordinate system was placed in the bike reference frame and hence independent of the relative flow direction.

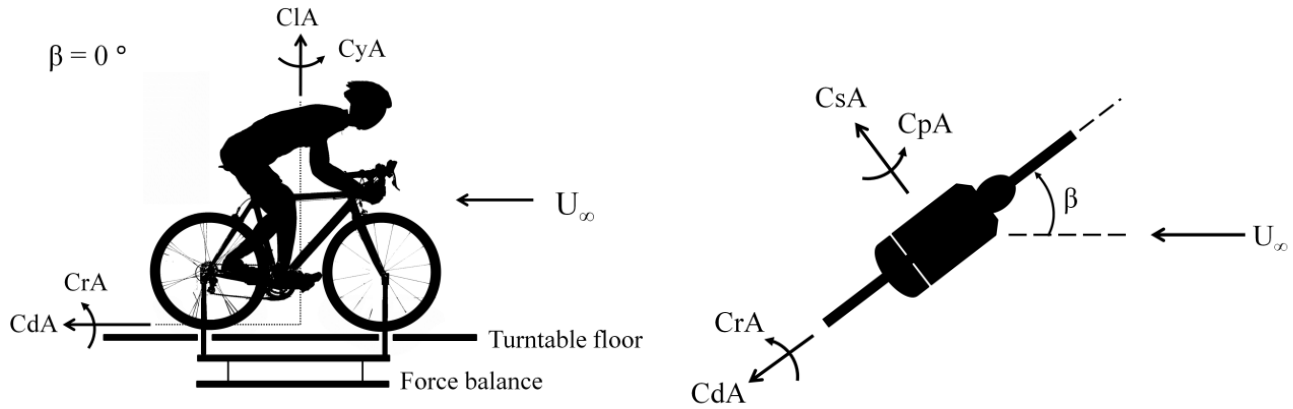


**Figure 6.1. Directions of the forces and moments: (a) side view, (b) top view.**

### 6.2.2 Aerodynamic testing

The sign convention adopted is illustrated in Figure 6.1. Yaw angles, β, of $0^o$, $15^o$, $30^o$, $45^o$, $60^o$, $75^o$ and $90^o$ were examined. Every yaw angle trial was repeated at least 3 times, determined from a confidence interval analysis with a significance level of 95 %. The total measured period was 80 seconds. The first 20 seconds allowed sufficient time for the flow in the wind tunnel to become stable. Only the final 60 seconds of the total measured data, in which the wind is steady, has been analysed. Firstly, the effect of yaw angle on the aerodynamic force coefficient at a constant wind speed has been determined. In all the experiments, a mannequin (PolyStar Man, Creatif Leven Displays Ltd, Gloucester, UK) was placed in a dropped position on a road bike (CIOCC Dragster, CIOCC ISB SRL, Bergamo, Italy) in a constant main flow velocity ($U_\infty$) of 9.91 m/s, unless otherwise stated (Figure 6.2(a)). Secondly, the individual contributions of the bike and uprights were evaluated for a range of yaw angles. Thirdly, the effect of torso angle on the aerodynamic responses at different yaw angles was measured. Two different torso angle positions were considered, i.e. $16^o$ and $24^o$ torso angle relative to the ground. In both configurations the hands were kept in the dropped position (Figure 6.2(a-b)). Finally, the aerodynamic behaviour of two isolated bikes was determined (Figure 6.2(c-d)). A road bike was compared with a time trial bike (Felt B12, Felt racing LLC, Irvine, USA) with a rear disk wheel (DT Swiss RRC, DT Swiss AG, Biel, Switzerland).

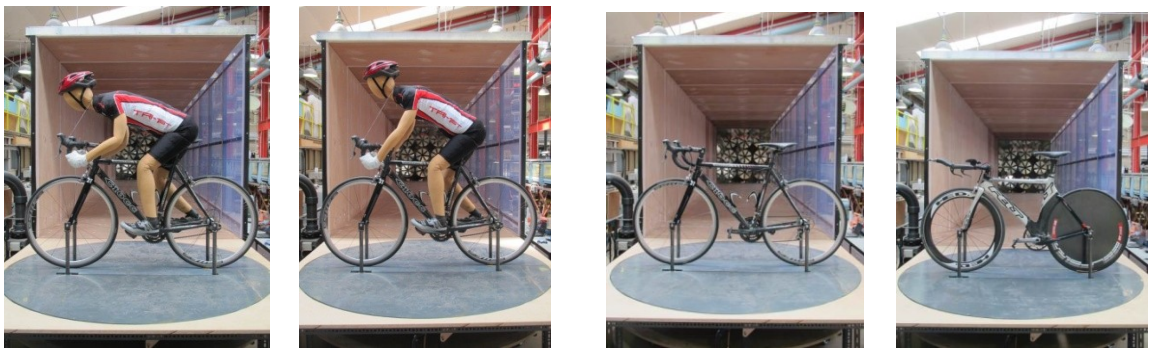

**Figure 6.2 Configurations: (a) $16^o$ torso angle position, (b) $24^o$ torso angle position, (c) road bike, (d) time trial bike.**

### 6.2.3 Data analysis

All data analysis was undertaken using Matlab (Matlab R2007B, The MathWorks Inc., Natick, USA). The recorded data was compensated for drift, calibration corrections, and two environmental variables, i.e. temperature and humidity. Finally, the data has been corrected for blockage area with the method of Mercker and Wiedemann (1996).

## 6.3 Results and Discussion

### 6.3.1 Force coefficients

In Figure 6.3 the force coefficient data relating to the mannequin and bike are shown. The data had an average standard deviation of around 0.02 $m^2$. It should be mentioned that error bars of the standard deviation are included in Figures 6.3-6.6. The side force coefficients, CsA, of the mannequin and bike increase with increasing yaw angles, whilst the opposite behaviour is noted in the drag force coefficients (CdA). The maximum side forces coefficients were more than twice the maximal drag forces coefficients. The measured lift force coefficients were small compared to both the side and drag force coefficient data. The maximal CdA was measured at $\beta = 15^o$. It should be noted that the largest gradients in CsA can be found for yaw angles up to $45^o$. The individual contributions of the uprights, bike and mannequin on the total aerodynamic force coefficients are also shown in Figure 6.3. For a pure head wind ($\beta = 0^o$) approximately 8 % of the drag is caused by the uprights and approximately 27 % of the drag coefficient is responsible for the combination of the road bike and the uprights. It is noticeable that the lift force is predominantly related to the mannequin for the majority of the yaw angles.

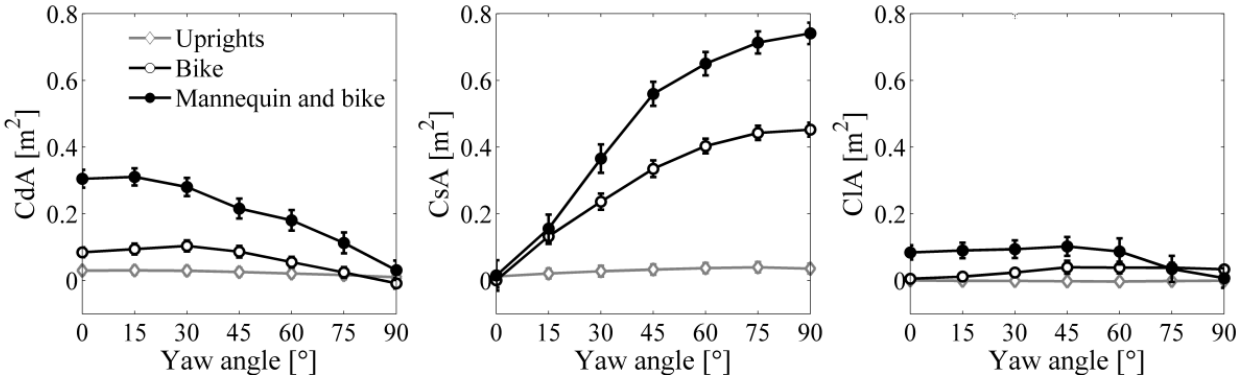


**Figure 6.3 Distribution of the aerodynamic coefficients between the uprights, bike and mannequin: (a) drag force coefficient, CdA, (b) side force coefficient CsA, (c) lift force coefficient ClA.**

At a 90$^o$ crosswind, approximately 61 % of the total side force coefficient is caused by the bike and uprights, whilst the uprights accounts for only about 5 % of the total side force coefficient. It should be noted that the use of uprights

does have a small contribution to the measured aerodynamic forces for all yaw angles.

The effects of two torso angle positions (16$^o$ and 24$^o$) on the aerodynamic responses are shown in Figure 6.4. The drag force coefficient significantly decreased with about 0.05 m$^2$ at a yaw angle of $\beta$ = 15$^o$ in a small torso angle position (16$^o$) compared to a more upright position (24$^o$). A drag force reduction up to 15 % can be experienced by lowering the torso angle. This reduction diminished with increasing torso angle. No significant difference in side and lift force coefficient was recorded between the two torso angle positions.

In Figure 6.5 the aerodynamic force coefficients acting on a time trial bike and road bike are shown. Although the drag force coefficients of a time trial bike are up to 50 % smaller (0.05 m$^2$) compared to a road bike, the side force coefficients were up to 34 % (0.15 m$^2$) higher for increasing yaw angles. The lift force coefficient on the road bike was positive with increasing angles, whilst negative for the time trial bike. Furthermore, the maximal drag force coefficient of the time trial bike is approximately 6 times smaller than the maximal side force coefficient.

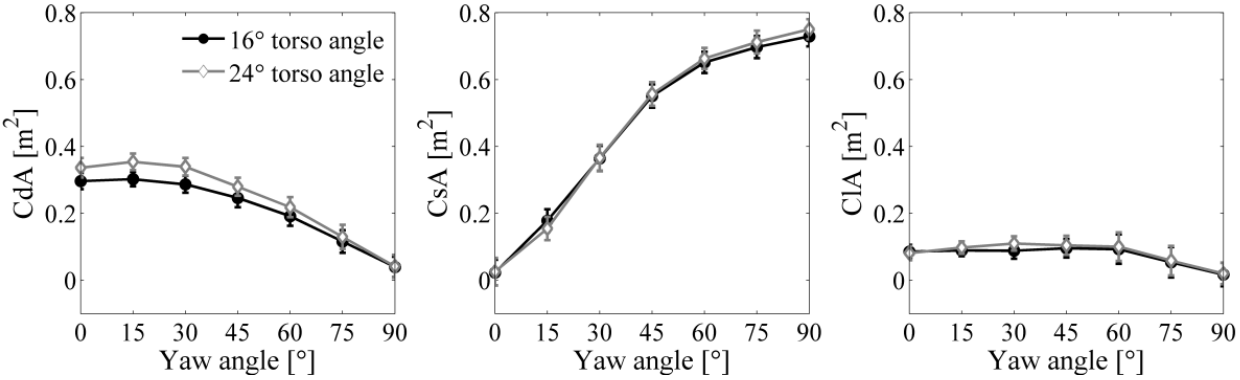


**Figure 6.4 Aerodynamic responses of the mannequin in a 16° and 24° torso angle position relative to the ground.**

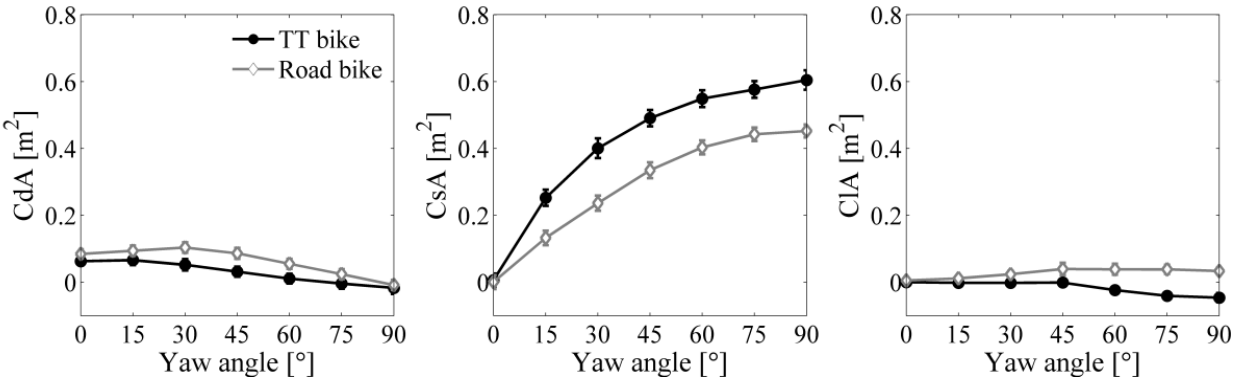


**Figure 6.5 Aerodynamic behaviour of a time trial bike and road bike at different angles of attack.**

### 6.3.2 Moment coefficients

.In Figure 6.6 the aerodynamic moment coefficients are shown. The rolling moment, CrA, increased significantly between $0^o$ and $60^o$, indicating the importance of considering the full range of yaw angles in stability analysis. The pitching moment, CpA, decreased (in absolute terms) as the yaw angle increased, whilst the maximum yawing moment is observed to occur at approximately $30^o$. The rolling moment coefficient CrA is mainly determined by the vertical moment arm of the side force. Hence, a close correlation ($p<.001$) can be seen between the CrA and side force coefficients CsA (see Figure 6.7).

The rolling moment coefficient CrA is mainly determined by the vertical moment arm of the side force. Hence, a close correlation ($p<.001$) can be seen between the CrA and side force coefficients CsA (see Figure 6.7). The corresponding phase plots show also a strong, almost

linear correlation. The behaviour observed in the CpA data is mainly determined by the vertical arm of the drag force, whilst the contribution to the yawing moment CyA is equally shared between the horizontal moment arm of the side forces and drag forces.

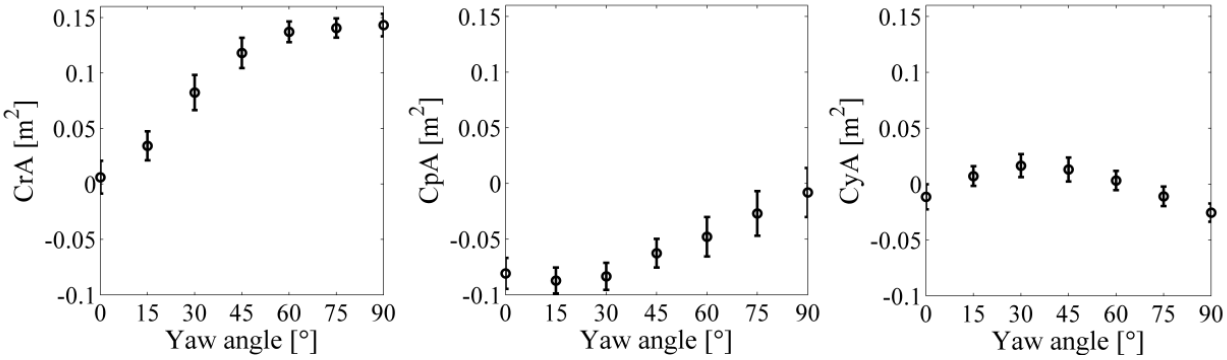


**Figure 6.6 Aerodynamic moment coefficients for different yaw angles: (a) rolling moment coefficient CrA, (b) pitching moment coefficient CpA, (c) yawing moment coefficient CyA.**

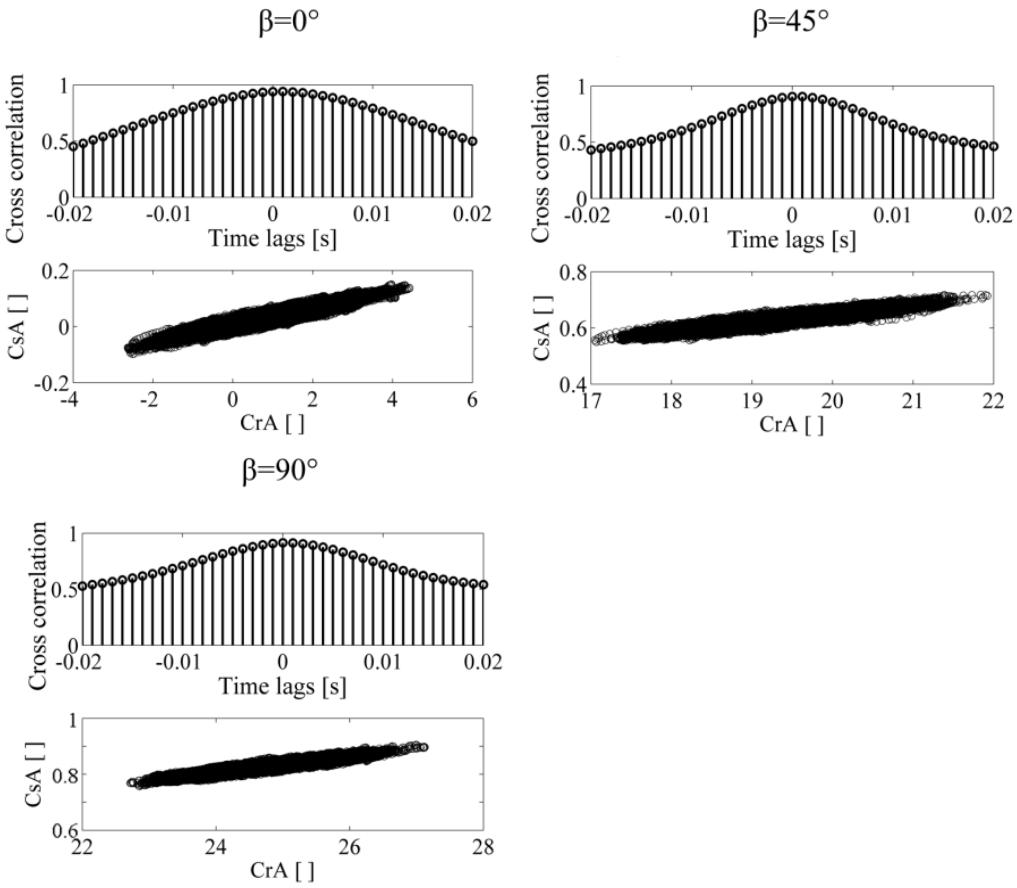


**Figure 6.7 Cross correlation and phase plot of side force coefficient CsA versus rolling moment coefficient CrA at different yaw angles (a) β = 0° ($R^2$=0.88, p<.001), (b) β = 45° ($R^2$=0.82, p<.001), (c) β = 90° ($R^2$=0.83, p<.001).**

## 6.4 Discussion

In this work, wind tunnel experiments were conducted to investigate the effect of crosswind on the aerodynamic load of cyclist. It has been shown that the aerodynamic force coefficients are strongly influenced by the yaw angle, in keeping with similar trends found in road and train vehicles studies. In general a peak lift force coefficient around $\beta = 45^{o}$ is obtained, which can be justified by the transition of a slender body to a bluff body behaviour (Bocciolone et al., 2008). However, it should be mentioned that the standard deviation of the lift forces are about 20 % of the measured data and for $\beta < 45^{o}$ the change in lift force is within the standard deviation of the data. It can be expected that the flow pattern around a cyclist differs for different angles of attack. At high yaw angles it is postulated that the aerodynamic force coefficients are influenced by the wake flow structures created by the cyclist. At these angles the wake structures on the lee side of the bike are likely to contribute strongly to both the lift and side forces. The maximum drag at low yaw angles ($\beta = 15^{o}$) can be explained by the non-aerodynamic shape and increased frontal area of the bike and mannequin.

This study also extended our knowledge on the parameters (cyclist position and bike type) that affect mostly the aerodynamic behaviour of a cyclist for an extensive range of crosswind angles. Results showed that the cyclist themselves accounts for the highest percentage of aerodynamic drag force coefficient (up to 74 % at $\beta = 0^{o}$), in line with Barry et al. (2012). Whereas previous studies investigated yaw angles up to $30^{o}$, the current study explored a wider range of yaw angles and showed that the bike has a progressively larger contribution to the total aerodynamic side forces as the yaw angle increases. When the yaw angle is 90°, up to half of the total aerodynamic side force coefficient contributes to the bike. Therefore, the side forces and corresponding rolling moments can be reduced by decreasing the side surface area of the bike. However, it is likely that this may lead to an increase in the total

aerodynamic drag force. For example, a rear disk wheel can decrease the aerodynamic drag by approximately 7 % at $\beta = 0^o$, but can also increase the aerodynamic side forces of the cyclist with about 20 % at $\beta = 90^o$ and hence may affect the safety of the cyclist. Therefore, cyclists should consider the potential risk of instability or falling by selecting their bike and wheel type depending on the wind conditions.

## 6.5 Conclusion

The effect of crosswind over a large range of yaw angles on the aerodynamic responses has been investigated. The results showed that crosswind has a significant effect on the aerodynamic forces and moments. In particular, the bike type does have a significant influence on the aerodynamic lateral load of a cyclist. A time trial bike with rear disk wheel can increase the lateral load of the cyclist up to 20 % compared to a road bike.

This study demonstrates that large crosswind yaw angles have a significant effect on the stability of the cyclist and shows the importance of the bike selection and design on the aerodynamic lateral load on a cyclist. These findings will help to improve the safety of cyclists and equipment, and to define guidelines for cycling lanes. Future analysis should attempt to gain insight of the flow pattern around a cyclist and the effect of a gust of wind on the aerodynamics and stability of cyclists by means of Computational Fluid Dynamic Simulations.

# CHAPTER 7

# Crosswinds: Numerical Study

**Abstract** [1]

For the first time, an extensive numerical study of the effect of crosswinds on the flow around a cyclist on a bicycle with stationary wheels has been undertaken for crosswind (yaw) angles ranging from $0^o$ - $90^o$. The flow field and the aerodynamic forces have been obtained using three numerical techniques: Reynolds Averaged Navier Stokes (RANS), Detached Eddy Simulation (DES) and Large Eddy Simulation (LES). RANS models have been undertaken for all the range of yaw angles to provide a general insight of the flow around a cyclist, whilst DES and LES have been undertaken at $15^o$ yaw angle in order to investigate the time-varying flow physics in detail. The aerodynamic forces have been compared with a series of wind tunnel experiments. The RANS results showed the development of large flow separation around the bicycle with increasing yaw angles. The instantaneous flow structures and the auto spectral densities of the time histories of the force coefficients are identified and revealed that the DES and LES turbulence models are able to predict the dominant frequencies found in the physical experiments. This work provides an improved understanding of the flow characteristics around a cyclist in crosswinds that will hopefully help to improve the safety of cyclists.

[1] This chapter has been published as: CFD simulations of the flow around a cyclist subjected to crosswinds. *Journal of Wind Engineering and Industrial Aerodynamics* (2015), doi: 10.1016/j.jweia.2015.05.009.

## 7.1 Introduction

Crosswinds can have an impact on the performance, stability and safety of cyclists, e.g., ~5 % of all single bicycle accidents are caused by crosswinds (Schepers and Wolt, 2012). Despite several fatalities, relatively little work has been undertaken investigating the effect of crosswinds with most numerical research focusing on minimising the overall aerodynamic drag (Defraeye et al., 2010a, Griffith et al., 2012, Hanna, 2002, Lukes et al., 2004). Two numerical cycling crosswind studies investigated the aerodynamics of isolated spoked bicycle wheels (Godo et al., 2009, Karabelas and Markatos, 2012). These studies enabled both the aerodynamic loads and flow structures around isolated bicycle wheels to be quantified. Both studies have demonstrated that the side forces acting on a spoked wheel are up to about 5 - 6 times higher than the drag forces, hence having an impact on the stability of the cyclist. However, a study by Barry et al. (2012), showed that the wheels and cyclist cannot be considered separately, due chiefly the flow interaction between them. In a numerical study reported by Hanna (2002), the full cyclist and bicycle system has been analysed. In the study a comparison has been made between disk and spoked rear wheels at different crosswind flow velocities (0-13 m/s). The side wind was positioned at a yaw angle of 90° to the cycling direction (the yaw angle is defined as the angle between the effective side wind, $U_{eff}$, and the direction of travel of the cyclist, $U_x$, as shown in Figure 7.1). The study showed that a disk wheel reduced the drag by approximately 2 % compared to spoked wheels, but in a crosswind of ~9 m/s the side forces were doubled. As the research has been conducted for the British Cycling team, details of the simulations and the results are limited and without validation precaution has to be taken about the validity of the results.

Barry et al. (2012) undertook a series of wind tunnel experiments to investigate the effect of crosswind on the bicycle system for yaw angles up to 30° and discovered that when

positioned in a time trial position, the side forces increase linearly with increasing yaw angles between 5-30°. It is found that the side forces are approximately double the drag forces at 15° yaw angle. It was also demonstrated that the wheel type, including spoked and disk wheels, has a significant effect on the aerodynamic drag and yaw moments. Although the work of Barry et al. study (2012) outlines the importance of examining crosswind at yaw angles often experienced by cyclists, it does not give real insight into the overall flow field. For many types of ground vehicles, the critical wind angle has been shown to be around 30°, such as busses (Hemida and Krajnović, 2009b, François et al., 2009), passenger cars (Ryan and Dominy, 1998) and trains (Hemida and Krajnović, 2009a, Diedrichs, 2010). For cyclists however, experimental results showed that there is no specific critical yaw angle (Fintelman et al., 2014a). It is likely that even at small crosswind yaw angles (~15°), the stability and performance of the cyclist will be influenced by crosswinds. It is however reasonable to assume that with increasing yaw angles, it becomes more difficult for cyclists to control the bicycle. Several bicycle accidents are reported as a result of crosswinds (7 News The Denver Channel, 2011, ABC News, 2012, The Guardian, 2001). The effect of crosswinds with yaw angles up to 90° has been investigated experimentally by Fintelman et al. (2014a). The results showed that the actual aerodynamic loads arising from crosswinds can be up to about 2.5 times the aerodynamic drag with spoke wheels and cyclist in dropped position. In addition, it has been observed that the torso angle of the cyclist has little effect on the side force coefficient. In contrast, the bicycle significantly affects the aerodynamic forces; at large yaw angles, the bicycle is responsible for approximately 60 % of the total side force coefficient. However, this study does not provide information about the flow characteristics around the cyclist that causes the aerodynamic forces and moments. Noting this, the research discussed below was undertaken in order to provide detailed information on the overall aerodynamic

forces and moments and to provide an insight into the surrounding flow field, thus laying the foundations for future improvements in cycling stability and performance.

In order to obtain accurate flow field and surface pressure of the bicycle and the cyclist, numerical simulations based on Reynolds Averaged Navier Stokes equations (RANS) using both k-ε and SST k-ω models have been undertaken. Yaw angles considered range between 0-90°. The surface pressure and the surface shear stresses are integrated to obtain the aerodynamic forces and moments on both the bicycle and cyclist with the results compared to previous physical simulations (Fintelman et al., 2014a). In addition, Detached Eddy Simulations (DES) and Large Eddy Simulations (LES) are undertaken on a bicycle and a cyclist in order to gain an insight in the instantaneous flow physics around the cyclist at 15° yaw angle, since this is found to be a common crosswind yaw angle (Guzik et al., 2013) in cycling.

Section 7.2 of this paper briefly outlines the wind tunnel experiments that were undertaken in order to compare the numerical simulations, whilst section 7.3 outlines details relating to the computational models. Section 7.4 addresses the numerical details of the simulations, whilst section 7.5 outlines the numerical accuracy. This is followed by the results and discussion in section 7.6 and finally in section 7.7 the main conclusions are drawn.

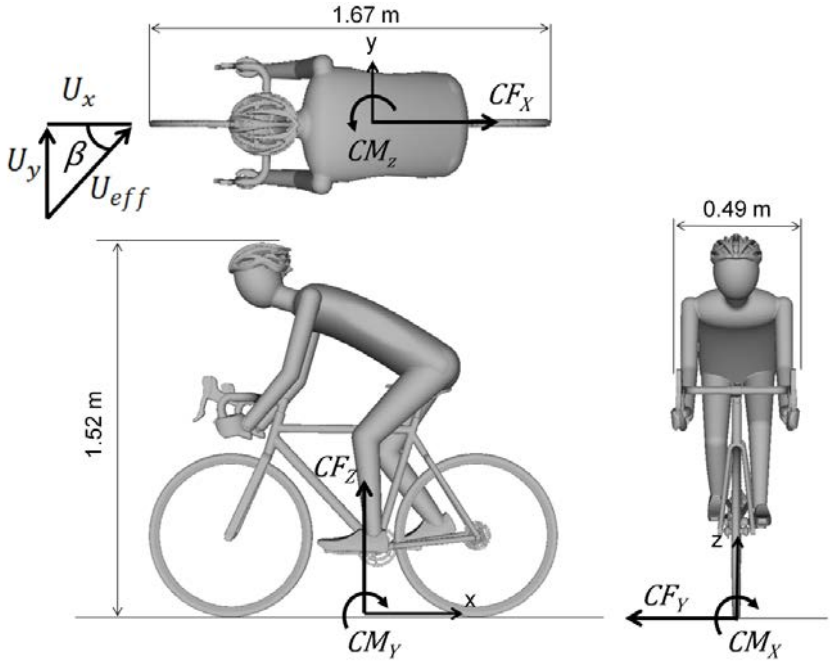


**Figure 7.1 Geometry and dimensions of cyclist and directions of the aerodynamic force and moment coefficients.**

## 7.2 Wind tunnel experiments

Details relating to the physical simulations can be found in Fintelman et al. (2014a) and are briefly reiterated for the benefit of the reader. The wind-induced forces on a bicycle with mannequin are measured in the open wind-tunnel facility at the University of Birmingham UK. The wind-tunnel has a cross-sectional area of 2x2 $m^2$ and length of 10 m. A constant crosswind flow velocity, $U_{eff}$, of 9.91 m/s is maintained in the wind tunnel with a corresponding average turbulence intensity of 0.67 %. The mannequin is placed in a dropped position on a road bicycle with stationary wheels as shown in Figure 7.2(a) and is connected to a six-component force balance (Kistler type 9281B, Kistler Instruments, Winterthur, Switzerland) which is used to measure the aerodynamic forces and moments. The aerodynamic forces were repeatable to within ± 0.05 N and the uncertainty was approximately 2 %.

(a) (b)

**Figure 7.2 (a) Full-scale bicycle and mannequin used in wind tunnel experiments and (b) geometry of the bicycle and cyclist in simulations.**

## 7.3 Computational models

To simulate realistic flow conditions, a high level of complexity and detail are maintained in the CAD model of the bicycle and mannequin (Figure 7.2(b)). However, modelling of small objects such as the spokes and cables have been omitted to simplify the geometry. A generalized computational domain is used as shown in Figure 7.3(a), in which H (1.52m) represents the height of the cyclist from the ground. The dimensions of the computational domain are large enough that blockage area effects can be neglected (maximal blockage area of 0.3 %). Similar to the wind tunnel setup, a uniform effective velocity, $U_{eff}$, of 9.91 m/s is applied for all different yaw angles, $\beta$. This gives a Reynolds number of 1.0x10$^6$, based on the effective wind velocity and the height of the cyclist from the ground. The velocity in the main inlet direction, $U_x$, and in the crosswind inlet direction , $U_y$, is calculated as:

$$U_x = U_{eff}\cos(\beta)\ , U_y = U_{eff}\sin(\beta). \tag{7.1}$$

No-slip boundary conditions are used on the surface of the model and on the ground to accurately match the wind tunnel experiments. A free-slip velocity boundary condition is applied on the upper boundary of the computational domain. In all simulations the wheels are considered static, as the effect of the rotation on the wheels without spokes is found to be

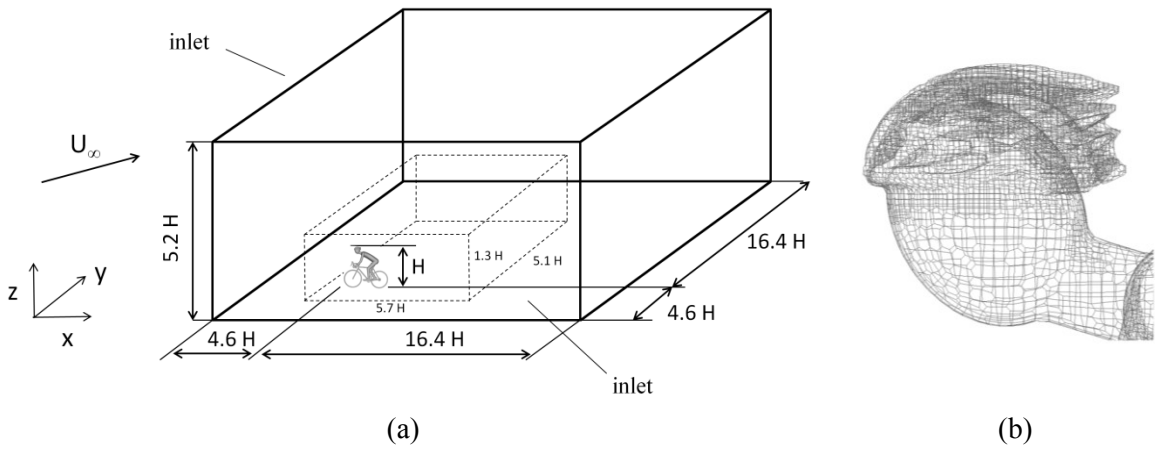


**Figure 7.3 (a) Computational domain, (b) surface mesh of the helmet of the cyclist for the RANS simulations.**

small; k-ε RANS simulations were undertaken without crosswinds and with crosswinds of 90°, in which the rims and tires rotated at 29.494 rad/s (equivalent to a tangential velocity of 9.91 m/s). The results (not reported here) showed that the aerodynamic coefficients in the main wind direction decreased by less than 1.8 % when implementing rotating rims and tires, which is within the limits of the uncertainties of the physical experiments. It is worth noting that rotation of the spokes can have an impact on the side force magnitude (Karabelas and Markatos, 2012). However for ease of simplicity, spoke and leg movement was not included in the simulations.

RANS simulations were used to predict the average flow velocity, pressure and aerodynamic responses. Two different steady RANS simulations were performed with different turbulence models: the standard k-ε and the SST k-ω models. Wall functions are applied close to the wall based on the log-law. These turbulence models are commonly applied in numerical sport simulations, for example in swimming (Zaïdi et al., 2008, Silva et al., 2008), rowing (Zhang et al., 2009), ski jumping (Meile et al., 2006) and bobsleigh (Dabnichki and Avital, 2006). They have also been shown to give a reasonable performance when applied in cycling (Defraeye et al., 2010b, Griffith et al., 2014).

In addition to the simulations using RANS models, the more computationally expensive but accurate standard detached eddy simulation (DES) are undertaken for the flow at 15$^{o}$ yaw angle. This is to provide information about the instantaneous and time-averaged flow at this particular yaw angle. The hybrid DES approach combines the RANS close to the walls and Large-eddy simulation (LES) in the region outside the boundary layers. This model replaces the turbulent length scale function $l_{RANS}$ with a modified length scale function, $l_{DES}$:

$$l_{DES} = \min\left(l_{RANS}, C_{DES}\Delta\right) \tag{7.2}$$

where $C_{DES}$ is a constant (0.65) and $\Delta$ is the largest dimension of the grid cell in all three directions, i.e., $\Delta = \max\left(\delta x, \delta y, \delta z\right)$. The length scales increases with the distance from the wall. Therefore, close to the wall the model behaves like the RANS model and the length scale is:

$$l_{DES} = l_{RANS} \ll C_{DES}\Delta\ . \tag{7.3}$$

In the far field the length scale is given by:

$$l_{DES} = C_{DES}\Delta \ll l_{RANS} \tag{7.4}$$

The most commonly used Spalart-Allmaras one-equation turbulent model is applied (Spalart and Allmaras, 1994). DES has been successfully used for the aerodynamics of a ground vehicle (Hemida and Krajnović, 2009b, Flynn et al., 2014).

Finally, the Large Eddy Simulations (LES) are used to make an accurate comparison of the simulation results of the different turbulence model approaches at a common crosswind yaw angle of 15°. LES is the most computational expensive turbulent model used in this research, but is considered to be the most accurate of all mentioned models, particularly when large scale flow unsteadiness is significant (which is likely to be the case for cyclists and bicycles). With the increase in computational power, LES has been used extensively in the study of the flow around small scale models of trains and cars subjected to cross winds (Hemida and

Baker, 2010, Hemida and Krajnović, 2010, Tsubokura et al., 2010). In the LES approach, the large eddies containing the most energy are resolved, whilst a sub-grid scale model is used for the eddies smaller than the grid size. The velocity is decomposed into a filtered part and sub-grid scale component. The filtered Navier-Stokes equations are derived for the large scale eddies. The filtered continuity and momentum equations for an incompressible flow are:

$$\frac{\partial \overline{\mathrm{u_i}}}{\partial \mathrm{t}} + \frac{\partial \overline{\mathrm{u_i}} \partial \overline{\mathrm{u_j}}}{\partial \mathrm{x_j}} = -\frac{1}{\rho}\frac{\partial \bar{\mathrm{p}}}{\partial \mathrm{x_i}} + 2\frac{\partial}{\partial \mathrm{x_j}}(\mathrm{v} + \mathrm{v}_t)\left(\bar{S}_{ij} - \partial \tau_{ij}^{r}\right), \tag{7.5}$$

$$\text{and} \qquad \frac{\partial \overline{\mathrm{u_i}}}{\partial \mathrm{x_i}} = 0,$$

where $\overline{\mathrm{u_i}}$ and $\bar{\mathrm{p}}$ are the filtered velocity and pressure, $\mathrm{v}_t$ the turbulent viscosity, $\bar{S}_{ij}$ the resolved strain rate tensor and $\tau_{ij}^{\mathrm{r}}$ the subrid scale stresses. The Smagorinsky sub-grid model is used to derive the sub-grid scale Reynolds stresses by calculating the turbulence viscosity:

$$\mathrm{v}_t = (C_S f_d \Delta)^2 \sqrt{2\bar{S}_{ij}\bar{S}_{ij}}, \tag{7.6}$$

where $C_S$ the Smagorinsky constant (0.1) and $f_d$ is the van Driest damping function.

## 7.4 Numerical details

The open-source CFD package "OpenFOAM" is used to perform all the simulations with the three dimensional finite volume to solve the flow. The SIMPLE algorithm is implemented in the simulations to couple the pressure and velocity. In the RANS simulations, the gradients are computed with a least square second order scheme. The pressure interpolation is performed with the second order central differencing scheme. The convection and viscous terms are solved with the second order upwind scheme. In the DES and LES simulations, the time discretization has been approximated by the second order implicit backward scheme. Gradients are computed with the second order central differencing scheme. A central difference-upwind stabilised transport scheme is used for the convection terms. This scheme

blends 25 % second order upwind with 75 % central difference interpolation to stabilise the solution whilst maintaining second order behaviour. The induced numerical dissipation plays an important role in stabilizing the convergence. In the transient simulations, a constant time step of $\Delta t = 0.00001$ sec has been used. This time step ensures that the maximum Courant-Friederichs-Lewy (CFL) number is lower than 1.0. The time history of the aerodynamic coefficients has been obtained for each time step. Convergence is monitored and simulations stopped when the residuals were stable and the maximum normalized residual of each turbulent equation has been converged to at least $10^{-4}$. The total wall time of the fine mesh of the RANS, DES and LES approach running at 16 processors was about 17 hours, 905 hours and 1357 hours respectively.

## 7.5 Numerical accuracy

To investigate the effect of the grid size on the RANS results, three different meshes (coarse, medium and fine) are evaluated with different number of nodes: $3.5 \times 10^6$, $8.7 \times 10^6$ and $17.9 \times 10^6$, respectively. The averaged normal wall distance $y^+$ of the cyclist for the different RANS meshes are 82, 60 and 43 respectively. Figure 7.3(b) shows an example of the surface mesh of the cyclist's helmet. Figure 7.4 shows the surface pressure of the cyclist at a height of 0.7 H, obtained from the RANS coarse, medium and fine meshes. The pressure distribution is expressed in terms of the local pressure coefficient, $C_p$, which is defined as:

$$C_p = \frac{p - p_\infty}{0.5 \rho {U_{eff}}^2}, \tag{7.7}$$

where $p$ is the local pressure, $p_\infty$ the free stream pressure and $\rho$ the air density. A good agreement (Root Mean Square error = 0.09) is found between the RANS fine and medium mesh.

In addition to the pressure distribution, the aerodynamic forces (expressed in coefficient form)

were compared. The drag force coefficient $CF_X$, side force coefficient $CF_Y$, lift force coefficient and $CF_Z$ are defined as:

$$CF_X = \frac{F_X}{0.5A\rho U_{\text{eff}}{}^2}, CF_Y = \frac{F_Y}{0.5A\rho U_{eff}{}^2}, \; CF_Z = \frac{F_Z}{0.5A\rho U_{eff}{}^2}, \tag{7.8}$$

where A is the total frontal area of the cyclist and bicycle at 0° yaw angle (0.55 $m^2$), $U_{eff}$ is the effective flow velocity (m/s), and $F_X$, $F_Y$, and $F_Z$ are the drag force, side force and lift force, respectively. The coordinate system adopted and thus the directions of these forces are shown in Figure 7.1. The aerodynamic force coefficient for the different grid sizes of the RANS models are shown in Table 7.1. The results of the RANS medium simulation compare well to those of the fine simulation. The grid convergence index (GCI) is used to quantify the error of the fine grid (Celik et al., 2008) and is defined as:

$$GCI_{fine} = \frac{F_S|\varepsilon|}{r^p - 1}, \tag{7.9}$$

where $F_S$ is the safety factor, $\varepsilon$ the relative error between the fine and medium mesh, $r$ the grid refinement factor and $p$ the order of accuracy. The safety factor is set to 1.25. The numerical uncertainty in the fine grid solution for the drag coefficient $CF_X$ and the side force coefficient $CF_Y$ are 0.4 % and 0.2 % respectively. These levels of agreement between the results obtained from the RANS fine and medium meshes suggest that the resolution of the fine mesh is adequate to correctly predict the flow and hence no further mesh refinement is needed. From this point all the RANS results are from the fine mesh unless otherwise explicitly stated.

In the RANS simulations, standard wall functions are used to solve the near wall region, requiring a less refined mesh close to wall. In the LES simulations, the accuracy of the results is dependent on the grid size. In particular in the near wall region a fine mesh is required. Therefore, an additional refinement box of dimensions 3.2 m x 0.8 m x 1.66 m (L x W x H) is added into the LES mesh. In addition, a higher surface based refinement level is applied. The

total number of nodes in the LES mesh is $26.7 \times 10^6$, consisting of 84 % of hexahedra elements, 15 % polyhedral elements and 1 % of prisms, tetrahedral wedges and tetrahedral elements. To be able to make an objective comparison between the LES and the DES simulation results, an identical mesh is used in both simulations. This allows a direct comparison of these two turbulence approaches, the grid influence being eliminated. This implies that the transition from LES to RANS in the DES will take place closer to the wall and consequently the DES will acts more like a LES model in most of the computational domain. A mesh sensitivity analysis has been carried out on the DES and LES simulation by performing a simulation on an even finer mesh, consisting of $41.7 \times 10^6$ nodes. The normal wall distances of the cyclist for the coarse and fine mesh are about 5.2 and 3.4 respectively. The results illustrate a reasonable agreement with the results of the coarser DES and LES mesh as shown in Table 7.1 ($CF_X$ error difference of about 1.0 % and 0.3 %, respectively).

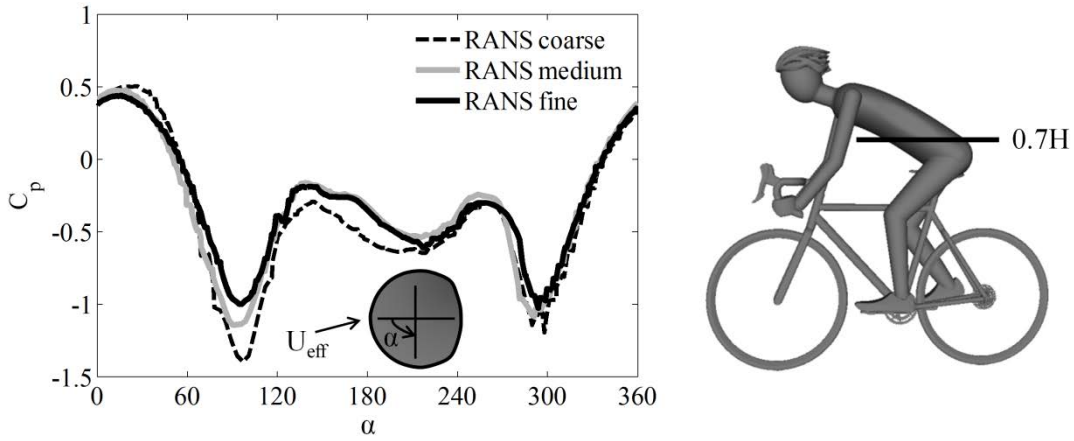


**Figure 7.4 Pressure distribution around the surface of the main body of the cyclist obtained from the coarse, medium and fine mesh of the RANS k-ε simulations at β=15°.**

**Table 7.1 Force coefficients refinement of the RANS k-ε model and the DES simulations.**

| | $CF_X$ | $CF_Y$ | $CF_Z$ |
|---|---|---|---|
| RANS Coarse | 0.653 | 0.148 | 0.116 |
| RANS Medium | 0.586 | 0.227 | 0.081 |
| RANS Fine | 0.596 | 0.231 | 0.099 |
| DES Coarse | 0.508 | 0.243 | 0.182 |
| DES Fine | 0.513 | 0.250 | 0.180 |
| LES Coarse | 0.612 | 0.211 | 0.184 |
| LES Fine | 0.610 | 0.232 | 0.160 |

## 7.6 Results and discussion

*7.6.1 Aerodynamic force coefficients*

Figure 7.5(a) shows the variation of the aerodynamic drag forces, side forces, lift forces and rolling moments of the bicycle and cyclist for different yaw angles, obtained from the RANS simulations and the experiments. The rolling moment coefficient $CM_X$ is defined as:

$$CM_X = \frac{M_X}{0.5AH\rho{U_{eff}}^2}, \tag{7.10}$$

where $M_X$ is the rolling moment. The direction of application of the rolling moment is shown in Figure 7.1. The rolling moment tends to rotate the bicycle about its longitudinal axis. For stability and safety, the side force and rolling moment coefficients are most important. The results show that the aerodynamic side force and the drag coefficients are a function of yaw angle and for the case of $CF_Y$, significant variations can be observed. Large side forces, yaw moments and roll moments are likely to have a strong impact on the bicycle stability. The RANS simulations illustrate similar trends to the experimental data with small variations in the drag force (~9 %) and lift force (~7 %) across the entire range of the examined yaw angles

(Figure 7.5(a)). Larger variations are observed for the side forces (~21 %) and the rolling moment (~11 %). Of the two RANS model approaches, the k-ε model demonstrates the best performance, showing a better prediction of the drag and side force coefficients. The better performance of the k-ε model is likely caused by the over prediction of the turbulent kinetic energy and hence the turbulent viscosity, which has an impact on the aerodynamic forces (Makowski and Kim, 2000). The overall under prediction of the aerodynamic forces of the k-ε and SST k-ω models are likely to be a consequence of the failure of the RANS models to correctly represent the flow physics in areas of considerable separation and reattachment. Furthermore, it is possible that for large yaw angles (> 60°), ~52 % of the under prediction of the side forces may be due the treatment of the modelling of the wheels (Kara belas and Markatos, 2012). However, it should be noted that this explanation should be interpreted with care since Karabelas and Markatos (2012) did not consider the interaction between bicycle and cyclist and this is felt to have a larger influence on the aerodynamics forces.

The results of the DES and LES are in a reasonable agreement with the experimental data as shown in Table 7.2 and Figure 7.5(b). It should be noted that at 15° yaw angle the actual magnitude of the side forces are small, which ensures that even small differences between the actual and predicted results in a relatively large percentage error. With increasing yaw angles, the percentage differences will reduce. All the CFD techniques under predict the drag and side force coefficients at the crosswind yaw angle of 15°. The under prediction could be assigned to a range of different small factors, which together add up to quantifiable differences. First of all there are small geometrical differences and simplification of the geometry, such as the exclusion cables and spokes. The contribution of the spokes to the total side forces at different yaw angles is numerically investigated by Karabelas and Markatos (2012). They found that

for an isolated stationary wheel at a yaw angle of 15°, the spokes increase the side forces by about 0.5N. The spokes could therefore explain approximately 60 % of the under prediction of the side forces. Secondly, it should be appreciated that in the physical modelling, there was slight buffeting of the mannequin in the y-direction largely due to the mannequin induced turbulence, which given the nature of the experiments meant that the geometry of the mannequin-cycle altered slightly during the tests compared to the numerical simulations. Finally, the variations could be associated with the inaccuracy of the turbulence models to capture all scales and to correctly predict the flow separation and attachments. The best performance is seen for the LES simulations, having a drag coefficient error of approximately 5 % compared with the experimental data (Figure 7.5(b)). The DES approach shows a reasonable good agreement for the lift and side forces (variation < 10 %), however larger discrepancies of about 17 % are found for the drag force, which is the dominating force direction at the 15° crosswind yaw angle. The less accurate performance of the DES compared with the LES is a result of the capturing of less eddies and the not resolving of the eddies scaled with the grid cells in the boundary layer.

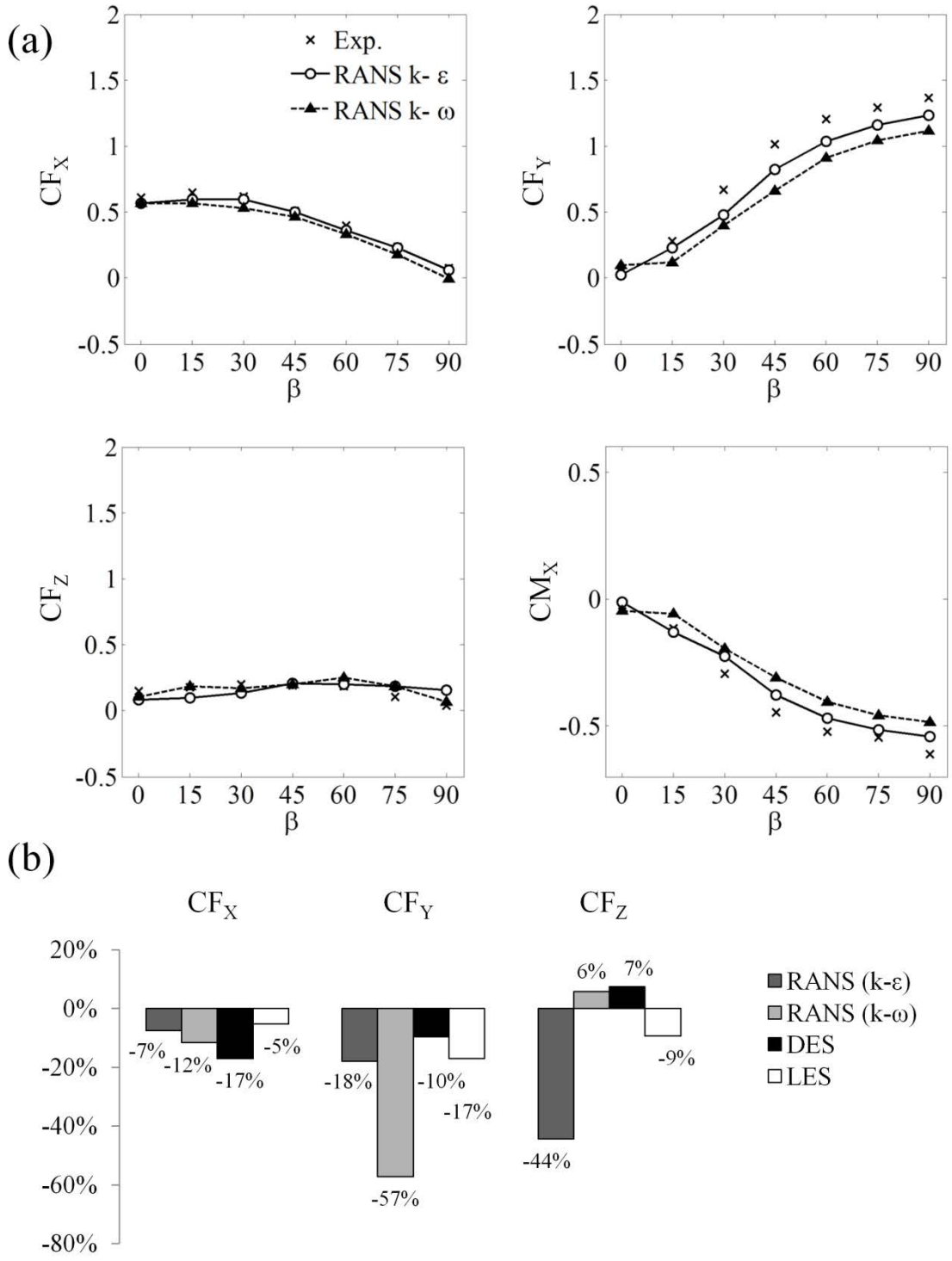


**Figure 7.5 Comparisons of the aerodynamic force coefficients obtained in the experiments and different turbulence models expressed as: (a) absolute value at different yaw angles, (b) percentage error for the drag at 15° crosswind yaw angle.**

The relative contributions of the mannequin and bicycle to the aerodynamic coefficients are shown in Table 7.2. Comparable results are found for the simulations and the experiments. About 70 % of the total drag force coefficients $CF_X$ and rolling moment coefficients $CM_X$ are caused by the mannequin in both the experimental work and simulations. The contribution is smaller for the side force coefficients $CF_Y$, where the mannequin contributed to about ~34% - 49 %. In the simulations, the bicycle has a lower contribution to the $CF_Y$, which is likely caused by the simplification of the geometry (i.e. no spokes, cables, chain etc). Finally, for both the experiments and the simulations, the main contribution of the lift force coefficients is the mannequin (around 90 – 110 %).

In the CFD results, a distinction is made between the pressure forces and the skin friction forces. The skin friction is caused by the viscous stress in the boundary layer around the bicycle and cyclist. In all the numerical investigations undertaken in this report, approximately 3 % of the total drag forces and approximately 2 % of the total side forces can be attributed to skin friction respectively. These relatively low viscous forces are comparable with similar investigations concerning an isolated cyclist (Defraeye et al., 2010b). As the mannequin-bicycle model used in the CFD calculations is smoother than that in the physical experiments, it is expected that the predicted viscous forces in the experiments are slightly higher than the computed ones. However, due to the nature of the physical experiments this hypothesis cannot be verified.

**Table 7.2 Aerodynamic force coefficients for the RANS k-ε, DES and LES simulations together with the experimental results at β=15°. The total aerodynamic coefficients and the relative contribution of the bicycle and mannequin are given. The percentage of the relative contribution of the mannequin and bicycle to the total aerodynamic coefficients are presented.**

| | | Total (Mannequin and Bicycle) | Mannequin | Bicycle |
|---|---|---|---|---|
| $CF_X$ | DES | 0.513 | 0.359 (70 %) | 0.154 (30 %) |
| | LES | 0.610 | 0.440 (72 %) | 0.171 (28 %) |
| | Experiments | 0.644 | 0.449 ( 70 % ) | 0.195 (30 %) |
| $CF_Y$ | DES | 0.250 | 0.123 (49 %) | 0.128 (51 %) |
| | LES | 0.232 | 0.107 (46 %) | 0.125 (54 %) |
| | Experiments | 0.281 | 0.095 ( 34 % ) | 0.186 (66 %) |
| $CF_Z$ | DES | 0.180 | 0.197 (109 %) | -0.015 (-8 %) |
| | LES | 0.160 | 0.171(107 %) | -0.011 (-7 %) |
| | Experiments | 0.178 | 0.155 ( 87 % ) | 0.023 (13 %) |
| $CM_X$ | DES | -0.107 | -0.070 (65 %) | -0.037 (35 %) |
| | LES | -0.104 | -0.069 (66 %) | -0.035 (34 %) |
| | Experiments | -0.114 | -0.083 (73 %) | -0.031 (27 %) |

### *7.6.2 Time-averaged flow*

Figure 7.6 shows the surface pressure distribution, obtained from the k-ε simulation at different yaw angles. At β = 0°, low pressure regions appear at the sides of the body where the vortex shedding takes place. By increasing the yaw angle, an area of suction pressure develops at the back of the cyclist and high pressure regions develop on the upper lower limbs and the abdomen. At 90° yaw angle, high pressure areas develop at the windward side of the cyclist, whilst the back and leeward sides of the cyclist are dominated by low pressure regions. At this yaw angle, the suction pressure is balanced by a developed suction pressure

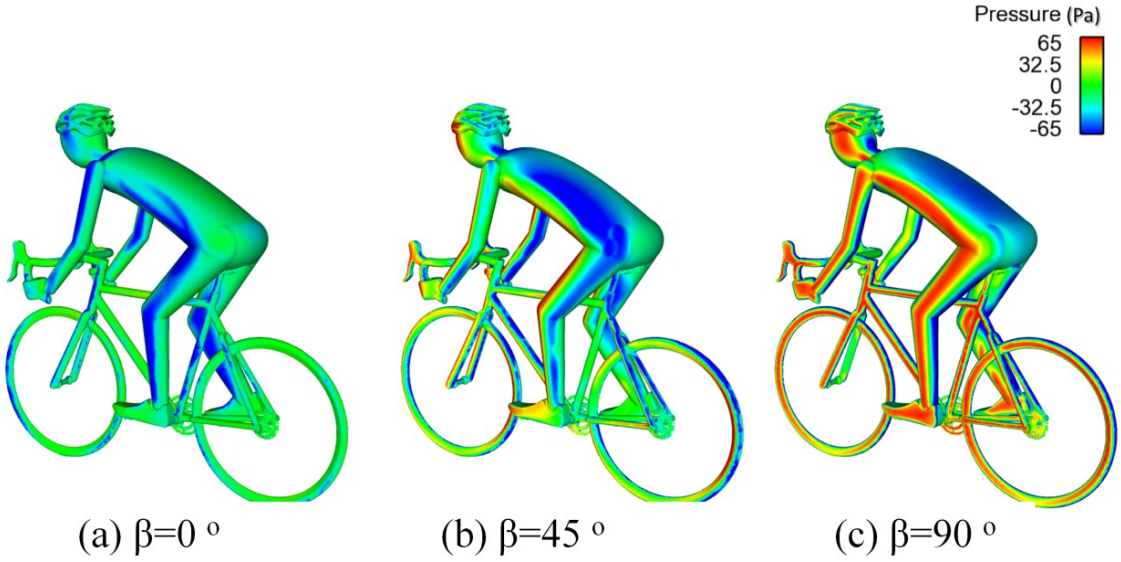


**Figure 7.6 Pressure distribution on the cyclist at different crosswind yaw angles obtained from the RANS k-ε simulations.**

on the front side of the cyclist (not shown in the Figure) and this explains the low drag coefficient at large yaw angles (> 60$^o$).

The isosurface of the pressure around the cyclist at $C_p$ = -0.240 for yaw angles of 0$^o$ and 60$^o$ is shown in Figure 7.7. For the case of no crosswind (0° yaw angle), the pressure is approximately symmetrical with the concentration of low pressure around the sides of the cyclist. However, at a yaw angle of 60°, the low pressure surface is located behind and at the leeward side of the cyclist and bicycle. In particular at large yaw angles, the bicycle starts to contribute to the turbulent flow around the cyclist which leads to an increase in the side force and rolling moment. This phenomenon has been also observed in the physical experiments, where for 60° yaw angle the bicycle was found to account for approximately 60 % of the total side force coefficient; whilst at 0° yaw angle the bicycle accounts for only about 20 % of the total drag (Fintelman et al., 2014a).

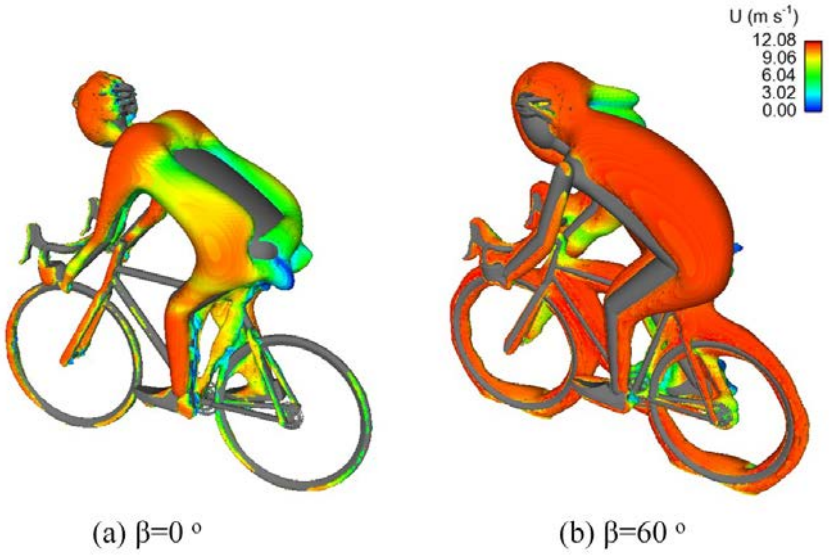


**Figure 7.7 Isosurface of the pressure at Cp = -0.240 at different yaw angles, coloured with the instantaneous velocity and obtained from the RANS k-ε simulations; (a) β=0°; (b) β=60°.**

The time-averaged pressure at different locations in the direction of the main flow at a crosswind yaw angle of β=15° is shown in Figure 7.8. The positions considered are at a distance of 0.3H, 0.5H, 0.7H and 0.9H from the cyclist. The negative peak pressure in the wake decreases with increasing distance from the cyclist. All turbulence models considered are approximately consistent with one another in terms of identifying the location of the peak pressure. The largest coefficient of pressure can be found at a height of about 0.6H, caused by flow structures that are separated from the back of the cyclist. The deviations with respect to the LES simulation are largest for the RANS k-ε simulation. Smaller deviations are observed between the more accurate LES and DES results.

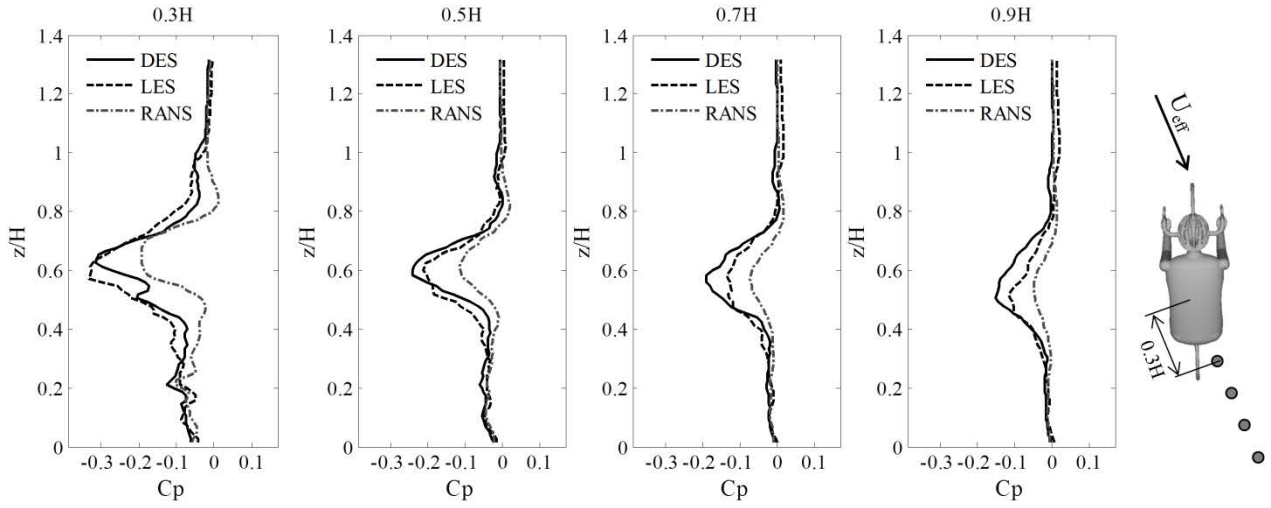


**Figure 7.8 Time-averaged vertical pressure lines at different locations in the wake of the cyclist at yaw angle β=15° and at a distance of 0.3H, 0.5H, 0.7H, 0.9H from the cyclist in the main flow direction.**

### *7.6.3 Instantaneous flow*

Although RANS simulations are computationally efficient due to their nature, obtaining instantaneous flow information by such methods is not possible. Therefore DES and LES are used to determine the instantaneous flow features. Figure 7.9 shows the isosurface of the instantaneous pressure around the cyclist at $C_p$ = -0.240 and a crosswind angle of 15° of the DES and LES simulations. As the centres of the flow vortices are normally associated with low pressure, these isosurface of constant pressure can be used to infer the flow structures around the bicycle and cyclist. The results of the DES (Figure 7.9(a)) and LES (Figure 7.9(b)) at random instantaneous time points look qualitatively similar. In both approaches the instantaneous flow structures show large vortices shed at the back and leeward side of the body into the wake flow. The flow separates at the back side of the helmet and the back of the cyclist to form large unsteady structures. Once these structures completely separate from the surface they tend to form vortex tubes with axis parallel to the flow direction as shown in Figure 7.9.

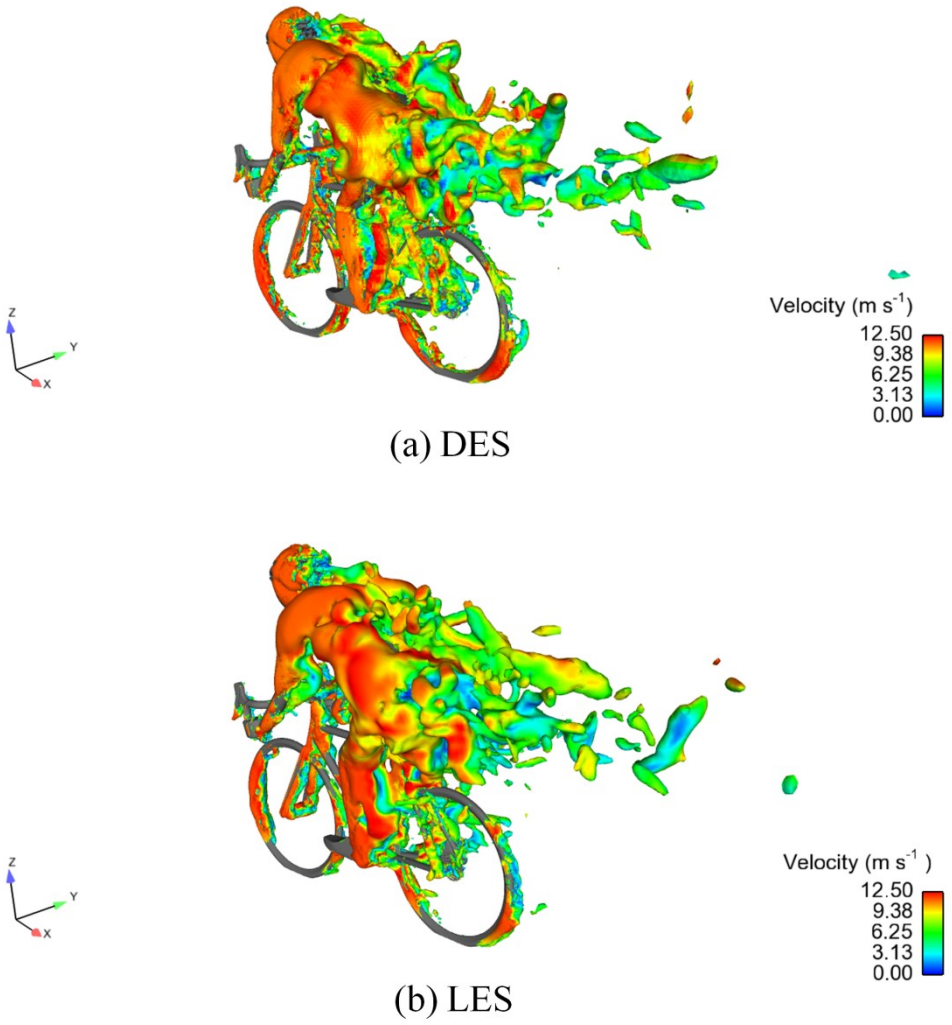


**Figure 7.9 Instantaneous flow structures around the cyclist subjected to crosswinds with a yaw angle of 15° at Cp= -0.240 and coloured with the instantaneous velocity, obtained from the (a) DES approach and (b) LES approach.**

The vortex cores of the flow around the cyclists are found by means of Eigen analysis. This method is based on an algorithm of Sujudi and Haimes (1995) and uses the Eigen value of the velocity gradient tensor to identify the vortex cores. The vortex cores help to give an insight into the possible distribution of the vortices around the cyclist. The locations of the instantaneous vortex cores in the flow around the bicycle at 15° yaw angle for the LES and DES turbulence models are shown in Figure 7.10. These vortices are predominantly developing and stretching along the direction of the main flow and showing the largest

strength closest to the body. This underpins the observation based on the pressure isosurface shown in Figure 7.9. Similar main flow vortices are obtained by LES and DES as shown in Figure 7.10 in terms of the instantaneous vortex cores. These main vortices are rather small and can be described as follows:

- Vortex V1 appears due to separation of the flow around the helmet.
- Vortex V2 originates from a focus very close to the cyclists' gluteus maximus.
- Vortex V3 and V4 appear at the leeward side of the upper body and originate very close to the back side of the upper arm.

The LES resolves more of the small vortex structures than the DES approach and thus many small-scale structures are found predominantly around the lower back of the cyclist compared to the DES simulations.

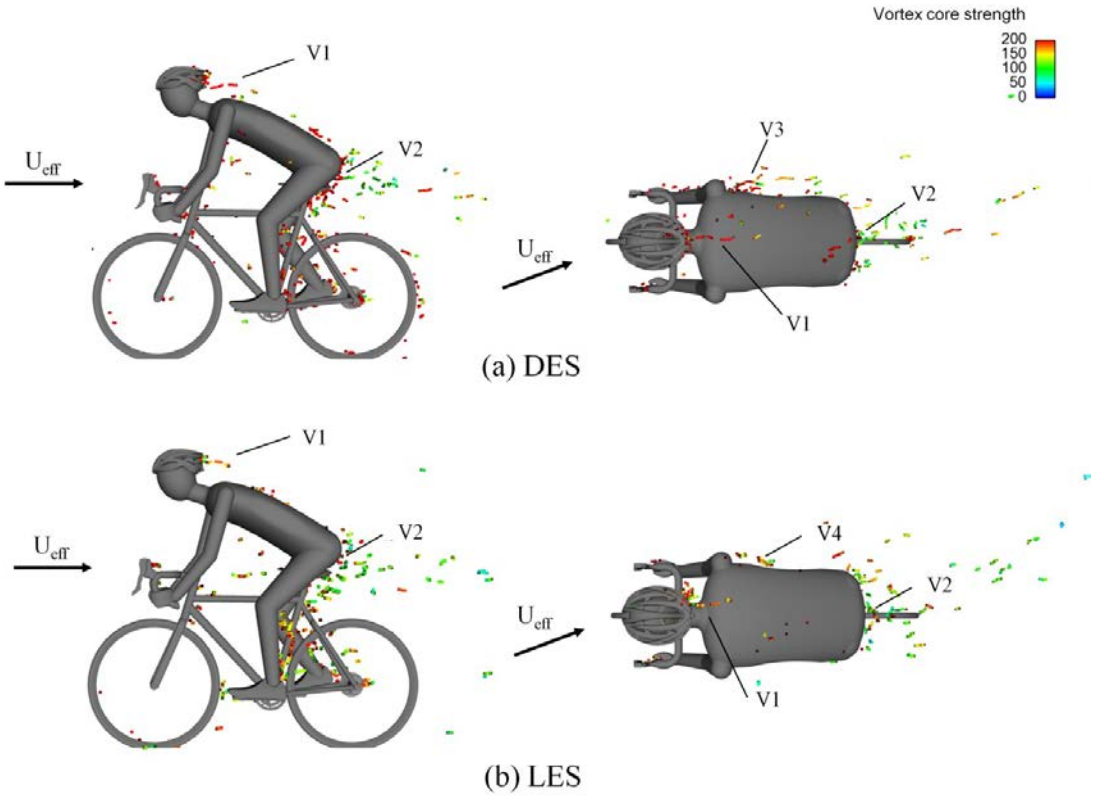


**Figure 7.10 Location of the instantaneous vortex cores in the flow around a cyclist shown from the side view and top view, obtained from the (a) DES simulation and (b) LES simulation. The vortex cores are coloured by the vortex core strength.**

The aerodynamic coefficient time histories are used to reveal the effect of the turbulence on the forces and moments. It is assumed that the flow is statistically stationary. The time, $t$, is expressed in a form of dimensionless time, $t^*$, as:

$$t^* = \frac{tU_{eff}}{H}. \tag{7.11}$$

The time histories of the drag force, side force, lift force and rolling moment coefficients obtained by the DES and LES simulations are shown in Figure 7.11. The shedding of vortices at the back and leeward side of the body into the wake flow shown in Figure 7.9, contributes to relatively large observed variation in the time history of the aerodynamic force coefficients $CF_X$ and $CF_Y$ shown in Figure 7.11. The largest variations in force coefficients are observed in the $CF_Y$, which is predominantly caused by the large vortices shed from the mannequin. As shown in Table 7.3, the standard deviations of the time histories of both turbulence model approaches are in the same order of magnitude. The standard deviations of the aerodynamic coefficients of the experiments are on average about 3 times larger than those of the simulations. These variations are likely not to be a result of the uncertainties of the force balance, but arise from vibrations and natural frequencies of the mannequin and bicycle system, causing stronger vortex shedding around the cyclist as shown in Figure 7.9.

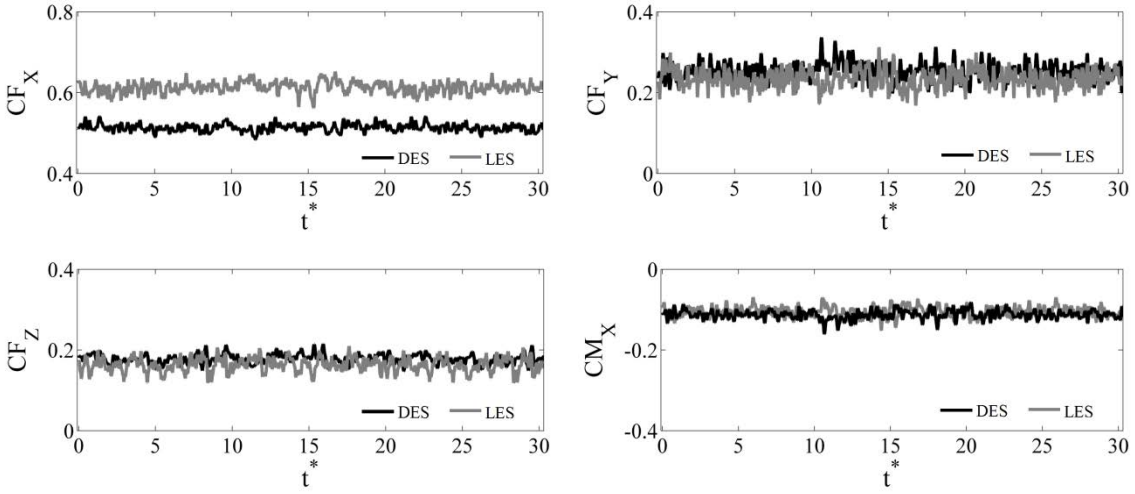


**Figure 7.11 Time history of the aerodynamic coefficients obtained from the fine DES and LES simulations.**

**Table 7.3 Mean and standard deviation of the aerodynamic force and moment responses of the DES simulations, LES simulations and wind tunnel experiments at 15° crosswind yaw angle**

| | Mean DES | Mean LES | Mean Exp | Std DES | Std LES | Std Exp |
|---|---|---|---|---|---|---|
| $CF_X$ | 0.513 | 0.610 | 0.644 | 0.010 | 0.014 | 0.046 |
| $CF_Y$ | 0.250 | 0.232 | 0.281 | 0.022 | 0.023 | 0.075 |
| $CF_Z$ | 0.180 | 0.160 | 0.178 | 0.012 | 0.017 | 0.042 |
| $CM_X$ | -0.107 | -0.104 | -0.114 | 0.011 | 0.013 | 0.016 |
| $CM_Y$ | 0.292 | 0.355 | 0.383 | 0.006 | 0.009 | 0.014 |
| $CM_Z$ | -0.017 | -0.018 | -0.008 | 0.004 | 0.004 | 0.010 |

A Fourier transform resulting in the power spectra of the time-varying force coefficients is used to resolve the dominating frequencies. The aerodynamic force frequencies provide an insight into the turbulent frequencies ($f$) in the flow and represent the crosswind induced force frequencies. The frequencies are expressed in Strouhal number:

$$St = \frac{fH}{U_{eff}} \tag{7.12}$$

The power spectra are normalized by the root means square of the turbulent frequencies. All high amplitude peaks in the auto spectral densities of the simulations (Figure 7.12(a) and 7.12(b)) can be found in the range $St$ = 0 – 7. For the DES simulations, the dominant peak in the drag force coefficient is found at $St$ = 0.49, which corresponds to 3.2 Hz. The dominant peak in the LES simulations is at $St$ = 0.99, corresponding to 6.5Hz. In the side force coefficients, multiple high amplitude peaks can be found. These peaks are caused by the large range of length scales due to variety of surfaces and angles of the cyclist and bicycle seen by the free stream flow. One of the main frequency components in the side force coefficient is at $St$ = 2.97 (E6), corresponding with 19.4 Hz. This frequency coincides with the frequency of the integral length scale of the drag coefficient. The integral length scale describes the size of the large energy containing eddies in the flow. In the side force coefficient frequency spectrum these large eddies originate from the mannequin. Two other dominant side force frequency are found at around $St$ = 0.61 (E4) and $St$ = 1.73 (E5), which corresponds to 4.0 Hz and 11.3 Hz respectively. The lift force of the DES simulations has a characteristic frequency at $St$ = 0.20, corresponding to 1.3 Hz. The dominant frequency of the LES simulation is at $St$ = 0.99. This peak in the lift force coefficients spectrum is identical to the dominant peak found in the drag forces of the LES simulations.

The auto spectral densities of the simulations are compared with experimental data. The experimental force coefficient time histories are shown in Figure 7.12(c) and are dominated by low frequency contents ranging between $St$ = 0 and $St$ = 5. The values of the dominant frequencies in the experimental work (E1-E7) can be found in Table 7.4. All dominant frequencies in the auto spectral density of the experiments are also found in the frequency spectra of the DES and LES simulations. This indicates that both approaches are able to predict the important instantaneous flow features. In the drag force coefficient spectrum,

which is the major wind direction, similar dominant frequencies (E1-E3) are found in the power spectrum of the LES. However, the highest absolute spectral power is observed in the side force coefficient direction. The dominant peaks E4 and E5 in the side force direction are identical to the dominant peaks of the LES and DES simulations. The normalized spectral power at these frequencies in the LES approach is higher than that of the DES simulations. This denotes that the LES simulations are better capable of predicting the reattachment and separation in the side force direction. Finally, the dominant lift force coefficient frequency, E7, is found in the simulations.

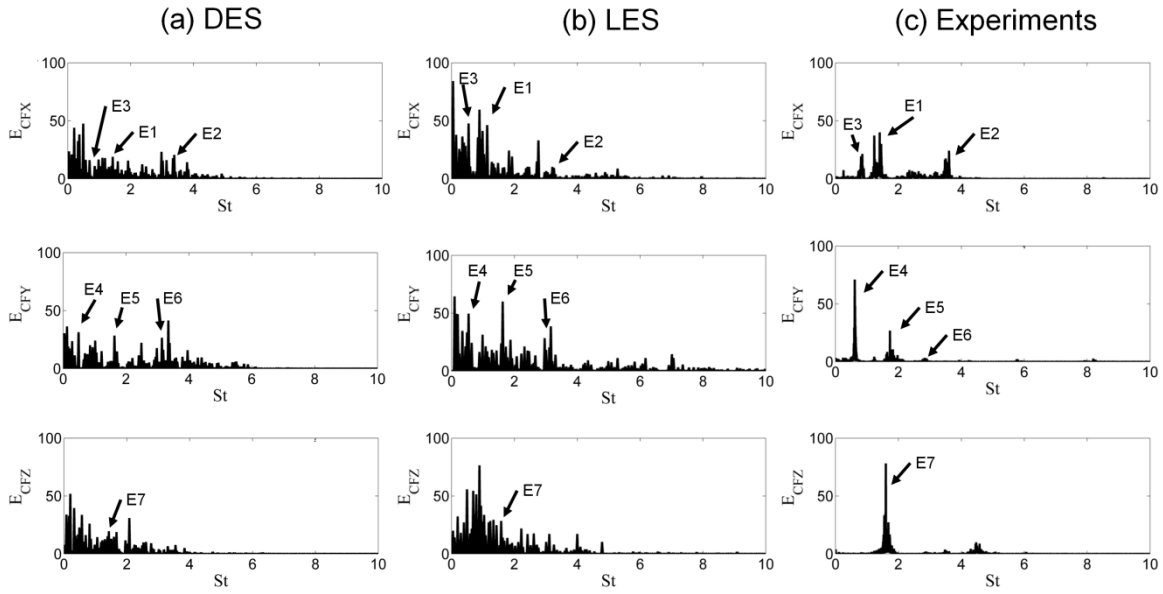


**Figure 7.12 Auto spectral density of the aerodynamic coefficients obtained from the fine mesh of the (a) DES simulation, (b) LES simulation, (c) experiments**

**Table 7.4 Dominant frequencies of the auto spectrum of the force coefficients of the experimental data.**

| | E1 | E2 | E3 | E4 | E5 | E6 | E7 |
|---|---|---|---|---|---|---|---|
| $St$ | 1.40 | 3.61 | 0.85 | 0.61 | 1.73 | 2.97 | 1.6 |
| $f$ (Hz) | 9.2 | 23.6 | 5.6 | 4.0 | 11.3 | 19.4 | 10.5 |

## 7.7 Conclusions

This is the first CFD study investigating the effect of crosswinds on a bicycle and cyclist for a range of yaw angles from 0 to 90$^{o}$. RANS analysis has been performed for all yaw angles whilst DES and LES have been restricted to 15$^{o}$ yaw angle. A reasonably good agreement has been found between the CFD results and the experimental data across a wide range of yaw angles (average drag coefficient error of approximately 10 %). The results showed that crosswinds have a significant effect on the aerodynamic force coefficients. All numerical simulations undertaken have been shown to under-predict the drag and side forces at 15$^{o}$ yaw angle. The LES simulations showed the best performance of all the approaches investigated (drag coefficient error of approximately 5 %). At small yaw angles, the upper body of the cyclist predominately affects the aerodynamic forces, whilst at large yaw angles the bicycle has been shown to have an increasing contribution. For the specific case of a 15° yaw angle, complex vortex structures have been identified in the flow and were found mainly in the direction of the free stream flow. These vortices predominantly appear in the flow due to the separation of the flow around the gluteus maximus, helmet, bicycle and upper body. Large vortex structures in the wake of the cyclist are predominantly found at a height of 0.6H. The main frequencies in the time histories of the force coefficients are indentified and compared with experimental data. It has been observed that both the LES and DES simulations predict all dominant frequencies found in the experimental work. It could be concluded that despite some dissimilarities between the DES and the LES results, the DES simulations is able to predict the main flow characteristics. This study shows that crosswinds significantly influence the cyclists' aerodynamic forces and the corresponding flow structures. The results therefore have significant influence with respect to the stability and safety of cyclists.

**Acknowledgement**

All simulations have been carried out on the Birmingham Environment for Academic Research (BEAR**)** computational facility. This work has been funded by the University of Birmingham.

# CHAPTER 8

# Position and crosswinds[1]

**Abstract**

The aim of this study was to investigate the effect of cycling position on the flow field around a cyclist and bicycle subjected to different crosswinds. The positions analysed were 0°, 8° and 16° torso angle time trial positions, and the 16° and 24° torso angle dropped positions. Crosswind yaw angles varied between 0°, 15°, 30° and 45°. The flow had a Reynolds number of 1.0 x $10^6$ based on the height of the cyclist from the ground. Reynolds Averaged Navier Stokes (RANS) simulations were used to determine the flow field around a bicycle and cyclist. Results showed that when lowering the torso angle within either the dropped position or time trial position, the wake area significantly reduces, which in return decreases both the drag force and the pitching moment. Moreover, it was demonstrated that the position (time trial versus dropped position) primarily influences the drag forces, side forces, pitching moments and rolling moments across different crosswind yaw angles. With no crosswind, higher drag forces are observed in the dropped position and these are associated with a larger wake area and additional vortices on the leeward side of the helmet and in the wake of the cyclist's arms. At large crosswind yaw angles, the time trial bicycle is responsible for a significant increase in the side forces compared to those of the road bicycle used in the

[1] This chapter is in preparation as: Computational fluid dynamics study of the effect of cycling position on the aerodynamic responses in crosswinds

dropped position. Isosurfaces of the pressure showed that the time trial bicycle changes the wake pressure. The results imply that in large yaw angle crosswinds not the cycling position but the cycling equipment (i.e. bicycle and helmet) plays a major role in the acting aerodynamic side forces and rolling moments, which may influence the stability of the bicycle.

## 8.1 Introduction

The main resistance force during cycling in still air is the aerodynamic drag (Kyle and Burke, 1984). By reducing drag, the performance of a cyclist can be optimised. The total aerodynamic drag can be split into two components: friction drag and form drag. A cyclist can be seen as a bluff body which means that the form drag tends to dominate. As the cyclist themselves account for approximately 70 - 80 % of the total drag (Defraeye et al., 2010a, Fintelman et al., 2014a), the most effective method of reducing the form drag is by changing the cyclist's position, thus decreasing the frontal area (Lukes et al., 2005). There are typically three cycling positions: upright position (hands on the hoods of the handlebar), dropped position, (hands on the dropped bars) and time trial position (hands on the time trial handlebars). When changing from either an upright position or a dropped position to a time trial position, the aerodynamic drag can be reduced by approximately 22 % and 13 % respectively (Defraeye et al., 2010a) . Lowering the torso angle within these positions could further reduce the drag (the torso angle is defined as the angle of the torso relatively to the ground). For example, in a dropped position, a drag reduction of 15 % has been estimated when lowering the torso angle position from 24° to 16° (Fintelman et al., 2014a). It is apparent that lowering body position is beneficial in reducing drag in windless environmental conditions. However, cyclists are regularly subjected to crosswinds and this can have a significant effect on the stability and safety of cyclists. Several accidents due to crosswinds

are reported with severe and fatal consequences (Schepers and Wolt, 2012). For example, in Australia in 2005, a female cyclist died after a strong gust of wind blew her into the path of a car when cycling in a classic tour ride (Barnes, 2005). A similar accident occurred in England in 2014, where a cyclist was severely injured after falling into the road due to a strong gust of wind and was subsequently hit by a car which was travelling behind (The Argus, 2014). It has been reported that about 5 % of all reported single bicycle accidents are caused by crosswinds (Schepers and Wolt, 2012). Fully understanding the flow structures on and around a cyclist is a perquisite in order to find solutions to minimise unwanted effects of crosswinds.

In order to reliably evaluate the aerodynamic forces acting on a cyclist, two types of approaches tend to be used: wind tunnel experiments and computational fluid dynamics simulations (CFD). The most commonly applied method of assessing posture differences is by wind tunnel experiments (Chabroux et al., 2012, Underwood et al., 2011, García-López et al., 2008, Grappe et al., 1997). In these studies the optimum aerodynamic positions are based on empirical (by trial and error) results, rather than evaluating the flow structures around a cyclist. Only a couple of experimental studies have investigated the effect of crosswinds on cyclists (Barry et al., 2012, Fintelman et al., 2014a). Both studies have shown that crosswinds have a significant effect on the aerodynamic force responses of the cyclist.

CFD offers the potential to provide a realistic insight into flow structures around a cyclist. However, to date this has not been extensively due to the relatively high computational power required in order to deal with the complex flow that occurs around the cyclist. However, this is slowly changing with the work of Hanna (2002), Lukes et al. (2004), Defraeye et al. (2010a) and Griffith et al. (2014) pioneering the way. It has been shown that CFD could provide reliable and accurate results compared to wind tunnel experiments and is therefore a valuable tool (Defraeye et al., 2010b). In a CFD study by Defraeye et al. (2010a) different

cycling positions (upright, dropped and time trial position) were validated and compared. It should be noted that the bicycle was excluded in these simulations. Their aerodynamic drag results were in reasonable good agreement with their wind tunnel experiments (relative difference smaller than 13 %) and showed the importance of CFD simulations in determining aerodynamic forces and moments. However, no attempt was made to understand the flow mechanisms or to investigate different wind conditions. Fintelman et al. (2014b) examined the flow structures which occurred as a result of a cyclist in dropped position subjected to crosswinds; unfortunately, the research was restricted to one cycling position. Further research is required since it is hypothesized that the aerodynamic forces and the flow structures alter with position and hence affect the stability and performance of the cyclist.

## 8.2 Numerical method

The time efficient steady Reynolds Averaged Navier Stokes (RANS) method has been used to investigate the flow field around a cyclist on a bicycle. The RANS method is commonly applied in numerical sport simulations, ranging from swimming (Zaïdi et al., 2008, Silva et al., 2008), rowing (Zhang et al., 2009), ski jumping (Meile et al., 2006) and bobsleigh (Dabnichki and Avital, 2006). The RANS equations for an incompressible Newtonian flow can be written as:

$$\rho\left(\frac{\partial \overline{u_i}}{\partial t} + \overline{u_j}\frac{\partial \overline{u_i}}{\partial x_j}\right) = -\frac{\partial \overline{p}}{\partial x_i} + \frac{\partial}{\partial x_j}\left(\mu\frac{\partial \overline{u_i}}{\partial x_j} - \rho\overline{u_i' u_j'}\right), \qquad (8.1)$$

where $\rho$ is the air density, $\mu$ is the dynamic viscosity and $t$, $u$, $p$ and $x_i$ are the time, velocity, pressure of the flow and coordinates respectively. The suffix notations $i$ and $j$ denotes x- and y-directions. The overhead bar denotes the time-averaged quantity and the term $\rho\overline{u_i' u_j'}$ the Reynolds stresses. These Reynolds stresses are a result of the turbulence and act on the mean flow. Turbulence models are used to close the system of mean flow equations. Turbulence

models can be split in two categories: the viscosity models and the stress models. In this work we only focus on the commonly used linear viscosity models. In these viscosity models, the Reynolds stresses are related by a linear relationship with the mean flow, defined as:

$$-\rho\overline{u_i'u_j'} = 2\mu_t S_{ij} - \frac{2}{3}\rho k\delta_{ij} \,, \tag{8.2}$$

where $\mu_t$ is the turbulent viscosity and $S_{ij}$ is the resolved rate of the strain expressed as:

$$S_{ij} = \frac{1}{2}\left(\frac{\partial\overline{u}_i}{\partial x_j} + \frac{\partial\overline{u_j}}{\partial x_i}\right). \tag{8.3}$$

The turbulent kinetic energy, *k,* is defined as:

$$k = \frac{1}{2}\overline{u_i'u_i'} \,, \tag{8.4}$$

and $\delta_{ij}$ the Kronecker delta, defined as:

$$\delta_{ij} = \begin{cases} 1 & \text{if } i = j \\ 0 & \text{otherwise} \end{cases}. \tag{8.5}$$

The standard two equation *k*-ε model turbulence model (Launder and Spalding, 1974) is used, as this turbulence model has been shown to give the most accurate RANS results compared with experiments (Fintelman et al., 2014b) (relative drag coefficient difference of 7 %). This was supported by Defraeye (2010b) who also demonstrated that the standard *k*-ε gives a reasonable accuracy for the aerodynamic drag compared to their wind tunnel experiments (relative difference of 4 %). The *k*-ε model adds two additional transport equations that represent the turbulence properties of the flow. The turbulent viscosity $\mu_t$ is not a constant, but is a function of $k$ and $\epsilon$:

$$\mu_t = \rho C_\mu \frac{k^2}{\epsilon} \,, \tag{8.6}$$

where $C_\mu$ is a constant set at 0.09 (Launder and Spalding, 1974).

## 8.3 Computational model

Two different cycling positions are investigated: the dropped position and the time trial position. Within these positions different torso angle positions are analysed. The torso angle's assessed in the time trial position are 0°, 8° and 16° relative to the ground, whilst in the dropped position the 16° and 24° torso angles are examined. These cycling positions are frequently used by cyclists (Fintelman et al., 2014c). The geometries used in the simulations are shown in Figures 8.1 and 8.2. These geometries were created in the commercial software package AutoDesk Inventor Professional 2013. The geometry (anthropometry) of the cyclist is kept constant in both cycling positions. In the time trial position, a time trial helmet and bicycle with time trial handlebars (Felt B12, Felt racing LLC, Irvine, USA) are included, whilst in the dropped position a road helmet and bicycle (CIOCC Dragster, CIOCC ISB SRL, Bergamo, Italy) are used. The time trial handlebar pads are positioned 100 mm apart. The geometries of all the parts of the bicycle are kept as close as possible to the actual dimensions and shapes. For simplicity, only the main details are included and small components such as cables and spokes are omitted. In addition, the computational resource required to resolve the flow around these components is considered excessive. The model has a length of 1.7 m and a width of 0.5 m in all considered cycling conditions. The model height is dependent on the torso angle position and is approximately 1.2 m, 1.3 m, 1.4 m and 1.5 m for the 0°, 8°, 16° and 24° torso angles respectively. Unless otherwise stated, all methodological approaches are similar across all cycling positions.

(a) (b)

**Figure 8.1 Representation of the dropped positions examined in the simulations. Torso angles adopted are the 16° and 24° relative to the ground; grey and orange jersey respectively. (a) frontal view; (b) side view.**

(a) (b)

**Figure 8.2 Representation of the time trial positions examined in the simulations. Torso angle positions adopted are the 0°, 8° and 16° relative to the ground; green, red and blue jersey respectively. (a) frontal view; (b) side view.**

### 8.3.1 Boundary conditions and computational domain

The bicycle with a cyclist is positioned in a computational domain of 32 m in the cycling travelling direction, comprising of a height of 8 m and a width of 32 m (Figure 8.3). The model is located 7 m from the two inlets to prevent interaction of the pressure field of the inlet with that around the model. Identical boundary conditions are applied in the different cycling position models. No-slip boundary conditions are used on the bicycle and cyclists' surface and on the floor of the computational domain. Inlet velocity boundary conditions were applied on the inlet and zero pressure boundary conditions were applied on the outlet boundaries of the domain. The flow enters the computational domain with uniform velocity constant in time with a turbulence intensity of 0.67 %. This is the observed turbulence intensity of the wind tunnel experiments of Fintelman et al. (2014a), to which the aerodynamic force coefficients will be compared. The inlet velocity is dependent on the yaw angle $\beta$ and is determined by:

$$U_x = U_\infty \cos(\beta)\ ,\ U_y = U_\infty \sin(\beta)\ , \tag{8.7}$$

where $U_x$ and $U_y$ are the inlet velocities in the x and y direction respectively and $U_\infty$ the free stream velocity of 9.91 m/s. The Reynolds number is 1.0 x $10^6$ based on the height of the cyclist from the ground, $H$, in the 24° torso angle dropped position, which has been taken as 1.52 m .

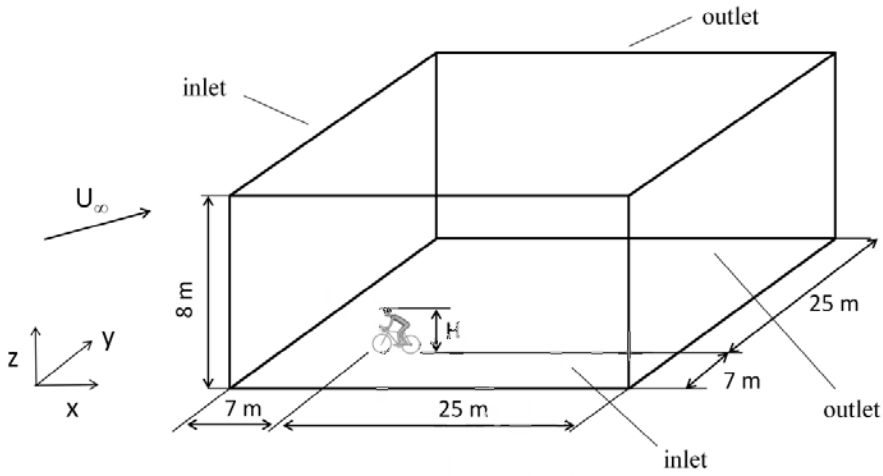


**Figure 8.3 Computational domain, where H is the height of the cyclist from the ground**

The turbulence in the boundary layer is estimated by standard wall functions based on the log law. In the turbulent region (log law region), a local equilibrium is assumed between the production and the dissipative kinetic energy. In this region the length scale grows linearly with the distance from the wall.

### 8.3.2 Mesh

The open source snappyHexMesh utitlity of OpenFOAM is used to create the surface mesh on the bicycle and cyclists and the mesh around it. To make a finer mesh close to the bicycle, a refinement area of 3.0 m x 1.4 m x 1.6 m is used. Another refinement area of 7.7 m x 8.6 m x 2 m is defined in the direction of the main flow originating at the upstream side of the bicycle. For a cyclist in dropped position, Fintelman et al. (2014b) examined three different meshes: coarse, medium and fine mesh with $7.3 \times 10^6$, $13.1 \times 10^6$ and $17.9 \times 10^6$ nodes, respectively. The meshes were formed of approximately 96 % of hexahedral elements and about 4 % of polyhedral elements. As shown by Fintelman et al. (2014b), a good agreement between the results obtained from the fine and medium meshes is shown. The numerical uncertainty in the

fine grid solution for the drag coefficient and the side force coefficient were 0.4 % and 0.2 %, respectively. This suggests that the resolution of the fine mesh is adequate to correctly predict the flow. Therefore in this study, all results are based on the aforementioned fine mesh.

### 8.3.3 Numerical implementations

The numerical flow is solved with the three-dimensional finite volume method. The convective and diffusion fluxes are approximated using a Gaussian second order upwind scheme. In order to limit numerical dissipation, second order discretisation schemes are used. The pressure and velocity are coupled with the SIMPLE algorithm.

## 8.4 Results and Discussion

RANS simulations are carried out for the flow around two bicycle and cyclist models, where the cyclist is positioned in a time trial or dropped position and in different torso angles. The aim of this study was to investigate the influence of different cycling positions on the flow field around a cyclist and bicycle subjected to crosswinds. Different visualisation techniques are used to visualise the time-averaged flow structures around the cyclist.

### 8.4.1 Aerodynamic forces and moments

The obtained aerodynamic forces and moments coefficients are defined as:

$$CF_X = \frac{F_X}{0.5A\rho{U_\infty}^2}, \qquad CF_Y = \frac{F_Y}{0.5A\rho{U_\infty}^2}, \qquad CF_Z = \frac{F_Z}{0.5A\rho{U_\infty}^2},$$
$$CM_X = \frac{M_X}{0.5HA\rho{U_\infty}^2}, \qquad CM_P = \frac{M_Y}{0.5HA\rho{U_\infty}^2}, \qquad CM_Z = \frac{M_Z}{0.5HA\rho{U_\infty}^2} \qquad (8.8)$$

where A is the total frontal area of the cyclist and bicycle in the 24° torso angle dropped position (0.55 $m^2$). $F_X$, $F_Y$ and $F_Z$ are the drag force, side force and lift force and $CM_X$, $CM_Y$ and $CM_Z$ are the rolling, pitching and yawing moment, respectively.

For each of the aerodynamic force coefficients, a similar behaviour across the different crosswind yaw angles are found, see Figure 8.4. The aerodynamic force coefficient findings are compared with wind tunnel results of Fintelman et al. (2014a). The numerical drag coefficient results are comparable with experimental results observed in the 16° and 24° dropped position, as shown in Table 8.1. The drag forces at zero crosswinds are underestimated by about 7 % and 11 % for the drag forces in the 16° and 24° torso angle positions, respectively. The side forces at β=45° are underestimated by 19 % and 18 %. The under prediction is likely caused by the simplification of the geometry, surface roughness dissimilarities, physical model uncertainties and small oscillations of the mannequin in the experiments, in particular at large yaw angles. It has been shown by

**Table 8.1 Force coefficients at different crosswinds yaw angle: β = 0° and β = 45°.**

| | $CF_X$ (β=0°) | Exp. $CF_X$ (β=0°) | $CF_Y$ (β=45°) | Exp. $CF_Y$ (β=45°) |
|---|---|---|---|---|
| 16° | 0.50 | 0.56 | 0.82 | 1.02 |
| 24° | 0.57 | 0.61 | 0.83 | 1.01 |

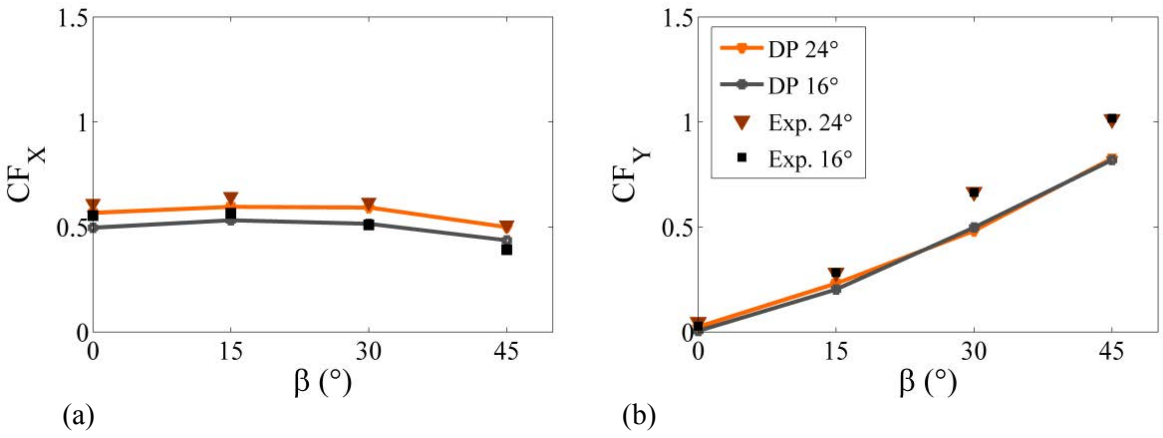


**Figure 8.4 Experimental and numerical force coefficients in the dropped position at a 16° and 24° torso angle, respectively. (a) drag force coefficient $CF_X$, (b) side force coefficient $CF_Y$.**

Karabelas and Markatos (2012) that for a stationary wheel at a 45° yaw angle, the spokes could increase the side forces by about 1.1 N. About 50 % of the under prediction at large yaw angles could therefore explained by the treatment of the modelling of the wheels.

Figure 8.5 shows the drag, side and lift forces together with the rolling, pitching and yawing moments at different crosswinds yaw angles and positions. It can be observed in Figure 8.5 that for a 16° torso angle, the time trial position significantly reduces the aerodynamic drag by about 18 % (0.413 vs 0.506) compared with the dropped position in windless conditions ($\beta$=0°). On the other hand, a significant higher side force up to 18 % can be experienced when riding in a time trial position with crosswinds up to 45°. The rolling and pitching moments significantly decrease in the time trial position across the different yaw angles. Although the lift forces are higher in a time trial position compared to a dropped position, the differences are marginal.

The torso angle has a significant effect on the aerodynamic drag within the two typical cycling positions, e.g. dropped and time trial position. When comparing the 16° and 24° torso angle dropped position in windless conditions, the drag is reduced by about 9 % (0.506 vs 0.554). Lowering the time trial position from 16° to 0° reduces the drag by about 11 % (0.413 vs 0.368). Across different crosswind yaw angles, the results show that in particular the drag forces and pitching moments are reduced by lowering the torso angle within either the time trial or dropped position. Negligible differences in crosswind effects are observed in the side forces, rolling and yawing moments with increasing yaw angles.

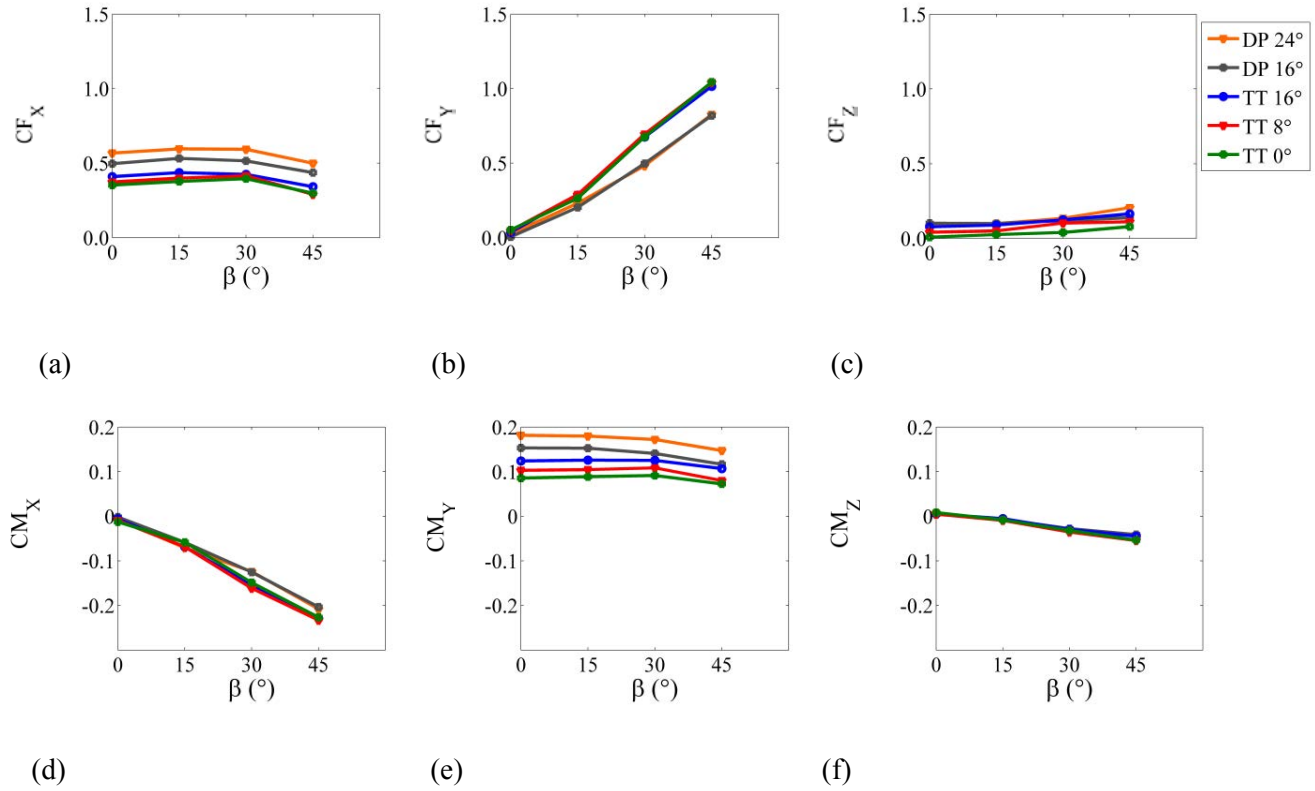


**Figure 8.5 Aerodynamic forces and moments coefficients in the different torso angle positions across different crosswind yaw angles, β. The dropped position (DP) and time trial position (TT) are used. Within these positions, the torso angle position is altered. (a) drag force coefficient, $CF_X$, (b) side force coefficient, $CF_Y$, (c) lift force coefficient, $CF_Z$, (d) rolling moment coefficient, $CM_X$, (e) pitching moment coefficient, $CM_Y$, (f) yawing moment coefficient, $CM_Z$.**

### 8.4.2 Streamlines

The streamlines are used to identify the circulation regions around the vortex cores. It should be noted that although the critical points in the three dimensional space are found, caution has to be taken in the data points far from the surface due to the fact that the streamlines are not Galilean invariant (Spalart and Shur, 1997). Figure 8.6 shows the time-averaged velocity streamlines projected on the x-z plane across different cycling positions at β = 0°. Two main vortices appear in the flow field in Figure 8.6. They can be described as follows: vortex Vc1 appears underneath the saddle of the bicycle and vortex Vc2 originates at the leeward side of the road helmet and only appears in the dropped position. The position of Vc1 depends on the

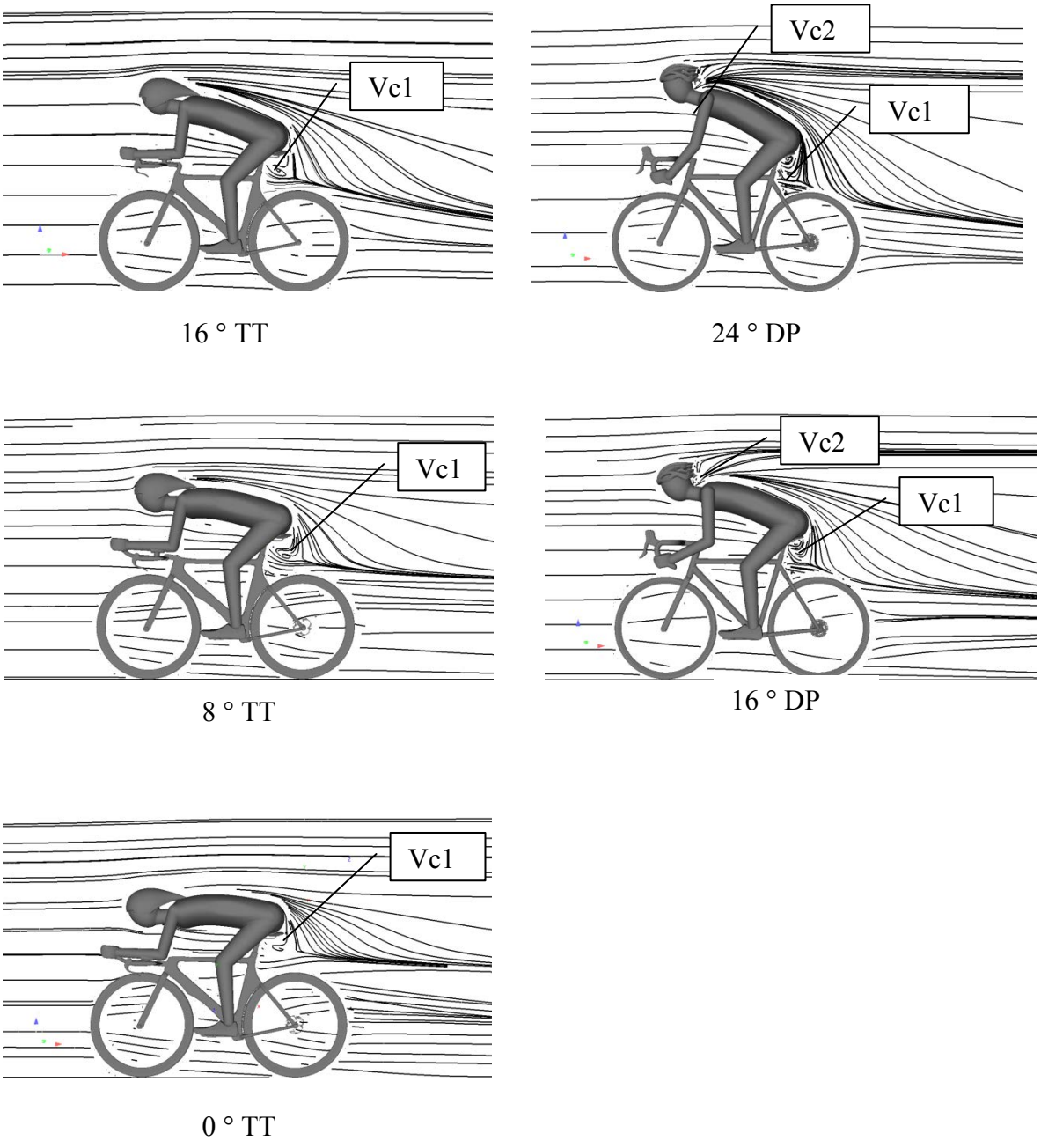


**Figure 8.6 Time averaged velocity streamlines projected on the x-z plane across different cycling positions, showing the development of the flow structures in the case of the 0° yaw angle. DP, dropped position; TT, time trial position.**

cycling position; this vortex appears higher (e.g. closer to the saddle) in the dropped position than in the time trial position. As the air from the back of the cyclist approaches the buttocks, the flow forces the side of the vortex Vc1 to rotate towards the bicycle. The circulation areas around Vc1 are comparable in size across the different cycling positions. Moreover the flow

remains attached to the upper body in the wake region in all conditions and the flow perfectly follows the shape outline of the upper body. However, the wake area increases at higher torso angle positions, whereas the velocity in the wake significantly decreases. In particular low flow velocities are found at the leeward side of the cyclist, hence increasing the cyclist's drag.

In Figure 8.7, the velocity streamlines are shown in case of a 45° yaw angle projected on a plane in the free stream flow direction. In these planes, no dominant critical points can be detected in the flow. It is interesting to note that the direction of the flow in the leeward site of the upper body of the cyclist changes due to the torso angle position. In the time trial position, the flow at the leeward side of the body is reflected in the positive z direction (upward), whilst for the dropped position the flow is moving in negative z direction (downward) and consequently decelerates the fluid flow.

In Figure 8.8(a) the velocity streamlines projected on a horizontal x-y plane at a height of 0.7H are shown for the time trial and dropped position at a torso angle of 16° and no crosswinds. It can be seen in Figure 8.8(a) that the width of the wake of the main body is significantly smaller in the time trial position than in the dropped position, which corresponds to the smaller total drag of the cyclist in the time trial position. This reduction is predominantly caused by differences in arm spacing. In the time trial position, the arms are positioned about twice as close together than in the dropped position at a height of 0.7H.

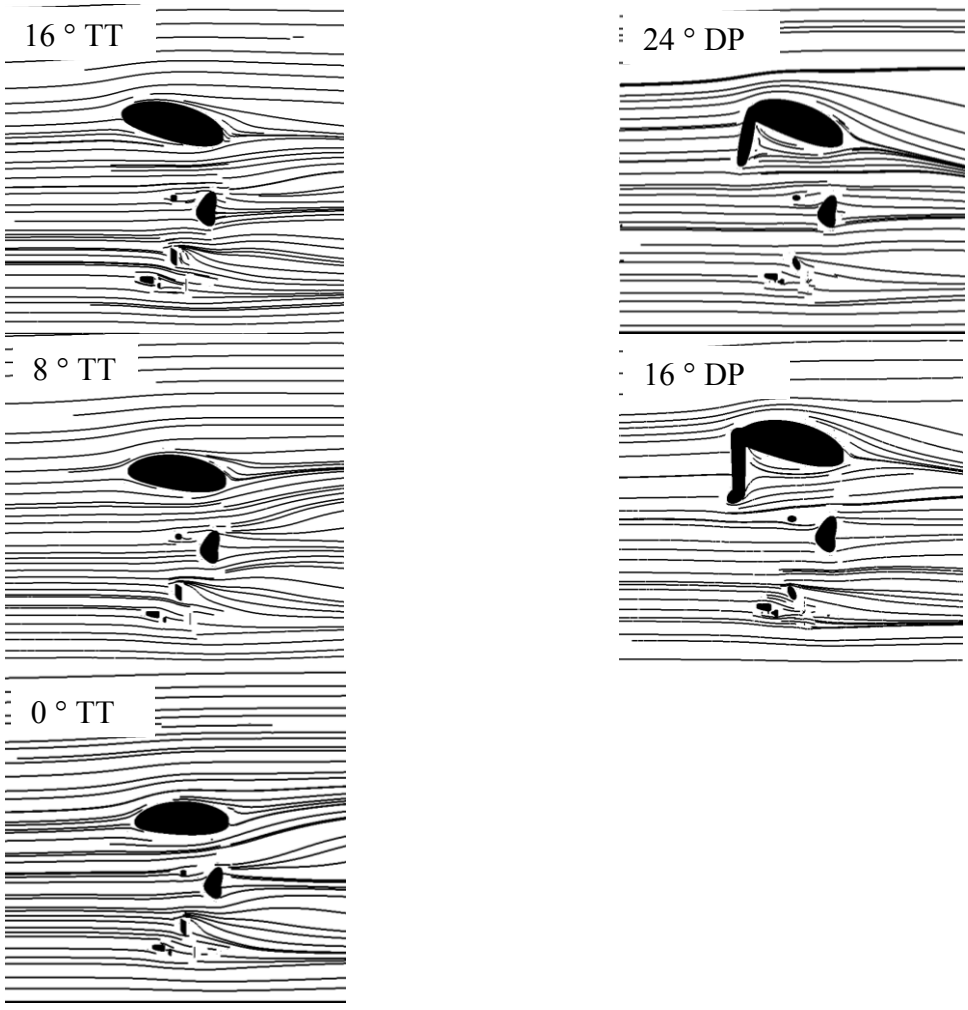


**Figure 8.7 Time averaged velocity streamlines projected on the 45° rotated x-z around the z axis across different cycling positions, showing the development of the flow structures in the case of the 45° yaw angle (plane in the main flow direction).**

In the dropped position significant flow separation and recirculation takes place at the leeward side of the arms, widening the wake of the flow. In the time trial position, the arms are in front of the body, resulting in a smaller wake area behind the arms and affecting the flow development to a lesser extent. The wake variations are a result of the cyclists' body upstream disturbance of the flow, influencing the flow field behind the arms as shown in the pressure fields of Figure 8.8(b). The interaction of the main body with the arms reduces the overpressure area in front of the main body, generating less flow separation and recirculation

behind the arms. A recent CFD study also showed that wider arm spacing in a time trial position increases the drag (Defraeye et al., 2014). It should be noted however that due to anthropometric differences between cyclists, the optimal arm spacing in time trial position is dependent on the cyclist (Defraeye et al., 2014, Underwood et al., 2011). At large crosswind yaw angles (β=45°), the development of the flow projected on the x-y plane at a height of 0.7H is comparable for both positions (dropped and time trial position). At this crosswind angle the arms do not contribute significantly to the wake area.

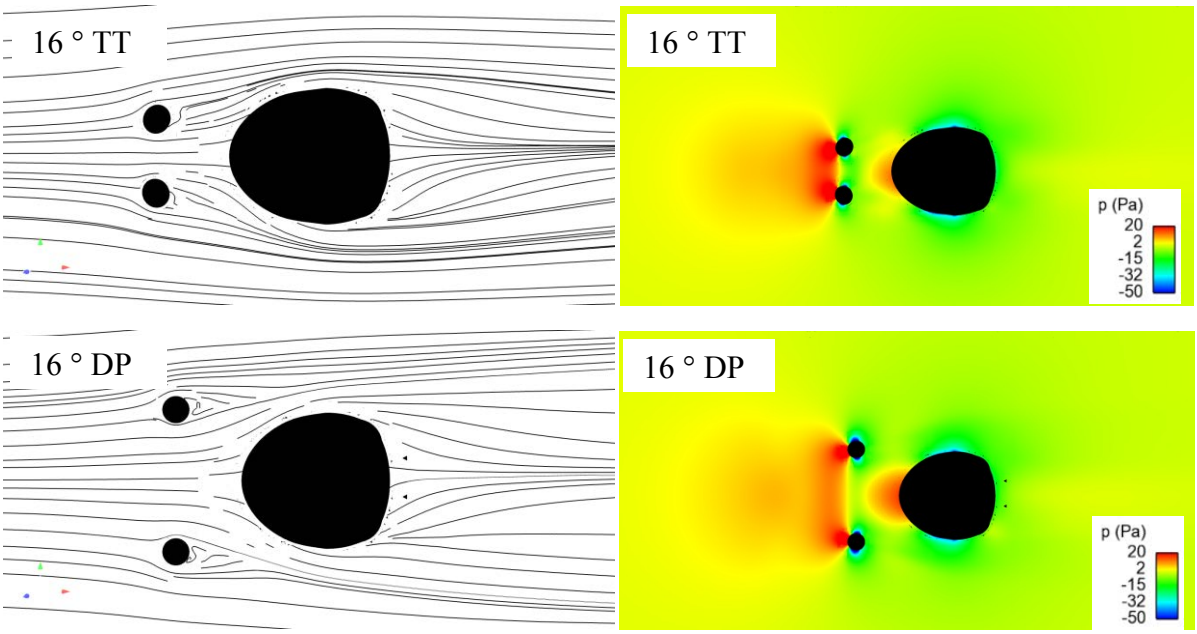


**Figure 8.8 Time averaged velocity streamlines and pressure projected on the x-y plane at 0.7H across different cycling positions , Dropped position (DP) and time trial position (TT) in the case of the 0° yaw angle (horizontal plane in the main flow direction): (a) time averaged velocity streamlines showing the development of the flow structures, (b) time averaged pressure showing the pressure interaction between arms and the body.**

### 8.4.3 Pressure distribution and contour lines

The pressure contour lines on the cyclist are shown in Figure 8.9. As expected, when changing the crosswind yaw angle from 0° to 45°, the high pressure areas move from the front to the side of the body. When comparing the dropped and time trial positions at $\beta = 0°$, in both positions high pressure regions are found on the windward side of the head, upper arms and legs. Low pressure regions are mainly found at the side of the upper arms and the legs, arising mainly from the flow separation at the sides of the limbs. These flow regions are comparable to those seen for a turbulent flow around a non-rotational cylinder, where the flow separates from an angle of ~90° with respect to the upstream flow (Achenbac, 1968). At $\beta = 0°$, the maximal negative pressure on the arms is significantly lower in the dropped position, $p = -94.7$ Pa, compared to the time trial position, $p = -65.1$ Pa. This corresponds with the difference in the flow structures seen in the streamlines and pressure field around the cyclists' body. Due to the reduction in arm spacing in the time trial position, the surface pressure is reduced contributing to the observed decrease in drag. At a large yaw angle ($\beta = 45°$), small differences are observed in the pressure levels in the two different cycling positions, see Figure 8.9. This is consistent with the slight changes in the flow field structures around the cyclists' body presented earlier. This implies that the pressure difference at large crosswind yaw angles does not contribute to increased aerodynamic responses found in the dropped position compared to the time trial position.

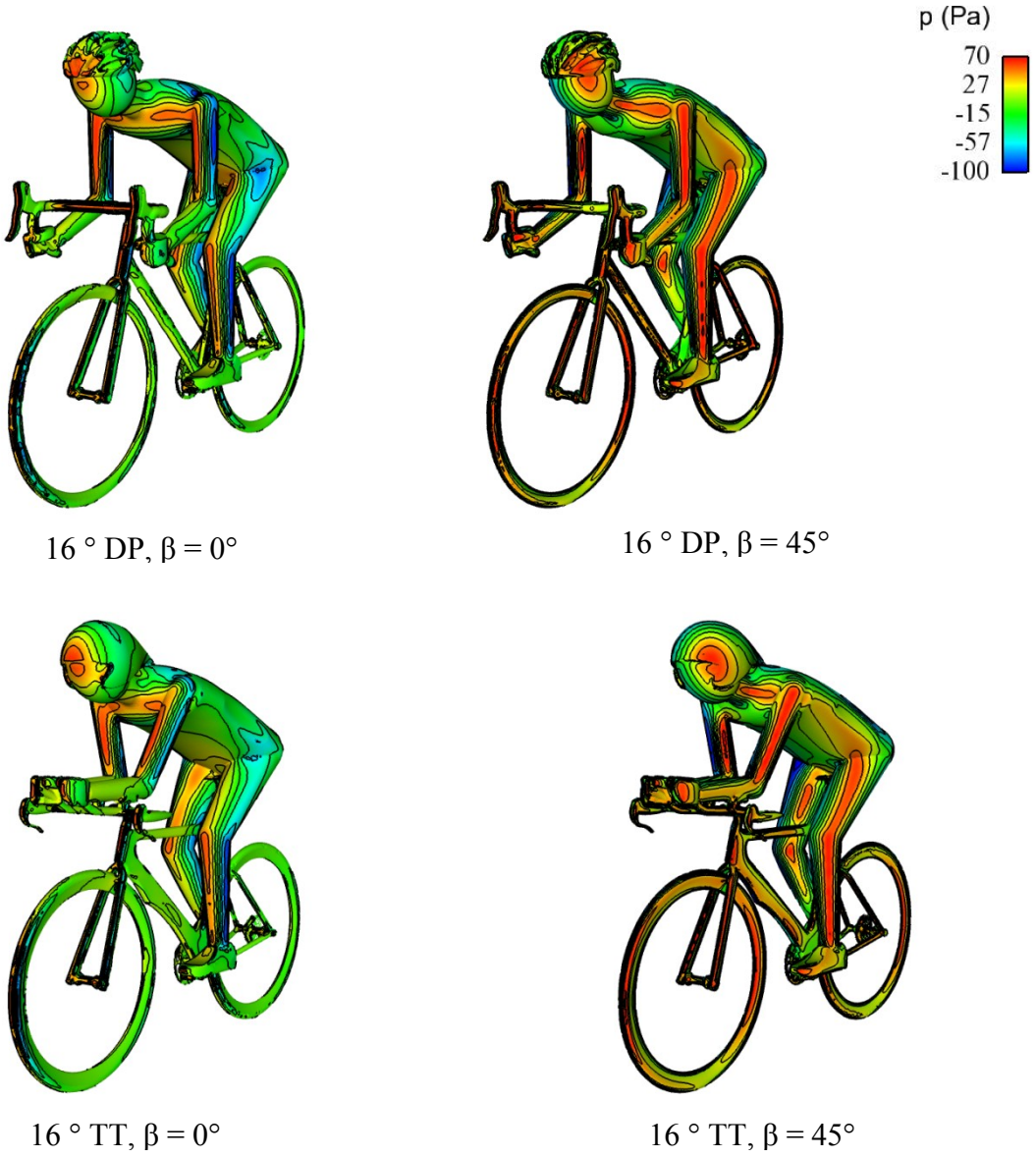


**Figure 8.9 Pressure surface and corresponding pressure contour lines on the surface of the cyclist in different cycling position and across different yaw angles.**

### 8.4.4 Isosurface pressure

The isosurface of the coefficient of pressure at $C_p = -0.240$ in different cycling positions are shown in Figure 8.10. For the case of no crosswind (β=0°), the time trial position and dropped position isosurface pressures are comparable. However, for a crosswind of 45° the surface pressure is significantly changed; larger isosurface pressure volumes are generated in the time trial position, in particular behind the time trial helmet, frame, and wheels of the time trial

bicycle. These results provide an insight as to why there is difference in side forces in crosswinds experienced by both the time trial and dropped positions.

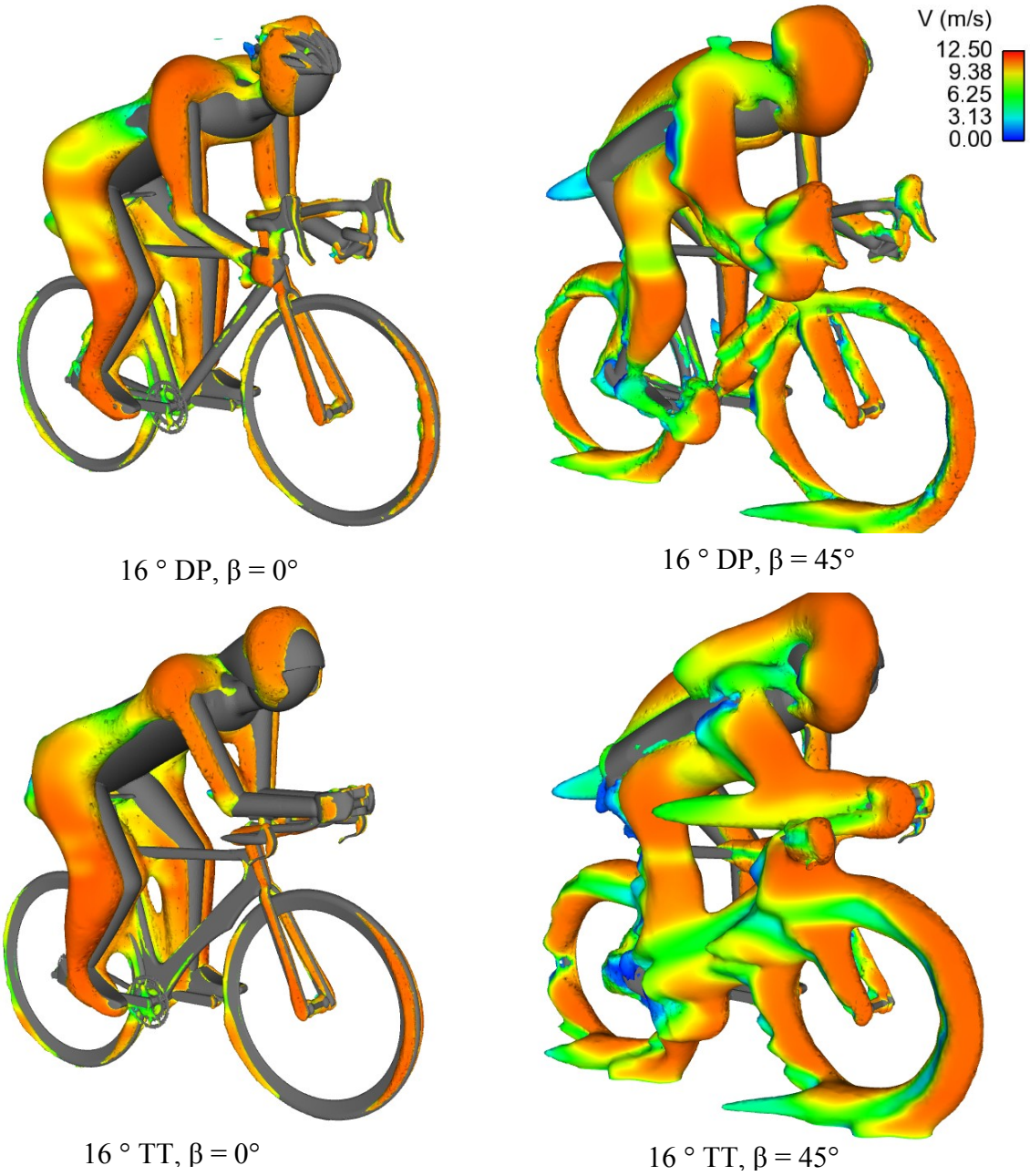


**Figure 8.10 Isopressure surface at Cp = -0.240 at different cycling positions (dropped position (DP) and time trial position (TT)) at a 16° torso angle and varying crosswind yaw angles (0°-45°). The isopressure is coloured by the flow velocity.**

## 8.5 Conclusion

The RANS simulations have provided new insight into how changes in the position of a cyclist and corresponding differences in yaw angles influence the flow structures in the flow around a cyclist. It has been observed that there are higher drag force coefficients in the dropped position compared to those of the time trial position at no crosswinds (β=0°). These are associated with an increased wake area, mainly originating from differences in arm spacing and helmet geometry. Moreover, additional vortices in the leeward side of the helmet and behind the arms are found in the dropped position. At large crosswind yaw angles (β=45°), in the time trial position large negative pressures are generated in the wake of the bicycle and cyclist. Significant changes in the flow structures around the time trial bicycle and helmet are found, whilst the surface pressure and the flow structures around the upper body are comparable with that of the dropped position. Lowering the torso angle position within a typical cycling position (dropped or time trial position) significantly reduces the wake and yields significant drag force and pitching moment reductions across different yaw angles. The results imply that at large crosswind yaw angles not the cycling position but the cycling equipment plays a major role in the acting aerodynamic side forces and rolling moments, which may influence the stability of the bicycle.

# CHAPTER 9

# Motorbike in crosswinds

**Abstract** [1]

Crosswinds have the potential to influence the stability and therefore the safety of a motorbike rider. Numerical computations using both Delayed Detached Eddy Simulations (DDES) and Reynolds-Averaged Navier-Stokes (RANS) were employed to investigate the flow around a motorbike subjected to crosswinds with yaw angles of 15, 30, 60 and 90 degrees. The Reynolds number was 2.2 million, based on the crosswind velocity and the height of the rider from the ground. The aerodynamic force coefficients and flow structures around the motorbike and rider were obtained and analysed. Although both DDES and RANS provided comparable overall aerodynamic forces, RANS failed to predict both the DDES surface pressures at the separation regions and location and size of the main circulation region. The DDES results showed that the drag coefficients decrease with increasing yaw angles, while the side force coefficients significantly increase. It was found that increasing yaw angles resulted in stronger vortex shedding around the windshield and helmet.

[1] This chapter has been published as: Numerical investigation of the flow around a motorbike subjected to crosswinds. *Engineering Applications of Computational Fluid Mechanics* (2015), doi: 10.1080/19942060.2015.1071524.

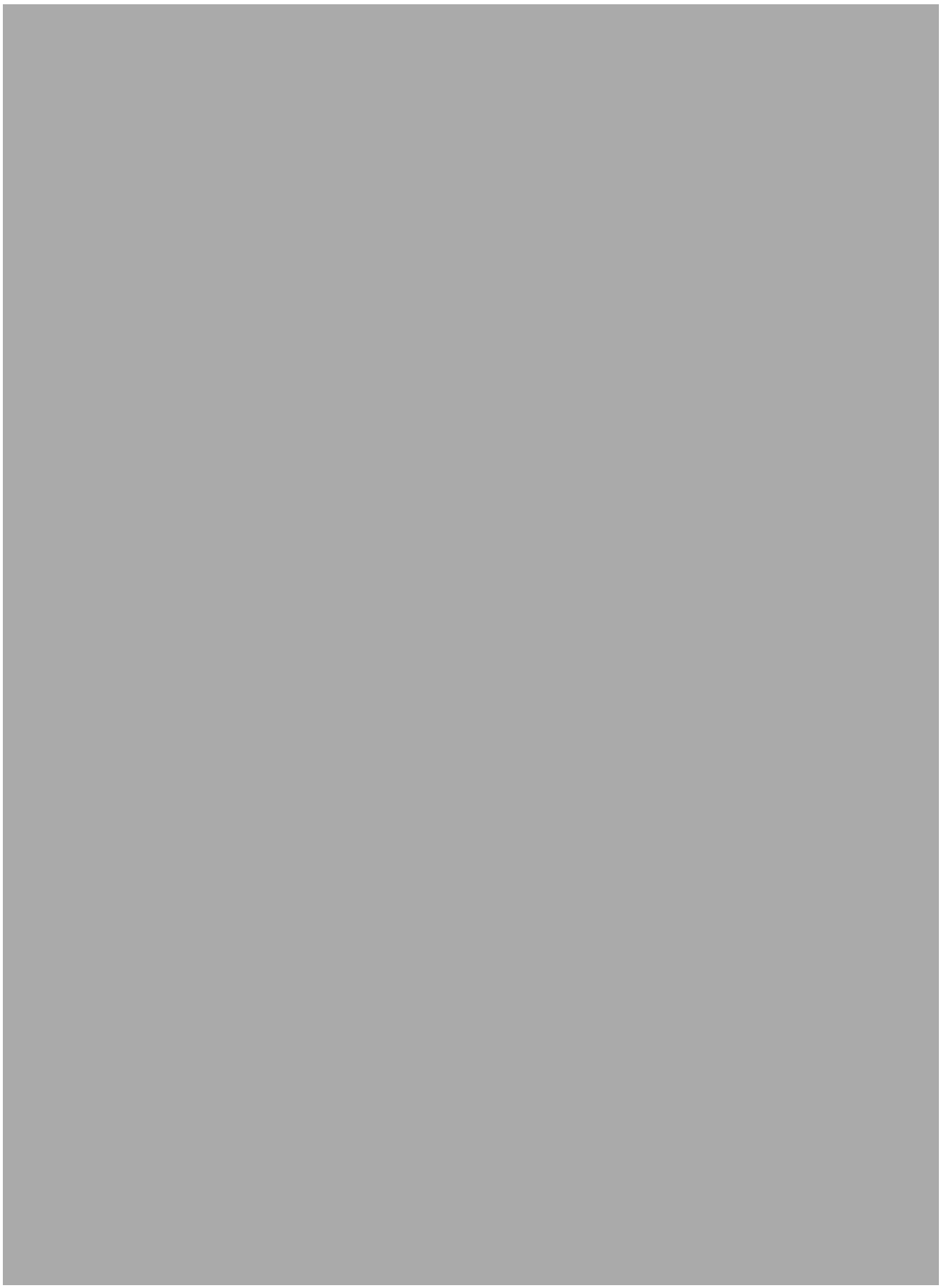

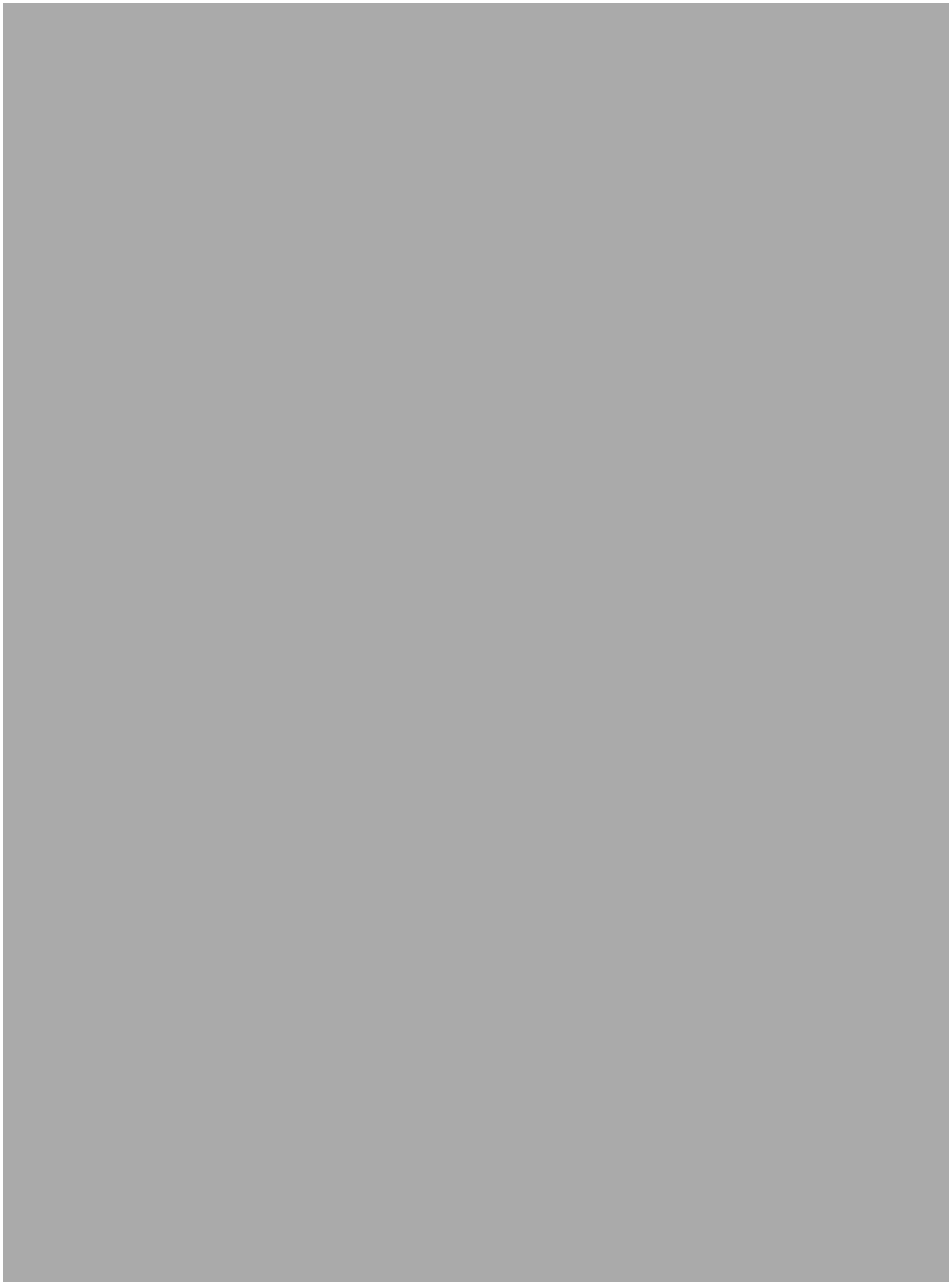

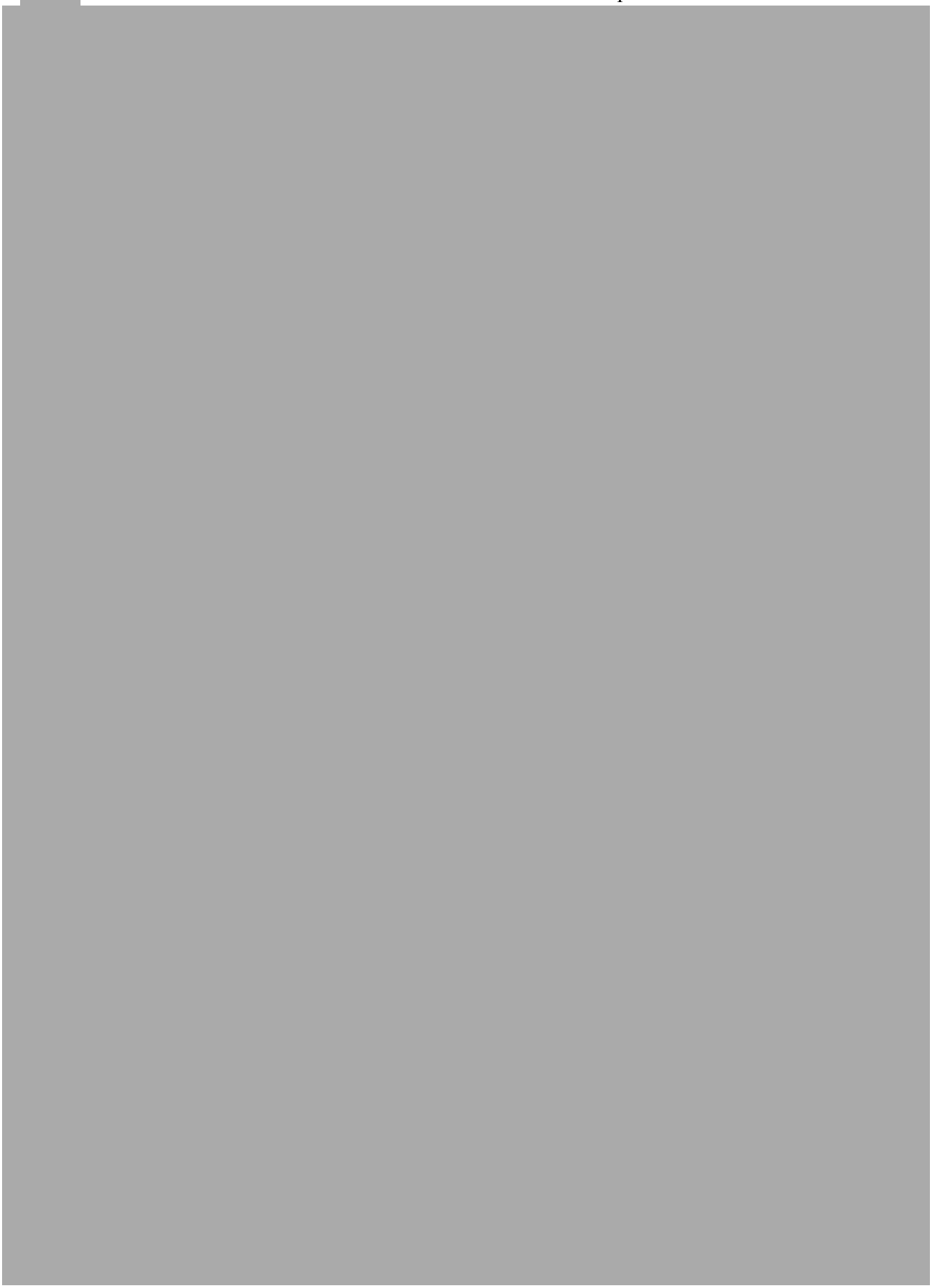

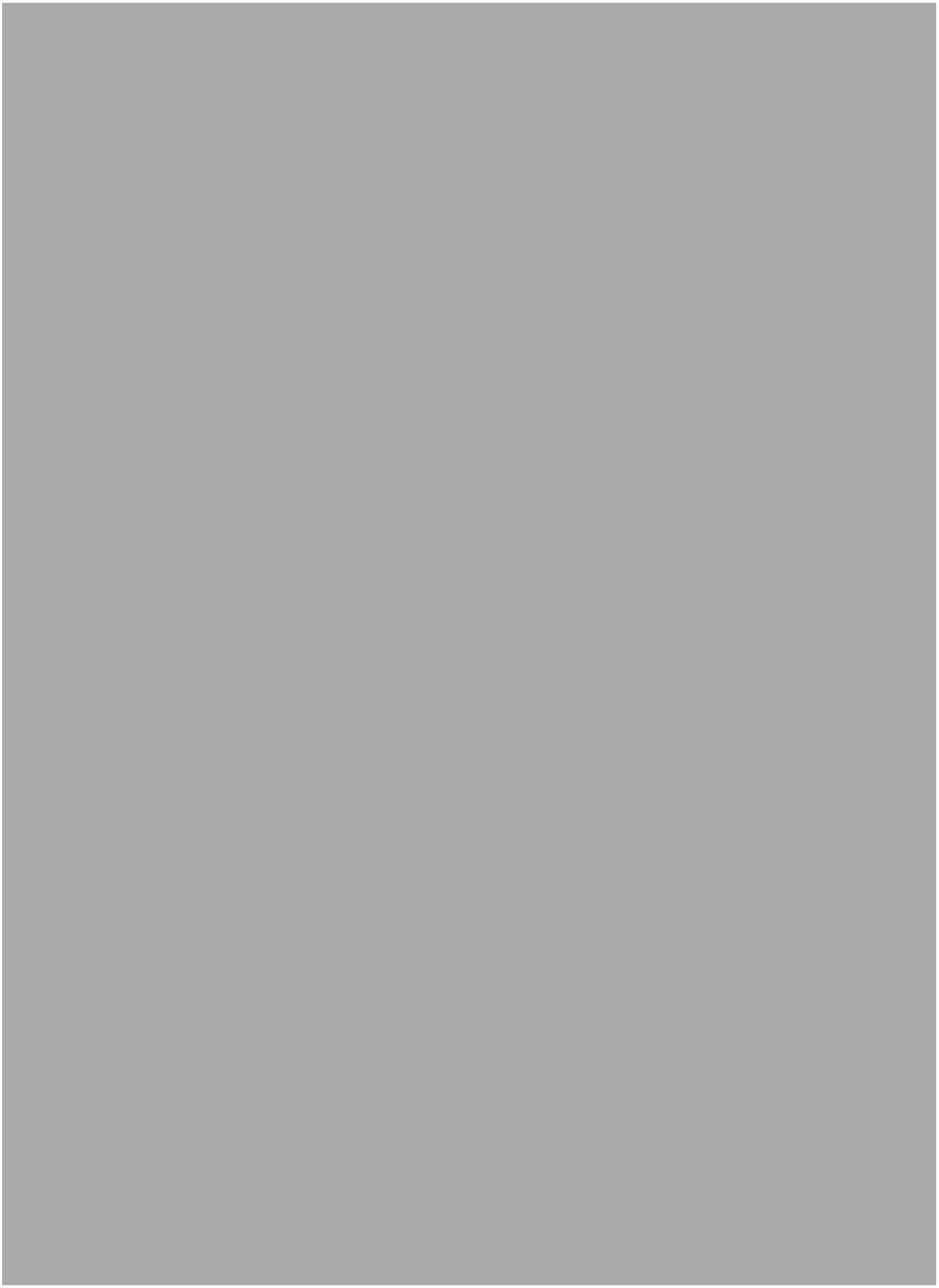

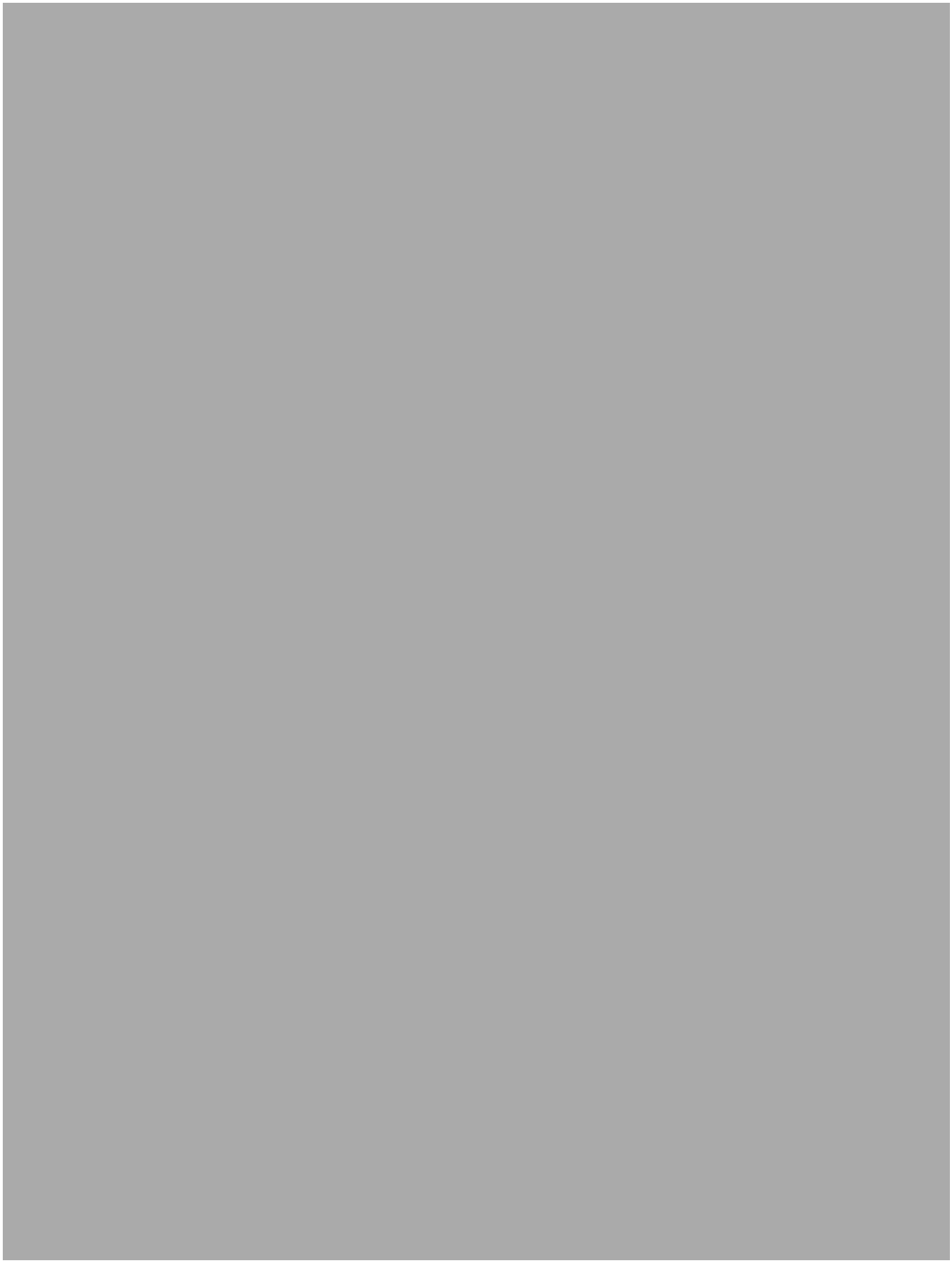

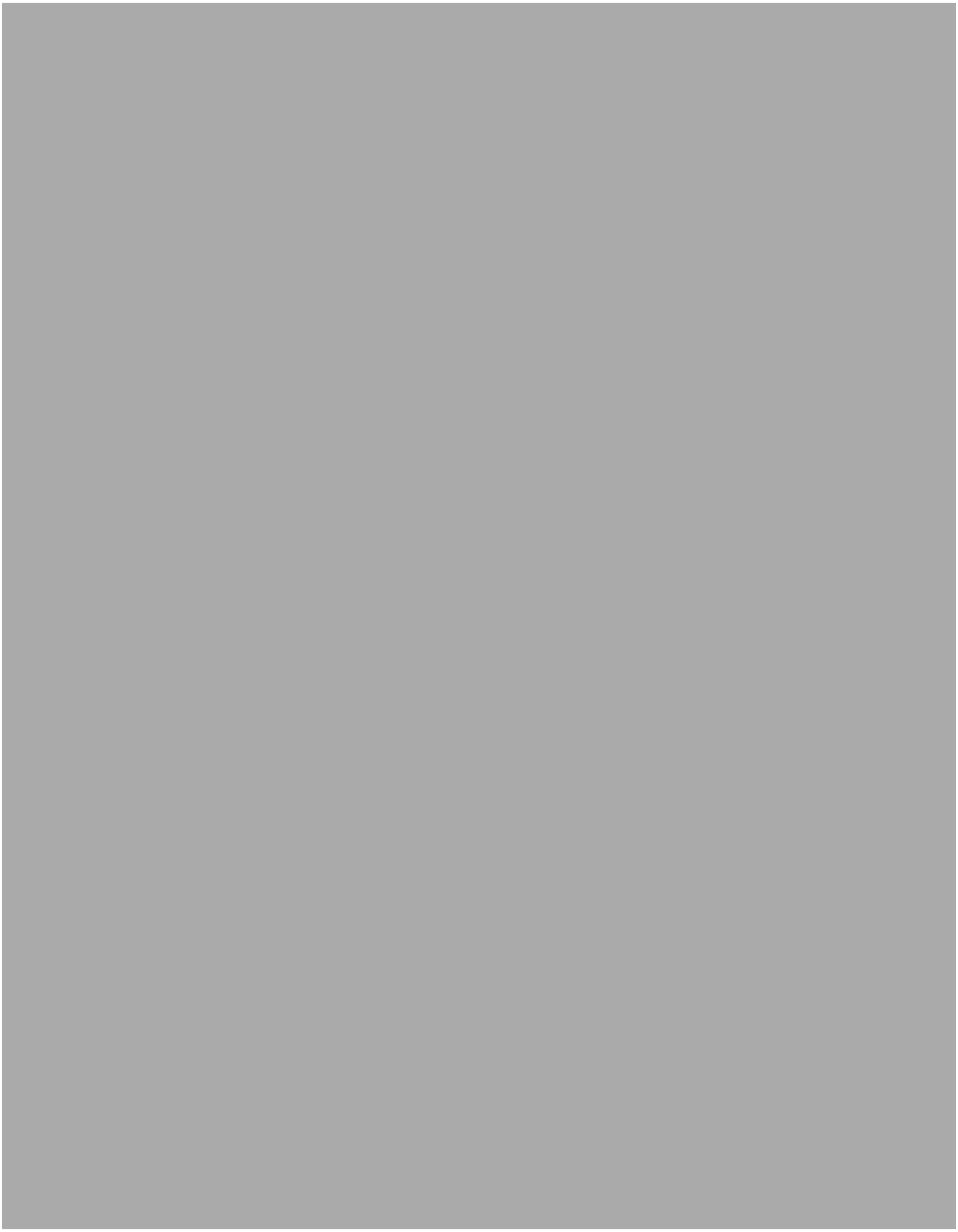

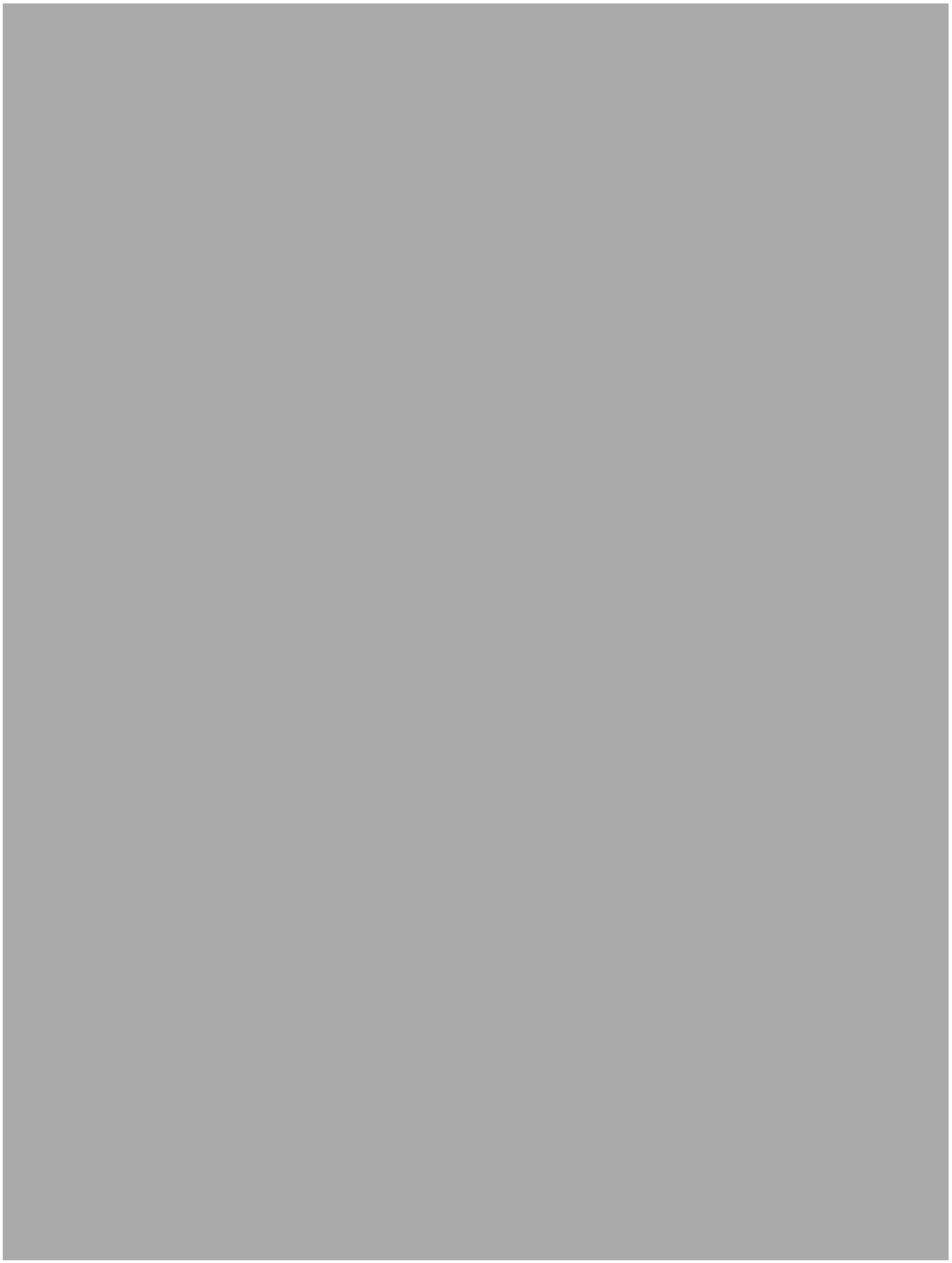

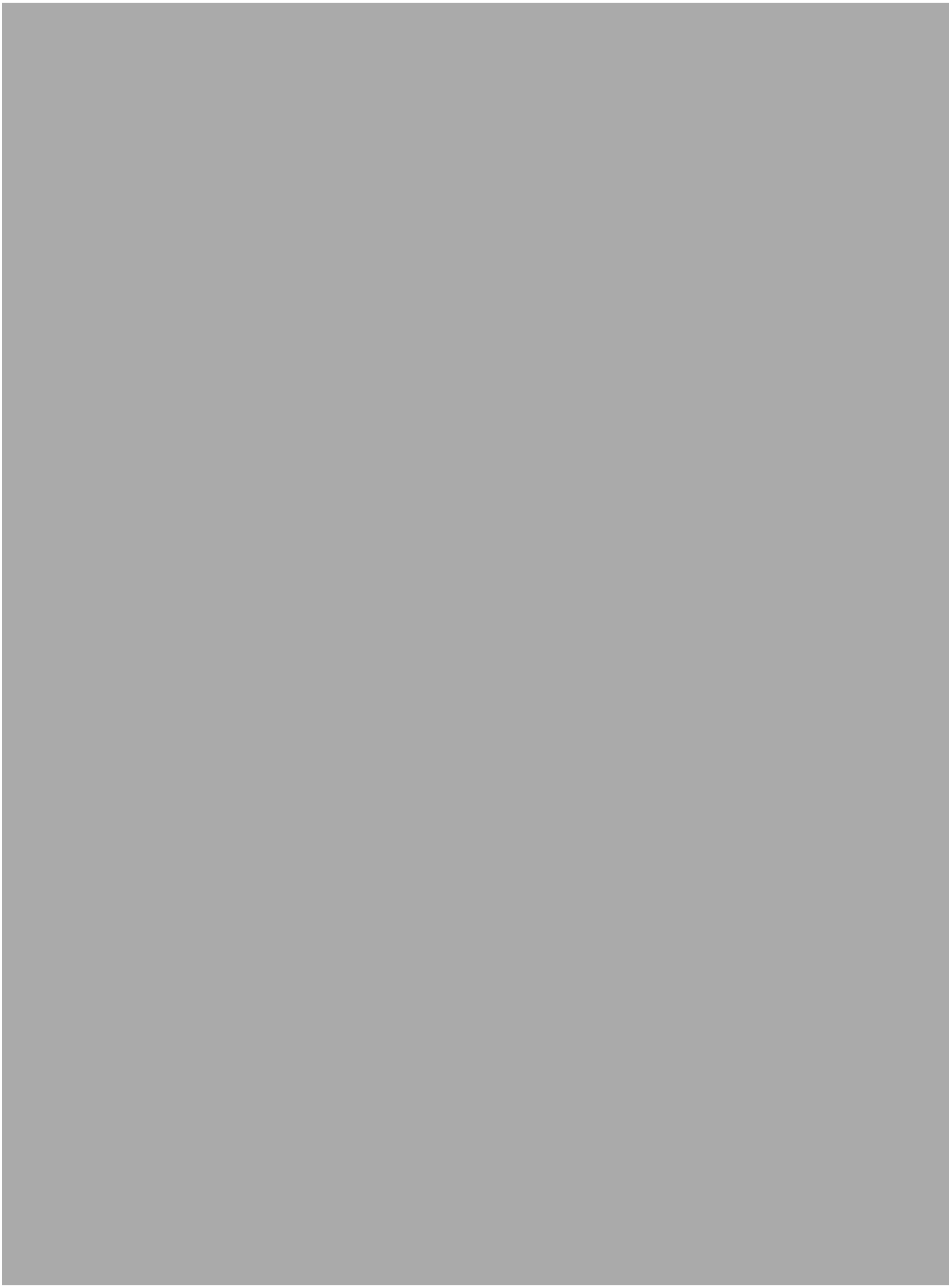

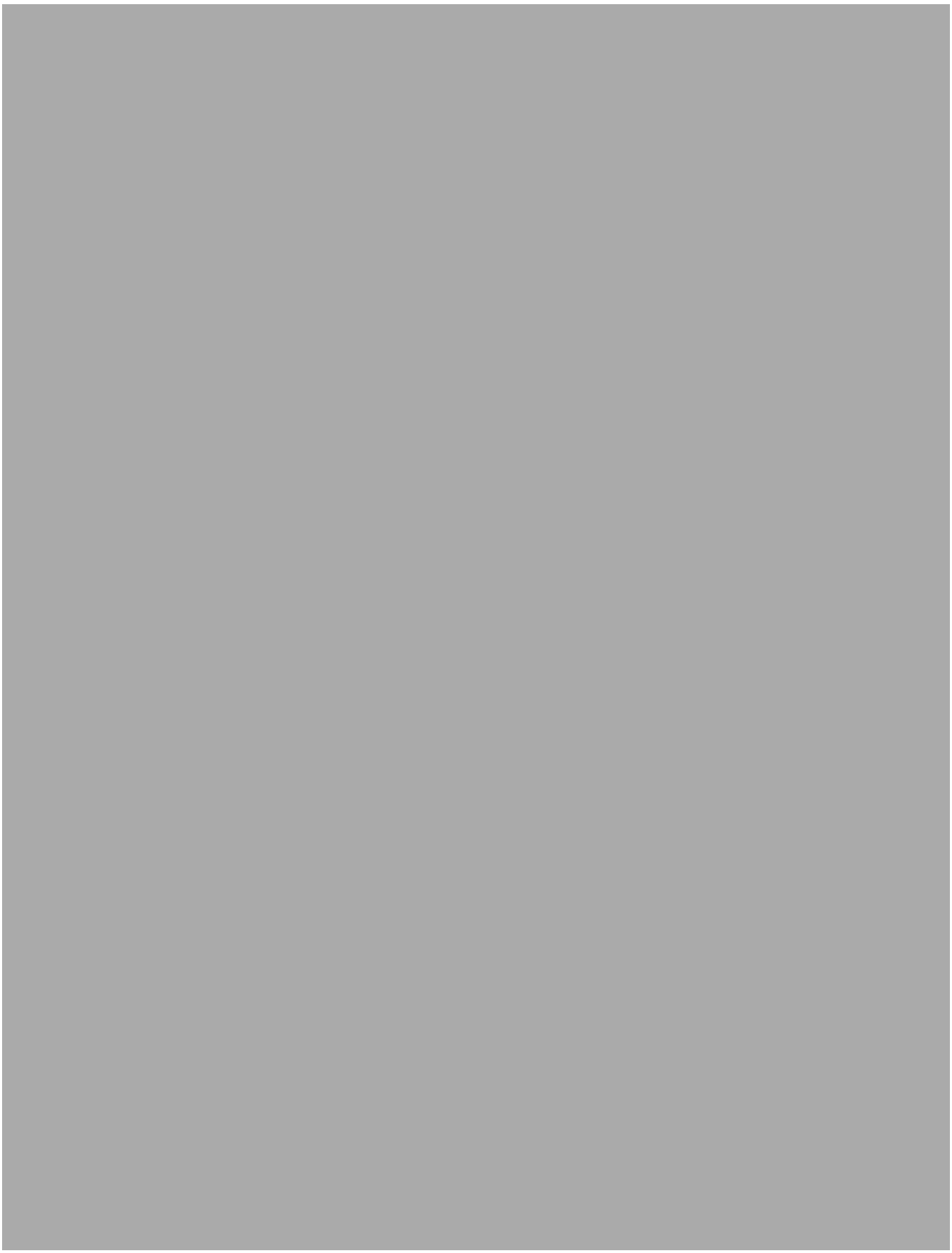

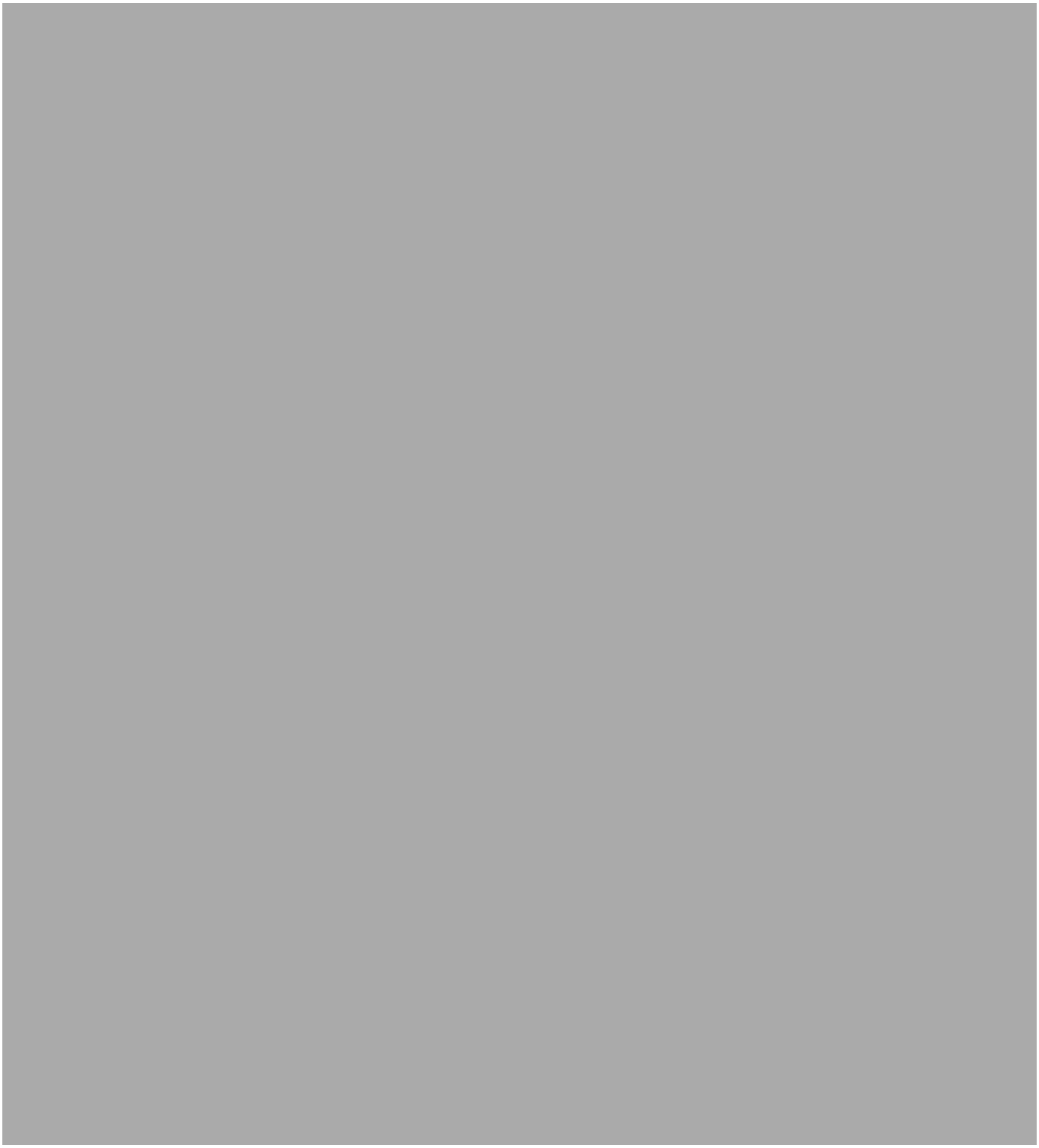

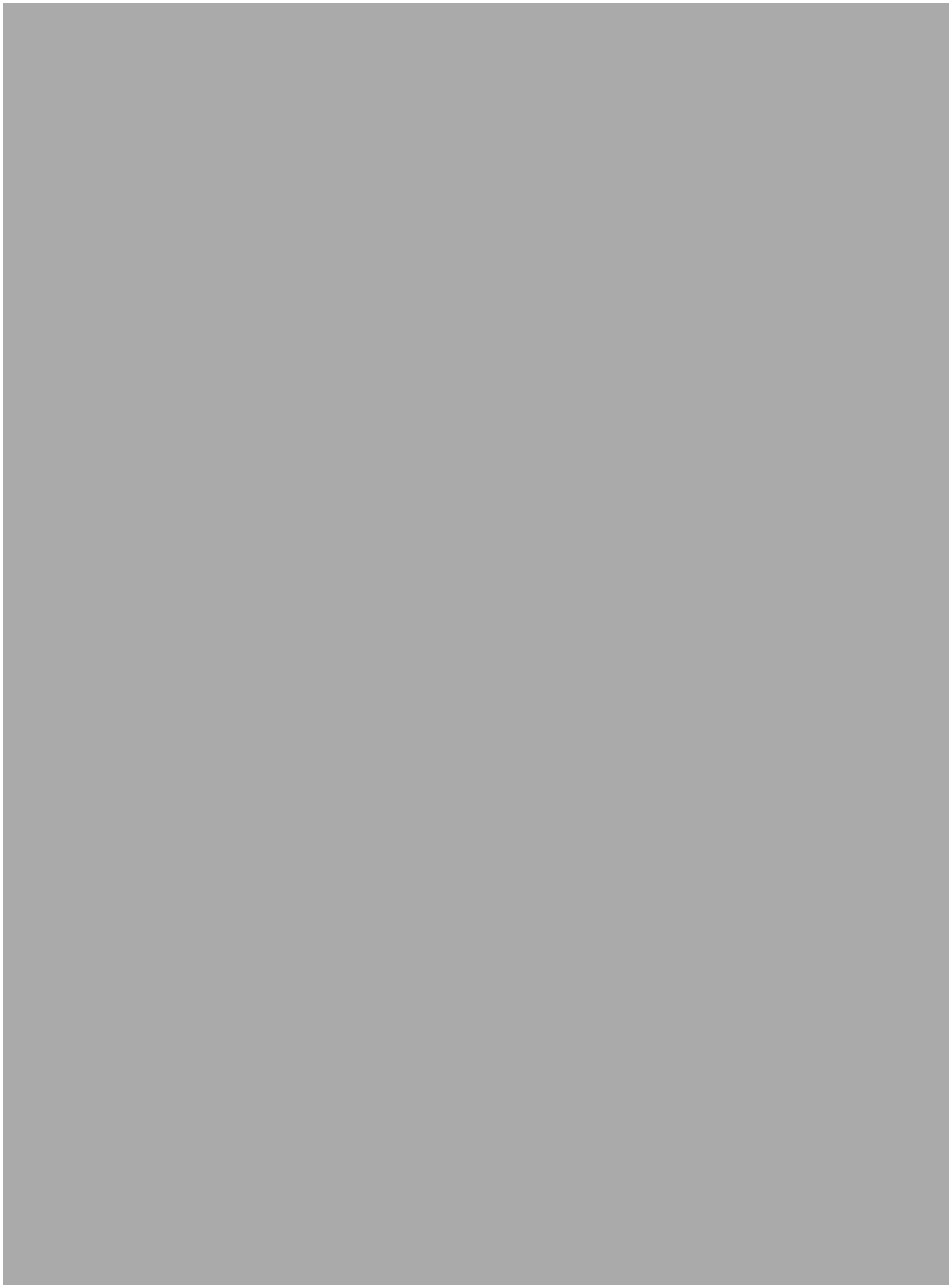

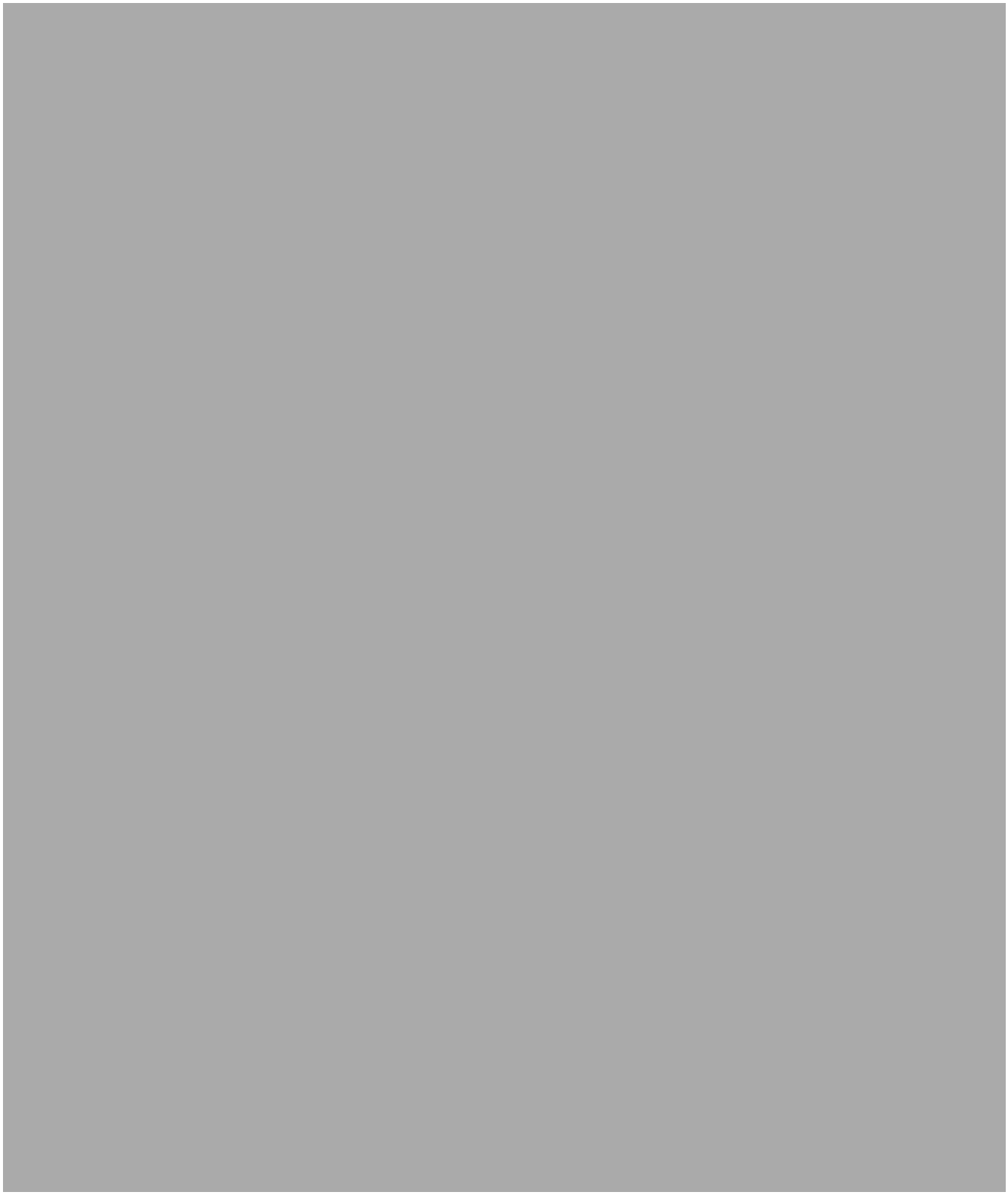

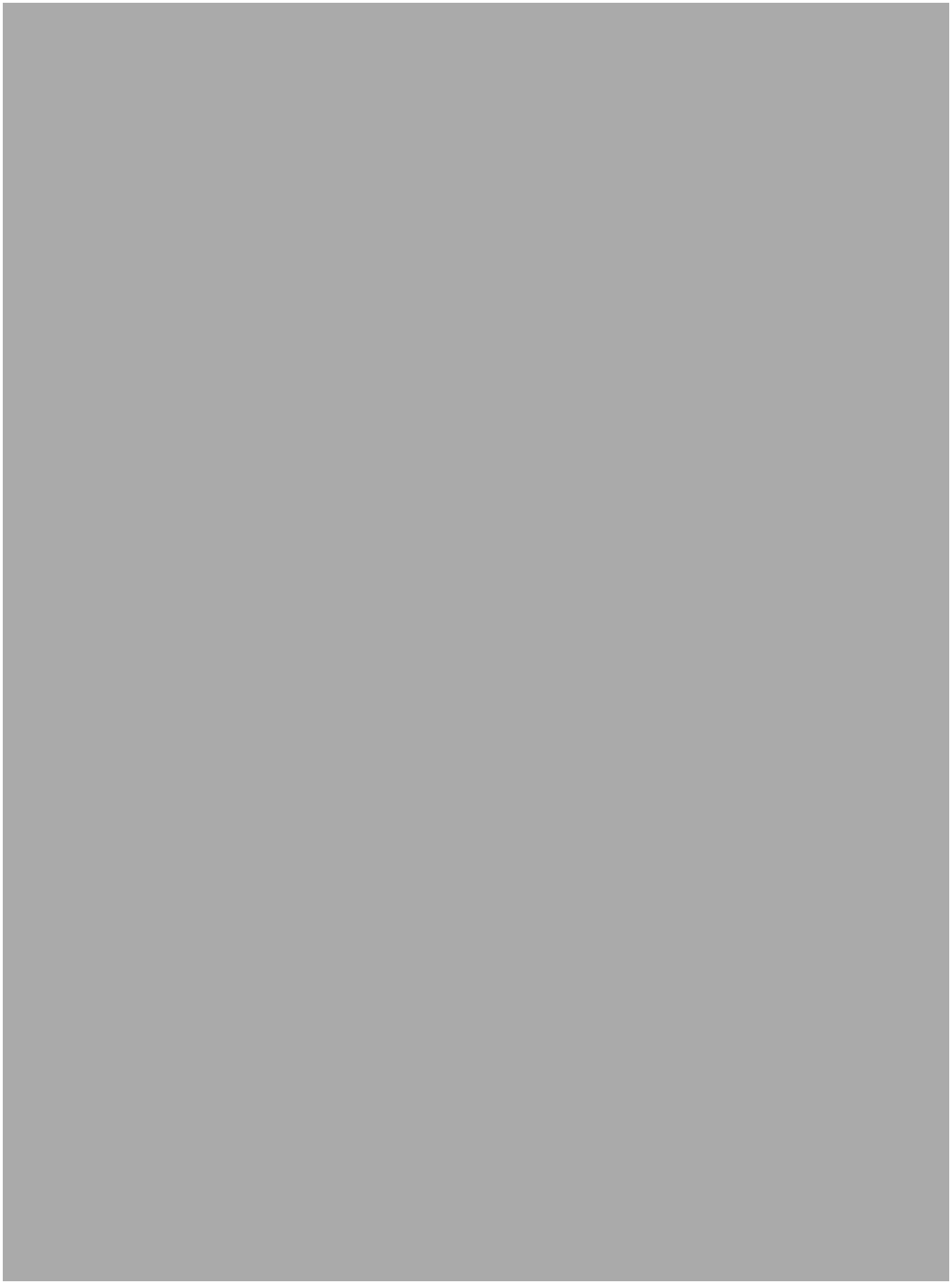

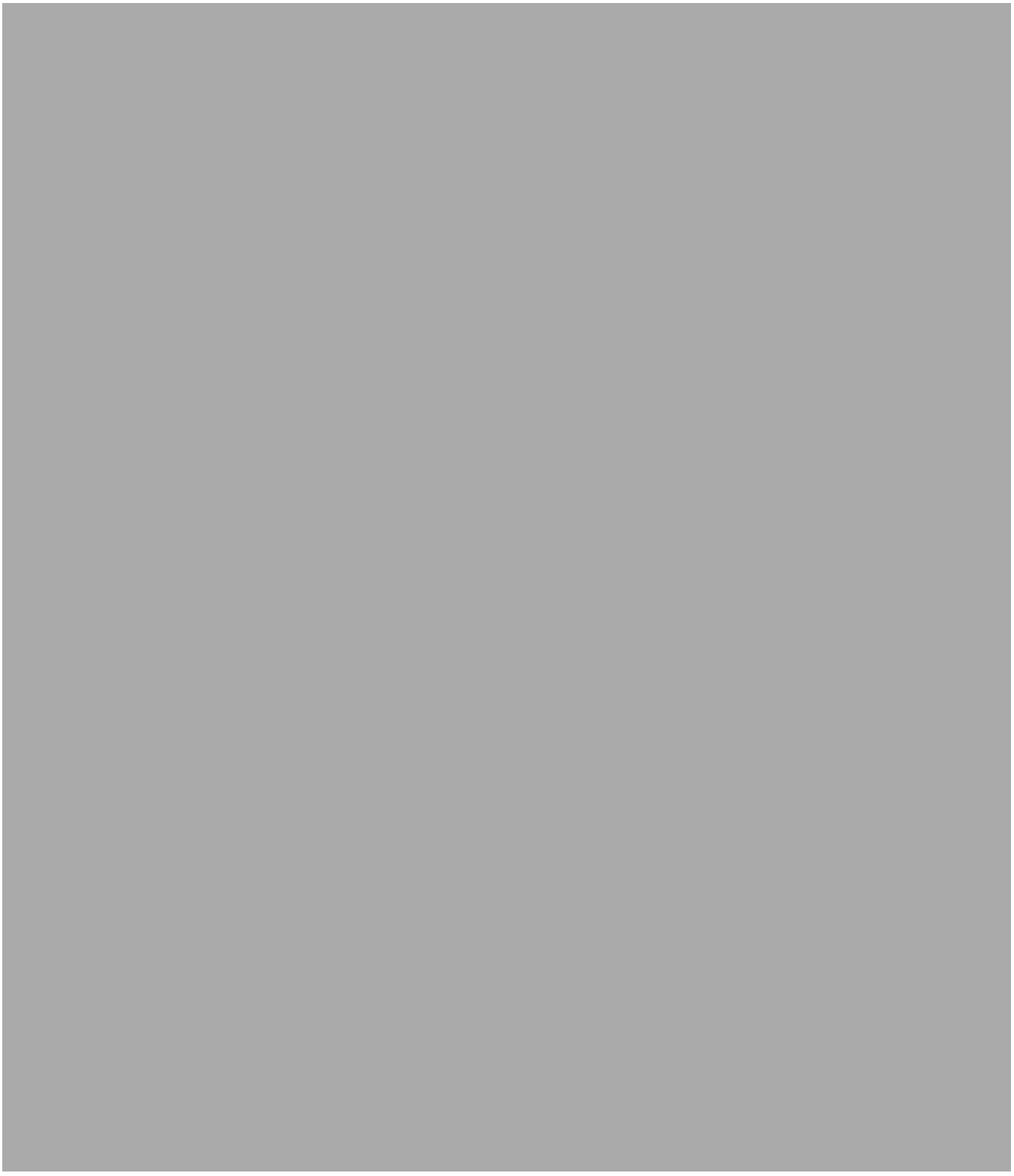

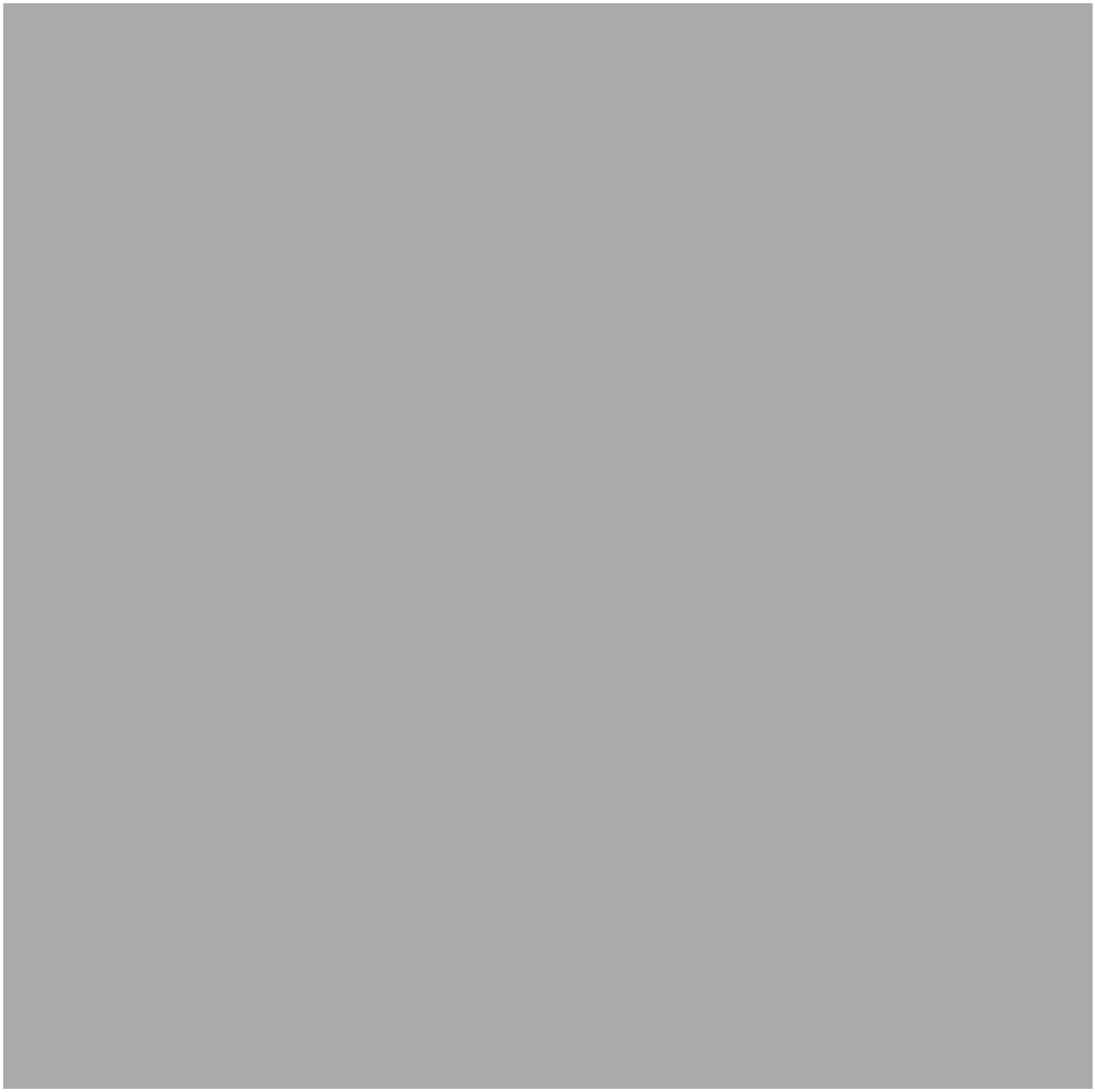

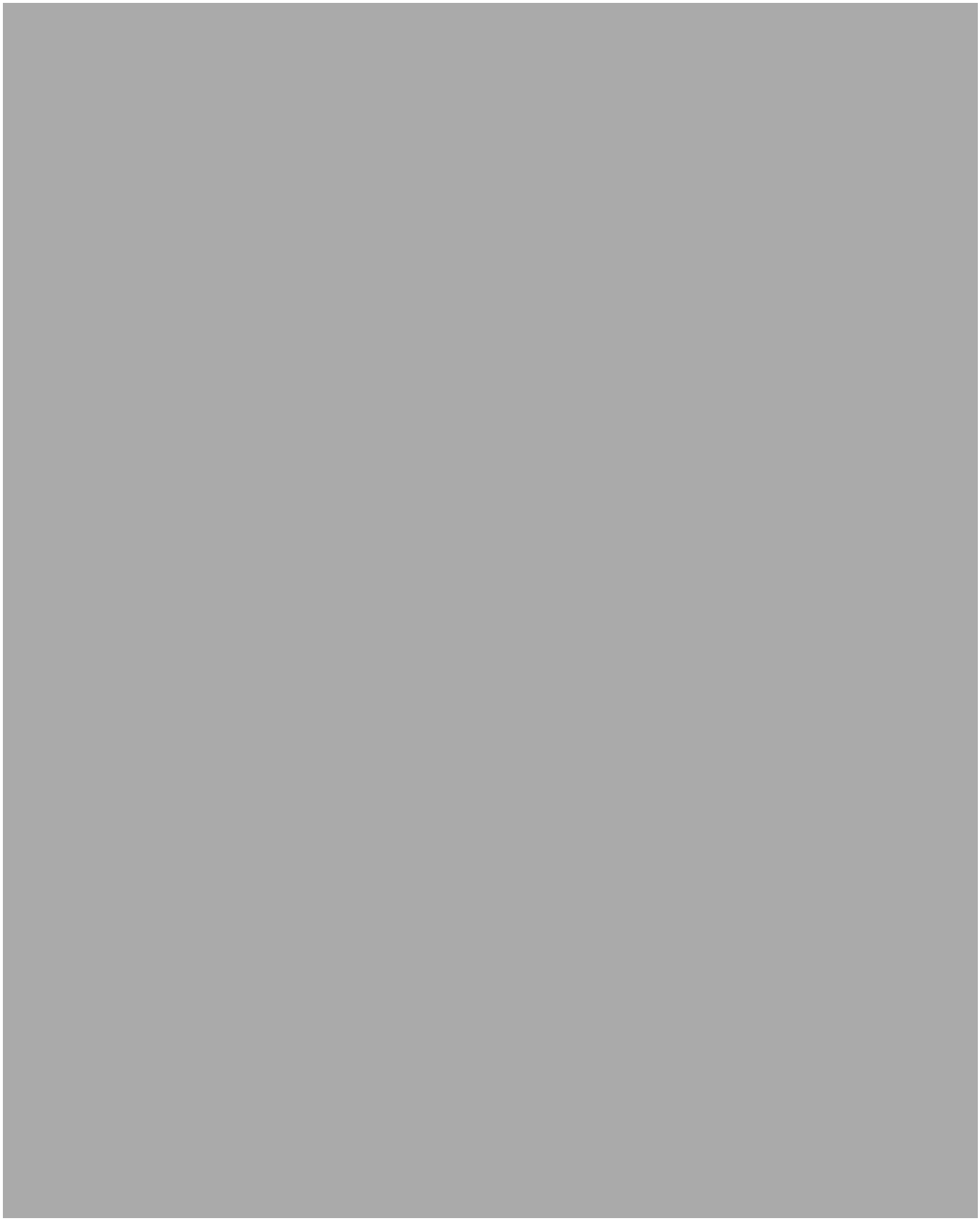

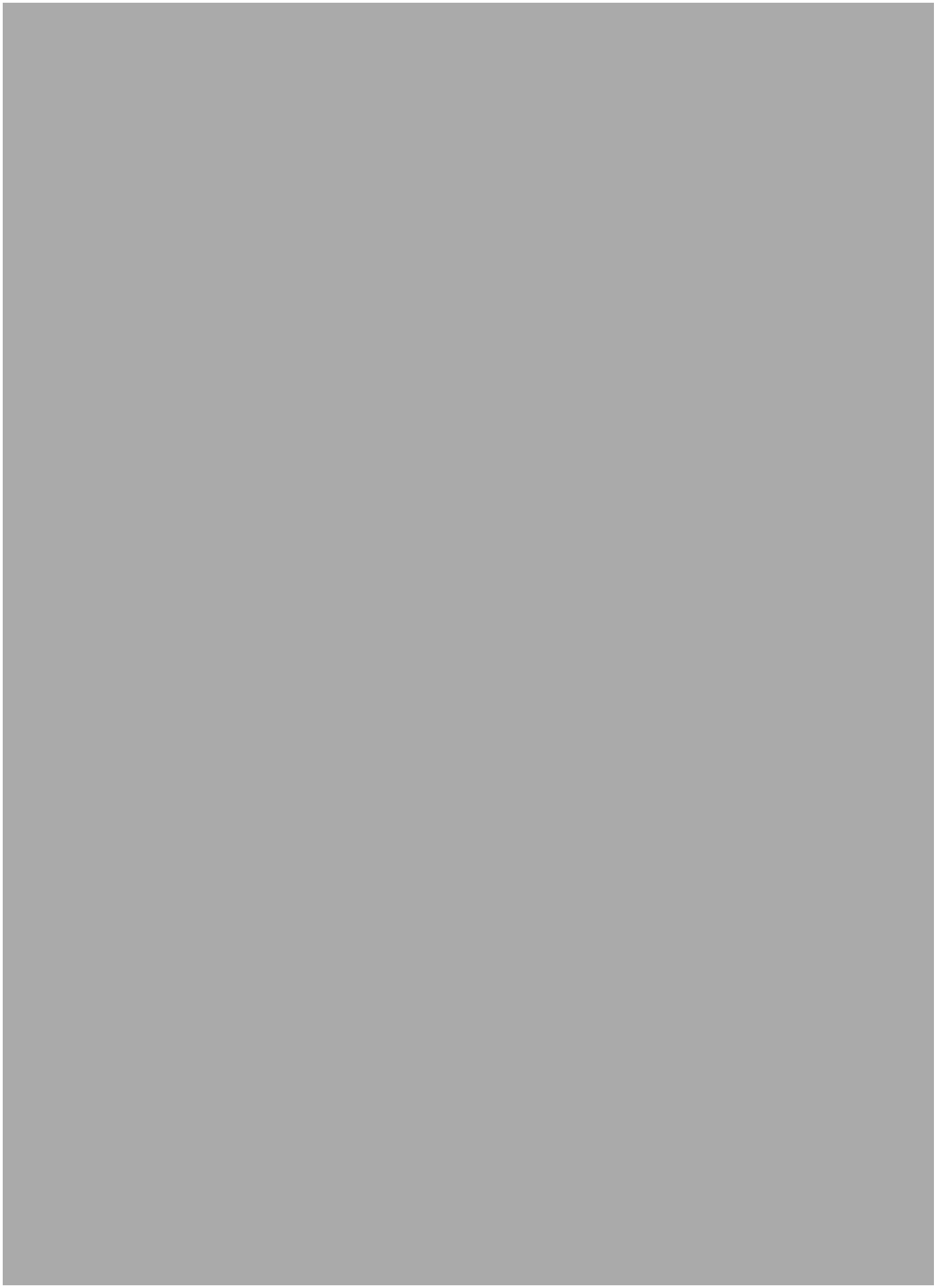

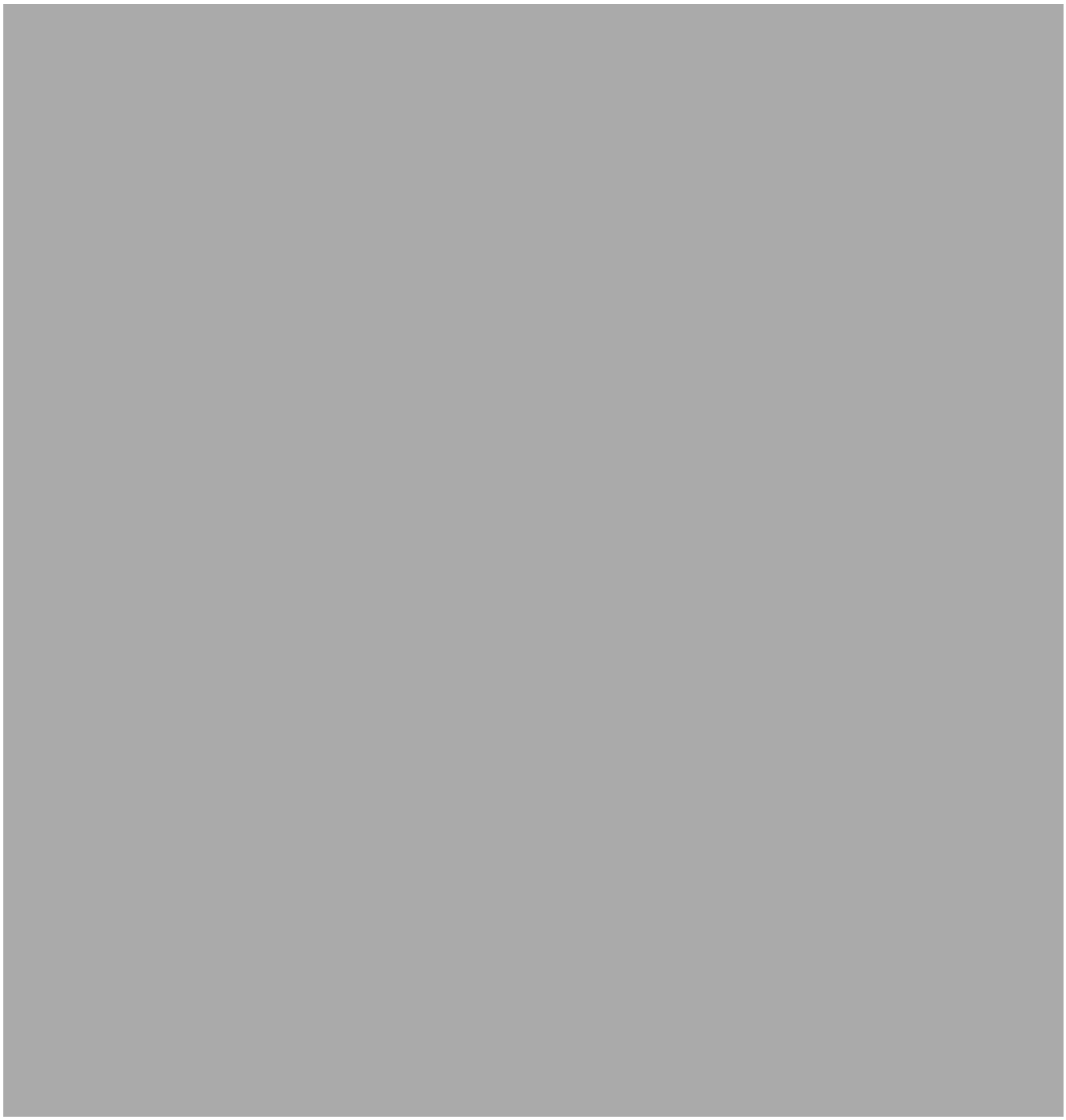

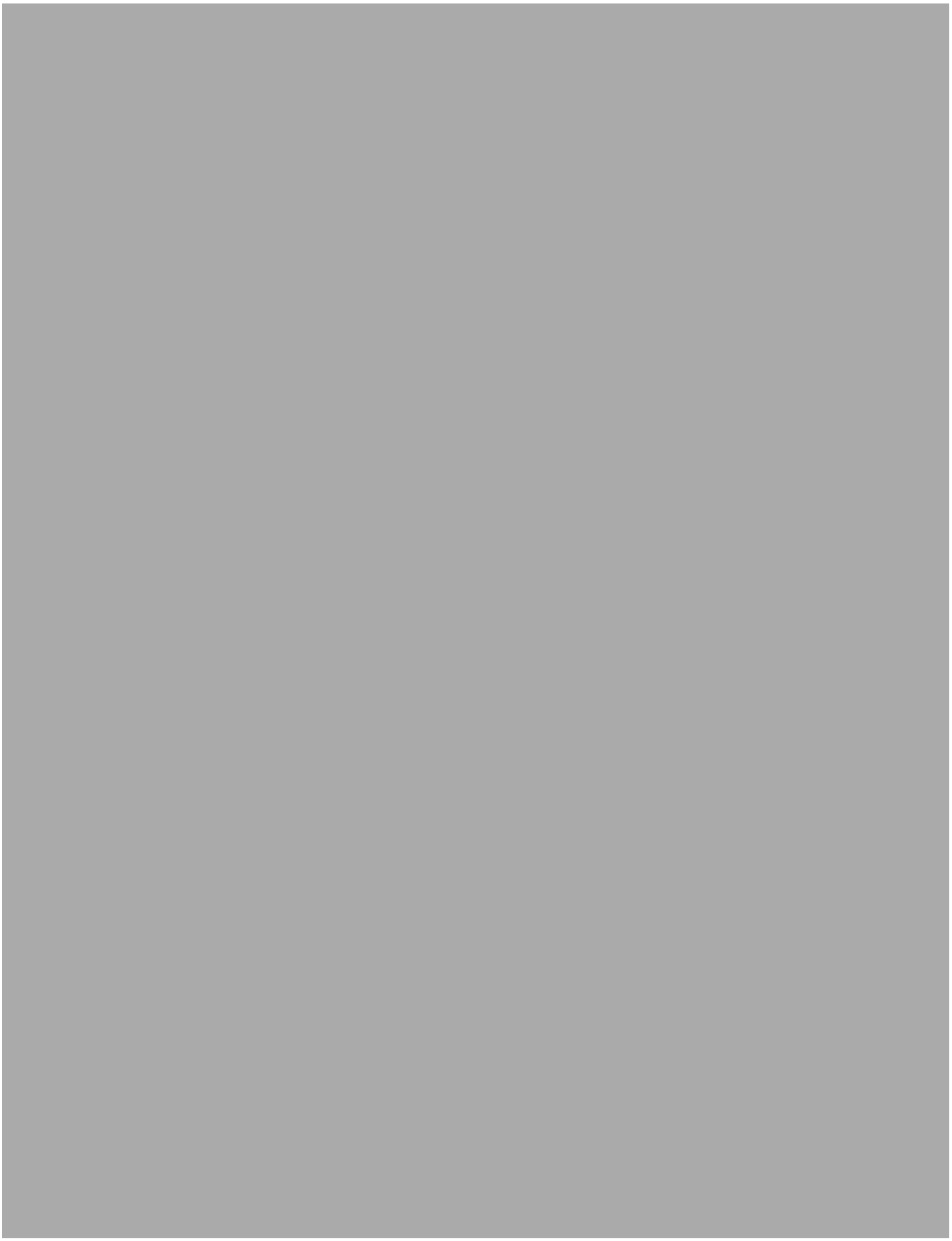

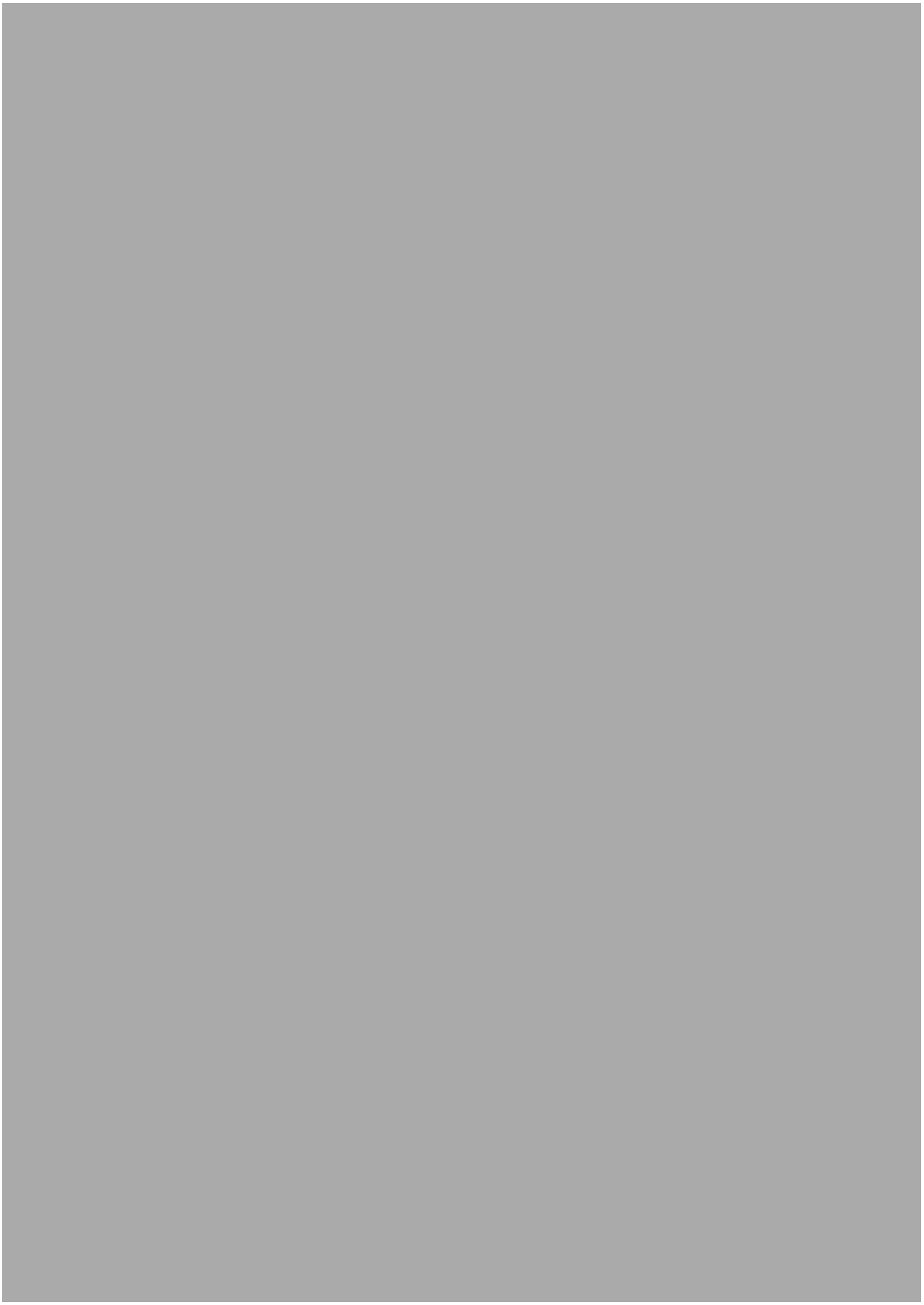

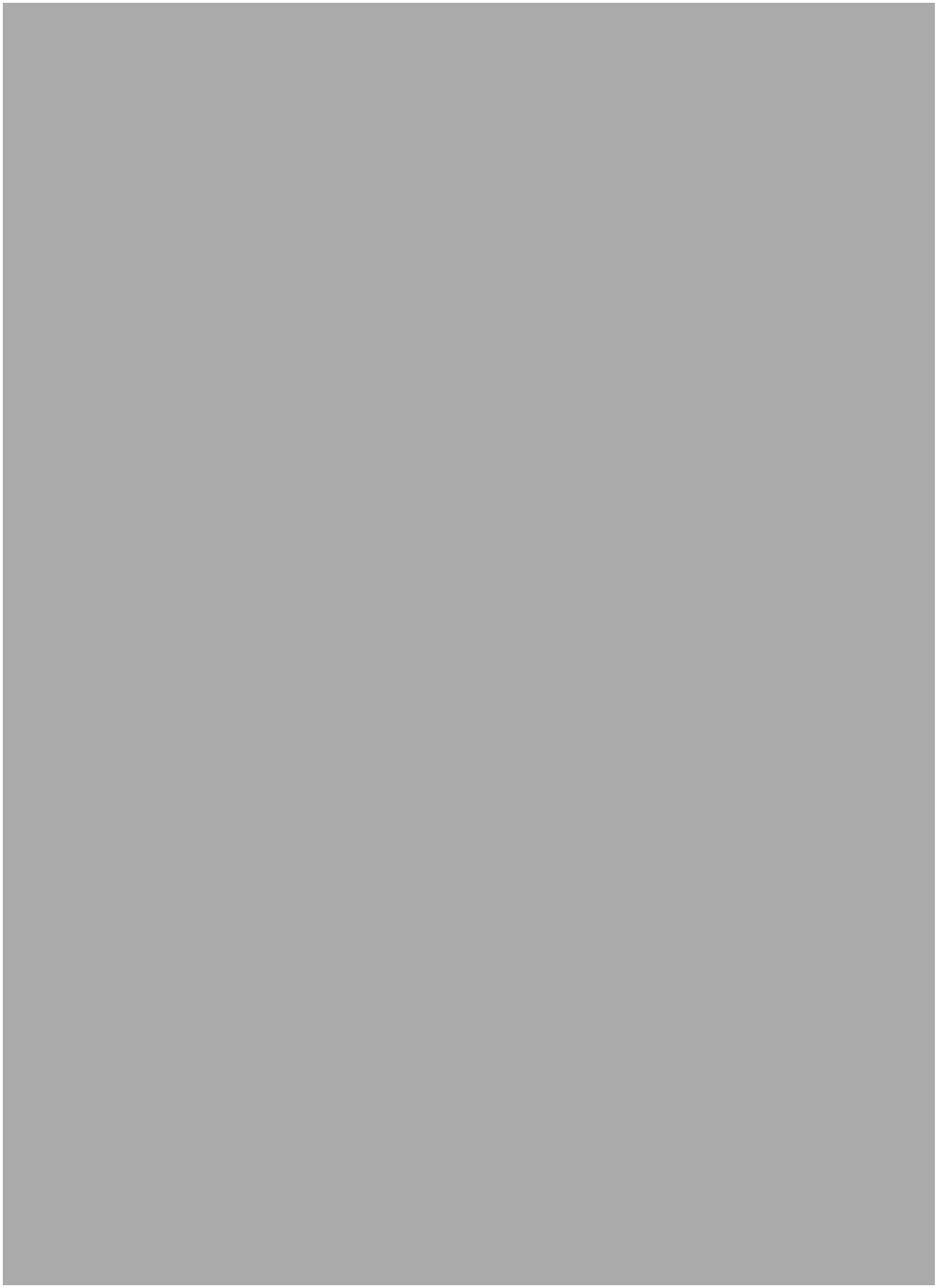

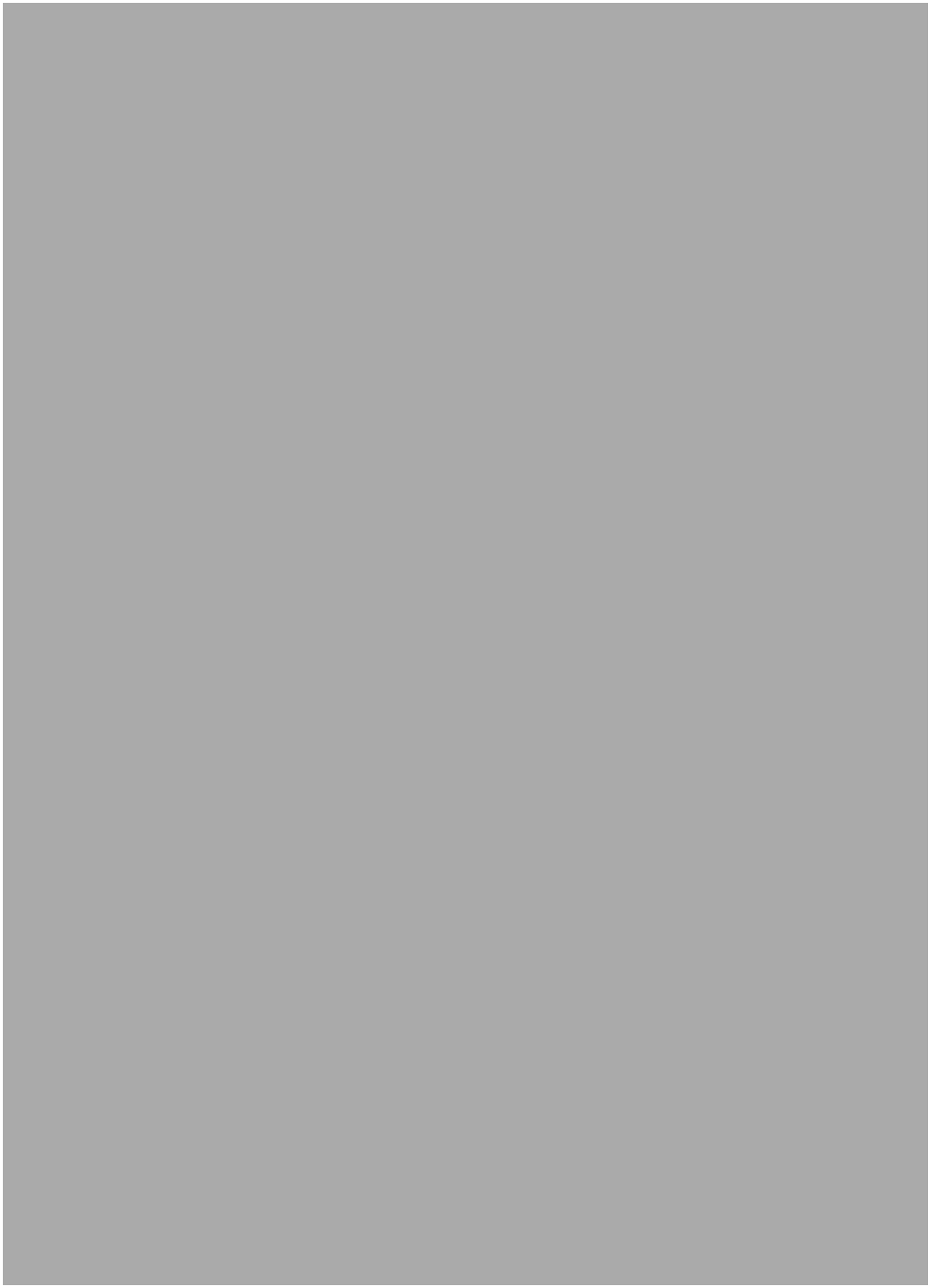

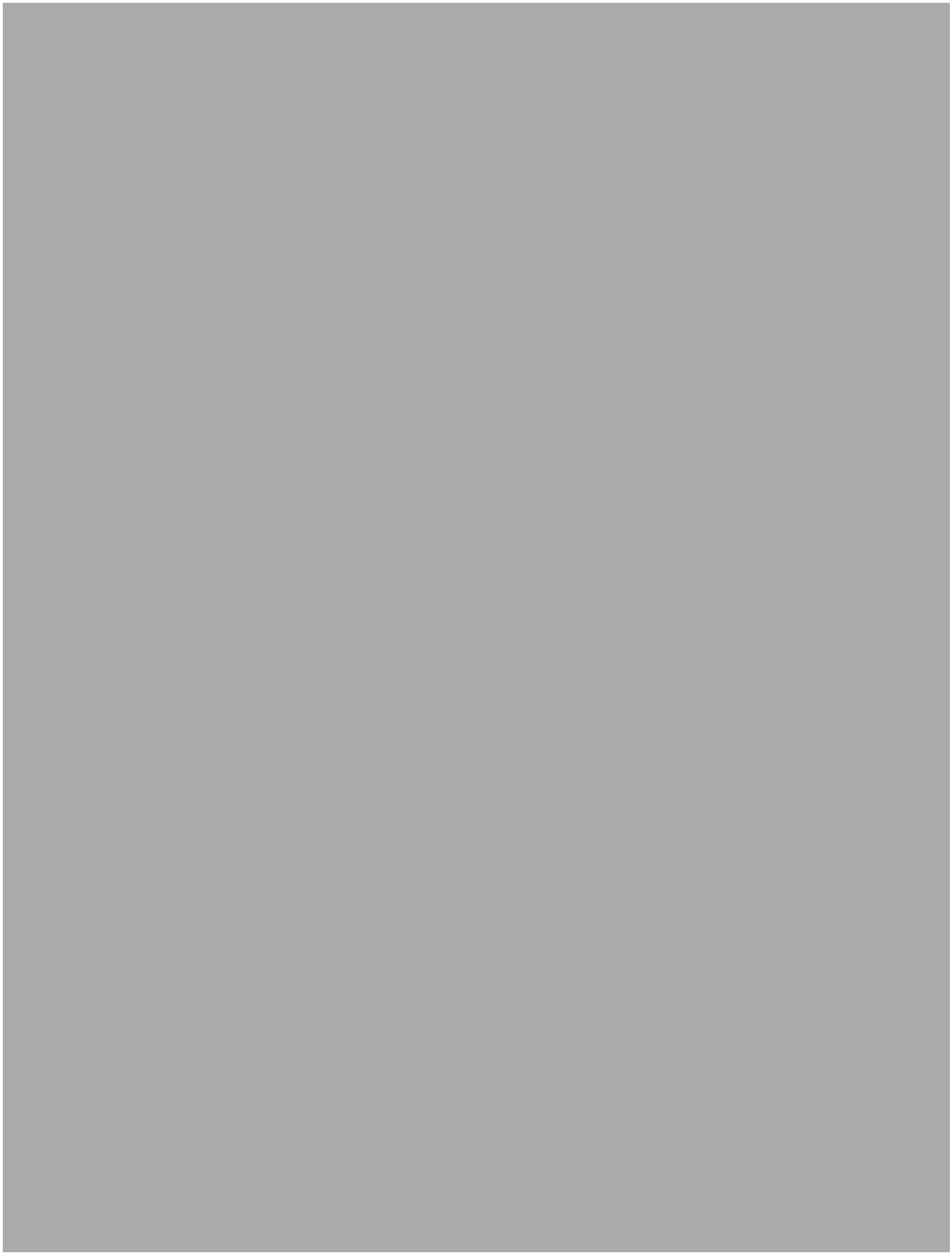

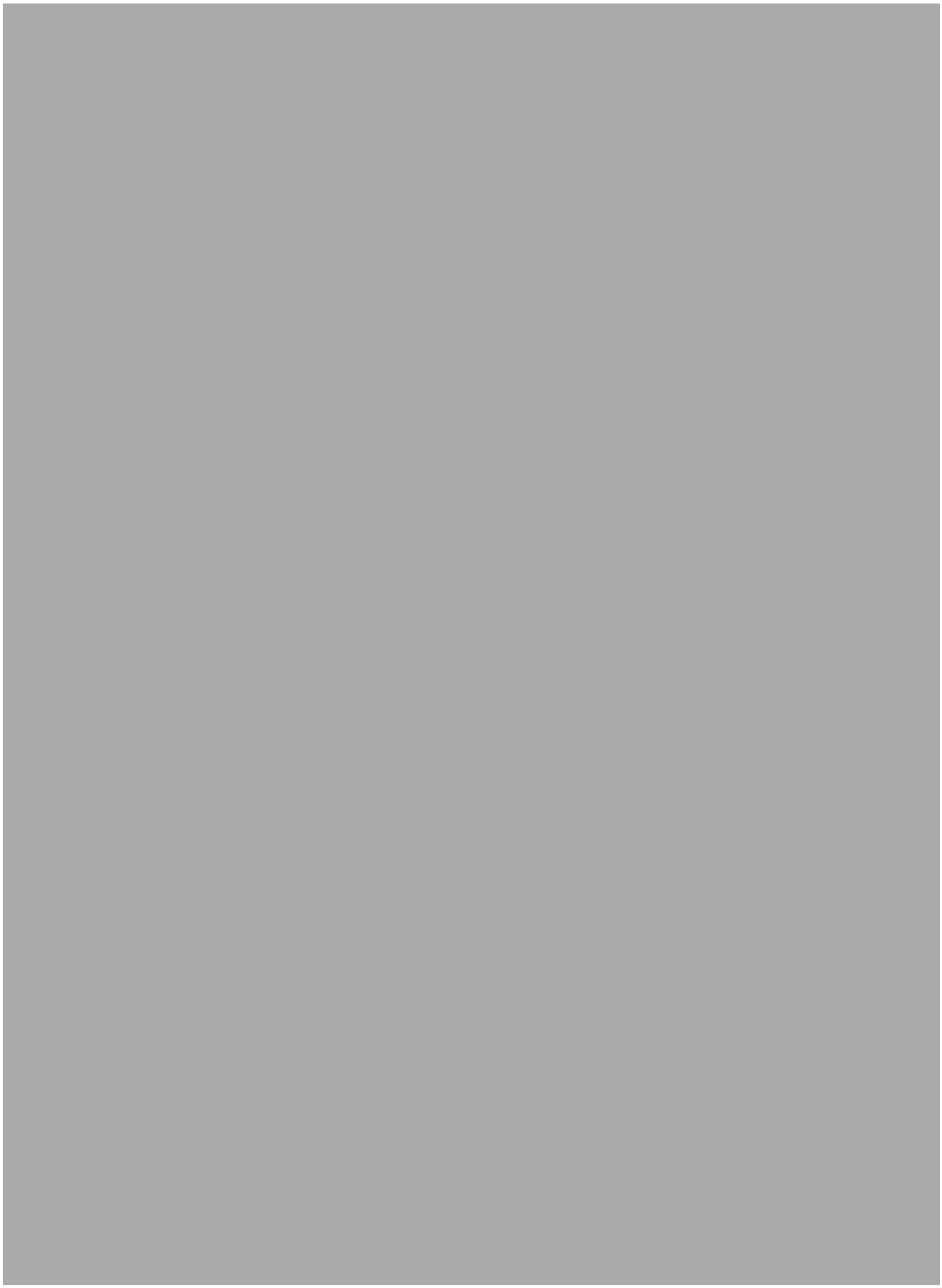

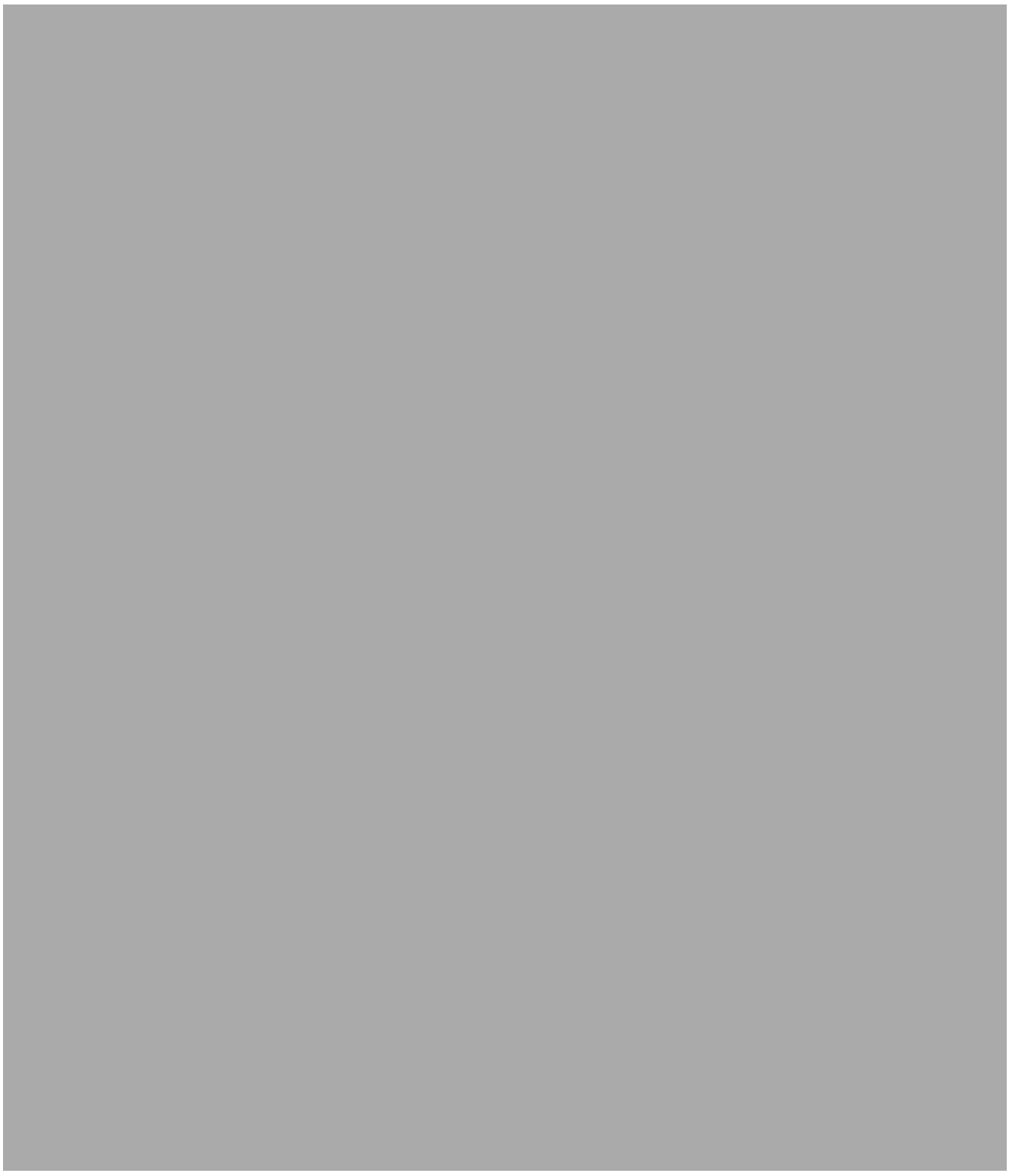

# CHAPTER 10

# General discussion

Due to the competitive nature of cycling, cyclists always aim to ride faster regardless of the wind conditions. As the aerodynamic drag is the main resistance force when cycling on a flat road, improving and exploring the aerodynamics associated with cycling is important to ensure gains in overall performance and safety. The main aim of this PhD thesis was to get an improved understanding of the effect of cycling position and crosswinds on the aerodynamics and performance of a cyclist. To accomplish this aim, two main objectives and hypothesizes were developed.

The first objective was to investigate the effect of position on the cyclists' physiology and aerodynamics. It was hypothesized that although lowering the time trial position will positively affect the aerodynamics, it will negatively affect the physiological and mechanical performance; therefore a trade-off between the physiological detriment and the aerodynamic gain was postulated. By means of a multidisciplinary approach, it has been observed that lowering the time trial torso angle indeed significantly reduces the aerodynamic drag. However, impairment in the power output and physiological performance has been found, which was closely related to a combination of neuromuscular and mechanical factors. The results suggested a trade-off between the impairment in physiological measures / power output and aerodynamic drag. Therefore a model was developed to determine the optimal torso angle for cyclists in a time trial position. The model demonstrated a trade-off in the

velocity range often used by competitive trained male cyclists, as hypothesized. In addition, it was shown that small torso angle positions lower than 5°, are not optimal.

The second objective was to investigate the effect of crosswinds on two-wheeled vehicles. Firstly, it was hypothesized that crosswinds significantly increase the side forces and rolling moments acting on a cyclist and motorbike rider. Secondly, it was hypothesized that lowering torso angle in cycling only reduces the drag force coefficients, whilst the side force and rolling moment coefficients remains unchanged. Wind tunnel measurements of a cyclist and bicycle showed that the aerodynamic forces and rolling moments are affected by crosswinds. The actual aerodynamic loads arising from such winds on a cyclist can be up to about 2.5 times the aerodynamic drag. When a cyclist is subjected to crosswinds, lowering time trial torso angle position was not shown to influence the side forces and rolling moments, which confirmed the hypothesis. However, it was demonstrated that the equipment (i.e. wheels and frame) plays an important role in the acting rolling moments (up to 60 %), hence affecting the stability and safety of the cyclist. The flow structures around a cyclist and motorbike rider were explored via CFD simulations. The current research showed that CFD simulations are a valuable tool to investigate the flow characteristics around two-wheeled vehicles in crosswinds with sufficient accuracy. Getting an insight into the surrounding flow field of two-wheeled vehicles lays the foundations for improvements in performance and stability.

## 10.1 Interpretation and discussion

In this thesis, it has been demonstrated that the metabolic costs are significantly affected at both maximal and submaximal intensities. Several factors can be suggested for the underlying mechanism of the physiological responses at small torso angles. First of all, it has been demonstrated in chapter 4, that the crank torque and muscle activation timing is changed

throughout the pedal cycle. Secondly, the hip and leg muscles are likely to operate at a different, less optimal length to produce optimal force of contraction (Dorel et al., 2009, Savelberg et al., 2003). However, the effect might be limited due to the relatively small torso angle changes. Thirdly, when cycling in a low torso angle, the abdominal compression could hinder the movement of the diaphragm and hence limit the lung volume (Ashe et al., 2003). Nevertheless, it should be noted that although in chapter 3 changes have been found in the breathing frequency and minute ventilation, the tidal volume was unaffected by position changes. In appendix C, a pilot study is presented that investigates whether the abdominal compression hinders the work of the diaphragm and the breathing volumes in different time trial cycling positions at rest. The results show that the exhale volume and velocity are primarily affected by lowering position, whilst the inspiration volumes remained relatively constant. This indicates that the lung restrictions due to lowering position are likely not a major limitation to cycling in small torso angle positions and will probably only affect the performance at high cycling intensities. Another suggestion for the change in metabolic functioning could be increased activation of the adductor muscles, to keep the leg movement in the sagittal plane (Gnehm et al., 1997). Finally, it could be suggested that the forces on the neck and upper limbs are marginally increased to maintain position (Gnehm et al., 1997).

Based on the aforementioned suggestions and results in this thesis, it can be concluded that the changed metabolic costs when lowering position are likely not caused by one specific mechanism, but by a combination of different factors, each contributing to a small extent to the general effect observed. In particular at low cycling speeds (< 30 km/h), these physiological effects are shown to be important. This trade-off between physiology/power output and aerodynamics has been nicely illustrated with the optimal torso angle model in chapter 5.

The torso angle position is the most important factor when optimising position in terms of reducing aerodynamic drag. Therefore focus was given on lowering the time trial torso angle position, whilst retaining the saddle and arm/hand position in cyclists' preferred position. Changes in arm position could slightly affect the fluid flow, hence improving the aerodynamic forces and cycling performance (Kyle, 1989, Underwood and Jermy, 2013). For example, it has been shown by Underwood and Jermy et al. (2013) that for male cyclists, optimising the arm position can reduce the aerodynamic drag by up to 2.5 %. In the numerical work of chapter 8, it was also shown that the arm position influences the vortex shading and reattachment of the flow. When placing the arms in a classical time trial position instead of a dropped position, the overpressure area in front of the main body has been reduced hence reducing the wake area and drag. Previous literature has demonstrated that when considering a time trial position, the aerodynamic drag has been shown to decrease when the arms are moved closer together to at least within the width of the upper body (Kyle, 1989, Underwood and Jermy, 2013). Albeit the arm position could further reduce the aerodynamic drag, it should be noted that changing the arm position might also alter the head position, which could again increase the aerodynamic drag (Underwood and Jermy, 2013). Additionally, close arm positions are likely to reduce the steering control of the bicycle, consequently affecting bicycle handling and stability. Besides changing the arm/hand position, the saddle position could be altered. To improve performance, time trial cyclists and triathletes often use steep saddle angles which effectively increase the saddle height and move the saddle forward (Burke and Pruitt, 2003, de Vey Mestdagh, 1998). This saddle position has been shown to reduce the oxygen consumption (Price and Donne, 1997, Heil et al., 1995) and to improve gross efficiency (Price and Donne, 1997). It should be noted that the forward position of the saddle is restricted by the international cycling union (UCI) when competing in endurance or

all mass start events (road, track and cyclo-cross). Regulation 1.3.013 states that the tip of the saddle must be a minimum of 5 cm behind the plane of the centre of the bottom bracket spindle. This rule does not apply for triathletes. For the saddle height position, it has been demonstrated by Oggiano (2008) that the lowest drag was found when the saddle height remained in the cyclists preferred position rather than in a 15 mm higher/lower position. Chabroux et al. (2012) also showed that increasing the saddle height could increase the aerodynamic drag by 3 %. It can be concluded that in addition to torso angle optimisation, in particular arm position alterations could further reduce the aerodynamic drag. Moreover, individual optimisation has been shown to improve the aerodynamic drag (Underwood and Jermy, 2013, Chabroux et al., 2012). As the aim of this PhD was to provide general insights into aerodynamic cycling performance, no attempt has been made to optimise the cycling position for individuals. In particular for competitive cycling events, where high cycling velocities are reached and time differences are small, the aerodynamic position needs to be individually optimised. Accurate drag measurements are required, such as wind tunnel experiments. This was not the case for the model input of chapter 5, in which the aerodynamic drag of the cyclists was estimated from frontal area measures. To predict the cycling performance in the optimised position, mathematical models driven by cyclists' specific data can be used. These kind of mathematical models have been shown to be successful in the past. For example, Hannas and Goff (2005) predicted the stage-winning times of the 2004 Tour de France. The results showed that the winning times were 0.05 % different from the actual times. Heil et al. (2005) estimated the world hour record at sea level and altitude and underestimated the UCI hour record at that time by -0.5 %. The aforementioned studies show that the application of models to predict general and individual performance is promising.

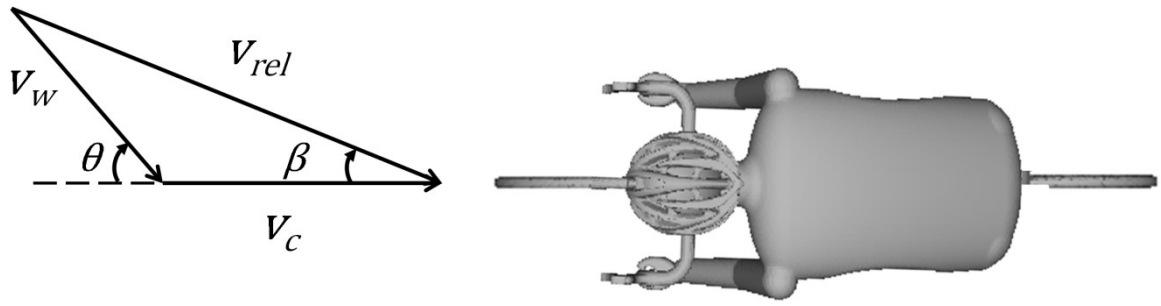


**Figure 10.1 Illustration of the contribution of the wind velocity, $v_w$, on the relative cycling velocity, $v_{rel}$, the cycling velocity $v_c$, the wind direction $\theta$ and the crosswind yaw angle β.**

In the presented optimal torso angle model, the forces induced by crosswinds were not taken into account. In spite of the significant effect of crosswinds on the aerodynamics demonstrated in this thesis, the expected change in cycling velocity has not been assessed (Iniguez-de-la-Torre and Iniguez, 2006) and could be predicted as follows. The total cycling power required for cycling in crosswinds, $P_{gen}$ at a flat road is:

$$P_{gen} = P_{roll} + P_{aer} \quad , \tag{10.1}$$

$$P_{aer} = \frac{1}{2}\rho A C_d \, (v_c + v_w \cos\theta)^3 \quad , \tag{10.2}$$

where $P_{roll}$ represents the rolling resistance power, $\rho$ the air density, $A$ the projected frontal area, $C_d$ the drag coefficient, $v_c$ the cycling velocity, $v_w$ the wind velocity, and $\theta$ the wind direction.

The yaw angle crosswind angle, β, is expressed as:

$$\beta = \tan^{-1}\left(\frac{v_w \sin\theta}{v_c + v_w \cos\theta}\right) \quad . \tag{10.3}$$

The change in effective cycling velocity used in the optimal position model could be predicted by:

$$\Delta v = v_w \cos\theta \quad . \tag{10.4}$$

From equation 10.4 and the model results, it can be implied that a more upright cycling position will be beneficial at high wind velocities and wind directions between $-\frac{1}{2}\pi < \theta < \frac{1}{2}\pi$. In all other wind directions, the effective cycling speed will likely increase and hence a lower position is optimal.

Bicycles are not the only two-wheeled vehicles that are influenced by crosswinds. Several accidents are reported for motorbikes due to wind induced forces and moments as discussed in chapter 9. Numerical simulations are therefore performed of the flow around both a cyclist and motorbike rider (chapters 7 - 9). To ensure numerical accuracy, the performance of different CFD approaches of the flow around two-wheeled vehicles are compared, such as the steady Reynolds averaged Navier Stokes (RANS), and the unsteady Detached-Eddy simulation (DES) and Large eddy simulation (LES). This thesis showed that the RANS simulations could provide reasonably good results around both a motorbike and cyclist. In the motorbike results, only at large yaw angles (>60°) the k-ε model over-predicted the acting side forces. This is likely caused by the over-prediction of the turbulent kinetic energy. However, for both vehicles, the more accurate LES and DES simulations outperform the RANS simulations and hence yield information of the unsteady, temporary changing flow field. For a cyclist, the LES simulations have shown to be more capable of predicting the reattachment and separation in the side force direction. Unfortunately, the LES and DES require much higher computational costs compared to RANS (about 10 times for DES and 17 times for LES). From a practical point of view, the less computationally expensive RANS simulation is more attractive when optimising position. Particularly as it is known that the simulation results differ to some extent from the reality, due to for example dissimilarities in environmental conditions and cyclists' body motion.

The numerical simulation has provided an estimation of the aerodynamic forces and moments acting on a bicycle and motorbike. Similar trends in the aerodynamic forces and moment coefficients are observed for both types of two-wheeled vehicles when subjected to crosswinds. The drag force coefficients decreases with increasing yaw angles, whilst the side forces increases along with the rolling moment coefficients. It has been observed that the maximal drag force coefficients are comparable for both types of two-wheeled vehicles. Although the windshield on motorbikes are designed to reduce the aerodynamic drag, for crosswind yaw angles > 30°, low pressure regions and vortex shading takes place around the windshield. The vortices are the major component of the turbulence flow and contribute to increased aerodynamic forces and moments. In cycling, in particular large flow separation develops around the bicycle at large yaw angles. For both two-wheeled vehicles, vortex cores are present behind the helmet in all crosswind yaw angle conditions. The time histories of the force coefficients are used to reveal the frequencies of the flow around the vehicles. The numerical bicycle results showed that the LES and DES approaches were able to predict the 'real' dominant frequencies. The frequencies found for the motorbike and bicycle is in the same Strouhal number range. It can be concluded that for both two-wheeled vehicles, crosswinds are shown to significantly affect the aerodynamics and it is likely that this will influence the performance and vehicle dynamics.

## 10.2 Practical applications

Although providing practical applications is not the main objective of this thesis, some findings lend themselves logically to practical cycling recommendations:

- Lowering position reduces power output and decreases maximal oxygen consumption and heart rate (chapter 3, Table 3.2).

- For non-elite competitive male time trial cyclists there exists a trade-off between physiological performance and aerodynamic drag. In contrast, in elite time trial cycling the aerodynamic drag reduction outweighs the physiological impairment due to the relatively high cycling velocities (about 40-50 km/h) (chapters 3 and 5).
- At cycling velocities above 45 km/h, low torso angle positions are optimal. However, small torso angles (< 5°) are not recommended (chapter 5, Figure 5.4).
- The bicycle itself is a dominant load factor (contributes to up to 60 % of the side forces) when subjected to crosswinds. To decrease the side forces and rolling moments of the bicycle in large yaw angle side winds, cyclists should avoid using a time trial bike or disk wheels (chapter 6, Figures 6.3 and 6.5).
- In strong side winds it is recommended to use an upright position instead of a time trial position, as it reduces the rolling moments, hence likely enhancing the bicycle stability (chapter 8, Figure 8.5).

## 10.3 Limitations and future research

All performance testing and torso angle position modelling presented in this thesis has been conducted for non-elite male competitive cyclists. Whether the results can be extrapolated to less trained counterparts or female cyclists is questionable. Ashe et al. (2003) investigated the physiological effect of male cyclists unfamiliar with time trial handlebars. They suggest that a period of training and adaptation is required to optimise performance in a time trial position; however, the duration of the training period was unidentified. A study of Hubenig et al. (2011) investigated the influence of altering position in females. Important morphological differences between male and females exist such that females are more flexible, they have an increased anterior pelvic tilt in the dropped position and a larger range of pelvic motion,

which might have an influence on the power output. Hubenig et al. (2011) showed differences in physiological response compared with similar cycling position studies in males. For example, contrary to the study of Ashe et al. (2003), in the latter study no relationship was found between experience or type of the participants (road cyclist or triathletes) and their power output. It could therefore be concluded that for these groups, further tests are required to be able to determine the optimal torso angle position and the effect of position on performance.

This research showed that with increasing cycling velocities, the cyclist should adopt a lower torso angle position irrespective of the detrimental effects on different physiological and mechanical factors. The acute change in position and short cycling duration might be attenuated via training. It is likely that training in a lower torso angle position can improve the power output production and oxygen consumption (Peveler et al., 2005, Heil et al., 1997), but the extent of these changes are not quantified yet. In addition, it is not clear how changes in the time trial position interact with factors such as fatigue and neck / back pain. No increased muscle activity has been observed whilst lowering torso angle in chapter 4. This indicates that in the range considered, lowering time trial position does not induce greater neuromuscular fatigue in the short term. Although it has been found by Duc et al. (2005) that the muscle activation does not increase during a 30 minute time trial at 74 % MAP, further research is needed to determine the effect of aerodynamic positions on fatigue at more ecologically valid cycling durations and conditions. Due to the relatively short cycling time duration of the laboratory sessions, no injuries or pain were reported associated with low torso angle position (e.g. torso angle <8°). However, it has been reported that decreasing torso angle could increase the risk of neck and back injuries (Deakon, 2012, Dettori and Norvell, 2006, Brown, 2002). A low torso angle position places the lumbar spine in a more horizontal position,

resulting in a higher strain on the lumbar spine which could cause lower back pain. It has also been stated that low cycling positions causes exaggerated lordosis, causing increased pressure on the posterior elements of the lumbar vertebra (Mellion, 1994). Neck pain is caused by increased tension on the upper 3 levels of the cervical spine to keep the neck in a hyper-extended position for a long time and the increased load on the arms and the shoulders to support the rider. The strain on the neck will be aggravated by vibrations from the road which are transmitted from the bike to the shoulders and the neck. It has been suggested that these injuries can be prevented by gradually lowering the torso during the cycling season (Deakon, 2012), but no scientific data exists to test this suggestion yet. In addition, the lumbar strain can be reduced by an anterior tilt of the saddle (Dettori and Norvell, 2006, Brown, 2002). It was observed that all participants in the studies arrived in the lab with either a level or anterior tilted saddle. Future research is needed to assess the long term effects of small torso angle positions on injuries and fatigue.

All presented experimental and numerical work has been conducted with a steady and uniform wind speed of about 10 m/s. Previous cycling literature has shown that there are no Reynolds number effects for speeds above 4 m/s (Zdravkovich et al., 1996) and within the cycling range typically used by cyclists (Defraeye et al., 2010a, Bassett et al., 1999). However, for accurate simulation of the flow around a cyclist, it is important to realistically simulate the atmospheric processes. In particular turbulence intensity can influence the attachment, reattachment of the flow and vortex shedding around bluff bodies (Johnson, 1998; Robinson et al., 1990). In the work presented, the bicycle was tested in a low turbulence wind tunnel, and hence the effect of the atmospheric boundary layer neglected. In reality, the turbulence intensity is high at vehicle level (Watkins et al., 1995). For example, at rural terrain and 2 m from the ground, the turbulence intensity could be around 26 % (Xu, 2013).

Future research should therefore include accurate simulation of the atmospheric boundary layer flow. Additionally, it can be expected that the stability of cyclists is in particular affected by strong gusts of winds, rather than a constant crosswind. These amplified gusts of wind are likely a result of surrounding high rise buildings or vehicles. To improve the safety of cyclists in gusts of winds, besides the equipment selection, the building environment needs to be investigated. To set guidelines for bicycle lanes, one will need the bicycle dynamics and the human control of the cyclist under these conditions. Bicycle stability has not been the subject of research for this thesis. Obviously, this is an important factor in terms of safety and the definition of guidelines. Future studies should therefore attempt to determine the effect of crosswinds on the bicycle dynamics. By performing experimental tests with realistic crosswind conditions or using a multi-body dynamics model (e.g. Whipple model, Meijaard et al. (2007)) driven by the present data, it would be possible to determine safety guidelines for cyclists subjected to crosswinds.

Another limitation of the crosswind studies presented in this thesis is the exclusion of the dynamic leg motion. The rotation of the legs will affect the flow field (García-López et al., 2008); however analysing static legs is a good starting point to study the fundamental flow characteristics. It should be noted that the velocity of the legs is relatively low compared to the upcoming flow (85 rpm = 1.4 Hz). It can be therefore assumed that the flow in the dynamic case will show similar flow features than that of in the static case. It is reasonable to assume that at higher cycling speeds the quasi-static assumption holds. Crouch et al. (2012) showed with a quasi-static approach that the leg position significantly changes the aerodynamic drag on a cyclist in windless conditions. Their experimental study showed variations up to 15 % in drag area when cycling in a time trial position. This is also confirmed by an extensive experimental and numerical analysis of the cycling aerodynamics (Griffith et

al., 2014). It has been suggested that these variations are primarily a result of changes in the flow field, rather than changes in frontal area; frontal area changes by less than 2 % over the pedal cycle. To investigate the effect of leg position in crosswinds, some additional simulations are performed and reported in Appendix D. The results show that in a 15° crosswind yaw angle, the drag varies by about 6 – 9 % between the different leg positions, whilst the projected frontal area changes by 3 – 8 %. The lowest drag is observed when the pedals are level in respect of each other and the highest drag when the pedal at the windward side of the cyclist is in the bottom dead centre (BDC). The side forces significantly reduce by about 25 % when the left pedal is at the TDC compared with level pedals, hence reducing the rolling moment. The lift forces are identical for the two cases where one pedal is in the TDC. From these preliminary results, it can be inferred that the aerodynamic force coefficients are affected by leg position in crosswinds. The results in the main body of this thesis, in which only level pedals are considered, might therefore slightly under-predict the aerodynamic forces experienced when pedaling. Future research should therefore attempt to investigate the effect of pedaling on the cycling aerodynamics in crosswinds.

Finally, drafting is one of the most efficient tactics to reduce aerodynamic drag and save energy. Reductions of up to 40 % power output were reported in windless conditions as shown previously in Table 1.2. In crosswinds however, cyclists commonly draft by using an echelon formation, where the cyclists are positioned at an angle with respect to each other. Although recent research has shown the optimal separation distance and savings for windless conditions (Defraeye et al., 2014), no studies have investigated the effect of drafting in crosswinds. For example, it is unknown what for example the optimal distance between the riders is or the optimal group size in crosswinds. Investigations will help to improve the drafting tactics and hence performance in cycling.

## 10.4 Conclusion

This thesis accentuates the importance of a multidisciplinary approach when optimising cycling performance. Without such an approach, this research would not have uncovered the trade-off between aerodynamics and power output. It is therefore suggested that applied sport sciences should more often use a multidisciplinary approach to study the cost-benefit of changes that aim to improve sports performance.

The CFD results have provided valuable data for other numerical and experimental work and are the first step in the process of investigating the effect of crosswinds on cyclists. Future research should attempt to reveal the aerodynamic and stability effect of gusts of winds on two-wheeled vehicles.

# APPENDIX A

## Wind tunnel calibration

The new low-speed wind tunnel at the University of Birmingham was calibrated before any experiments were undertaken. The flow velocity in the wind tunnel was measured with a 3D sonic anemometer (Windmaster, Gill Instruments Ltd, Lymington, UK). The anemometer was placed in the middle of the free stream (1m from the top and 1 m from the side of wind tunnel), whilst the bicycle with mannequin was placed in front of the wind tunnel in a crosswind position (yaw angle of 90°). Measurements were taken every 1m along the entire length of wind tunnel; starting from the end of the wind tunnel towards the diffuser (Figure A.1). A sampling frequency of 10 Hz was used. All fans were running at a constant maximal fan power. To improve the flow quality, a honeycomb was placed behind the diffuser to reduce the lateral velocity. The data was captured for 3 minutes. The data was analysed between the 2nd and 3rd minute to eliminate initial start-up unsteadiness in the flow.

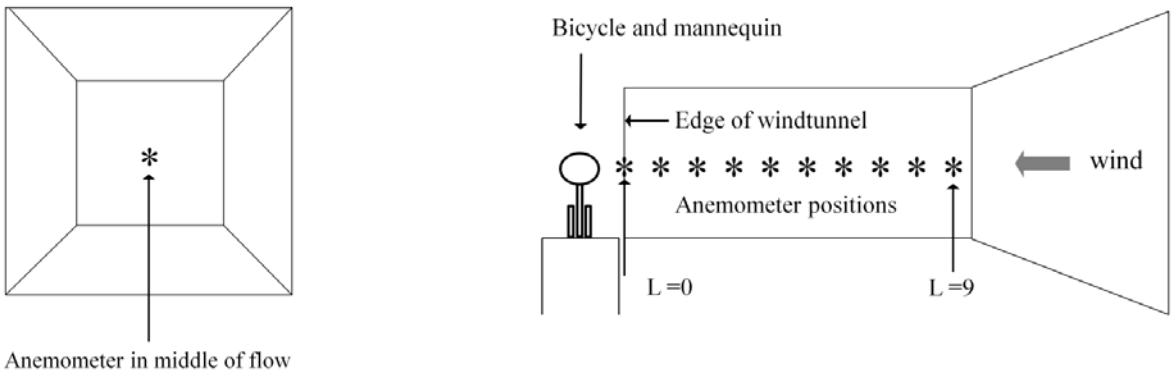


(a) (b)

**Figure A.1 Positions of the sonic anemometer in the wind tunnel to investigate the straightening effect and flow characteristics of the wind tunnel. (a) frontal view (b) side view.**

**Tilt correction**

The anemometer was not placed completely in the streamwise coordinate system, therefore the anemometer data was corrected for tilt. The following equations were used to correct for the anemometer tilt:

$$u_g = [u\cos\theta + v\sin\theta]\cos\phi + w\sin\phi \tag{A.1}$$

$$v_g = -u\,sin\theta + v\cos\theta \tag{A.2}$$

$$w_g = w\cos\phi - [u\cos\theta + \ v\,sin\,\theta]\sin\phi \tag{A.3}$$

where

$$\theta = \arctan\frac{\bar{v}}{\bar{u}} \tag{A.4}$$

$$\phi = \arctan\frac{\bar{w}}{\bar{u_g}} \tag{A.5}$$

where $u$ is the streamwise component of the flow, $v$ the lateral component and $w$ the vertical component and $\bar{u}$, $\bar{v}$ and $\bar{w}$ the mean of the velocity in the different directions.

The tilt correction equations were applied on all captured data. Velocity differences were only found for the lateral and vertical components of the velocity (difference < 0.25 m/s). In the streamwise velocity direction, the velocity differences due to tilt were small (difference < 0.0079 m/s).

**Mean velocity**

The mean of the streamwise component of the flow was calculated by:

$$\bar{u} = \frac{1}{N}\sum_{i=1}^{N} u\,(i) \tag{A.6}$$

The streamwise is shown in Figure A.2, where the dotted lines are the standard deviation. It could be seen that the streamwise velocity increased towards the end of the wind tunnel.

This might be caused by the fact that the flow becomes straighter along the wind tunnel hence

reducing pressure and increasing velocity. Another explanation could be that the effective cross-sectional area of the wind tunnel decreases due to boundary layer growth, resulting in an increased velocity (the boundary layer is a thin layer of viscous fluid close to the wall which is in contact with the flow and has a flow velocity varying from zero close to the wall to up to 99 % of the free stream velocity). At the end of the wind tunnel at L=0m the wind speed decreased, which is as result of the inference of the bicycle with the flow. The standard deviation of the velocity shows that fluctuations were higher close to the diffuser (standard deviation = 0.116) and lower towards the end of the wind tunnel (standard deviation = 0.093).

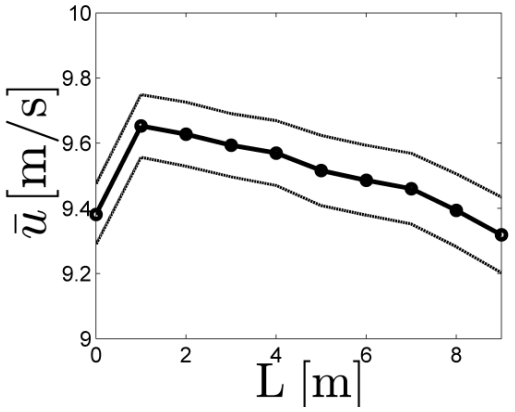


**Figure A.2 Mean streamwise flow as function of different positions in the length of the wind tunnel, including standard deviation (dotted lines). Anemometer was placed in the middle of the streamwise flow. L =0 corresponds to the end of wind tunnel and L=9 corresponds to the beginning of wind tunnel.**

### Turbulent flow fluctuations

The measured streamwise speed $u$ can be split into the mean velocity $\bar{u}$ and turbulent fluctuations $u'$:

$$u = \bar{u} + u' \tag{A.7}$$

Figure A.3 shows the streamwise fluctuations of the flow at the beginning and end of the wind tunnel. The turbulent flow fluctuations were calculated in the middle of the flow. The data showed that the amplitude of the fluctuations decreased towards the end of the wind tunnel. The wind tunnel effectively straightened the flow.

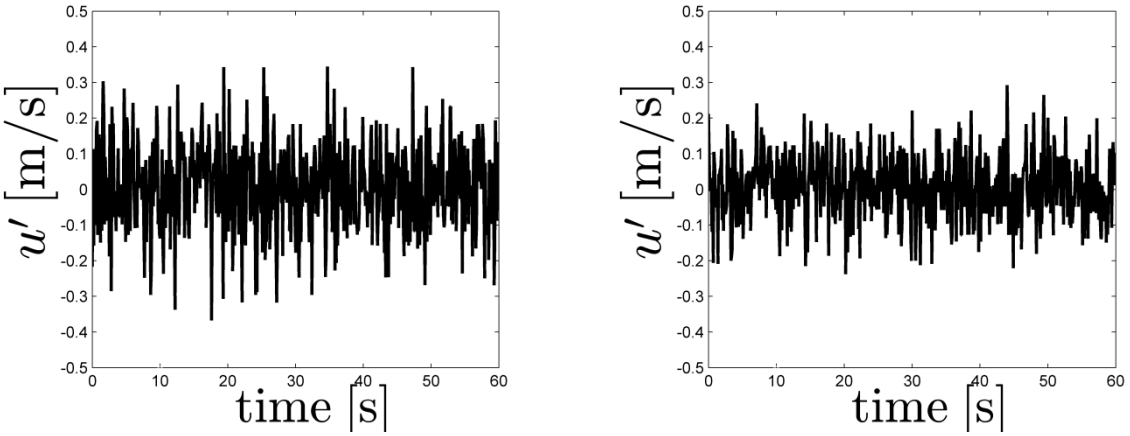


(a) (b)

**Figure A.3 Streamwise fluctuations as function of time at maximal fan power and at different locations: (a) at beginning of wind tunnel, L =0m and (b) at the end of the wind tunnel just after the diffuser, L=9m.**

### Turbulence intensity

The turbulence intensity was defined as:

$$I = \frac{U_{RMS}}{\bar{U}} \tag{A.8}$$

where the $U_{RMS}$ is the root-means-square of the turbulent fluctuations of the mean flow and $\overline{U}$ the mean flow velocity. The root-mean-square of the turbulent fluctuations of the mean flow, $U_{RMS}$ was defined by:

$$U_{RMS} = \sqrt{\frac{1}{3}({u_{RMS}}^2 + {v_{RMS}}^2 + {w_{RMS}}^2)} \tag{A.9}$$

Whereas the mean velocity of the flow can be calculated from the mean velocity components in all directions:

$$\overline{U} = \sqrt{(\bar{u}^2 + \bar{v}^2 + \bar{w}^2)} \tag{A.10}$$

The turbulence intensity decreased from the beginning of the wind tunnel L=9, towards the end of the wind tunnel L=0 (Figure A.4). At L=0, the turbulence intensity was about 0.67 %.

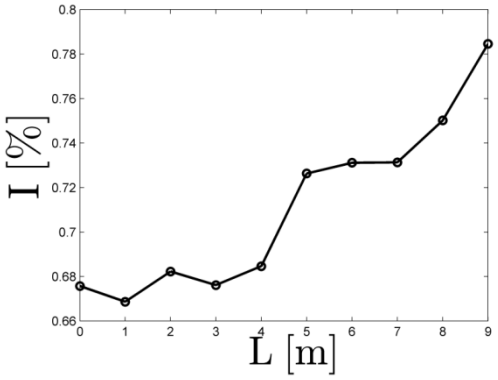


**Figure A.4 Turbulence intensity as function of the position across the length of the wind tunnel.**

### Turbulent kinetic energy

The turbulent kinetic energy, $k$, was calculated by:

$$k = \frac{3}{2} {U_{RMS}}^2 \tag{A.11}$$

where the $U_{RMS}$ is the root-means-square of the turbulent fluctuations of the mean flow. The turbulent kinetic energy at L =0 was about 0.0062 $m^2/s^2$.

### Specific turbulent dissipation rate

The specific turbulent dissipation rate, $\omega$, was calculated by:

$$\omega = \frac{{C_\mu}^{-0.25} k^{0.5}}{\tilde{L}} \tag{A.12}$$

where $C_\mu$ is the turbulent model constant and usually set at 0.09, $k$ the turbulent kinetic energy and $\tilde{L}$ the characteristic length scale. The characteristic length scale was estimated by

$$\tilde{L} = 0.07\, D_{tunnel} \tag{A.13}$$

where $D_{tunnel}$ is the tunnel 'diameter', defined as 2 m. The characteristic length scale was 0.14 m. This gave a specific turbulent dissipation rate of 1.03 $s^{-1}$ at the end of the wind tunnel at L=0.

**Start-up time**

The start-up time of the wind tunnel has been investigated by measuring the streamwise speed response at different positions along the length of the wind tunnel, L=0-9 m. The sonic anemometer was manually synchronised with the wind tunnel software. In Figure A.5 the streamwise speed directly after turning on the wind tunnel is shown. There was approximately a 2 seconds delay between turning on the wind tunnel and the fans starting to rotate. To increase the speed from 0-8 m/s took about 5 seconds from the first movement of the fans.

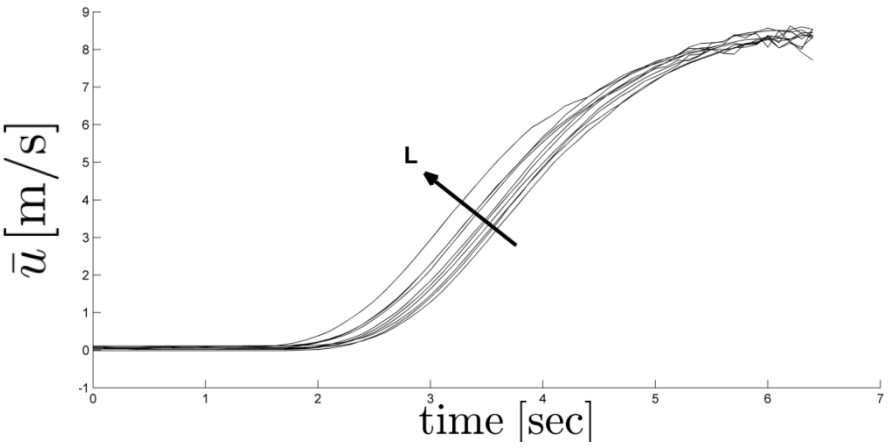


**Figure A.5 Start-up time as of the streamwise speed at different positions in the wind tunnel; from beginning of wind tunnel (L=9m) till the end of the wind tunnel (L=0m).**

**Slow down time**

When turning off the wind tunnel, it takes time to slow down the flow velocity due to the inertia of the fans. It is important that before each trial there were windless environmental conditions, as the force platform was being offset before each trial. This improves the accuracy of the force measurements. Therefore the time between the trials was dependent on the slowdown time of the wind tunnel. In Figure A.6, the streamwise speed profile after turning off the wind tunnel is shown. From this plot it is suggested that a waiting time of approximately 2 minutes is needed to reach windless environmental conditions and this has therefore been applied for all trials presented in this thesis.

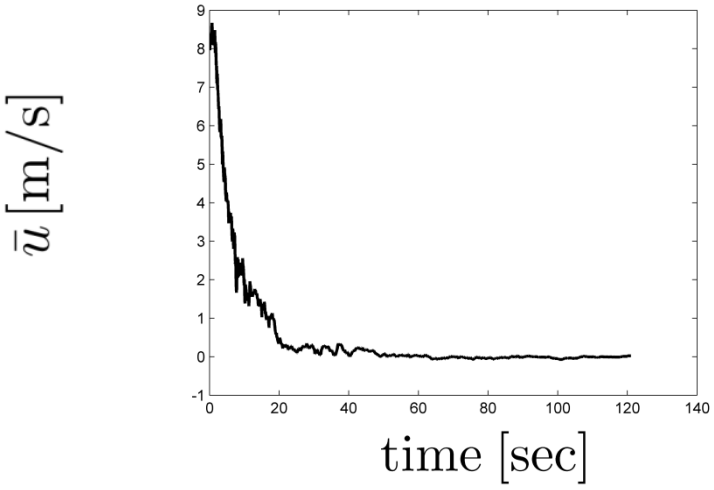


**Figure A.6 Streamwise velocity as function of time after turning off the wind tunnel.**

### Frequency spectrum of streamwise wind speed

The frequency spectrum was used to identify the turbulence frequencies, which can be compared with the dominant frequencies of the force signal. The frequency spectrum of the streamwise speed was calculated by using the Fast Fourier Transform (FFT) of the data. At the end of the wind tunnel, L = 0m (Figure A.7(a)) and at the beginning, L = 9m (Figure A.7(b)) the frequency spectrum of the streamwise speed were determined. In particular high frequencies are induced by the wind. However, no clear dominant peaks were found in the frequency spectra of the measured wind velocities.

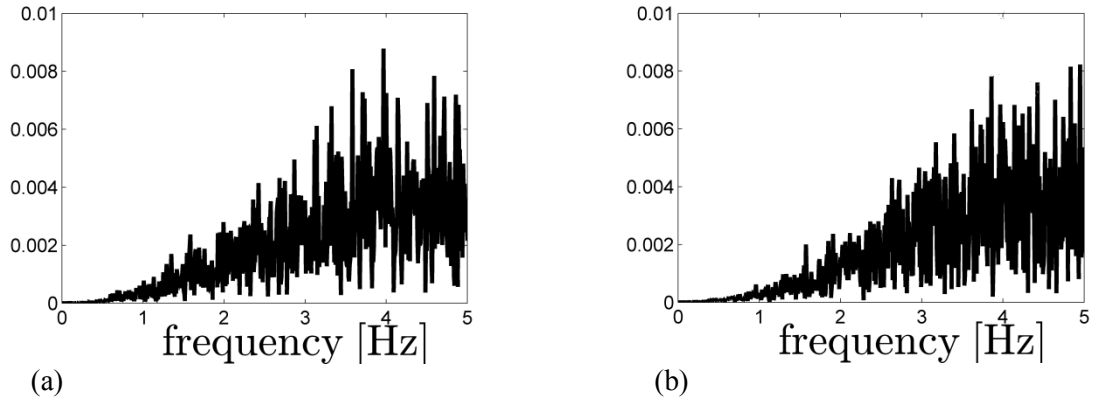


**Figure A.7 Fourier Transfer of the streamwise speed of 2 minutes of captured data: (a) at end of wind tunnel L=0m, (b) at beginning of wind tunnel L=9m.**

**Wind speed outside wind tunnel without bicycle**

The flow velocity, 1 m in front of the wind tunnel, were measured at three different locations: in the middle of the flow and 20 cm from the edge of the platform at both sides and at a height of 1m from the floor of the wind tunnel. As shown in Figure A.8, the flow velocity decreased by approximately 6 %. This could be caused by the interaction of the flow with the motionless flow around the wind tunnel or the boundary layer of the wind tunnel.

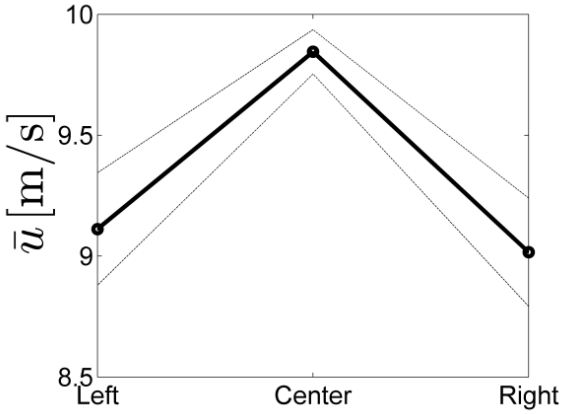


**Figure A.8 Flow velocity 1 m outside the wind tunnel at three different locations measured in the middle of the flow.**

**Wind velocity in wind tunnel with bicycle in different configurations**

The effect of the interference effect of the bicycle on the streamwise velocity was determined. Three different configurations were analysed: 1) bicycle and mannequin in headwind, yaw angle 0°, 2) bicycle and mannequin in crosswind, yaw angle 90°, 3) no bicycle. The streamwise velocity in the final 2m of the wind tunnel in the different conditions is shown in Figure A.9. The streamwise velocity decreases when the bicycle with mannequin was positioned in either a headwind or crosswind configuration compared with no bicycle. A mean velocity reduction of about 4 % was found in a headwind and about 5.4 % in a crosswind at the edge of the wind tunnel (L=0m).

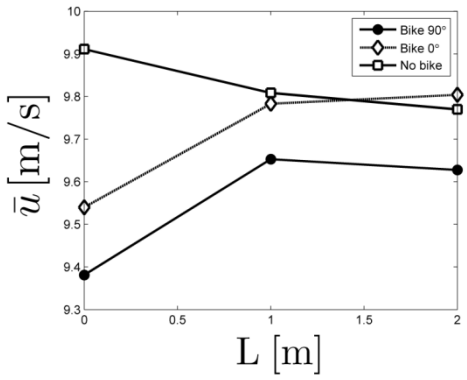


**Figure A.9 Flow velocities in the final 2 m of the wind tunnel in 3 different configurations: no bike and bike with mannequin at 0° and 90° yaw angle.**

## Boundary layer thickness

The boundary layer thickness, $\delta$, is the distance across a boundary layer from the object surface to where the flow has practically reached the free stream flow velocity $U_e$, as shown in Figure A.10. It is relatively difficult to measure the boundary thickness of the wind tunnel experimentally. Therefore CFD simulations were used to estimate the boundary layer thickness along the length of the wind tunnel with the commercial software Ansys CFX. The boundary thickness on a flat plate is defined as 99 % of the free stream velocity. However, in this particular situation, the free stream velocity is non-uniform along the width of the wind tunnel. Therefore the forward differential of the velocity has been used to determine the boundary layer thickness. The boundary layer was determined when the absolute value of dy < 0.01.

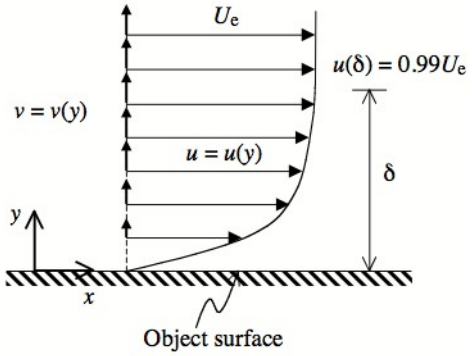


**Figure A.10 Boundary layer thickness (Courtesy of http://aerospaceengineeringblog.com/bio-mimetic-drag-reduction-part-2-aero-and-hydrodynamics/)**

In the CFD simulations, all dimensions were identical to the wind tunnel (Figure A.11). The honeycomb was excluded from the simulations, as it was assumed that it only affects the turbulent intensity rather than the flow velocity. A wall boundary condition was applied on all gray coloured walls in Figure A.11, which are representing the walls of the building. On the two transparent walls, an opening boundary condition was applied. An inlet boundary was applied at the inlet of the diffuser. A k-ε model turbulence model was used in the simulations. The initial flow velocity at the inlet of the wind tunnel was set to 1.338 m/s, resulting in a flow velocity at the end of the wind tunnel of 9.9 m/s, which is comparable with the wind tunnel experiments. The roughness of the wall was set to a smooth wall.

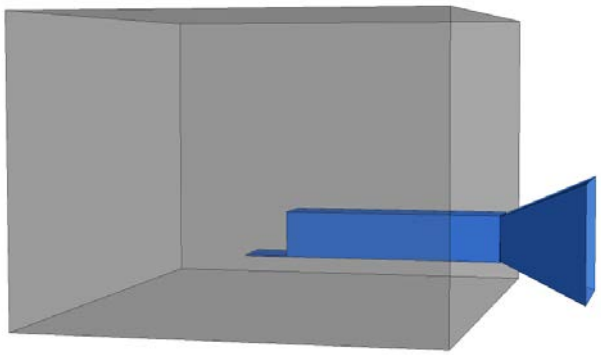

**Figure A.11 Computational domain of the wind tunnel**

The velocity distribution seen from the side and top of the wind tunnel is shown in Figure A.12. The streamwise velocity is almost constant along the length of the wind tunnel. The flow is distributed in all directions when the flow hits the wall. No flow separation exists at the beginning of the wind tunnel directly after the diffuser. Moreover, no boundary layer separation was found in the wind tunnel. From the top view A12.a, it could be seen that the flow hits the wall directly behind the wind tunnel and mainly follows the wall closest to the wind tunnel. In particular on the right side of the wind tunnel an increased velocity area appears.

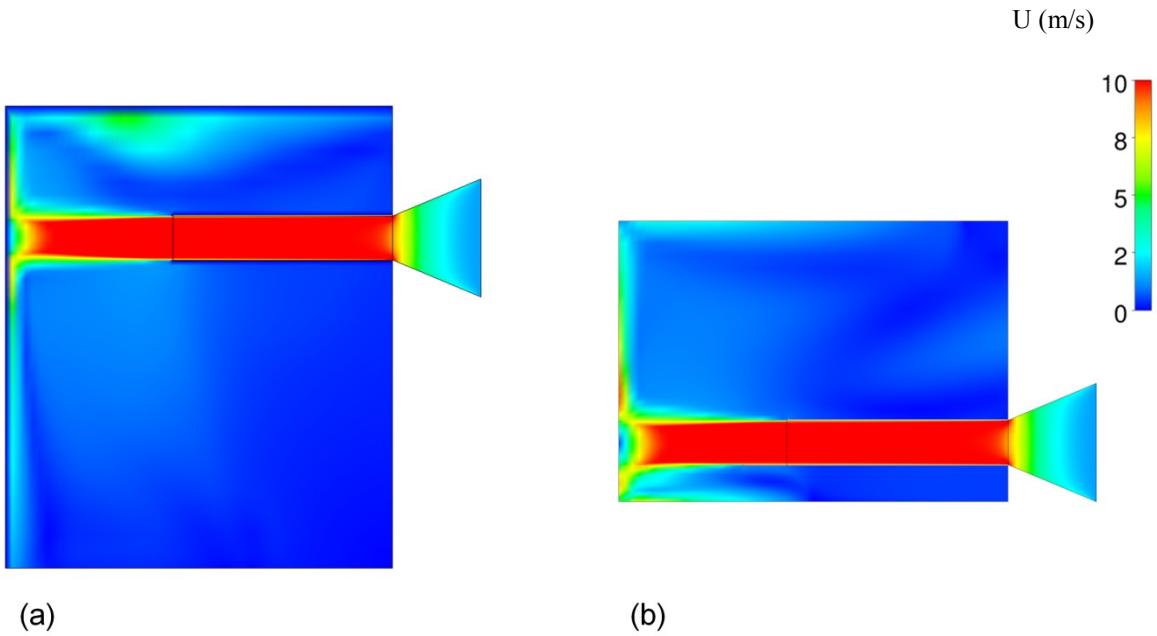


**Figure A.12 Pressure distribution in and around wind tunnel: (a) top view, (b) side view.**

The streamwise velocity $\bar{u}$ at different positions across the length of the wind tunnel from one wall of the wind tunnel to another is shown in Figure A.13. It could be seen that the boundary layer increases closer to the end of the wind tunnel. In addition, the mean velocity increases along the wind tunnel. It should be noticed that the velocity was non-uniform throughout the wind tunnel.

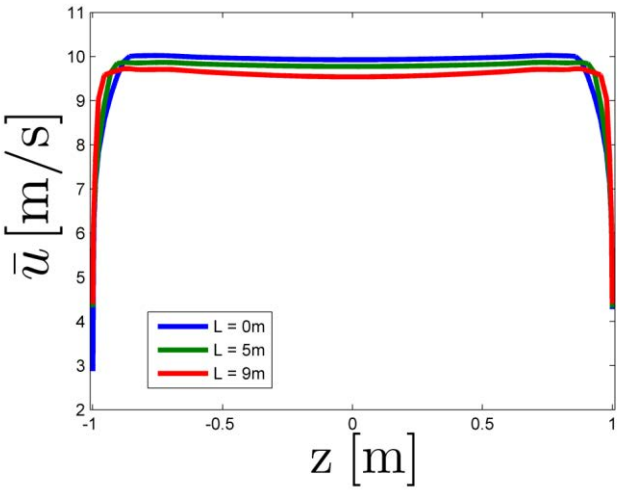


**Figure A.13 Velocity distribution along the height of the wind tunnel at different locations across the length of the wind tunnel.**

Figure A.14 shows the simulated boundary layer thickness at different positions along the length of the wind tunnel. The boundary layer thickness increases towards the edge of the wind tunnel. At the end of the wind tunnel the boundary layer thickness is increased to around 145 mm, whilst at the beginning of the wind tunnel it was only 50 mm.

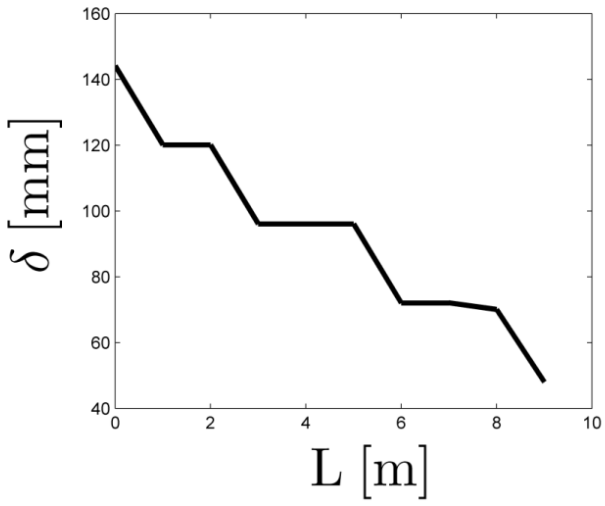


**Figure A.14 Boundary layer thickness along the length of the wind tunnel obtained from CFD simulations.**

# APPENDIX B

# Aerodynamic coefficient corrections

The aerodynamic coefficients were compensated for fluctuating environmental conditions and inference effects of the wind tunnel as they slightly influence the recorded data.

**Environmental conditions correction**

The main changing environmental conditions considered were the air density and temperature. The density ratio between the standard environmental conditions (defined as 20°C and 35 % humidity) and current environmental conditions was calculated. The density of humid air was defined by:

$$\rho_{air} = \frac{p_v}{R_v(T+273.15)} + \frac{p_d}{R_d(T+273.15)} \quad \text{(B.1)}$$

where $p_v$ is the water vapor pressure, $R_v$ the specific gas constant of water vapor, 461.058 J/(kg K) , $T$ the temperature in °C, $p_d$ the dry air pressure and $R_d$ the specific gas constant of dry air, 287.058 J/(kg K). The water vapor pressure was estimated by:

$$p_v = \Phi\left(6.1078 \cdot 10^{\left(\frac{7.5T}{T+237.3}\right)}\right) \quad \text{(B.2)}$$

where $\Phi$ is the relative humidity. Finally the dry air pressure was calculated by subtracting the atmospheric pressure from the water vapour pressure:

$$p_v = 101325 - p_v \quad \text{(B.3)}$$

One correction factor for temperature was applied for the mean temperature and humidity of all trials in each yaw angle condition.

**Wind tunnel interference correction**

The blockage area of the bicycle with mannequin at a 0° and 90° yaw angle was 13.8 % and 21.9 % respectively. This was determined based on the method of Barelle et al (2010), as described in Chapter 2. As the blockage area was > 10 %, a correction was required. In contrast with a closed wind tunnel, where the solid blockage increases the kinetic pressure on the model, an open wind tunnel has a negative blockage effect leading to lower loads on the bicycle. This interference effect is mainly caused by the over-expansion of the flow at the bicycle, reducing the velocity at the position of the bicycle. The flow is also decelerated at the end of the wind tunnel due to the blockage of the bicycle. Although the blockage effect is smaller compared to a closed return wind tunnel, a correction factor has to be applied to correct for the blockage effects when presenting the data. The method of Mercker and Wiedemann (1996) was used to correct for blockage effects of an open wind tunnel. Two interference effects were included:

1. Nozzle blockage: the interference of the bicycle on the flow at the end of the wind tunnel.
2. Flow expansion and solid blockage: the flow will over-expand at the bicycle.

The nozzle blockage, $\epsilon_n$, was calculated by:

$$\epsilon_n = \varepsilon_{qn}\left[\frac{{R_n}^3}{\left({x_m}^2+{R_n}^2\right)^{3/2}}\right] \tag{B.4}$$

where $R_n$ is the hydraulic radius of the duplex nozzle, $x_m$ the distance of the bicycle to the

end of the wind tunnel, and $\varepsilon_{qn}$ the perturbation velocity at the nozzle plane due to the nozzle blockage:

$$B = \frac{A_m(\beta)}{2C}\left[1 + \frac{x_s}{({x_s}^2 + {R_n}^2)}\right] \tag{B.5}$$

$$\epsilon_{qn} = \frac{B}{1-B} \tag{B.6}$$

where $A_m$ is the duplex frontal area of the bicycle and mannequin, $C$ is the cross-section of the wind tunnel and $x_s$ the distance of the nozzle to the source point and defined as:

$$x_s = -x_m + \frac{L}{2} - \left(\frac{A_m(\beta)}{2\pi}\right)^{1/2} \tag{B.7}$$

where L is the length of the bicycle.

The solid blockage, $\epsilon_s$, was calculated by

$$\epsilon_s(\beta) = \tau\left(\frac{V}{L}\right)^{1/2}\frac{A_m(\beta)}{{A_D}^{3/2}} \tag{B.8}$$

where $\tau$ is the wind tunnel shape factor, $V$ the volume of the bicycle and mannequin, and $A_D$ the reduced cross-section of the wind tunnel and is calculated by:

$$A_D = \frac{C}{1+\epsilon_{qn}} \tag{B.9}$$

The correction factor of the aerodynamic forces $CF_i$ was expressed as:

$$\left(\frac{CF_i}{CF_{ic}}\right) = \left(\frac{q_c}{q_u}\right) = (1+\epsilon)^2 = (1 + \epsilon_n + \epsilon_s(\beta))^2 \tag{B.10}$$

where $CF_{ic}$ is the corrected force coefficient value.

# APPENDIX C

# Position and pulmonary functioning

**Introduction**

By lowering the time trial handlebar position, the pulmonary functioning of a cyclist can be affected due to the restricted movement of the diaphragm. Craig et al. (1960) demonstrated that when changing from a sitting position to a leaned forward sitting position the respiratory reserve volume significantly increased. However, this change in lung volume is not supported by previous cycling literature. Berry et al. (1994) have shown that there is no significant effect of altering position on the lung volumes and capacities. It should be noted that the positions analysed were an upright position and a large torso angle time trial position. The effect of small torso angles towards more relevant small time trial torso angle positions has not been examined yet. Therefore the aim of this study was to investigate the effect of different time trial positions on the pulmonary functioning. It was hypothesized that the lung volumes and capacities are reduced and the respiratory reserve volume is increased when lowering position.

**Method**

Spirometry measurements were taken from 10 male participants to determine the inhale and exhale volume of air as a function of time in the 0° and 16° torso angle cycling positions in rest (i.e. no physical activity). The participants were between the ages of 21-49 years and physically fit and healthy. It should be noted that only one of the participants was a time trial

cyclist. The participant characteristics are shown in Table C.1.

The spirometry was undertaken with a Jaeger Oxycon Pro system (Erich Jaeger GmbH, Hoechberg, Germany). The breath to breath analyser has been calibrated prior to each test. Measured variables were the forced vital capacity (FVC), maximal volume exhaled in the first second of the forced expiration (FEV1), forced expiratory ratio (FER), expiratory reserve volume (ERV), tidal volume (VT), vital capacity inspiration (VC IN) and vital capacity expiration (VC EX). A schematic representation of the measured pulmonary functions is shown in Figure C.1. The FVC is the volume of maximal forced expiration starting from a full slow inspiration and FER is expressed as the fraction between FVC and FEV1. The inspiratory reserve volume (IRV) was determined from the vital capacity minus the expiratory reserve volume and tidal volume. The tidal volume was determined from 10 consistent normal breaths that met the criteria set by Jaeger Oxycon Pro.

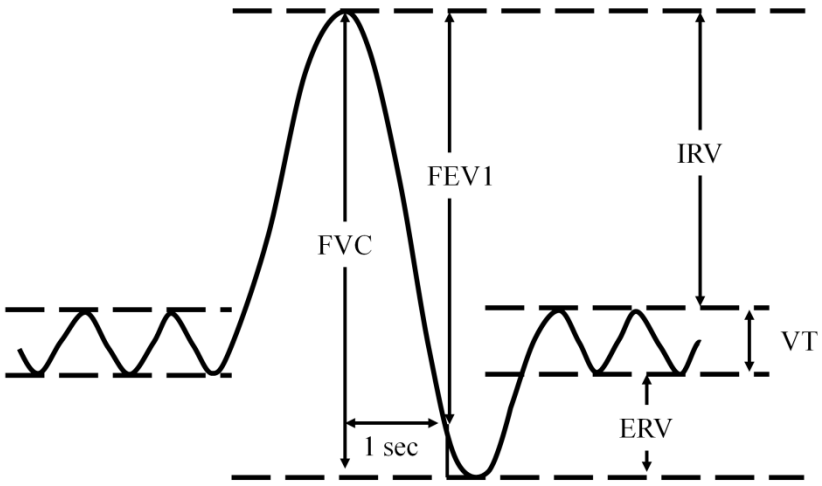


**Figure C.1 Schematic representation of the measured pulmonary variables: forced vital capacity (FVC), maximal volume exhaled in the first second of the forced expiration (FEV1), expiratory reserve volume (ERV), inspiratory reserve volume (IRV), tidal volume (VT).**

**Table C.1 Participant characteristics (n=10).**

| | Age (yr) | Height (m) | Weight (kg) |
|---|---|---|---|
| Value | 26.7± 8.4 | 1.84 ± 0.1 | 79.3 ± 8.9 |

All tests were repeated at least three times and until the between test criteria of the European Respiratory Journal (Miller et al., 2005) were fulfilled. The maximal measured spirometry values were reported. Differences between the pulmonary function in the two different cycling positions were analysed with a paired samples t test. The significance level was set at 0.05.

**Results**

Lung capacities and volumes in the two cycling positions are shown in Table C.2. There was a significant difference in vital capacity expiration (VC EX) in the different torso angle positions; $t(9) = 2.454$, $p = 0.037$. Furthermore, a significant effect of position has been found on the FEV1; $t(9) = 2.291$, $p = 0.048$. Although the FVC reduced by lowering position, the results were not significantly different; $t(9) = 2.065$, $p = 0.069$. All other lung volumes and capacities were not significantly affected by torso angle position.

**Discussion**

The results show that the pulmonary functioning was slightly affected by position when the body was at rest (i.e. no physical activity). Only the expiratory variables VC EX and FEV1 were different, indicating that primarily the exhale volume and velocity are affected by the position, whilst the inspiration volumes remained relatively constant. It should be noted that the non-significant findings could be a result of the combination of the small sample size used and the large variability often encountered in pulmonary function measurements. Main sources of the inter-subject variability in this study are physical fitness, age, weight, and genetic characteristics (Becklake, 1986). Despite the limited number of participants, the results show that the lung restrictions due to lowering position are not a major limitation to cycling in small torso angle positions. Moreover, the restricted lung volume will likely only

affect the performance at high cycling intensities. Caution has to be taken in extrapolating the findings from rest to a physical active cycling state, as the pulmonary function increases and changes due to intensity and fatigue (Berry et al., 1994).

**Table C.2 Lung volumes and capacities in the 0° and 16° torso angle position (n=10) in rest (e.g. no physical activity).**

| | 16° position | 0° position |
|---|---|---|
| VT (L) | 0.91 ± 0.24 | 0.83 ± 0.17 |
| ERV (L) | 2.21 ± 0.54 | 2.25 ± 0.46 |
| IRV (L) | 2.34 ± 0.54 | 2.07 ± 0.43 |
| VC IN (L) | 5.49 ± 0.68 | 5.19 ± 1.20 |
| VC EX (L) | 5.71 ± 0.96 | 5.33 ± 0.99* |
| FEV1 (L) | 4.52 ± 0.81 | 4.28 ± 0.89* |
| FVC (L) | 5.47 ± 0.64 | 5.16 ± 0.74 |
| FER (%) | 82.5 ± 10.2 | 82.5 ± 9.3 |

*VT, tidal volume; ERV, expiratory reserve volume; IRV, inspiratory reserve volume; VC IN, vital capacity inspiration; VC EX, vital capacity expiration; FEV1, forced expiratory volume at the end of the first second; FVC, forced volume capacity; FER, forced expiratory ratio.*

* Significant different from the 16° torso angle position, $p < 0.05$

# APPENDIX D

# Leg position and crosswinds

**Introduction**

The position of the cyclist's legs changes throughout the pedal cycle. Variations of the flow have been observed across different static crank angles (Griffith et al., 2014, Crouch et al., 2012, Crouch et al., 2014a). For example, it has been shown by Crouch et al. (2012) that the leg position significantly changes the aerodynamic forces on a cyclist. Their experimental study showed variations of up to 15 % in drag area when cycling in a time trial position. This is also confirmed by an extensive experimental and numerical analysis of the cycling aerodynamics (Griffith et al., 2014). It has been suggested that these variations are primarily a result of changes in the flow field, rather than changes in frontal area. It has been shown that the frontal area changes by less than 2 % over the pedal cycle. According to the knowledge of the authors, previous literature focused on windless conditions, whilst cyclists' are commonly subjected to crosswinds. Therefore this side-investigation aims to determine the effect of leg configuration on the aerodynamic forces in crosswinds. It has been hypothesized that the aerodynamic drag is lowest when the pedals are level and that the leg configuration alters the aerodynamic side forces when subjected to crosswinds.

**Methods**

Three different leg positions are compared and shown in Figure D.1: (a) pedals level; (b) left pedal at top dead centre, TDC; (c) right pedal at top dead centre, TDC. The positions are close

to the positions corresponding to the minimal and maximum drag force value observed within the pedal cycle (Crouch et al., 2012). Two CFD approaches are used to determine the forces on a cyclist: the RANS k-ε model approach and the DES approach. For both approaches the computational methods are similar to those described in Chapter 7. As the pedal frequency is relatively slow compared to the flow velocity, a quasi-static approach has been assumed. A recent cycling study has shown that the quasi-static approach provides similar fundamental fluid mechanics than that of the dynamic pedaling approach (Crouch et al., 2014b). Two different crosswind conditions are investigated: the 15° crosswind yaw angle condition and the 90° condition. A steady crosswind of 9.91 m/s is applied. The RANS and DES mesh consisted of 17.8 and 26.8 million nodes, respectively. As this is a preliminary study, the 90° yaw angle condition has only been investigated with steady RANS simulations.

(a) Pedals level (b) Left pedal at TDC (c) Right pedal at TDC

**Figure D.1 Representation of the different cycling position examined: (a) pedals level, (b) left pedal at top dead centre, (c) right pedal at top dead centre**

### Results: crosswind yaw angle of 15°

The aerodynamic force and moment results of the DES simulations in the different leg position configurations are shown in Table D.1. The results show drag coefficient ($CF_X$) variations of 14 – 16 % between the different leg positions. The lowest drag is observed when

the pedals are level, whilst the highest drag is found when the pedal at the leeward side of the cyclist (right pedal) is in the top dead centre. The side force coefficients ($CF_Y$) significantly reduce by about 19 % when the left pedal is at the TDC compared with level pedals, hence reducing the rolling moment coefficients ($CM_X$). The lift force coefficients ($CF_Z$) are slightly decreased and comparable for the two cases where one pedal is in the TDC. The drag forces are similar to the results of (Crouch et al. (2012)), despite of a couple of methodological differences such as the cycling positions used (dropped versus time trial position) and differences in flow directions (crosswind versus no crosswind).

**Table D.1 Aerodynamic forces and moments of the cyclist obtained with DES with the legs in three different positions and at a crosswind yaw angle of 15°: pedals level, left pedal at top dead centre and right pedal at top dead centre. The percentage difference between the pedals level and the left/ right pedal at the top dead centre are included.**

| | | Pedals level | Left pedal at TDC | Right pedal at TDC |
|---|---|---|---|---|
| Value | $CF_X$ | 0.513 | 0.579 | 0.590 |
| % Difference Level | | | +13.9 % | +16.1 % |
| % Frontal area | | | +3 % | +8 % |
| Value | $CF_Y$ | 0.250 | 0.203 | 0.295 |
| % Difference Level | | | -18.8 % | +18.0 % |
| % Frontal area | | | +1 % | -1 % |
| Value | $CF_Z$ | 0.180 | 0.176 | 0.158 |
| % Difference Level | | | -2.2 % | -12.2 % |
| % Frontal area | | | -3 % | -3 % |
| Value | $CM_X$ | -0.107 | -0.093 | -0.110 |
| % Difference Level | | | -13.1 % | +2.8 % |
| Value | $CM_Y$ | 0.292 | 0.324 | 0.319 |
| % Difference Level | | | 10.9 % | 9.2 % |

The time-averaged iso-surface pressure at Cp=-0.240 of the flow around a cyclist in the different pedal positions are shown in Fig. C.2. It can be clearly seen that in the case of the left pedal at TDC, the iso-pressure in the wake is stretched and increased in length, whilst the flow velocity is higher compared to the other pedal positions. This reflects the higher side forces shown for this leg configuration. This stretched flow structure is also observed for the time-varying iso-pressure in Figure D.3. When the left pedal is at the TDC, large elongated structures are formed at the back of the cyclist on the left side and extended in the wind-ward direction. More symmetrical flow mechanics are observed when the pedals are level compared to the other leg configurations.

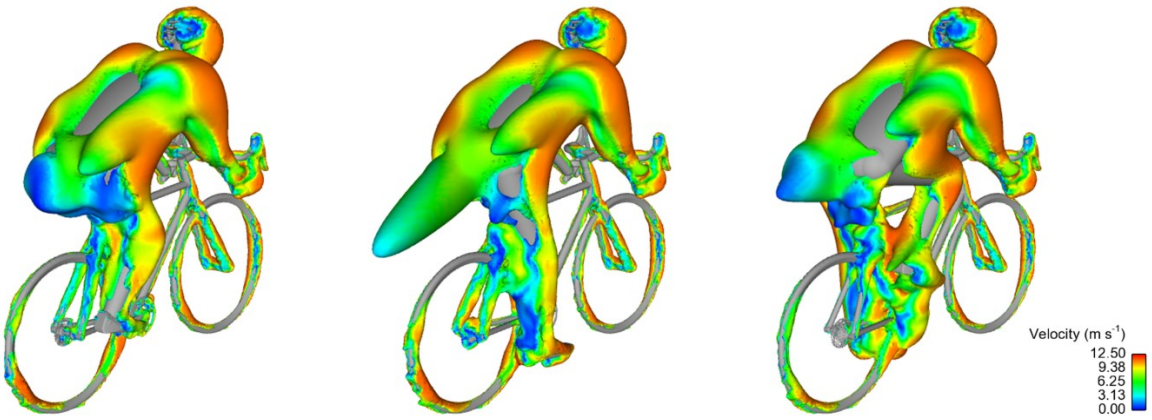


(a) Pedals level (b) Left pedal at TDC (c) Right pedal at TDC

**Figure D.2 Iso-surface of the pressure around a cyclist across the three different leg configurations obtained with DES. The iso-surface is coloured with the flow velocity.**

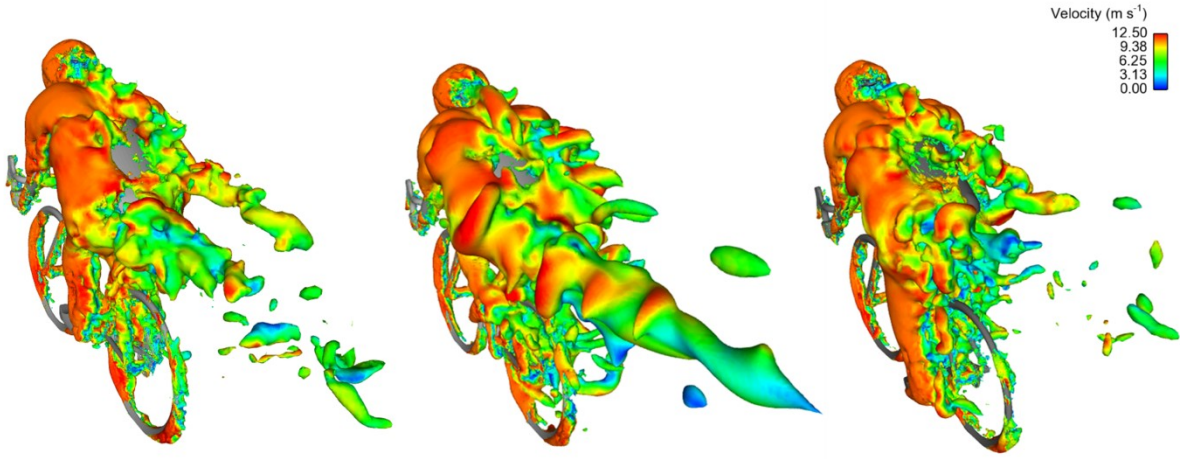


(a) Pedals level (b) Left pedal at TDC (c) Right pedal at TDC

**Figure D.3 Time-varying iso-surface of the pressure around a cyclist across three different leg positions obtained with the DESsimulations. The iso-surface is coloured with the flow velocity.**

In Figure D.4, the time-averaged pressure in three horizontal planes at different heights (0.7H, 0.6H and 0.4H) is shown. Comparable pressure fields are obtained at a height of 0.7H and 0.4H. Largest differences are shown for the plane at 0.6H. In this plane, it could be seen that when the legs are level, the pressure fields of the two legs are interacting. The largest pressure region is observed in front of the leg which is in the bottom dead centre. This region is largest for the case when the right pedal is the TDC, as shown in Figure D.4(c).

The streamlines projected on a horizontal plane at a height of 0.6H and 0.4H is shown in Figure D.5. It can be clearly seen that the flow mechanics change due to the different leg configurations. In particular at a height of 0.6H, the flow directions changes as a result of the interaction of the two legs. The absolute width of the wake is however comparable for the different leg configuration which is caused by the fixed position of the arms in all three configurations.

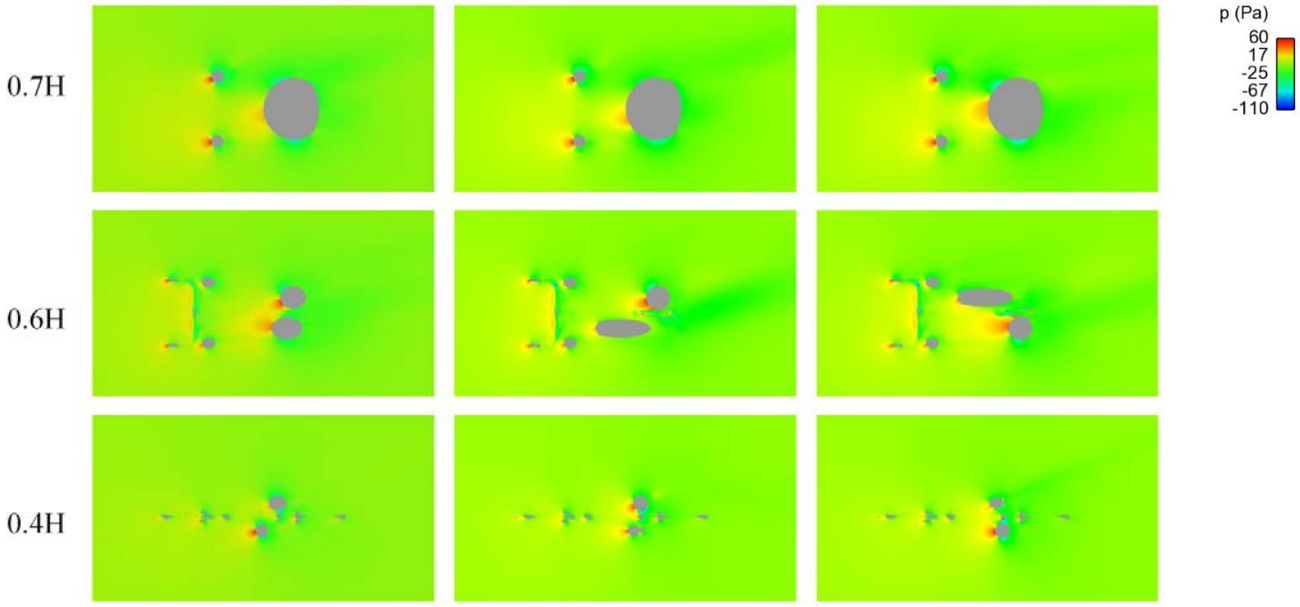


(a) Pedals level (b) Left pedal at TDC (c) Right pedal at TDC

**Figure D.4 Time-averaged pressure in the x-y plane across different leg configurations and at a height of 0.7H, 0.6H and 0.4H.**

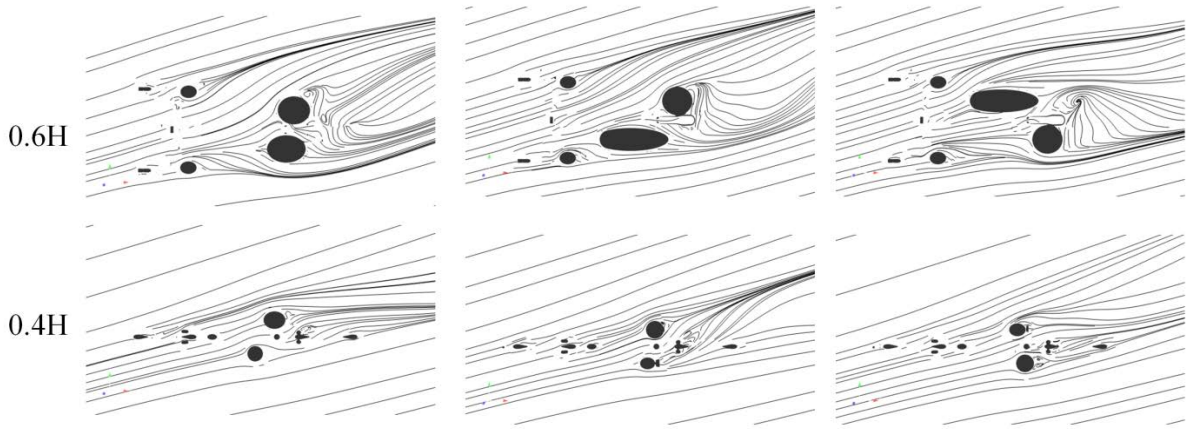


(a) Pedals level (b) Left pedal at TDC (c) Right pedal at TDC

**Figure D.5 Time-averaged streamlines in the x-y plane across different leg configurations and at a height of 0.7H, 0.6H and 0.4H.**

**Results: crosswind yaw angle of 90°**

The RANS results of a bicycle in different leg configurations at a crosswind yaw angle of 90° are shown in Table D.2. The side, lift and rolling moments are increased when one of the legs is in the TDC compared to level pedals. The side forces coefficients increase by up to about 16 %, despite the fact that the side area significantly decreases by about 3 %. The highest side force coefficients and rolling moment coefficients are observed when the right pedal (leeward side of bike) is at the top dead centre.

The iso-surface pressure at Cp=0.240 are shown in Figure D.6. Comparable flow structures are shown for the pedals level and left pedal at TDC, Figure D.6(a) and D.6(b) respectively. However, it could be seen that when the left pedal is at the TDC (Figure D.6(b)), a low pressure area is stretched to the ground. In case of the right pedal at the TDC, low pressure structures develop around the rear wheel and hip. These vortex structures contribute to the higher observed side forces compared to the other two leg configurations.

**Table D.2 Aerodynamic forces and moments of the cyclist obtained with RANS with the legs in three different positions and at a crosswind yaw angle of 90°: pedals level, left pedal at top dead centre and right pedal at top dead centre. The percentage difference between the pedals level and the left/ right pedal at the top dead centre are included.**

| | | Pedals level | Left pedal at TDC | Right pedal at TDC |
|---|---|---|---|---|
| Value | $CF_Y$ | 1.235 | 1.309 | 1.430 |
| % Difference Level | | | +5.9 % | +16.2 % |
| % Frontal area | | | -5 % | -5 % |
| Value | $CF_Z$ | 0.157 | 0.193 | 0.120 |
| % Difference Level | | | +23.6 % | +23.7 % |
| % Frontal area | | | -3 % | -3 % |
| Value | $CM_X$ | -0.541 | -0.592 | -0.621 |
| % Difference Level | | | +9.4 % | +14.8 % |

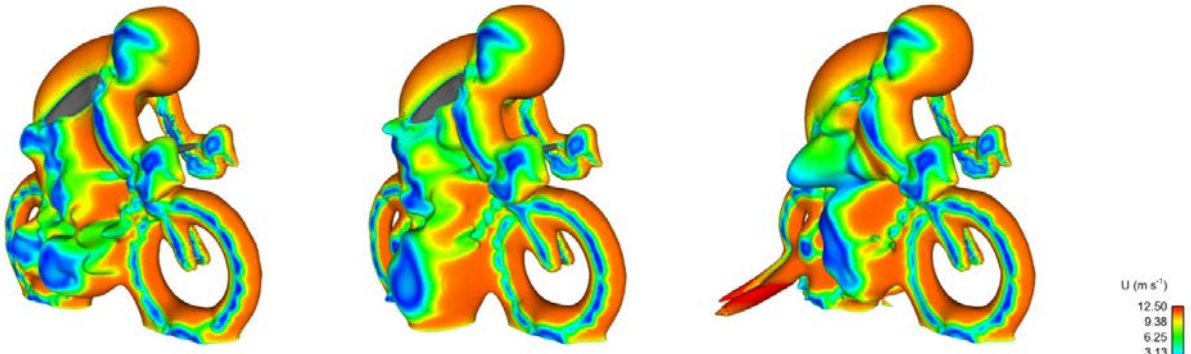


(a) Pedals level (b) Left pedal at TDC (c) Right pedal at TDC

**Figure D.6 Iso-surface of the time-averaged pressure around the cyclist across the three different leg configurations at 90 degrees crosswind yaw angle. The iso-surface is coloured with the flow velocity.**

## Conclusion

The results show that the aerodynamic forces and moments are significantly affected by the leg configuration. The forces in the free stream flow direction are increased by up to 16 % when one of the pedals is in the top dead centre of the pedal revolution. For a yaw angle of 15° and 90°, the highest force and moment coefficients are found for the right pedal in the top dead centre and the windward pedal in the bottom dead centre. In addition, variations in the flow structures are observed with different leg configurations. The altered flow characteristics are not a result of modified area, but by changes in the flow field.

# REFERENCES


ACHENBAC, E. 1968. Distribution of Local Pressure and Skin Friction around a Circular Cylinder in Cross-Flow up to Re=5x106. *Journal of Fluid Mechanics,* 34**,** 625-639.

ANGELETTI, M., SCLAFANI, L., BELLA, G. and UBERTINI, S. 2003. The Role of CFD on the Aerodynamic Investigation of Motorcycles. *SAE Technical Paper* 2003-01-0997.

ARAKI, Y. and GOTOU, K. 2001. Development of aerodynamic characteristics for motorcycles using scale model wind tunnel. *SAE Technical Paper* 2001-01-1851.

*The Argus*. 2014. Man blown off bike then hit by car, 12th May 2014. Available: http://www.theargus.co.uk/ [Accessed 12th May 2014].

ASHE, M. C., SCROOP, G. C., FRISKEN, P. I., AMERY, C. A., WILKINS, M. A. and KHAN, K. M. 2003. Body position affects performance in untrained cyclists. *British Journal of Sports Medicine,* 37**,** 441-444.

BAKER, C., CHELI, F., ORELLANO, A., PARADOT, N., PROPPE, C. and ROCCHI, D. 2009. Cross-wind effects on road and rail vehicles. *Vehicle System Dynamics,* 47**,** 983-1022.

BAKER, C. J. 1991. Ground vehicles in high cross winds part I: Steady aerodynamic forces. *Journal of Fluids and Structures,* 5**,** 69-90.

BALMER, J., DAVISON, R. C. R. and BIRD, S. R. 2000. Peak power predicts performance power during an outdoor 16.1-km cycling time trial. *Medicine and Science in Sports and Exercise,* 32**,** 1485-1490.

BANKS, D. C. and SINGER, B. A. 1994. Vortex Tubes in Turbulent Flows - Identification, Representation, Reconstruction. *Institute for Computer Applications in Science and Engineering.* Hampton: NASA Langley Research Center.

BARELLE, C., CHABROUX, V. and FAVIER, D. 2010. Modeling of the time trial cyclist projected frontal area incorporating anthropometric, postural and helmet characteristics. *Sports Engineering,* 12**,** 199-206.

*The Age*. 2005. Cyclist killed on Great Victorian Bike Ride, November 28, 2005. Available: http://www.theage.com.au/articles/2005/11/28/1133026378716.html?from=top5 [Accessed November 28, 2005].

BARRY, N., BURTON, D., CROUCH, T., SHERIDAN, J. and LUESCHER, R. 2012. Effect of crosswinds and wheel selection on the aerodynamic behavior of a cyclist. *Procedia Engineering,* 34**,** 20-25.

BARRY, N., SHERIDAN, J., BURTON, D. and BROWN, N. A. T. 2014. The Effect of Spatial Position on the Aerodynamic Interactions between Cyclists. *Procedia Engineering,* 72**,** 774-779.

BASSETT, D. R., KYLE, C. R., PASSFIELD, L., BROKER, J. P. and BURKE, E. R. 1999. Comparing cycling world hour records, 1967-1996: modeling with empirical data. *Medicine and Science in Sports and Exercise,* 31**,** 1665-1676.

*BBC*. 2014. UK storms: Strong winds shut Bridgewater Place. Available: http://www.bbc.co.uk/.

BECKLAKE, M. R. 1986. Concepts of Normality Applied to the Measurement of Lung-Function. *American Journal of Medicine,* 80**,** 1158-1164.

BERRY, M. J., POLLOCK, W. E., VANNIEUWENHUIZEN, K. and BRUBAKER, P. H. 1994. A Comparison between Aero and Standard Racing Handlebars during Prolonged Exercise. *International Journal of Sports Medicine,* 15**,** 16-20.

BEST, J. 2013. Main road into Leeds 'should be closed in high winds' after pedestrian was killed by flying lorry. *Mirror.* UK.

BLOCKEN, B. and CARMELIET, J. 2004. Pedestrian Wind Environment around Buildings: Literature Review and Practical Examples. *Journal of Thermal Envelope and Building Science,* 28**,** 107-159.

BLOCKEN, B., DEFRAEYE, T., KONINCKX, E., CARMELIET, J. and HESPEL, P. 2013. CFD simulations of the aerodynamic drag of two drafting cyclists. *Computers & Fluids,* 71**,** 435-445.

BOCCIOLONE, M., CHELI, F., CORRADI, R., MUGGIASCA, S. and TOMASINI, G. 2008. Crosswind action on rail vehicles: Wind tunnel experimental analyses. *Journal of Wind Engineering and Industrial Aerodynamics,* 96**,** 584-610.

BRIDGES, P. and RUSSELL, J. B. 1987. The Effect of Topboxes on Motorcycle Stability. *Vehicle System Dynamics,* 16**,** 345-354.

BRIER, S. R. and NYFIELD, B. 1995. A Comparison of Hip and Lumbopelvic Inflexibility and Low-Back-Pain in Runners and Cyclists. *Journal of Manipulative and Physiological Therapeutics,* 18**,** 25-28.

BROKER, J. P., KYLE, C. R. and BURKE, E. R. 1999. Racing cyclist power requirements in the 4000-m individual and team pursuits. *Medicine and Science in Sports and Exercise,* 31**,** 1677-1685.

BROWN, D. A., KAUTZ, S. A. and DAIRAGHI, C. A. 1996. Muscle activity patterns altered during pedaling at different body orientations. *Journal of Biomechanics,* 29**,** 1349-1356.

BROWN, G. 2002. Injury Prevention and Management. *In:* JEUKENDRUP, A. (ed.) *High-performance cycling.* USA: Human Kinetics.

BROWNLIE, L., KYLE, C. R., CARBO, J., DEMAREST, N., HARBER, E., MACDONALD, R. and NORDSTROM, M. 2009. Streamlining the time trial apparel of cyclists: the Nike Swift Spin project. *Sports Technology,* 2**,** 53-60.

BURKE, E. R. and PRUITT, A. L. 2003. Body positioning for cycling, Chapter 3. *In:* BURKE, E. (ed.) *High-tech cycling.* 2nd ed. United States of America: Human Kinetics.

CAPELLI, C. and DIPRAMPERO, P. E. 1995. Effects of Altitude on Top Speeds during 1 H Unaccompanied Cycling. *European Journal of Applied Physiology and Occupational Physiology,* 71**,** 469-471.

CARR, A. 2011. *Fatal Motorcycle Crash, Wind Gust Causes Sherman Wreck* [Online]. Available: http://www.post-journal.com/page/content.detail/id/583501/Fatal-Motorcycle-Crash.html?nav=5192.

CELIK, I. B., GHIA, U., ROACHE, P. J. and FREITAS, C. J. 2008. Procedure for estimation and reporting of uncertainty due to discretization in CFD applications. *Journal of Fluids Engineering-Transactions of the Asme,* 130.

CHABROUX, V., BARELLE, C. and FAVIER, D. 2012. Aerodynamics of Cyclist Posture, Bicycle and Helmet Characteristics in Time Trial Stage. *Journal of Applied Biomechanics,* 28**,** 317-323.

*7 News The Denver Channel*. 2011. Bike Rider Blown Over By Heavy Wind, Jun 17 Available: http://www.thedenverchannel.com/ [Accessed Jun 17 ].

CHAPMAN, A. R., VICENZINO, B., BLANCH, P., KNOX, J. J., DOWLAN, S. and HODGES, P. W. 2008. The influence of body position on leg kinematics and muscle recruitment during cycling. *Journal of Science and Medicine in Sport,* 11**,** 519-526.

CHELI, F., BELFORTE, P., MELZI, S., SABBIONI, E. and TOMASINI, G. 2006a. Numerical-experimental approach for evaluating cross-wind aerodynamic effects on heavy vehicles. *Vehicle System Dynamics,* 44**,** 791-804.

CHELI, F., BOCCIOLONE, M., PEZZOLA, M. and LEO, E. Numerical and experimental approaches to investigate the stability of a motorcycle vehicle. Proceedings of the 8th Biennial Conference on Engineering Systems Design and Analysis, 4-7 July 2006 2006b Turin, Italy. 105-114.

CHILLÓN, P., CASTRO-PIÑERO, J., RUIZ, J. R., SOTO, V. M., CARBONELL-BAEZA, A., DAFOS, J., VICENTE-RODRÍGUEZ, G., CASTILLO, M. J. and ORTEGA, F. B. 2010. Hip flexibility is the main determinant of the back-saver sit-and-reach test in adolescents. *Journal of Sports Sciences,* 28**,** 641-648.

CHOWDHURY, H. and ALAM, F. 2012. Bicycle aerodynamics: an experimental evaluation methodology. *Sports Engineering,* 15**,** 73-80.

CHOWDHURY, H., ALAM, F. and MAINWARING, D. 2011. A full scale bicycle aerodynamics testing methodology. *Procedia Engineering,* 13**,** 94-99.

CHOWDHURY, H., ALAM, F. and SUBIC, A. 2010. Aerodynamic performance evaluation of sports textile. *Procedia Engineering,* 2**,** 2517-2522.

CHU, L. M., CHANG, M. H., HSU, H. C., CHIEN, W. T. and LIU, C. H. 2008. Simulation and experimental measurement of flow field within four-stroke motorcycle engines. *Journal of the Chinese Society of Mechanical Engineers,* 29**,** 149-158.

CONNICK, M. J. and LI, F. X. 2013. The impact of altered task mechanics on timing and duration of eccentric bi-articular muscle contractions during cycling. *Journal of Electromyography and Kinesiology,* 23**,** 223-229.

COOPER, K. R. 1983. The Effect of Handlebar Fairings on Motorcycle Aerodynamics. *SAE Technical Paper,* 830156.

CRAIG, A. B. 1960. Effects of Position on Expiratory Reserve Volume of the Lungs. *Journal of Applied Physiology,* 15**,** 59-61.

CROUCH, T., SHERIDAN, J., BURTON, D., THOMPSON, M. and BROWN, N. A. T. 2012. A quasi-static investigation of the effect of leg position on cyclist aerodynamic drag. *Procedia Engineering,* 34**,** 3-8.

CROUCH, T. N., BURTON, D., BROWN, N. A. T., THOMPSON, M. C. and SHERIDAN, J. 2014a. Flow topology in the wake of a cyclist and its effect on aerodynamic drag. *Journal of Fluid Mechanics,* 748**,** 5-35.

CROUCH, T. N., BURTON , D., THOMPSON , M. C., MARTIN , D. T., BROWN, N. A. T. and SHERIDAN, J. 2014b. A Phase-Averaged Analysis of the Pedalling Cyclist Wake. *19th Australasian Fluid Mechanics Conference.* Melbourne, Australia.

DABNICHKI, P. and AVITAL, E. 2006. Influence of the postion of crew members on aerodynamics performance of two-man bobsleigh. *Journal of Biomechanics,* 39**,** 2733-2742.

DALMONTE, A., LEONARDI, L. M., MENCHINELLI, C. and MARINI, C. 1987. A New Bicycle Design Based on Biomechanics and Advanced Technology. *International Journal of Sport Biomechanics,* 3**,** 287-292.

DE VEY MESTDAGH, K. 1998. Personal perspective: in search of an optimum cycling posture. *Applied Ergonomics,* 29**,** 325-334.

DEAKON, R. T. 2012. Chronic Musculoskeletal Conditions Associated With the Cycling Segment of the Triathlon; Prevention and Treatment With an Emphasis on Proper Bicycle Fitting. *Sports Medicine and Arthroscopy Review,* 20**,** 200-205.

DEBRAUX, P., BERTUCCI, W., MANOLOVA, A. V., ROGLER, S. and LODINI, A. 2009. New Method to Estimate the Cycling Frontal Area. *International Journal of Sports Medicine,* 30**,** 266-272.

DEBRAUX, P., GRAPPE, F., MANOLOVA, A. V. and BERTUCCI, W. 2011. Aerodynamic drag in cycling: methods of assessment. *Sports Biomechanics,* 10**,** 197-218.

DEFRAEYE, T., BLOCKEN, B., KONINCKX, E., HESPEL, P. and CARMELIET, J. 2010a. Aerodynamic study of different cyclist positions: CFD analysis and full-scale wind-tunnel tests. *Journal of Biomechanics,* 43**,** 1262-8.

DEFRAEYE, T., BLOCKEN, B., KONINCKX, E., HESPEL, P. and CARMELIET, J. 2010b. Computational fluid dynamics analysis of cyclist aerodynamics: Performance of different turbulence-modelling and boundary-layer modelling approaches. *Journal of Biomechanics,* 43**,** 2281-2287.

DEFRAEYE, T., BLOCKEN, B., KONINCKX, E., HESPEL, P. and CARMELIET, J. 2011. Computational fluid dynamics analysis of drag and convective heat transfer of individual body segments for different cyclist positions. *Journal of Biomechanics,* 44**,** 1695-1701.

DEFRAEYE, T., BLOCKEN, B., KONINCKX, E., HESPEL, P., VERBOVEN, P., NICOLAI, B. and CARMELIET, J. 2014. Cyclist Drag in Team Pursuit: Influence of Cyclist Sequence, Stature, and Arm Spacing. *Journal of Biomechanical Engineering-Transactions of the Asme,* 136.

DELTA 2007. TU sluit Mekelweg af tijdens storm.

DETTORI, N. J. and NORVELL, D. C. 2006. Non-traumatic bicycle injuries - A review of the literature. *Sports Medicine,* 36**,** 7-18.

DIEDRICHS, B. 2010. Aerodynamic crosswind stability of a regional train model. *Proceedings of the Institution of Mechanical Engineers Part F-Journal of Rail and Rapid Transit,* 224**,** 580-591.

DONELL, S. 2010. Wind Blamed in Fatal Motorcycle Accident. *NBC Washington.*

DOREL, S., COUTURIER, A. and HUG, F. 2009. Influence of different racing positions on mechanical and electromyographic patterns during pedalling. *Scandinavian Journal of Medicine & Science in Sports,* 19**,** 44-54.

DUC, S., BETIK, A. C. and GRAPPE, F. 2005. EMG activity does not change during a time trial in competitive cyclists. *International Journal of Sports Medicine,* 26**,** 145-150.

EDWARDS, A. G. and BYRNES, W. C. 2007. Aerodynamic Characteristics as Determinants of the Drafting Effect in Cycling. *Medicine & Science in Sports & Exercise,* 39**,** 170-176 10.1249/01.mss.0000239400.85955.12.

ERICSON, M. 1986. On the Biomechanics of Cycling - a Study of Joint and Muscle Load during Exercise on the Bicycle Ergometer. *Scandinavian Journal of Rehabilitation Medicine,* 16**,** 1-43.

EVANGELISTI, M. I., VERDE, T. J., ANDRES, F. F. and FLYNN, M. G. 1995. Effects of Handlebar Position on Physiological Responses to Prolonged Cycling. *The Journal of Strength and Conditioning Research,* 9**,** 243-246.

FARIA, I., DIX, C. and FRAZER, C. 1978. Effect of Body Position during Cycling on Heart-Rate, Pulmonary Ventilation, Oxygen-Uptake and Work Output. *Journal of Sports Medicine and Physical Fitness,* 18**,** 49-56.

FARIA, I. E. 1992. Energy Expenditure, Aerodynamics and Medical Problems in Cycling. *Sports Medicine,* 14**,** 43-63.

FINTELMAN, D., HIGHTON, P., ADAMS, T., STERLING, M., HEMIDA, H. and LI, F.-X. 2013. Cycling time trial position: torso angle affects metabolic and physiological variables *ECSS annual conference.* Barcelona.

FINTELMAN, D. M., STERLING, M., HEMIDA, H. and LI, F. X. 2014a. The effect of crosswind on cyclists: an experimental study. *Procedia Engineering,* 72**,** 720-725.

FINTELMAN, D. M., STERLING, M., HEMIDA, H. and LI, F. X. 2014b. The effect of crosswinds on cyclists. *6. International Symposium on Computational Wind Engineering.* Hamburg, Germany.

FINTELMAN, D. M., STERLING, M., HEMIDA, H. and LI, F. X. 2014c. Optimal cycling time trial position models: Aerodynamics versus power output and metabolic energy. *Journal of Biomechanics,* 47**,** 1894-1898.

FINTELMAN, D. M., STERLING, M., HEMIDA, H. and LI, F. X. 2015. The effect of time trial cycling position on physiological and aerodynamic variables. *Journal of Sports Sciences***,** 1-8.

FLYNN, D., HEMIDA, H., SOPER, D. and BAKER, C. 2014. Detached-eddy simulation of the slipstream of an operational freight train. *Journal of Wind Engineering and Industrial Aerodynamics,* 132**,** 1-12.

FRANÇOIS, D., DELNERO, J., COLMAN, J., MARAÑÓN, D. L. J. and CAMOCARDI, M. Experimental determination of Stationary Aerodynamics loads on a double deck Bus. 11th Americas Conference on Wind Engineering, San Juan, Puerto Rico, 2009.

FRANKE, W. D., BETZ, C. B. and HUMPHREY, R. H. 1994. Effects of Rider Position on Continuous-Wave Doppler Responses to Maximal Cycle Ergometry. *British Journal of Sports Medicine,* 28**,** 38-42.

GARBY, L. and ASTRUP, A. 1987. The Relationship between the Respiratory Quotient and the Energy Equivalent of Oxygen during Simultaneous Glucose and Lipid Oxidation and Lipogenesis. *Acta Physiologica Scandinavica,* 129**,** 443-444.

GARCÍA-LÓPEZ, J., RODRÍGUEZ-MARROYO, J. A., JUNEAU, C., PELETEIRO, J., MARTÍNEZ, A. C. and VILLA, J. G. 2008. Reference values and improvement of aerodynamic drag in professional cyclists. *Journal of Sports Sciences,* 26**,** 277-286.

GAUGER, W. 2013. *Fatal motorcycle crash in Waupaca Co.* [Online]. Fox 11 News. Available: http://www.fox11online.com/dpp/news/local/fox_cities/fatal-motorcycle-crash-in-waupaca-co [Accessed 14 August 2013.

GENTILLI, R., ZANFORLIN, S. and FRIGO, S. Numerical and experimental analysis on a small GDI, stratified charge, motorcycle engine. Proceedings of the 8th Biennial Conference on Engineering Systems Design and Analysis, 4-7 July 2006 2006 Turin, Italy. 575-581.

GIBERTINI, G., CAMPANARDI, G., GRASSI, D. and MACCHI, C. 2008. Aerodynamics of biker position. *BBAA VI International Colloquium on: Bluff Bodies Aerodynamics & Applications.*

GNEHM, P., REICHENBACH, S., ALTPETER, E., WIDMER, H. and HOPPELER, H. 1997. Influence of different racing positions on metabolic cost in elite cyclists. *Medicine and Science in Sports and Exercise,* 29**,** 818-823.

GODO, M. N., CORSON, D. and LEGENSKY, S. M. 2009. An Aerodynamic Study of Bicycle Wheel Performance using CFD. *47th AIAA Aerospace Sciences Meeting Including The New Horizons Forum and Aerospace Exposition.*

GRAPPE, F., CANDAU, R., BELLI, A. and ROUILLON, J. D. 1997. Aerodynamic drag in field cycling with special reference to the Obree's position. *Ergonomics,* 40**,** 1299-1311.

GRAPPE, F., CANDAU, R., BUSSO, T. and ROUILLON, J. D. 1998. Effect of cycling position on ventilatory and metabolic variables. *International Journal of Sports Medicine,* 19**,** 336-341.

GREENWELL, D. I., WOOD, N. J., BRIDGE, E. K. L. and ADDY, R. J. 1995. Aerodynamic Characteristics of Low-Drag Bicycle Wheels. *Aeronautical Journal,* 99**,** 109-120.

GRIFFITH, M., CROUCH, T., THOMPSON, M., BURTON, D. and SHERIDAN, J. 2012. Elite Cycling Aerodynamics: Wind Tunnel Experiments and CFD. *18th Australasian Fluid Mechanics Conference.* Lauceston, Australia.

GRIFFITH, M., CROUCH, T., THOMPSON, M., BURTON, D. and SHERIDAN, J. 2014. Computational Fluid Dynamics Study of the Effect of Leg Position on Cyclist Aerodynamic Drag. *Journal of Fluids Engineering*.

*The Guardian*. 2001. Cyclist's death was an accident, Nov 02. Available: http://www.retfordtoday.co.uk/ [Accessed Nov 02].

GUILMINEAU, E. and CHOMETON, F. 2009. Effect of Side Wind on a Simplified Car Model: Experimental and Numerical Analysis. *Journal of Fluids Engineering,* 131**,** 021104.

GUZIK, D., HARDER, P., SUZUKI, M., LAVERY, M. and MATSON, C. 2013. 2014 Speed concept. Trek Bicycle Corporation.

HAHN, A. G. and GORE, C. J. 2001. The effect of altitude on cycling performance - A challenge to traditional concepts. *Sports Medicine,* 31**,** 533-557.

HANNA, R. K. 2002. Can CFD make a performance difference in sport? *In:* UJIHASHI, S. and HAAKE, S. J. (eds.) *The engineering of sport 4.* Oxford: Blackwell Science Ltd.

HANNAS, B. L. and GOFF, J. E. 2005. Inclined-plane model of the 2004 Tour de France. *European Journal of Physics,* 26**,** 251.

HARGREAVES, D. M., MORVAN, H. P. and WRIGHT, N. G. 2006. CFD modeling of high-sided vehicles in cross-winds. *The Fourth International Symposium on Computational Wind Engineering (CWE2006).* Yokohama, Japan.

HAWLEY, J. A. and NOAKES, T. D. 1992. Peak Power Output Predicts Maximal Oxygen-Uptake and Performance Time in Trained Cyclists. *European Journal of Applied Physiology and Occupational Physiology,* 65**,** 79-83.

HEIL, D. H. 2001. Body mass scaling of projected frontal area in competitive cyclists. *European Journal of Applied Physiology,* 85**,** 358-366.

HEIL, D. P. 2005. A Mathematical Model Of The 2004 Tour De France l'Alped'Huez Time-trial Winning Performance. *Medicine and Science in Sports and Exercise,* 37**,** S105-S105.

HEIL, D. P., DERRICK, T. R. and WHITTLESEY, S. 1997. The relationship between preferred and optimal positioning during submaximal cycle ergometry. *European Journal of Applied Physiology and Occupational Physiology,* 75**,** 160-165.

HEIL, D. P., WILCOX, A. R. and QUINN, C. M. 1995. Cardiorespiratory Responses to Seat-Tube Angle Variation during Steady-State Cycling. *Medicine and Science in Sports and Exercise,* 27**,** 730-735.

HEMIDA, H. and BAKER, C. 2010. Large-eddy simulation of the flow around a freight wagon subjected to a crosswind. *Computers & Fluids,* 39**,** 1944-1956.

HEMIDA, H. and KRAJNOVIĆ, S. 2009a. Exploring Flow Structures Around a Simplified ICE2 Train Subjected to A 30° Side Wind Using LES. *Engineering Applications of Computational Fluid Mechanics,* 3**,** 28-41.

HEMIDA, H. and KRAJNOVIĆ, S. 2009b. Transient Simulation of the Aerodynamic Response of a Double-Deck Bus in Gusty Winds. *Journal of Fluids Engineering-Transactions of the Asme,* 131.

HEMIDA, H. and KRAJNOVIĆ, S. 2010. LES study of the influence of the nose shape and yaw angles on flow structures around trains. *Journal of Wind Engineering and Industrial Aerodynamics,* 98**,** 34-46.

HENNEKAM, W. 1990. The speed of a cyclist. *Physics Education,* 25**,** 141.

HERMENS, H. J., MERLETTI, R. and FRERIKS, B. 1999. *SENIAM,* Enschede, The Netherlands, Roessingh Research and Development.

HUBENIG, L. R., GAME, A. B. and KENNEDY, M. D. 2011. Effect of Different Bicycle Body Positions on Power Output in Aerobically Trained Females. *Research in Sports Medicine,* 19**,** 245-258.

HUG, F. and DOREL, S. 2009. Electromyographic analysis of pedaling: A review. *Journal of Electromyography and Kinesiology,* 19**,** 182-198.

INIGUEZ-DE-LA-TORRE, I. and INIGUEZ, J. 2006. Cycling and wind: does sidewind brake? *European Journal of Physics,* 27**,** 71-74.

INIGUEZ-DE-LA TORRE, A. and INIGUEZ, J. 2009. Aerodynamics of a cycling team in a time trial: does the cyclist at the front benefit? *European Journal of Physics,* 30**,** 1365-1369.

ISSA, R. I. 1986. Solution of the implicitly discretised fluid flow equations by operator-splitting. *Journal of Computational Physics,* 62**,** 40-65.

JEUKENDRUP, A. E. and MARTIN, J. 2001. Improving Cycling Performance: How Should We Spend Our Time and Money. *Sports Medicine,* 31**,** 559-569.

JOBSON, S. A., NEVILL, A. M., GEORGE, S. R., JEUKENDRUP, A. E. and PASSFIELD, L. 2008. Influence of body position when considering the ecological validity of laboratory time-trial cycling performance. *Journal of Sports Sciences,* 26**,** 1269-1278.

JOBSON, S. A., NEVILL, A. M., PALMER, G. S., JEUKENDRUP, A. E., DOHERTY, M. and ATKINSON, G. 2007. The ecological validity of laboratory cycling: Does body size explain the difference between laboratory- and field-based cycling performance? *Journal of Sports Sciences,* 25**,** 3-9.

JOHNSON, R. W. 1998. Handbook of fluid dynamics. ed United States of America: Crc Press.

JOHNSON, S. and SCHULTZ, B. 1990. The physiological effects of aerodynamic handlebars. *Cycling Science,* 2**,** 9-12.

KARABELAS, S. J. and MARKATOS, N. C. 2012. Aerodynamics of Fixed and Rotating Spoked Cycling Wheels. *Journal of Fluids Engineering-Transactions of the Asme,* 134.

KOLMOGOROV, A. N. 1941. Local structure of turbulence in an incompressible viscous fluid at very large Reynolds numbers. *Doklady Akademiia Nauk SSSR,* 30**,** 299.

KYLE, C. R. 1979. Reduction of Wind Resistance and Power Output of Racing Cyclists and Runners Traveling in Groups. *Ergonomics,* 22**,** 387-397.

KYLE, C. R. 1988. The mechanics and aerodynamics of cycling. *In:* BURKE, E. R. and NEWSOM, M. M. (eds.) *Medical and Scientific Aspects of Cycling.* Champaign IL: Human Kinetics.

KYLE, C. R. 1989. The aerodynamics of handlebars and helmets. *Cycling Science,* 1**,** 22-25.

KYLE, C. R. 1991. The effect of crosswinds upon time trials. *Cycling Science,* 3**,** 51-6.

KYLE, C. R. 2003. Selecting Cycling Equipment, Chapter 1. *In:* BURKE, E. R. (ed.) *High-tech Cycling.* 2nd ed. United States of America: Human Kinetics.

KYLE, C. R. and BURKE, E. 1984. Improving the Racing Bicycle. *Mechanical Engineering,* 106**,** 34-45.

LAUNDER, B. E. and SPALDING, D. B. 1974. The numerical computation of turbulent flows. *Computer Methods in Applied Mechanics and Engineering,* 3**,** 269-289.

LI, L. and CALDWELL, G. E. 1998. Muscle coordination in cycling: effect of surface incline and posture. *Journal of Applied Physiology,* 85**,** 927-934.

LOPEZ-MINARRO, P. A., ANDUJAR, P. S. D. and RODRIGUEZ-GARCIA, P. L. 2009. A comparison of the sit-and-reach test and the back-saver sit-and-reach test in university students. *Journal of Sports Science and Medicine,* 8**,** 116-122.

LUKES, R., CHIN, S. and HAAKE, S. 2005. The understanding and development of cycling aerodynamics. *Sports Engineering,* 8**,** 59-74.

LUKES, R. A., CHIN , S. B., HART, J. H. and HAAKE, S. J. 2004. The aerodynamics of mountain bicycles: the role of computational fluid dynamics. *In:* HUBBARD, M., MEHTA, R. D. and PALLIS, J. M. (eds.) *The engineering of sport 5.*

MAKOWSKI, F. T. and KIM, S.-E. 2000. Advances in External-Aero Simulation of Ground Vehicles Using the Steady RANS Equations. *SAE Technical Paper,* 2000-01-0484.

MARSH, A. P. and MARTIN, P. E. 1995. The Relationship between Cadence and Lower-Extremity Emg in Cyclists and Noncyclists. *Medicine and Science in Sports and Exercise,* 27**,** 217-225.

MARTIN, J. and COBB, J. 2002. Body position and Aerodynamics. *In:* JEUKENDRUP, A. (ed.) *High-performance Cycling.* 1st ed. United States of America: Human Kinetics.

MARTIN, J. C., GARDNER, A. S., BARRAS, M. and MARTIN, D. T. 2006. Modeling sprint cycling using field-derived parameters and forward integration. *Medicine and science in sports and exercise,* 38**,** 592-597.

MARTIN, J. C., MILLIKEN, D. L., COBB, J. E., MCFADDEN, K. L. and COGGAN, A. R. 1998. Validation of a Mathematical Model for road Cycling Power. *Journal of Applied Biomechanics,* 14**,** 276-219.

MEIJAARD, J. P., PAPADOPOULOS, J. M., RUINA, A. and SCHWAB, A. 2007. Linearized dynamics equations for the balance and steer of a bicycle: a benchmark and review. *Proceedings of the Royal Society a-Mathematical Physical and Engineering Sciences,* 463**,** 1955-1982.

MEILE, W., REISENBERGER, E., MAYER, M., SCHMÖLZER, B., MÜLLER, W. and BRENN, G. 2006. Aerodynamics of ski jumping: experiments and CFD simulations. *Experiments in Fluids,* 41**,** 949-964.

MELLION, M. B. 1994. Neck and Back Pain in Bicycling. *Clinics in Sports Medicine,* 13**,** 137-164.

MENTER, F. R. 1992. Improved two-equation k-omega turbulence models for aerodynamic flows. *NASA-TM-103975,* NASA-TM-103975.

MERCKER, E. and WIEDEMANN, J. 1996. On the Correction of Interference Effects in Open Jet Wind Tunnels. SAE International.

MILLER, M. R., HANKINSON, J., BRUSASCO, V., BURGOS, F., CASABURI, R., COATES, A., CRAPO, R., ENRIGHT, P., VAN DER GRINTEN, C. P. M., GUSTAFSSON, P., JENSEN, R., JOHNSON, D. C., MACINTYRE, N., MCKAY, R., NAVAJAS, D., PEDERSEN, O. F., PELLEGRINO, R., VIEGI, G. and WANGER, J. 2005. Standardisation of spirometry. *European Respiratory Journal,* 26**,** 319-338.

MOSELEY, L. and JEUKENDRUP, A. E. 2001. The reliability of cycling efficiency. *Medicine and Science in Sports and Exercise,* 33**,** 621-7.

MURAKAMI, S., UEHARA, K. and KOMINE, H. 1979. Amplification of Wind Speed at Ground-Level Due to Construction of High-Rise Building in Urban Area. *Journal of Industrial Aerodynamics,* 4**,** 343-370.

NEPTUNE, R. R., KAUTZ, S. A. and HULL, M. L. 1997. The effect of pedaling rate on coordination in cycling. *Journal of Biomechanics,* 30**,** 1051-1058.

*ABC News*. 2012. Bobridge blown off his bike, 11 Jan. Available: http://www.abc.net.au/ [Accessed 11 Jan].

OGGIANO, L., LEIRDAL, S., SAETRAN, L. and ETTEMA, G. 2008. Aerodynamic optimization and energy saving of cycling postures for international elite level cyclists. *Engineering of Sport 7, Vol 1***,** 597-604.

OGGIANO, L., TROYNIKOV, O., KONOPOV, I., SUBIC, A. and ALAM, F. 2009. Aerodynamic behaviour of single sport jersey fabrics with different roughness and cover factors. *Sports Engineering,* 12**,** 1-12.

OLDS, T. 1992. The optimal altitude for cycling performance: A mathematical model. *Excel,* 8**,** 155-159.

ORIGENES, M. M., BLANK, S. E. and SCHOENE, R. B. 1993. Exercise ventilatory response to upright and aero-posture cycling. *Medicine and Science in Sports and Exercise,* 25**,** 608-12.

PADILLA, S., MUJIKA, I., ANGULO, F. and GOIRIENA, J. J. 2000. Scientific approach to the 1-h cycling world record: a case study. *Journal of Applied Physiology,* 89**,** 1522-1527.

PEVELER, W., BISHOP, P., SMITH, J. and RICHARDSON, M. 2005. Effects of training in an aero position on metabolic economy. *Journal of Exercise Physiology,* 8**,** 44-50.

PRICE, D. and DONNE, B. 1997. Effect of variation in seat tube angle at different seat heights on submaximal cycling performance in man. *Journal of Sports Sciences,* 15**,** 395-402.

PRILUTSKY, B. I., GREGOR, R. J. and RYAN, M. M. 1998. Coordination of two-joint rectus femoris and hamstrings during the swing phase of human walking and running. *Experimental Brain Research,* 120**,** 479-486.

RICHARDSON, R. S. and JOHNSON, S. C. 1994. The Effect of Aerodynamic Handlebars on Oxygen-Consumption While Cycling at a Constant-Speed. *Ergonomics,* 37**,** 859-863.

ROBINSON, C.G. and BAKER, C.J. 1990. The effect of atmospheric turbulence on trains. *Journal of Wind Engineering and Industrial Aerodynamics,* 34, 251-272.RYAN, A. and DOMINY, R. G. 1998. The Aerodynamic Forces Induced on a Passenger Vehicle in Response to a Transient Cross-Wind Gust at a Relative Incidence of 30°. *SAE Technical Paper,* 980392.

RYAN, B. 2012. Andy Schleck crashes in Critérium du Dauphiné time trial. *Cycling news.* UK.

RYSCHON, T. W. and STRAY-GUNDERSEN, J. 1991. The effect of body position on the energy cost of cycling. *Med Sci Sports Exerc,* 23**,** 949-53.

SAKAGAWA, K., YOSHITAKE, H. and IHARA, E. 2005. Computational Fluid Dynamics for Design of Motorcycles (Numerical Analysis of Coolant Flow and Aerodynamics). *SEA Technical Paper,* 2005-32-0033.

SARRE, G., LEPERS, R., MAFFIULETTI, N., MILLET, G. and MARTIN, A. 2003. Influence of cycling cadence on neuromuscular activity of the knee extensors in humans. *European Journal of Applied Physiology,* 88**,** 476-479.

SAUNDERS, M. J., EVANS, E. M., ARNGRIMSSON, S. A., ALLISON, J. D., WARREN, G. L. and CURETON, K. J. 2000. Muscle activation and the slow component rise in oxygen uptake during cycling. *Medicine and Science in Sports and Exercise,* 32**,** 2040-2045.

SAVELBERG, H. H. C. M., VAN DE PORT, I. G. L. and WILLEMS, P. J. B. 2003. Body configuration in cycling affects muscle recruitment and movement pattern. *Journal of Applied Biomechanics,* 19**,** 310-324.

SCHEPERS, P. and WOLT, K. 2012. Single-bicycle crash types and characteristics. *Cycling Research International,* 2**,** 119-135.

SCIBOR-RYLSKI, A. J. and SYKES, D. M. 1984. *Road Vehicle Aerodynamics,* Plymouth, Pentech Press.

SHINOHARA, M. and MORITANI, T. 1992. Increase in neuromuscular activity and oxygen uptake during heavy exercise. *Annual Journal of Physiology Anthropology,* 11**,** 257-262.

SHUHEI, A. 2006. Fuel Cell Powered Motorcycles. *Journal of the Society of Automotive Engineers of Japan,* 60**,** 90-93.

SILVA, A. J., ROUBOA, A., MOREIRA, A., REIS, V. M., ALVES, F., VILAS-BOAS, J. P. and MARINHO, D. A. 2008. Analysis of drafting effects in swimming using computational fluid dynamics. *Journal of sports sciences and Medicine,* 7**,** 60-66.

SPALART, P. R. and ALLMARAS, S. R. 1994. A One-Equation Turbulence Model for Aerodynamic Flows. *Recherche Aerospatiale***,** 5-21.

SPALART, P. R., DECK, S., SHUR, M. L., SQUIRES, K. D., STRELETS, M. K. and TRAVIN, A. 2006. A new version of detached-eddy simulation, resistant to ambiguous grid densities. *Theoretical and Computational Fluid Dynamics,* 20**,** 181-195.

SPALART, P. R. and SHUR, M. 1997. On the sensitization of turbulence models to rotation and curvature. *Aerospace Science and Technology,* 1**,** 297-302.

STERLING, M., QUINN, A. D., HARGREAVES, D. M., CHELI, F., SABBIONI, E., TOMASINI, G., DELAUNAY, D., BAKER, C. J. and MORVAN, H. 2010. A comparison of different methods to evaluate the wind induced forces on a high sided lorry. *Journal of Wind Engineering and Industrial Aerodynamics,* 98**,** 10-20.

SUJUDI, D. and HAIMES, R. 1995. Identification of swirling flow in 3-D vector fields. *12th Computational Fluid Dynamics Conference.* American Institute of Aeronautics and Astronautics.

TAKAHASHI, Y., KURAKAWA, Y., SUGITA, H., ISHIMA, T. and OBOKATA, T. 2009. CFD Analysis of Airflow around the Rider of a Motorcycle for Rider Comfort Improvement. *SAE Technical paper,* 2009-01-1155.

TEW, G. S. and SAYERS, A. T. 1999. Aerodynamics of yawed racing cycle wheels. *Journal of Wind Engineering and Industrial Aerodynamics,* 82**,** 209-222.

TOO, D. 1990. Biomechanics of Cycling and Factors Affecting Performance. *Sports Medicine,* 10**,** 286-302.

TRANSPORT, D. F. 2012. Reported Road Casualties in Great Britain: Main Results 2011. *Statistical Release.*

TSUBOKURA, M., NAKASHIMA, T., KITAYAMA, M., IKAWA, Y., DOH, D. H. and KOBAYASHI, T. 2010. Large eddy simulation on the unsteady aerodynamic response of a road vehicle in transient crosswinds. *International Journal of Heat and Fluid Flow,* 31**,** 1075-1086.

UBERTINI, S. and DESIDERI, U. 2002. Aerodynamic Investigation of a Scooter in the University of Perugia Wind Tunnel Facility. 2002-01-0254. Available: http://dx.doi.org/10.4271/2002-01-0254.

UNDERWOOD, L. and JERMY, M. 2013. Optimal handlebar position for track cyclists. *Sports Engineering,* 16**,** 81-90.

UNDERWOOD, L. and JERMY, M. C. 2011. Fabric testing for cycling skinsuits. *5th Asia-Pacific Congress on Sports Technology (Apcst),* 13**,** 350-356.

UNDERWOOD, L., SCHUMACHER, J., BURETTE-POMMAY, J. and JERMY, M. 2011. Aerodynamic drag and biomechanical power of a track cyclist as a function of shoulder and torso angles. *Sports Engineering,* 14**,** 147-154.

WALTON, D., DRAVITZKI, V. K., CLELAND, B. S., THOMAS, J. A. and JACKETT, R. 2005. *Balancing the needs of cyclist and motorist,* Wellington, New Zealand.

WANG, B., XU, Y. L., ZHU, L. D., CAO, S. Y. and LI, Y. L. 2013. Determination of Aerodynamic Forces on Stationary/Moving Vehicle-Bridge Deck System under Crosswinds Using Computational Fluid Dynamics. *Engineering Applications of Computational Fluid Mechanics,* 7**,** 355-368.

WANG, B., XU, Y. L., ZHU, L. D. and LI, Y. L. 2014. Crosswind Effect Studies on Road Vehicle Passing by Bridge Tower Using Computational Fluid Dynamics. *Engineering Applications of Computational Fluid Mechanics,* 8**,** 330-344.

WATANABE, T., OKUBO, T., IWASA, M. and AOKI, H. 2003. Establishment of an aerodynamic simulation system for motorcycle and its application. *Jsae Review,* 24**,** 231-233.

WATKINS, S., SAUNDERS, J.W., and HOFFMANN, P.H. 1995. Turbulence experienced by moving vehicles. Part I. Introduction and turbulence intensity. J*ournal of Wind Engineering and Industrial Aerodynamics*, 57, 1-17.

WELBERGEN, E. and CLIJSEN, L. P. V. M. 1990. The Influence of Body Position on Maximal Performance in Cycling. *European Journal of Applied Physiology and Occupational Physiology,* 61**,** 138-142.

WILSON, D. G. 2004. Bicycle science. *In:* PAPADOPOULOS, J. M. (ed.) 3d ed. ed. United States of America: MIT press.

XU, Y.-L., 2013. Wind effects on cable bridges. ed. Singapore: John Wiley & Sons.

YAMAHA. 2009. *YZF-R1: History 1998-2010* [Online]. Available: http://www.yamaha-motor.eu/designcafe/en/about-bikes/supersport/index.aspx?view=article&id=442650.

ZAÏDI, H., TAÏAR, R., FOHANNO, S. and POLIDORI, G. 2008. Analysis of the effect of swimmer's head position on swimming performance using computational fluid dynamics. *Journal of Biomechanics,* 41**,** 1350-1358.

ZDRAVKOVICH, M. M., ASHCROFT, M. W., CHISHOLM, S. J. and HICKS, N. 1996. Effect of cyclist's posture and vicinity of another cyclist on aerodynamic drag. *Engineering of Sport***,** 21-28.

ZHANG, D. Y., ZHENG, W. T., MA, Q. Z. and YANG, P. 2009. Numerical Simulation of Viscous Flow around Rowing Based on FLUENT. *2009 Isecs International Colloquium on Computing, Communication, Control, and Management, Vol I***,** 429-433.